VOL. 696 NO. 2 14 APRIL 1995
THIS ISSUE COMPLETES VOL. 696

JOURNAL OF CHROMATOGRAPHY A

INCLUDING ELECTROPHORESIS AND OTHER SEPARATION METHODS

ELSEVIER

JOURNAL OF CHROMATOGRAPHY A

INCLUDING ELECTROPHORESIS AND OTHER SEPARATION METHODS

Scope. The *Journal of Chromatography A* publishes papers on all aspects of **chromatography, electrophoresis** and related methods. Contributions consist mainly of research papers dealing with chromatographic theory, instrumental developments and their applications. In the *Symposium volumes*, which are under separate editorship, proceedings of symposia on chromatography, electrophoresis and related methods are published. *Journal of Chromatography B: Biomedical Applications* —This journal, which is under separate editorship, deals with the following aspects: developments in and applications of chromatographic and electrophoretic techniques related to clinical diagnosis or alterations during medical treatment; screening and profiling of body fluids or tissues related to the analysis of active substances and to metabolic disorders; drug level monitoring and pharmacokinetic studies; clinical toxicology; forensic medicine; veterinary medicine; occupational medicine; results from basic medical research with direct consequences in clinical practice.

Submission of Papers. The preferred medium of submission is on disk with accompanying manuscript (see *Electronic manuscripts* in the Instructions to Authors, which can be obtained from the publisher, Elsevier Science B.V., P.O. Box 330, 1000 AH Amsterdam, Netherlands). Manuscripts (in English; *four* copies are required) should be submitted to: Editorial Office of *Journal of Chromatography A*, P.O. Box 681, 1000 AR Amsterdam, Netherlands, Telefax (+31-20) 485 2304, or to: The Editor of *Journal of Chromatography B: Biomedical Applications*, P.O. Box 681, 1000 AR Amsterdam, Netherlands. Review articles are invited or proposed in writing to the Editors who welcome suggestions for subjects. An outline of the proposed review should first be forwarded to the Editors for preliminary discussion prior to preparation. Submission of an article is understood to imply that the article is original and unpublished and is not being considered for publication elsewhere. For copyright regulations, see below.

Publication information. *Journal of Chromatography A* (ISSN 0021-9673): for 1995 Vols. 683–714 are scheduled for publication. *Journal of Chromatography B: Biomedical Applications* (ISSN 0378-4347): for 1995 Vols. 663–674 are scheduled for publication. Subscription prices for *Journal of Chromatography A*, *Journal of Chromatography B: Biomedical Applications* or a combined subscription are available upon request from the publisher. Subscriptions are accepted on a prepaid basis only and are entered on a calendar year basis. Issues are sent by surface mail except to the following countries where air delivery via SAL is ensured: Argentina, Australia, Brazil, Canada, China, Hong Kong, India, Israel, Japan, Malaysia, Mexico, New Zealand, Pakistan, Singapore, South Africa, South Korea, Taiwan, Thailand, USA. For all other countries airmail rates are available upon request. Claims for missing issues must be made within six months of our publication (mailing) date. Please address all your requests regarding orders and subscription queries to: Elsevier Science B.V., Journal Department, P.O. Box 211, 1000 AE Amsterdam, Netherlands. Tel.: (+31-20) 485 3642; Fax: (+31-20) 485 3598. Customers in the USA and Canada wishing information on this and other Elsevier journals, please contact Journal Information Center, Elsevier Science Inc., 655 Avenue of the Americas, New York, NY 10010, USA, Tel. (+1-212) 633 3750, Telefax (+1-212) 633 3764.

Abstracts/Contents Lists published in Analytical Abstracts, Biochemical Abstracts, Biological Abstracts, Chemical Abstracts, Chemical Titles, Chromatography Abstracts, Current Awareness in Biological Sciences (CABS), Current Contents/Life Sciences, Current Contents/Physical, Chemical & Earth Sciences, Deep-Sea Research/Part B: Oceanographic Literature Review, Excerpta Medica, Index Medicus, Mass Spectrometry Bulletin, PASCAL-CNRS, Referativnyi Zhurnal, Research Alert and Science Citation Index.

US Mailing Notice. *Journal of Chromatography A* (ISSN 0021-9673) is published weekly (total 52 issues) by Elsevier Science B.V., (Sara Burgerhartstraat 25, P.O. Box 211, 1000 AE Amsterdam, Netherlands). Annual subscription price in the USA US$ 5389.00 (US$ price valid in North, Central and South America only) including air speed delivery. Second class postage paid at Jamaica, NY 11431. **USA POSTMASTERS**: Send address changes to *Journal of Chromatography A*, Publications Expediting, Inc., 200 Meacham Avenue, Elmont, NY 11003. Airfreight and mailing in the USA by Publications Expediting.

See inside back cover for Publication Schedule, Information for Authors and information on Advertisements.

0021-9673/95/$09.50

Printed in the Netherlands

CONTENTS

(Abstracts/Contents Lists published in Analytical Abstracts, Biochemical Abstracts, Biological Abstracts, Chemical Abstracts, Chemical Titles, Chromatography Abstracts, Current Awareness in Biological Sciences (CABS), Current Contents/Life Sciences, Current Contents/Physical, Chemical & Earth Sciences, Deep-Sea Research/Part B: Oceanographic Literature Review, Excerpta Medica, Index Medicus, Mass Spectrometry Bulletin, PASCAL-CNRS, Referativnyi Zhurnal, Research Alert and Science Citation Index)

REGULAR PAPERS

(Continued overleaf)

ELSEVIER

Journal of Chromatography A, 696 (1995) 165–172

JOURNAL OF CHROMATOGRAPHY A

Theoretical interpretation of the retention of system peaks in partition chromatography with a mobile phase containing electrolytes

Masami Shibukawa

Laboratory for Analytical Chemistry, Faculty of Engineering, Chiba University, 1-33, Yayoi-cho, Inage-ku, Chiba 263, Japan

First received 9 August 1994; revised manuscript received 20 December 1994; accepted 27 December 1994

Abstract

Theoretical equations were developed to describe the retention dependence of system peaks generated in partition chromatography with a mobile phase containing electrolytes on the composition of the mobile phase electrolytes, on the basis of the model regarding the partitioning of ionic solutes and Knox and Kaliszan's general equations for the retention of system peaks. The predictions from the equations agreed well with experimental results obtained on hydrophilic polymer packings for both water and acetone–water mobile phase systems containing two or three background electrolytes. This means that the retention of system peaks can be predicted even for three or more mobile phase component systems, once the dependence of the distribution of each mobile phase component between the mobile and stationary phases on the composition of the mobile phase has been elucidated.

1. Introduction

The use of multi-component mixtures as mobile phases leads to the formation of extra peaks that do not correspond to any component of the separated sample. These extraneous peaks are generally called systems peaks. System peaks can be visualized if at least one of the mobile phase components can be detected. Therefore, the system peaks can cause several chromatographic problems such as co-elution with solute peaks and incorrect assignment of peak identities [1].

Many investigators have examined various aspects of system peaks [1–25] and it is known that system peaks appear in the chromatograms due to the perturbation of the equilibrium composition of the mobile phase components caused by sample introduction. The equilibrium disturbances that occur when a sample solute is injected was extensively treated by Helfferich and Klein [26]. More recently, Knox and Kaliszan [27] developed a general theory on the generation of system peaks and presented a useful equation for interpreting the retention of the system peaks. The equations presented are expected to be used for the prediction of the capacity factors of the system peaks. However, the theory appears to have been substantiated by experiments only for two-component systems and not yet for three- or more-component systems.

In order to calculate the capacity factors of the system peaks, one would need to know all of the relevant sorption isotherms of the mobile phase

0021-9673/95/$09.50
SSDI 0021-9673(94)01283-0

components. Although isotopically labelled mobile phase components could be used for this purpose, it is tedious, especially for systems of three or more components, to obtain the isotherms from the retention volumes of the labelled components.

Another approach is to use a system where the dependence of the retention of the mobile phase components on the mobile phase composition has been clarified. We have shown that the effects of the background electrolytes in the mobile phase on the retention of ionic solutes on non-ionic polymer gels with water [28] or aqueous acetone [29] can be well interpreted by the stoichiometric model presented regarding the partitioning of ionic solutes. This ion partition model was also used successfully to account for the retention dependence of ionic solutes on the composition of the background electrolytes in these systems [30]. It was felt that this partition chromatographic system should provide an opportunity not only to demonstrate the practical validity of Knox and Kaliszan's theory but also to clarify the effect of the composition of background electrolytes in the mobile phase on the retention of the system peaks. It will be shown in this paper that the dependence of the capacity factors of the system peaks on hydrophilic porous polymers with acetone–water or water alone for three- or more-component systems can indeed be interpreted on the basis of the theoretical equations derived from Knox and Kaliszan's equation and the ion partition model.

2. Experimental

2.1. Materials

All chemicals were of analytical-reagent grade unless indicated otherwise.

HPLC-grade acetone was obtained from Kanto (Tokyo, Japan). Water purified through a Millipore Milli-Q water purification system was used throughout.

The column packings used were a cross-linked dextran gel, Sephadex G-25 (10–40 μm), purchased from Pharmacia (Uppsala, Sweden) and a cross-linked polyacrylamide gel, Bio-Gel P-2 (200–400 mesh), from Bio-Rad Labs. (Richmond, CA, USA). These polymer gels were washed with water, ethanol and acetone in that order and dried at 90°C before use.

2.2. Chromatographic conditions

The column packings were allowed to swell for 24 h in a large excess of the eluent solvent to be used, the solvent being decanted several times. The swollen gels were slurry packed into a 250 × 4 mm I.D. stainless-steel column. The column was thermostated at 25.0 ± 0.1°C through a column jacket, using a Yamato (Tokyo, Japan) Model BH-71 constant-temperature circulator.

The pump was a Kyowa Seimitsu (Tokyo, Japan) KHP-010 solvent-delivery system. The eluent reservoir was a commercially available glass syringe of 200-ml capacity [31]. Mobile phases were water or acetone–water (70:30, v/v) containing sodium salts. Elutions were carried out at a constant flow-rate of ca. 0.8 ml/min. Exact values of the volumetric flow-rate were measured using a burette designed to prevent vaporization of solvent. Portions of 5 μl of the sample solutions were injected into the column with a Kyowa Seimitsu KHP-UI-130A injection valve. The system peaks were monitored with a Tosoh (Tokyo, Japan) CM-8 conductivity detector and an Erma (Tokyo, Japan) ERC-7510 differential refractometer.

The mobile phase volume was determined according to the method proposed by Shibukawa and Ohta [32].

3. Results and discussion

3.1. Theoretical background

If the equilibrium composition of a mobile phase containing $N + 1$ components is perturbed by sample introduction, N system peaks will be generated. Knox and Kaliszan [27] showed that the relative velocities, R, of the system peaks for an $(N + 1)$-component mobile phase system are given by N roots of the following equation:

$$\begin{vmatrix} \left(f_{11}-\frac{1}{R}\right) & f_{12} & \cdots & f_{1N} \\ f_{21} & \left(f_{22}-\frac{1}{R}\right) & \cdots & f_{2N} \\ \vdots & \vdots & & \vdots \\ f_{N1} & f_{N2} & \cdots & \left(f_{NN}-\frac{1}{R}\right) \end{vmatrix} = 0 \quad (1)$$

where

$$f_{ij} = \left(\frac{\partial y_i}{\partial x_j}\right)_{x_k(k\neq j,N+1)=\text{constant}} \quad (2)$$

and x and y are the volume fraction of each component in the mobile phase and that in the liquid phase within the column, respectively.

Eq. 1 was derived for the distribution between the bulk mobile phase and the space within the column bed. In this case, R is defined by

$$R = \frac{V_t}{V_R} \quad (3)$$

where V_t is the total volume of all mobile phase components within the column and V_R is the retention volume.

It is more convenient to use the capacity factor, which describes the solute distribution between the mobile phase and the stationary phase, to express the retention of the system peaks observed in partition chromatography of ionic solutes than to use R. It is then a simple matter to replace volume fraction by amount, n, and R by the capacity factor, k', to give

$$\begin{vmatrix} (g_{11}-k') & g_{12} & \cdots & g_{1N} \\ g_{21} & (g_{22}-k') & \cdots & g_{2N} \\ \vdots & \vdots & & \vdots \\ g_{N1} & g_{N2} & \cdots & (g_{NN}-k') \end{vmatrix} = 0 \quad (4)$$

where

$$g_{ij} = \left(\frac{\partial n_{s,i}}{\partial n_{m,j}}\right)_{n_{m,k}(k\neq j,N+1)=\text{constant}} \quad (5)$$

and subscripts m and s denote the mobile and stationary phases, respectively.

In order to solve Eq. 4, all of the differentials in this equation, $g_{11}, g_{12}, \ldots, g_{NN}$, must be obtained. It is possible to calculate these differentials provided that the dependence of the retention of each mobile phase component on the composition of the mobile phase has previously been clarified. The author has recently presented the equations that represent the dependence of the retention of ionic analytes on the composition of the mobile phase electrolytes in partition chromatography [30]. The basic assumption of the ion partition model used for the derivation of the equations is that the association of each ion with counter ions is negligible in both the mobile and stationary phases [28].

When the mobile phase contains N univalent anions, $X_1^-, \cdots, X_N^-$ and a common univalent cation, Y^+, the capacity factor of an analyte anion, A^{p-}, $k'^{Y(X_1+\cdots+X_N)}_A$, is given by [30]

$$k'^{Y(X_1+\cdots+X_N)}_A = \frac{n_{s,A}}{n_{m,A}} = \left\{\frac{\sum[X_i^-]}{\sum\frac{[X_i^-]}{(k'^{YX_i}_A)^{2/p}}}\right\}^{p/2} \quad (6)$$

where $k'^{YX_i}_A$ is the capacity factor of A^{p-} when eluted with a single electrolyte, YX_i ($i = 1, \cdots, N$), and $[X_i^-]$ is the concentration of X_i^- is the mobile phase.

In a similar manner, the capacity factor of an anion, which is one of the components of the mobile phase, X_j^-, can be expressed as

$$k'^{Y(X_1+\cdots+X_N)}_{X_j} = \frac{n_{s,X_j}}{n_{m,X_j}} = \left\{\frac{\sum[X_i^-]}{\sum\frac{[X_i^-]}{(k'^{YX_i}_{X_j})^2}}\right\}^{1/2} = \left\{\frac{\sum n_{m,X_i}}{\sum\frac{n_{m,X_i}}{(k'^{YX_i}_{X_j})^2}}\right\}^{1/2} \quad (7)$$

We see that Eq. 7 enables us to calculate $g_{X_iX_j}$ for any combinations of the mobile phase component anions.

3.2. One solvent–two electrolyte system

Let us consider a mobile phase that consists of one solvent and two electrolytes, YX_1 and YX_2. This mobile phase is regarded as a three-component system since X_1^- and X_2^- must be accompanied by their counter cation, Y^+, in both the mobile and stationary phases. Hence we can write

$$\begin{vmatrix} (g_{X_1X_1} - k') & g_{X_1X_2} \\ g_{X_2X_1} & (g_{X_2X_2} - k') \end{vmatrix} = 0 \quad (8)$$

We obtain $g_{X_1X_1}$, $g_{X_2X_2}$, $g_{X_1X_2}$ and $g_{X_2X_1}$ from Eq. 7 as

$$g_{X_1X_1} = \frac{k'^{YX_2}_{X_1}\{[X_1^-](k'^{YX_1}_{X_1}/k'^{YX_1}_{X_2})(2[X_1^-] + [X_2^-]) + [X_2^-](3[X_1^-] + 2[X_2^-])\}}{2([X_1^-] + [X_2^-])^{1/2}\{[X_1^-](k'^{YX_1}_{X_1}/k'^{YX_2}_{X_2}) + [X_2^-]\}^{3/2}} \quad (9)$$

$$g_{X_2X_2} = \frac{k'^{YX_1}_{X_2}\{[X_2^-](k'^{YX_2}_{X_2}/k'^{YX_2}_{X_1})(2[X_2^-] + [X_1^-]) + [X_1^-](3[X_2^-] + 2[X_1^-])\}}{2([X_1^-] + [X_2^-])^{1/2}\{[X_2^-](k'^{YX_2}_{X_2}/k'^{YX_2}_{X_1}] + [X_1^-]\}^{3/2}} \quad (10)$$

$$g_{X_1X_2} = \frac{k'^{YX_2}_{X_1}[X_1^-]^2\{(k'^{YX_1}_{X_1}/k'^{YX_1}_{X_2}) - 1\}}{2([X_1^-] + [X_2^-])^{1/2}\{[X_1^-](k'^{YX_1}_{X_1}/k'^{YX_1}_{X_2}) + [X_2^-]\}^{3/2}} \quad (11)$$

$$g_{X_2X_1} = \frac{k'^{YX_1}_{X_2}[X_2^-]^2\{(k'^{YX_2}_{X_2}/k'^{YX_2}_{X_1}) - 1\}}{2([X_1^-] + [X_2^-])^{1/2}\{[X_2^-](k'^{YX_2}_{X_2}/k'^{YX_2}_{X_1}) + [X_1^-]\}^{3/2}} \quad (12)$$

Comparison of the theory with experiments through Eqs. 8–12 requires a knowledge of four k' values, $k'^{YX_1}_{X_1}$, $k'^{YX_2}_{X_1}$, $k'^{YX_1}_{X_2}$ and $k'^{YX_2}_{X_2}$. However, it is not necessary to determine all of the four values experimentally. $k'^{YX_2}_{X_1}$ and $k'^{YX_2}_{X_2}$ can be calculated from $k'^{YX_1}_{X_1}$ and $k'^{YX_1}_{X_2}$ as follows [28]:

$$k'^{YX_2}_{X_1} = \left[\frac{(k'^{YX_1}_{X_1})^3}{k'^{YX_1}_{X_2}}\right]^{1/2} \quad (13)$$

$$k'^{YX_2}_{X_2} = (k'^{YX_1}_{X_1}k'^{YX_1}_{X_2})^{1/2} \quad (14)$$

$k'^{YX_1}_{X_1}$ can be assumed to be the same as the capacity factor of the system peak observed when a solution of YX_1 with a concentration different from that of the mobile phase is injected into the column, provided that the mobile phase concentration of YX_1 is low enough to be within the portion of the isotherm that is linear from the origin [2]. Since an aqueous solution of YX_1 is a two-component system, only one system peak is generated, the capacity factor of which is given by

$$k' = g_{X_1X_1} = \frac{\partial n_{s,X_1}}{\partial n_{m,X_1}} \quad (15)$$

We compared the predictions of the theory with the experiments carried out on Sephadex G-25 and Bio-Gel P-2 with aqueous solutions of NaCl and $NaClO_4$. It has been shown that the effect of various types of electrolytes on the retention of inorganic ions on non-ionic hydrophilic porous polymers such as Sephadex G-25 and Bio-Gel P-2, when water is used as the mobile phase solvent can well be interpreted by the ion partition model [28]. The retention of an ion in these systems can be regarded as being governed by the partitioning of the ion between the external bulk water and the water in polymer gels, which has properties different from those of ordinary bulk water.

Figs. 1 and 2 show the capacity factors of the system peaks on Sephadex G-25 and Bio-Gel P-2 as a function of ClO_4^- in the mobile phase containing NaCl and $NaClO_4$; the total concentration of Cl^- and ClO_4^-, that is, the concentration of Na^+, was kept constant at 0.1 *M*. The solid lines represent the k' values calculated from Eqs. 8–12 using experimental data obtained in the NaCl mobile phase system. $k'^{NaClO_4}_{Cl}$ and $k'^{NaClO_4}_{ClO_4}$ were calculated by substituting k'^{NaCl}_{Cl} and $k'^{NaCl}_{ClO_4}$ into Eqs. 13 and 14, respectively. It is seen from Figs. 1 and 2 that the calculated k' values are in good agreement with

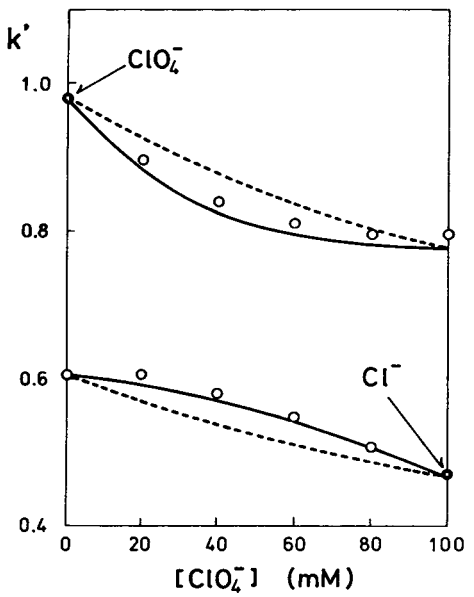

Fig. 1. Capacity factors of system peaks on Sephadex G-25 as a function of concentration of ClO_4^- in aqueous solution containing NaCl and $NaClO_4$. The solid lines were calculated from Eqs. 8–12. The dashed lines, which represent the capacity factors of Cl^- and ClO_4^- as analyte ions, were calculated according to Eq. 6. $[Na^+] = [Cl^-] + [ClO_4^-] = 100$ m*M*. ● = Analyte peak; ○ = system peak.

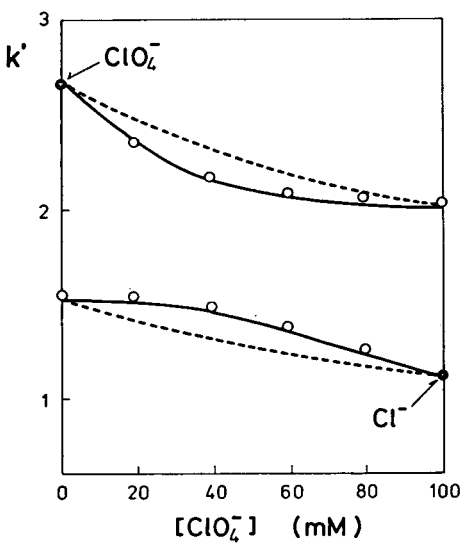

Fig. 2. Capacity factors of system peaks on Bio-Gel P-2 as a function of concentration of ClO_4^- in aqueous solution containing NaCl and $NaClO_4$. For other details, see Fig. 1.

the experimental values. It should be noted that the capacity factors of Cl^- and ClO_4^- as analyte ions injected (dashed lines), evaluated using Eq. 6, are different from those of the system peaks.

3.3. Two solvent–two electrolyte system

As the second object of this study, Sephadex G-25 equilibrated with acetone–water containing two electrolytes, YX_1 and YX_2, was chosen. Sephadex G-25 preferentially takes up water when it is brought into contact with a mixture of water and acetone and then forms a typical normal-phase partition system where the retention of inorganic ions is governed by the simple ion partition mechanism [29].

The mobile phase adopted here is a four-component system, the capacity factors of three system peaks observed in this system being given by the three roots of the equation

$$\begin{vmatrix} (g_{X_1X_1} - k') & g_{X_1X_2} & g_{X_1Ac} \\ g_{X_2X_1} & (g_{X_2X_2} - k') & g_{X_2Ac} \\ g_{AcX_1} & g_{AcX_2} & (g_{AcAc} - k') \end{vmatrix} = 0 \quad (16)$$

where the subscript Ac represents acetone.

If the concentrations of the mobile phase ions are negligibly smaller than those of the component solvents and the concentrations of the solvents in the stationary phase can be regarded as being constant regardless of the composition of the mobile phase electrolytes, we can write

$$g_{AcX_1} = g_{AcX_2} = 0 \quad (17)$$

Eqs. 16 and 17 then give

$$(g_{AcAc} - k') \begin{vmatrix} (g_{X_1X_1} - k') & g_{X_1X_2} \\ g_{X_2X_1} & (g_{X_2X_2} - k') \end{vmatrix} = 0 \quad (18)$$

It is expected from Eq. 18 that the k' value of one of the three system peaks generated in this system should be constant, independent of the composition of the mobile phase electrolytes, whereas the values of the remaining two peaks are given by substituting Eqs. 9–12 into Eq. 8 in

a similar manner as described for a one solvent–two electrolyte system.

Fig. 3 shows the chromatograms of conductivity and refractive index detector responses for the injection of an acetone–water mixture with a concentration of acetone slightly less than that in the mobile phase into a column equilibrated with acetone–water (70:30, v/v) containing 8 m*M* $NaNO_3$ and 2 m*M* $NaClO_4$. The dependence of the k' values for the three system peaks in the conductivity trace on the concentration of ClO_4^- is illustrated in Fig. 4, where the total concentration of NO_3^- and ClO_4^- was kept constant at 10 m*M*. As expected, one of the system peaks, the positive peak in the conductivity trace, which corresponds to the peak observed in the refractive index response, has a constant k' value of 0.81, whereas the other two peaks exhibit k' values that depend on the composition of the mobile phase electrolytes. The theoretical k' values (solid lines) were calculated from Eqs. 8–12 using experimental data obtained in the $NaClO_4$ system. $k'^{NaNO_3}_{ClO_4}$ and $k'^{NaNO_3}_{NO_3}$ were obtained by substituting $k'^{NaClO_4}_{ClO_4}$ and $k'^{NaClO_4}_{NO_3}$ into Eqs. 13 and 14, respectively. Fig. 4 shows

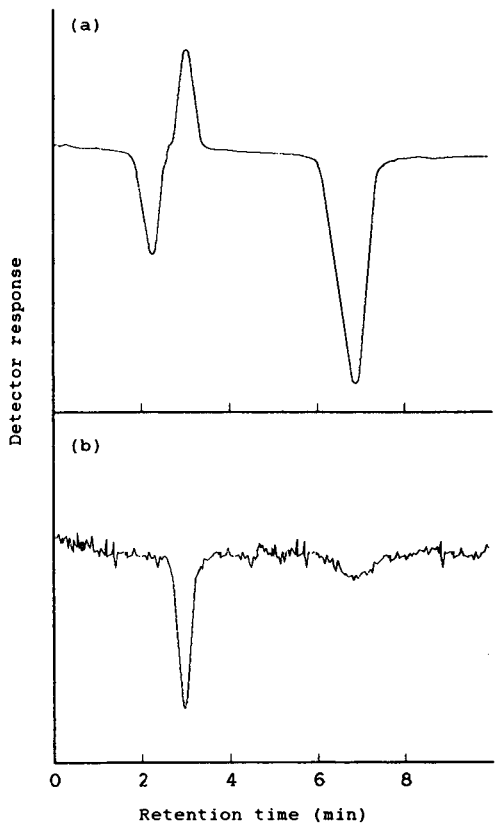

Fig. 3. Chromatograms of (a) conductivity and (b) refractive index detector responses resulting from an injection of an acetone–water mixture that is slightly enriched in water compared with the mobile phase. Column, Sephadex G-25 (250 × 4 mm I.D.); mobile phase, acetone–water (70:30, v/v) containing 8 m*M* $NaNO_3$ and 2 m*M* $NaClO_4$.

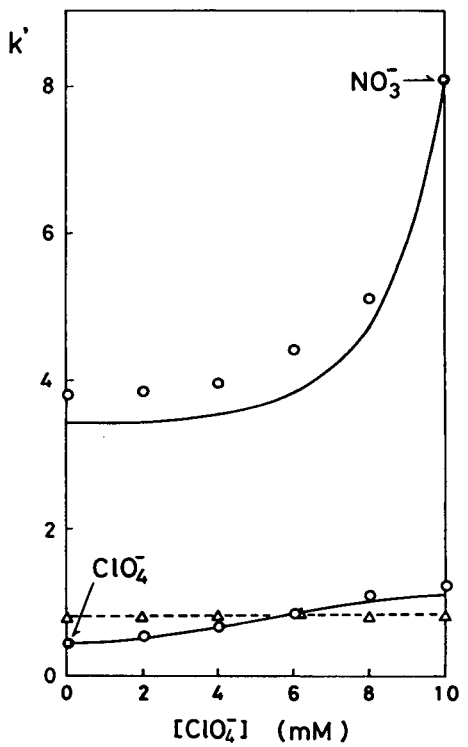

Fig. 4. Capacity factors of system peaks on Sephadex G-25 as a function of concentration of ClO_4^- in acetone–water (70:30, v/v) containing $NaNO_3$ and $NaClO_4$. The solid lines were calculated from Eqs. 8–12. $[Na^+] = [NO_3^-] + [ClO_4^-] =$ 10 m*M*. ● = Analyte peak; ○ = system peak which depends on the composition of mobile phase electrolytes; △ = system peak which does not depend on the composition of mobile phase electrolytes.

that there is fairly good agreement between the experimental and calculated k' values. This result indicates that the retention of the system peaks in this system can be predicted from Eq. 18 and the ion partition model.

3.4. Two solvent–three electrolyte system

We extend the theoretical approach described above to a two solvent–three electrolyte system. If acetone–water to be used as the mobile phase solvent contains three anions, X_1^-, X_2^- and X_3^-, and a common cation, Y^+, it is regarded as a five-component system. The capacity factors to be generated are given by the four roots of the following equation, provided that the distribution of acetone on Sephadex G-25 does not depend on the composition of the mobile phase electrolytes:

$$(g_{AcAc} - k') \begin{vmatrix} (g_{X_1X_1} - k') & g_{X_1X_2} & g_{X_1X_3} \\ g_{X_2X_1} & (g_{X_2X_2} - k') & g_{X_2X_3} \\ g_{X_3X_1} & g_{X_3X_2} & (g_{X_3X_3} - k') \end{vmatrix} = 0 \quad (19)$$

The evaluation of $g_{X_1X_1}$, $g_{X_1X_2}$, ..., $g_{X_3X_3}$ from Eq. 7 involves simple but detailed manipulations too long to reproduce here. The result for the system acetone–water (70:30, v/v) containing NaCl, $NaNO_3$ and $NaClO_4$ is shown in Fig. 5, where the solid lines represent the theoretical k' values calculated by using the experimental k' data obtained in the $NaNO_3$ system. Table 1 compares the calculated and experimental k' values for the three system peaks which depend on the mobile phase electrolyte composition. The calculated and experimental values agree well with each other, which indicates that the k' values of the system peaks in two solvent–three

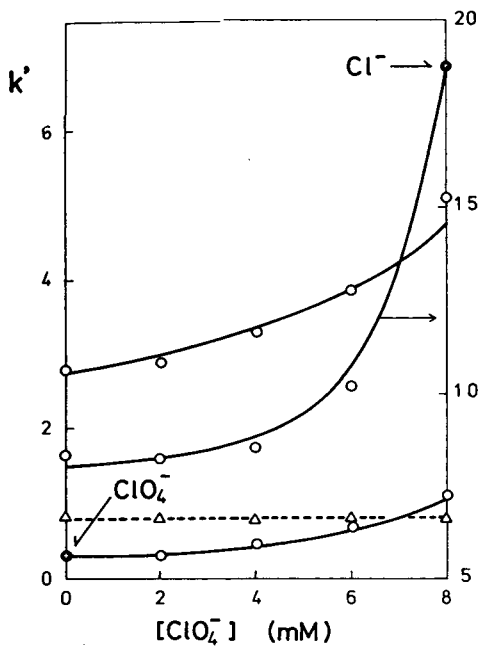

Fig. 5. Capacity factors of system peaks on Sephadex G-25 as a function of concentration of ClO_4^- in acetone–water (70:30, v/v) containing $NaNO_3$, NaCl and $NaClO_4$. $[NO_3^-] = 2$ mM; $[Na^+] = [NO_3^-] + [Cl^-] + [ClO_4^-] = 10$ mM. For other details, see Fig. 4.

Table 1
Calculated and experimental capacity factors of system peaks on Sephadex G-25 with acetone–water (70:30, v/v) containing NaCl, $NaNO_3$ and $NaClO_4$

Concentration of mobile phase anions (mM)				Capacity factor of system peak		
				No. 1	No. 2	No. 3
ClO_4^-	NO_3^-	Cl^-				
2	2	6	Exptl.	0.311	2.88	8.10
			Calcd.	0.389	2.91	7.61
2	4	4	Exptl.	0.405	3.46	8.90
			Calcd.	0.423	3.25	8.19
2	6	2	Exptl.	0.443	3.89	10.18
			Calcd.	0.474	3.51	9.51
4	2	4	Exptl.	0.456	3.28	8.50
			Calcd.	0.495	3.32	8.26
4	4	2	Exptl.	0.527	3.96	10.55
			Calcd.	0.560	3.62	9.88
6	2	2	Exptl.	0.674	3.85	10.15
			Calcd.	0.671	3.88	10.20

electrolyte system can also be accurately predicted from Eqs. 7 and 19.

4. Conclusions

Theoretical equations concerning the dependence of retention of system peaks on the composition of the mobile phase electrolytes were developed on the basis of the model for partition chromatography of ionic solutes in the presence of background electrolytes and Knox and Kaliszan's theory. The capacity factors of the system peaks predicted from the equations were in good agreement with the experimental values obtained with both single (water) and binary solvent (acetone–water) systems containing two or three electrolytes. The results described above indicate that the relationship between the retention of the system peaks and the mobile phase composition can be obtained, once the dependence of the distribution of each mobile phase component between the mobile and stationary phases on the composition of the mobile phase is known, although it may sometimes be fairly complicated.

References

[1] P.E. Jackson and P.R. Haddad, *J. Chromatogr.*, 346 (1985) 125–137.
[2] R.M. McCormack and B.L. Karger, *Anal. Chem.*, 52 (1980) 2249–2257.
[3] J.J. Stranahan and S.N. Deming, *Anal. Chem.*, 54 (1982) 1540–1546.
[4] K. Fukuhara, A. Nakamura and M. Tsuboi, *Bull. Chem. Soc. Jpn.*, 56 (1983) 2169–2170.
[5] W.R. Melander, J.F. Erard and Cs. Horváth, *J. Chromatogr.*, 282 (1983) 229–248.
[6] B. Buszewski, T. Bleha and D. Berek, *J. High Resolut. Chromatogr. Chromatogr. Commun.*, 8 (1985) 860–862.
[7] A. Sokolowski, *Chromatographia*, 22 (1986) 177–182.
[8] S. Levin and E. Grushka, *Anal. Chem.*, 58 (1986) 1602–1607.
[9] S. Levin and E. Grushka, *Anal. Chem.*, 59 (1987) 1157–1164.
[10] M.C. Gennaro, *J. Liq. Chromatogr.*, 10 (1987) 3347–3375.
[11] T. Takeuchi, S. Watanabe, K. Murase and D. Ishii, *Chromatographia*, 25 (1988) 107–110.
[12] R.A. Djerki and R.J. Laub, *J. Liq. Chromatogr.*, 11 (1988) 327–332.
[13] H. Poppe, *J. Chromatogr.*, 506 (1990) 45–60.
[14] L. Hackzell and G. Schill, *Chromatographia*, 15 (1982) 437–444.
[15] J. Crommen, G. Schill, D. Westerlund and L. Hackzell, *Chromatographia*, 24 (1987) 252–260.
[16] E. Arvidsson, J. Crommen, G. Schill and D. Westerlund, *Chromatographia*, 24 (1987) 460–468.
[17] A. Sokolowski, T. Fornstedt and D. Westerlund, *J. Liq. Chromatogr.*, 10 (1987) 1629–1662.
[18] J. Crommen, G. Schill and P. Herne, *Chromatographia*, 25 (1988) 397–403.
[19] E. Arvidsson, L. Hackzell, G. Schill and D. Westerlund, *Chromatographia*, 25 (1988) 430–436.
[20] E. Arvidsson, J. Crommen, G. Schill and D. Westerlund, *Chromatographia*, 26 (1988) 45–52.
[21] E. Arvidsson, J. Crommen, G. Schill and D. Westerlund, *J. Chromatogr.*, 461 (1989) 429–441.
[22] A. Sokolowski, *J. Chromatogr.*, 384 (1987) 1–12.
[23] A. Sokolowski, *J. Chromatogr.*, 384 (1987) 13–24.
[24] T. Fornstedt, D. Westerlund and A. Sokolowski, *J. Chromatogr.*, 506 (1990) 61–74.
[25] C.W. Hsu and W.T. Cooper, *J. Chromatogr.*, 603 (1992) 63–71.
[26] F. Helfferich and G. Klein, *Multicomponent Chromatography*, Marcel Dekker, New York, 1970.
[27] J.H. Knox and R. Kaliszan, *J. Chromatogr.*, 349 (1985) 211–234.
[28] M. Shibukawa and N. Ohta, *Chromatographia*, 22 (1986) 261–267.
[29] M. Shibukawa, N. Ohta and T. Koya, *J. Chromatogr. Sci.*, 26 (1988) 325–330.
[30] M. Shibukawa, *J. Chromatogr. A*, 655 (1993) 199–205.
[31] K. Saitoh and N. Suzuki, *Anal. Chem.*, 52 (1980) 30–32.
[32] M. Shibukawa and N. Ohta, *Chromatographia*, 25 (1988) 288–294.

ELSEVIER

Journal of Chromatography A, 696 (1995) 173–183

JOURNAL OF CHROMATOGRAPHY A

Preparation and application of an (*S*)-naproxen chiral stationary phase

Myung Ho Hyun[a,*], Yoon Jae Cho[a], Jae-Jeong Ryoo[a], Kyung Kyu Jyung[b], Gwi Suk Heo[c]

[a]*Department of Chemistry, Pusan National University, Pusan 609-735, South Korea*
[b]*Department of Chemistry Education, Pusan National University, Pusan 609-735, South Korea*
[c]*Korea Research Institute of Standards and Science, P.O. Box 3, Daedeog-Danji, Daejon 305-606, South Korea*

First received 18 August 1994; revised manuscript received 25 November 1994; accepted 21 December 1994

Abstract

A chiral stationary phase (CSP) for the liquid chromatographic separation of enantiomers was prepared by immobilizing the 3,5-dimethylanilide derivative of (*S*)-naproxen on silica gel through the 6-methoxy-2-naphthyl functionality of (*S*)-naproxen. The enantioselectivities exerted by this π-basic CSP for resolving π-acidic racemates were generally greater than those on the previously reported CSPs prepared by immobilizing an alkylamide of (*S*)-naproxen on silica gel through the alkylamide functionality. Based on the chromatographic resolution trends, two chiral recognition mechanisms are proposed. One mechanism applied for the resolution of N-(3,5-dinitrobenzoyl)-α-amino esters is proposed to utilize the 6-alkoxy-2-naphthyl group of the CSP as a π-basic interaction site for enantioselective $\pi-\pi$ complexation with the 3,5-dinitrobenzoyl group of the analyte and the other mechanism is proposed to utilize the 3,5-dimethylanilide group of the CSP in resolving N-(3,5-dinitrobenzoyl)-α-arylalkylamines.

1. Introduction

The two enantiomers of racemic drugs often show different pharmacological effects in living systems [1]. In consequence, the enantiomeric composition of pharmaceuticals has been an important issue in the drug development and in the clinical use of drugs and there has been a widespread need for techniques that afford a means of determining enantiomeric composition and absolute configuration and obtaining each of the two enantiomers in an enantiomerically pure form [2,3]. Among various techniques, chiral liquid chromatography based on chiral stationary phases (CSPs) has been widely accepted as a convenient and accurate means to meet such a need [4].

The resolution of racemates by chiral liquid chromatography is now fairly common because various CSPs are available [5]. Among others, Pirkle-type CSPs have been known to resolve two enantiomers through the $\pi-\pi$ interaction between the CSP and the analytes [6]. To utilize the effective $\pi-\pi$ interaction, Pirkle-type CSPs are usually designed to contain a π-basic or a π-acidic aryl functional group [7,8]. In relation to this point, (*S*)-naproxen which is a well known anti-inflammatory drug sold as an optically active

* Corresponding author.

0021-9673/95/$09.50
SSDI 0021-9673(94)01285-7

form, is an attractive candidate for new Pirkle-type CSPs because the 6-methoxy-2-naphthyl group of the compound can be utilized as a strong π-basic aryl functionality. Previously, (*S*)-naproxen has been used as a π-basic chiral selector in chiral liquid chromatography. For example, CSPs such as **1**, **2** and **3** consisting of (*S*)-naproxen immobilized on silica gel via an amide linkage [9,10], an ester linkage or an ionic linkage [11] have been reported. Recently, Pirkle *et al.* [12] reported doubly tethered CSP **4** prepared by immobilizing (*S*)-naproxen diallylamide to silica gel through the diallylamide functionality and compared its efficiencies with CSP **1**. All of these (*S*)-naproxen-derived CSPs utilize the carboxylic acid functionality of (*S*)-naproxen in immobilization.

In contrast, in this paper we report a CSP (**5**) prepared by immobilizing the 3,5-dimethylanilide of (*S*)-naproxen on silica gel through the 6-methoxy-2-naphthyl functionality of (*S*)-naproxen, the connection mode of which has been verified as useful in preparing other (*S*)-naproxen-derived CSPs in our laboratory [13,14]. Previously, it has been reported that arylamide derivatives of ibuprofen, which has a structure similar to that of naproxen, are resolved better than simple alkylamide derivatives on the π-

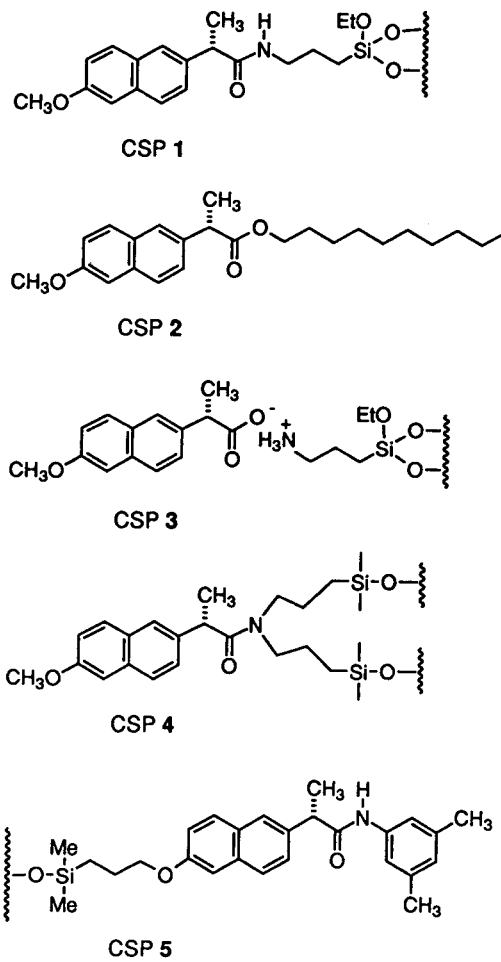

FORMULA A.

acidic CSP derived from (*R*)-N-(3,5-dinitrobenzoyl)phenylglycine and the resolutions are improved as the electron-donating power of the substituent on the aromatic derivatizing group increases [15]. We also found that arylamide derivatives of racemic naproxen are generally resolved better than simple alkylamide derivatives on the same CSP. In consequence, CSP **5** derived from (*S*)-naproxen arylamide containing two electron-donating substituents such as a methyl functionality on the aromatic ring of the aryl amide group is expected to be better than the CSPs derived from alkylamide derivatives of naproxen in resolving π-acidic racemic analytes based on the reciprocity concept of chiral recognition [16].

In addition, CSP **5** actually contains two π-basic functional groups that can act as a π-donor site, i.e., 6-alkoxy-2-naphthyl and 3,5-dimethylphenyl groups. Either of the two π-basic functional groups of CSP **5** may be used for face-to-face $\pi-\pi$ complexation with π-acidic racemates, which is known to be essential for chiral recognition by Pirkle-type CSPs [6]. Therefore, the role of the two π-basic aromatic functional groups contained in CSP **5** in resolving π-acidic racemates is of interest and is discussed herein.

2. Experimental

^{1}H NMR spectra were recorded on a Varian Gemini 300 spectrometer (300 MHz). Chemical shifts are reported in parts per million (ppm) relative to tetramethylsilane as the internal standard. IR spectra were measured with a Mattson Polaris Fourier transform (FT) IR spectrometer. Melting points were taken on a Rigaku TAS 100 thermal analyzer. Optical rotations were measured on a Rudolph Autopol III automatic polarimeter. Elemental analyses were performed at the OCRC Centre, Sogang University, Seoul, Korea.

The analytes used in this study were either available from prior studies or prepared in the manner described previously [14]. (*S*)-Naproxen, (+)-6-methoxy-α-methyl-2-naphthaleneacetic acid, was purchased from Aldrich. Solvents for HPLC analysis were of HPLC grade. All reagents purchased from commercial suppliers were of analytical-reagent grade and used without further purification, unless indicated otherwise. All reactions were performed under an argon atmosphere.

HPLC analyses were performed using a HPLC system consisting of a Waters Model 510 pump, a Rheodyne Model 7125 injector with a 20-μl sample loop, a Youngin (Seoul, Korea) Model 710 absorbance detector with a 254-nm UV filter and a Youngin D520B computing integrator. The volume of sample injected was usually 5 μl.

2.1. Preparation of CSP 5

(S) - α - (6-Methoxy-2-naphthyl)propion - 3,5-dimethylanilide (6)

(*S*)-Naproxen (7.38 g, 0.032 mol) and thionyl chloride (9.35 ml, 0.128 mol) were dissolved in 100 ml of benzene and then the stirred mixture was refluxed for 2 h. After cooling to room temperature, the mixture was evaporated to dryness using a rotary evaporator. The residue was dissolved in 80 ml of dry dichloromethane and then a mixture of 3,5-dimethylaniline (3.99 ml, 0.032 mol) and triethylamine (4.46 ml, 0.032 mol) diluted in 20 ml of dry dichloromethane was added slowly with stirring. The reaction mixture was stirred at room temperature for 2 h and then washed successively with 100 ml of saturated $NaHCO_3$ solution, 100 ml of 2 *M* HCl and brine. The organic solution was dried over anhydrous Na_2SO_4 and evaporated. The residue was purified by flash column chromatography on silica gel [ethyl acetate–hexane–dichloromethane (1:5:1–1:3:1, v/v/v)] to afford a white solid. Crystallization of the white solid in hexane afforded amide **6** (10.41 g) in 98% yield. The enantiomeric purity of amide **6** was greater than 98% by the HPLC analysis on a previously described CSP [17]; m.p. 153–155°C. ^{1}H NMR (C^2HCl_3), δ 1.67 (d, 3H), 2.23 (s, 6H), 3.84 (q, 1H), 3.94 (s. 3H), 6.70 (s, 1H), 6.99–7.78 (m, 9H). IR (KBr) cm^{-1}, 3436, 3305, 1661, 1607, 1532. $[\alpha]_D^{25}$ +103.7 (*c* 1.0, CH_2Cl_2).

(S) - α - (6-Hydroxy-2-naphthyl)propion - 3,5-dimethylanilide (7)

Amide **6** (5.0 g, 0.015 mol) was placed in a 250-ml round-bottomed flask with 70 ml of dry dichloromethane. The solution was cooled to −78°C and then a solution of BBr_3 (3.58 ml, 0.038 mol) in 15 ml of dry dichloromethane was added over 1 h with stirring. The reaction mixture was allowed to warm to room temperature over 1 h and then stirred for an additional 1 h. At this stage, the formation of a white solid was observed. The mixture was cooled to 0°C and then water was added slowly with stirring until no more white fumes (probably HBr gas) evolved. After stirring for an additional 3 h, the white solid was filtered off and dissolved in a mixture of acetone (130 ml) and ethyl acetate (600 ml). The organic solution was washed with brine, dried over anhydrous Na_2SO_4 and then evaporated. The residue was purified by flash column chromatography on silica gel [acetone–dichloromethane (1:20, v/v)] to afford hydroxy compound **7** (4.16 g, 87% yield) as a white solid. The enantiomeric purity of hydroxy compound **7** was greater than 98% by the HPLC analysis on a previously described CSP [17]; m.p. 161–163°C. ^1H NMR (acetone-$^2H_6$), δ 1.57 (d, 3H), 2.24 (s, 6H), 3.97 (q, 1H), 6.70 (broad s, 1H), 7.15–7.80 (m, 9H), 9.06 (s, 1H). IR (KBr) cm^{-1}, 3298, 2974, 1618, 1547. $[\alpha]_D^{25}$ + 105.4 (*c* 1.0, CH_3OH).

(S) - α - (6-Allyloxy-2-naphthyl)proprion - 3,5-dimethylanilide (8)

Hydroxy compound **7** (2.0 g, 0.0063 mol) was dissolved in 100 ml of dry CH_3CN and then stirred with K_2CO_3 (1.12 g, 0.0081 mol) at room temperature for 2 h in a 150-ml round-bottomed flask. Allyl bromide (1.35 ml, 0.0156 mol) was added to the reaction mixture and then the whole mixture was heated to reflux. After refluxing for 2 h, the solvent was evaporated and the residue was dissolved in diethyl ether. The diethyl ether solution was washed successively with 100 ml of 1 *M* NaOH solution and 100 ml of brine, dried over anhydrous $MgSO_4$ and concentrated. The residue was purified by silica gel column chromatography [ethyl acetate–hexane (1:6–1:3, v/v)] to afford allyloxy compound **8** (2.14 g, 95% yield) as a white solid. The enantiomeric purity of allyloxy compound **8** was greater than 98% by the HPLC analysis on a previously described CSP [17]; m.p. 136–137°C. ^1H NMR (C^2HCl_3), δ 1.67 (d, 3H), 2.24 (s, 6H), 3.84 (q, 1H), 4.66–4.69 (m, 2H), 5.32–5.38 (m, 1H), 5.45–5.53 (m, 1H), 6.08–6.09 (m, 1H), 6.71 (s, 1H), 7.00–7.76 (m, 9H). IR (KBr) cm^{-1}, 3281, 1653, 1604, 1531. $[\alpha]_D^{25}$ + 88.6 (*c* 1.0, CH_2Cl_2).

(S) - α - [6-(3-Ethoxydimethylsilylpropoxy) - 2-naphthyl)]proprion - 3,5 - dimethylanilide (9)

Compound **8** (2.0 g, 0.0056 mol) was placed in a 100-ml round-bottomed flask with 50 ml of dry dichloromethane. Dimethylchlorosilane (25 ml) was added to the reaction mixture, followed by addition of $H_2PtCl_6 \cdot 6H_2O$ (*ca.* 10 mg) dissolved in 1 ml of dry tetrahydrofuran. The reaction mixture was heated to reflux and checked periodically by TLC. After checking that there was no starting material in the reaction mixture, dichloromethane and excess dimethylchlorosilane were removed by simple distillation and then under reduced pressure. The residue was dissolved in 60 ml of dry dichloromethane and then 10 ml of triethylamine—absolute ethanol (1:1, v/v) were added slowly with stirring. The mixture was stirred at room temperature for 1 h, concentrated and chromatographed on silica gel [ethyl acetate–hexane (1:6, v/v)] to afford silyl compound **9** (2.26 g, 88% yield) as a highly viscous, colourless liquid. The enantiomeric purity of **9** was greater than 98% by the HPLC analysis on a previously described CSP [17]. ^1H NMR (C^2HCl_3), δ 0.15 (s, 6H), 0.74–0.79 (m, 2H), 1.20 (t, 3H), 1.64 (d, 3H), 1.88–1.96 (m, 2H), 2.21 (s, 6H), 3.69 (q, 2H), 3.81 (q, 1H), 4.05 (t, 2H), 6.68 (s, 1H), 7.04–7.72 (m, 9H). IR (CH_2Cl_2) cm^{-1}, 3299, 2934, 1659, 1605, 1559. $[\alpha]_D^{25}$ + 65.9 (*c* 0.8, CH_2Cl_2).

*Preparation of CSP **5** and HPLC column packing*

A 100-ml flask equipped with a Dean–Stark trap, a condenser and a magnetic stirring bar was

charged with Regis Rexchrom silica gel (5 μm, 4.5 g) and toluene (90 ml). After heating the heterogeneous silica gel–toluene mixture to reflux until the complete azeotropic removal of water, silyl compound **9** (1.28 g, 0.0028 mol) dissolved in 20 ml of toluene was added and the whole mixture was heated at reflux for 83 h. The modified silica gel was filtered, washed successively with toluene, methanol, acetone, ethyl acetate, hexane and diethyl ether and then dried under vacuum. Elemental analysis of the modified silica gel (C 10.48, H 1.07, N 0.42%) showed a loading of 0.34 mmol of chiral selector per gram of stationary phase based on C or 0.30 mmol of chiral selector per gram of stationary phase based on N. The modified silica gel was slurried in methanol and packed into a 250 mm × 4.6 mm I.D. stainless-steel HPLC column using a conventional slurry packing method with an Alltech slurry packer. After washing the HPLC chiral columns thus packed with 100 ml of dichloromethane, a solution of 2 ml of hexamethyldisilazane in 50 ml of dichloromethane was eluted through the column to end-cap the residual silanol groups and then dichloromethane was eluted to wash out unreacted hexamethyldisilazane.

3. Results and discussion

CSP **5** was prepared as shown in Fig. 1. To summarize, (*S*)-naproxen was converted into the acid chloride and then treated with 3,5-dimethylaniline in the presence of triethylamine to afford the 3,5-dimethylanilide derivative **6** of (*S*)-naproxen. Treatment of **6** with boron tribromide at −78°C afforded the 6-hydroxy-2-naphthyl com-

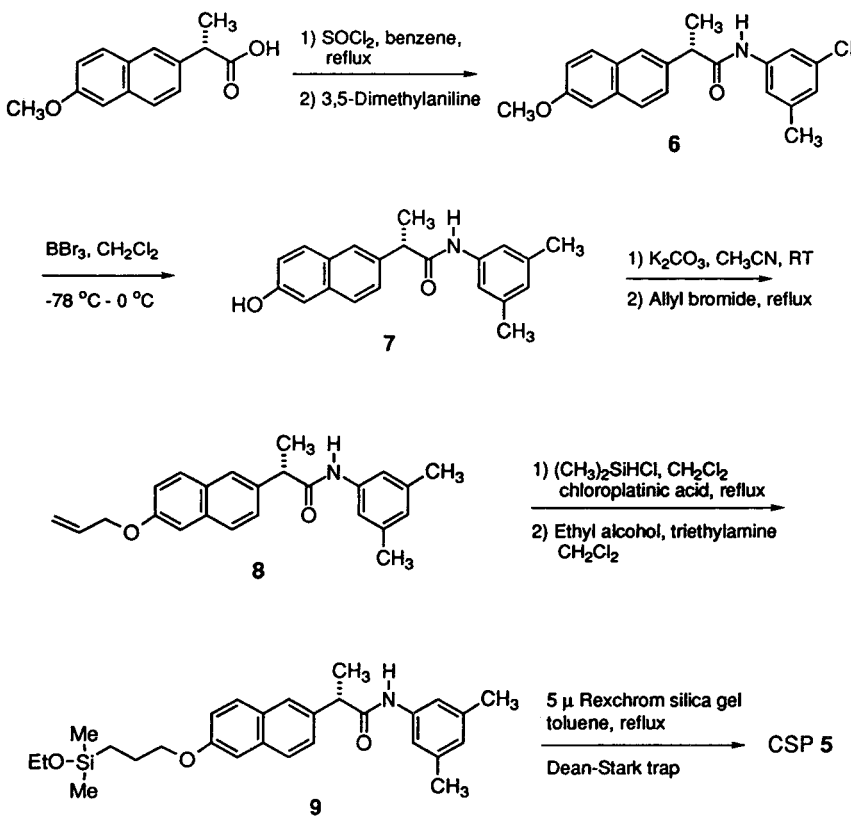

Fig. 1. Scheme for the preparation of CSP **5**.

pound **7**. Reaction of **7** with K_2CO_3 in acetonitrile at room temperature and then with allyl bromide under reflux gave the 6-allyloxy-2-naphthyl compound **8**. Finally, hydrosilylation of **8** to give silyl compound **9** and treatment of **9** with 5-μm silica gel produced CSP **5**. In each step, no racemization was observed by HPLC analysis on a previously described CSP [17].

The enantioselectivities exerted by CSP **5** for resolving various π-acidic racemates shown in Fig. 2 are summarized in Table 1. As shown in Table 1, N-(3,5-dinitrobenzoyl) derivatives of α-amino esters (analytes **10a–o**), α-amino amides (analytes **10p–r**) and α-arylalkylamines (analytes **11**) and 3,5-dinitroanilide derivatives of anti-inflammatory drugs related to α-arylpropionic acids (analytes **12**) are resolved with reasonable to good separation factors on CSP **5**. In addition, N-(3,5-dinitrobenzoyl) derivatives of other racemic compounds (analytes **13–15**) are resolved with reasonable separation factors on CSP **5**. By comparing the separation factors shown in Table 1 with those reported previously by Pirkle *et al.* [12], we found that CSP **5** is generally better than CSP **1** in terms of chiral recognition denoted by separation factors (α values) but worse than CSP **4** except for resolving N-(3,5-dinitrobenzoyl)leucine alkyl esters. In resolving N-(3,5-dinitrobenzoyl)leucine alkyl esters, CSP **5** showed the best resolution results. The elution orders shown in Table 1 for resolving N-(3,5-dinitrobenzoyl) derivatives of racemates on CSP **5** were identical with those on CSPs **1** and **4**.

In an effort to elucidate the chiral recognition mechanism manifested by CSP **5**, N-(3,5-dinitrobenzoyl) derivatives of a series of α-alkylglycine ethyl esters (analytes **10a–e**) and leucine alkyl esters (analytes **10g–m**) were prepared and resolved on CSP **5**. The use of homologous series of analytes has been often utilized as mechanistic probes to investigate the origins of enantioselectivity exerted by a certain Pirkle-type CSP. For example, increasing or decreasing trends in the separation factors of a homologous series of analytes with variation of the length of the substituent have been used as evidence for the intercalation of alkyl substituents of analytes between the adjacent strands of the bonded phase during the chiral recognition [18,19]. However, the separation factors for resolving N-(3,5-dinitrobenzoyl) derivatives of a series of α-alkylglycine ethyl esters (analytes **10a–e**) and leucine alkyl esters (analytes **10g–m**) on CSP **5** remain almost constant as

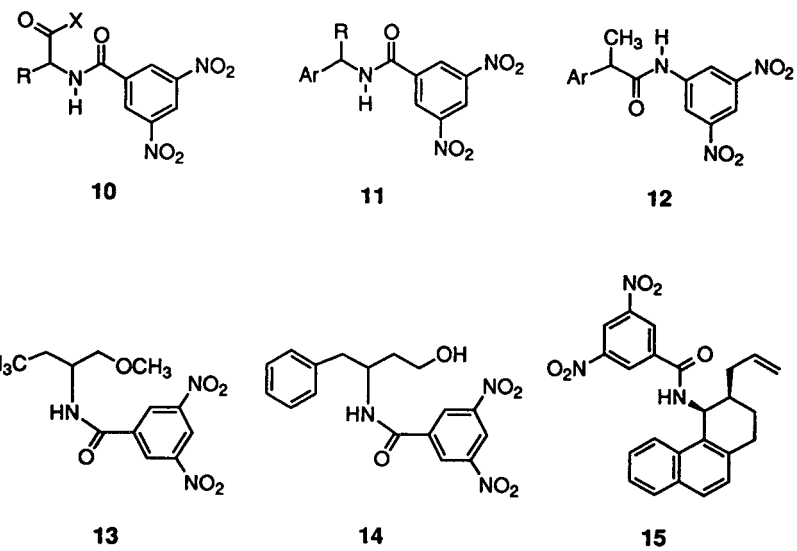

Fig. 2. Structures of the racemic compounds resolved on CSP **5** in this study.

Table 1
Resolution of various π-acidic racemates on CSP **5**

Analyte	R (or Ar)	X (or R)	$k_1'^a$	$k_1'^b$	α^c	Configuration[d]
10a	CH_3	OCH_2CH_3	14.77	23.01	1.56	*R*
b	$(CH_2)_2CH_3$	OCH_2CH_3	13.89	30.57	2.20	
c	$(CH_2)_4CH_3$	OCH_2CH_3	12.67	26.29	2.07	
d	$(CH_2)_6CH_3$	OCH_2CH_3	11.74	25.82	2.20	
e	$(CH_2)_7CH_3$	OCH_2CH_3	10.99	24.07	2.19	
f	$CH(CH_3)_2$	OCH_2CH_3	12.44	25.39	2.04	*R*
g	$CH_2CH(CH_3)_2$	OCH_3	15.07	37.98	2.52	*R*
h	$CH_2CH(CH_3)_2$	OCH_2CH_3	12.56	32.15	2.56	*R*
i	$CH_2CH(CH_3)_2$	$O(CH_2)_2CH_3$	11.79	29.45	2.50	
j	$CH_2CH(CH_3)_2$	$O(CH_2)_3CH_3$	11.39	28.73	2.52	
k	$CH_2CH(CH_3)_2$	$O(CH_2)_5CH_3$	10.83	26.72	2.47	
l	$CH_2CH(CH_3)_2$	$O(CH_2)_9CH_3$	8.90	21.98	2.47	
m	$CH_2CH(CH_3)_2$	$O(CH_2)_{15}CH_3$	7.36	18.16	2.47	
n	Phenyl	OCH_3	28.45	32.99	1.16	*R*
o	Benzyl	OCH_3	37.25	57.70	1.55	*R*
p	CH_3	$NH(CH_2)_2CH_3$	4.21	4.94	1.17	*R*
q	$CH(CH_3)_2$	$NH(CH_2)_2CH_3$	2.05	3.35	1.63	*R*
r	$CH_2CH(CH_3)_2$	$NH(CH_2)_2CH_3$	2.31	3.95	1.71	*R*
11a	Phenyl	CH_3	35.52	38.67	1.19	*R*
b	Phenyl	CH_2CH_3	36.04	49.23	1.37	
c	Phenyl	$(CH_2)_4CH_3$	34.88	46.83	1.34	
d	Phenyl	$(CH_2)_7CH_3$	27.03	38.64	1.43	
e	Phenyl	$(CH_2)_{11}CH_3$	21.81	33.31	1.53	
f	4-CH_3-Phenyl	CH_3	30.19	35.00	1.16	
g	4-$CH_3(CH_2)_2$-phenyl	CH_3	27.09	31.06	1.15	
h	4-$CH_3(CH_2)_7$-phenyl	CH_3	22.41	23.51	1.05	
i	4-$CH_3(CH_2)_{11}$-phenyl	CH_3	19.42	19.42	1.00	
j	4-Methoxyphenyl	CH_3	42.96	53.49	1.25	*R*
k	4-Methoxyphenyl	$(CH_2)_7CH_3$	35.92	51.13	1.42	
l	4-Methoxyphenyl	$(CH_2)_{16}CH_3$	25.38	39.63	1.56	
m	α-Naphthyl	CH_3	40.63	60.61	1.49	*R*
12a	3-Phenoxyphenyl		11.45	13.65	1.19	
b	3-Benzoylphenyl		13.19	16.38	1.24	
c	6-Methoxy-2-naphthyl		17.54	20.12	1.15	*S*
13			15.98	24.88	1.56	
14			16.66	19.03	1.14	
15			35.68	116.67	3.27	

All data were collected using 20% 2-propanol in hexane at a flow-rate of 2.0 ml/min. Void volumes were measured using 1,3,5-tri-*tert*.-butylbenzene.
[a] Capacity factors of the first-eluted enantiomers.
[b] Capacity factors of the second-eluted enantiomers.
[c] Separation factors.
[d] Absolute configuration of the second-eluted enantiomers. For blank entries, the elution orders have not been established.

the length of the alkyl chain of analytes increases as shown in Table 1. Note that relatively small separation factor for resolving N-(3,5-dinitrobenzoyl)alanine ethyl ester (**10a**, α-alkyl = methyl) on CSP **5** compared with the separation factors of other N-(3,5-dinitrobenzoyl)-α-alkylglycine

ethyl esters may stem from conformational factors, as described previously [19]. From these results, we excluded the possibility of a chiral recognition mechanism involving the process of intercalating the ester alkyl tail or the α-alkyl tail of N-(3,5-dinitrobenzoyl)-α-alkylamino alkyl esters between the adjacent strands of the bonded phase. Instead, we propose, from a study of the CPK molecular models, a possible chiral recognition mechanism that does not involve the intercalation process for resolving N-(3,5-dinitrobenzoyl)-α-alkylamino alkyl esters.

Fig. 3 shows the proposed chiral recognition model for resolving N-(3,5-dinitrobenzoyl)-α-alkylamino alkyl esters on CSP **5**. In this model, CSP **5** and the analyte are represented in conformations which are presumed to be of relatively low energy and hence preferentially populated [11,18]. CSP **5** and the analyte interact through the face-to-face $\pi-\pi$ complexation between their respective 6-alkoxy-2-naphthyl (NAPH) and 3,5-dinitrophenyl (DNP) groups and the simultaneous face-to-edge $\pi-\pi$ interaction, which has received increased attention as an associative force between aromatic rings [18,19], between the 3,5-dimethylphenyl (DMP) group of the CSP and the DNP group of the analyte and through the hydrogen bonding between the amide NH hydrogen of the CSP and the carbonyl oxygen of the 3,5-dinitrobenzoyl group of the analyte. In this event, the alkoxy oxygen of the ester functionality of the *R*-enantiomer can also interact with the amide NH hydrogen of the CSP and in consequence the diastereomeric *R,S*-complex shown in Fig. 3 is energetically more favorable than the *S,S*-complex. Note that in this model both of the ester alkyl group (Y) and the α-aklyl substituent (denoted by R in the model) of the analyte are away from the connecting tether of the CSP and in consequence the intercalation of either the Y or the R group of the analyte between the connecting tethers of the CSP is not possible. When the ester alkoxy group of the analyte is changed to an amide NH group, the second hydrogen bonding shown in Fig. 3 between the alkoxy oxygen of the ester functionality of the *R*-enantiomer and the amide NH hydrogen of the CSP is not possible. This may be the reason for the shorter retention times and lower separation factors observed for resolving N-(3,5-dinitrobenzoyl)-α-aminoamides (analytes **10p–r**) on CSP **5** than those for resolving N-(3,5-dinitrobenzoyl)-α-amino esters shown in Table 1.

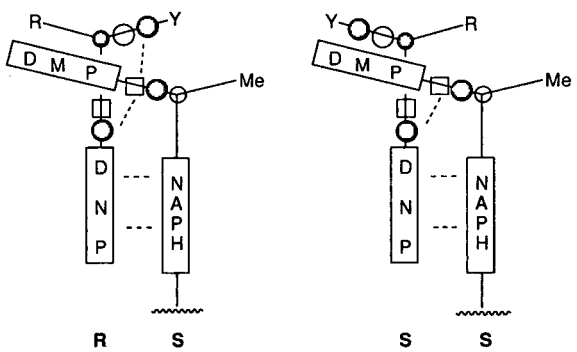

Fig. 3. Proposed chiral recognition model for resolving N-(3,5-dinitrobenzoyl)-α-alkylamino alkyl esters on CSP **5**. The *R,S*-complex is more stable than the *S,S*-complex.

The separation factors for resolving a series of N-(3,5-dinitrobenzoyl)-α-phenylalkylamines (analytes **11a–e**) on CSP **5** increase whereas those for resolving a series of N-(3,5-dinitrobenzoyl)-α-(*p*-alkylphenyl)ethylamines (analytes **11f–i**) decrease as the alkyl substituent of analytes increases in length, as shown in Table 1, and these trends are illustrated with more relevant data included in Figs. 4 and 5. As shown in Fig. 4, the capacity factors of the *S*-enantiomers of N-(3,5-dinitrobenzoyl)-α-phenylalkylamines decrease more rapidly than those of the more retained *R*-enantiomers as the length of the α-alkyl substituent of the analyte increases and in consequence separation factors increase continuously. The discrepancy in the continuous increase of separation factors at $n = 2$ noted in Fig. 4 may also originate from conformational reasons, as described previously [19]. However, Fig. 5 shows that the capacity factors of the more

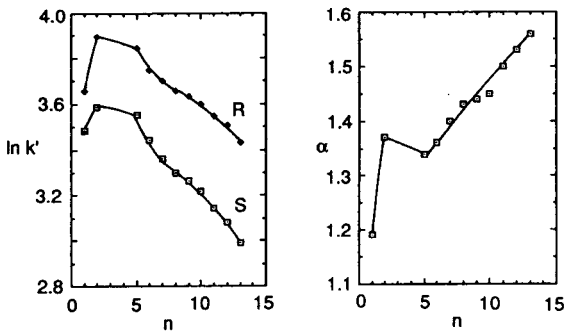

Fig. 4. Trends in the retention (ln k') of the two enantiomers and the enantioselectivity (α) for resolving N-(3,5-dinitrobenzoyl)-α-phenylalkylamines on CSP **5**. The length of the alkyl substituent [$-(CH_2)_nH$] at the chiral centre of the analyte is denoted by n on the abscissa. For chromatographic conditions, see Experimental and the footnote to Table 1.

retained *R*-enantiomers of N-(3.5-dinitrobenzoyl)-α-(p-alkylphenyl)ethylamines decrease more rapidly than the *S*-enantiomers as the length of the p-alkyl substituent of the analyte increases, and in consequence the separation factors decrease and finally no resolution is observed with the p-alkyl substituent reaches n-decyl.

From the trends shown in Figs. 4 and 5, we can imagine that the alkyl substituent at the chiral centre of the *S*-enantiomers of N-(3,5-dinitrobenzoyl)-α-phenylalkylamines intercalates between the strands of bonded phase during the chiral recognition and the intercalation process experiences more difficulty as the alkyl substituent increases in length. Similarly, the p-alkyl substituent of the *R*-enantiomers of N-(3,5-dinitrobenzoyl)-α-(p-alkylphenyl)ethylamine intercalates between the strands of bonded phase during the chiral recognition and the separation factors decrease as the p-alkyl substituent increases in length.

A possible chiral recognition mode which involves such intercalation processes and explains the trends shown in Figs. 4 and 5 is proposed as shown in Fig. 6. In this model, the CSP has the same conformation as drawn in the model shown in Fig. 3 and the analyte is presumed to be in its lowest energy conformation as described previously [20]. As shown in Fig. 6, CSP **5** utilizes the DMP instead of the NAPH group as a π-basic interaction site for the face-to-face $\pi-\pi$ complexation with the DNP group of the analyte and the carbonyl oxygen for the simultaneous hydrogen bonding with the NH hydrogen of the analyte. The alternative hydrogen bonding interaction between the NH hydrogen of the CSP and the carbonyl oxygen of the analyte seems also to be possible. However, from study of the CPK molecular models we found that the hydrogen bonding interaction between the carbonyl oxygen of the CSP and the

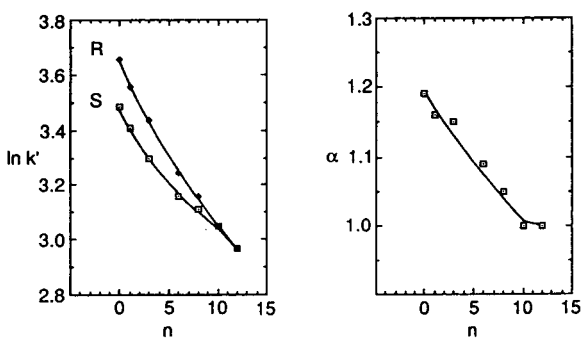

Fig. 5. Trends in the retention (ln k') of the two enantiomers and the enantioselectivity (α) for resolving N-(3,5-dinitrobenzoyl)-α-(p-alkylphenyl)ethylamines on CSP **5**. The length of the p-alkyl substituent [$-(CH_2)_nH$] of the analyte is denoted by n on the abscissa. For chromatographic conditions, see Experimental and the footnote to Table 1.

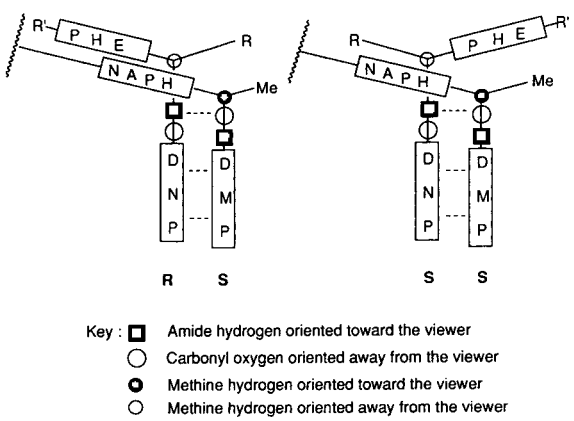

Fig. 6. Proposed chiral recognition model for resolving N-(3,5-dinitrobenzoyl)-α-arylalkylamines on CSP **5**. The *R*,*S*-complex is more stable than the *S*,*S*-complex.

NH hydrogen of the analyte shown in Fig. 6 might make possible the secondary hydrogen bonding interaction between the NH hydrogen of the CSP and the oxygen of the nitro group of the analyte, a hydrogen bonding interaction similar to which has been proposed previously [20], and consequently we presumed the model shown in Fig. 6 to be more plausible.

In this instance, the alkyl substituent (denoted by R in the model) at the chiral centre of the *R*-analyte is oriented to the direction of the methyl group of the CSP whereas that of the *S*-analyte is more parallel to the connecting tether of the CSP. As a consequence, the retention time of the initially less retained *S*-enantiomer decreases more rapidly than that of the initially more retained *R*-enantiomer and the separation factor (α) increases as the length of the alkyl substituent at the chiral centre of the analyte increases as shown in Fig. 4. However, the origin of the more retention of the *R*-enantiomer than that of the *S*-enantiomer on CSP **5** is not clear at present. Based on the chiral recognition model shown in Fig. 6, we propose that the two aromatic functional groups such as the phenyl group (PHE) of the *R*-enantiomer of the analyte and the NAPH group of the CSP may induce an attractive interaction between them. In this event, the diastereomeric *R,S*-complex should be more favorable than the *S,S*-complex.

In resolving N-(3,5-dinitrobenzoyl)-α-(*p*-alkylphenyl)ethylamines on CSP **5**, the *p*-alkyl group of the *R*-enantiomer is directed alongside the connecting tether of the CSP whereas that of the *S*-enantiomer is oriented towards the direction of the methyl group of the CSP as shown in Fig. 6. In this instance, the retention time of the *R*-enantiomer of the analyte decreases more rapidly than that of the *S*-enantiomer because of the suppressed intercalation process as the *p*-alkyl group of the analyte increases in length and consequently the separation factor decreases. All of these are consistent with the trends shown in Fig. 5.

The use of different π-basic aromatic groups of CSP **5** in resolving N-(3,5-dinitrobenzoyl)-α-alkylamino alkyl esters and N-(3,5-dinitrobenzoyl)-α-arylalkylamines illustrated in Figs. 3 and 6 may be evidenced by comparison of the enantioselectivities with those obtained with a CSP derived from the 3,5-dinitroanilide derivative of (*S*)-naproxen. Previously, we prepared a CSP that has the same structure as that of CSP **5** except for the 3,5-dimethylanilide group by immobilizing the 3,5-dinitroanilide derivative of (*S*)-naproxen on silica gel and reported the resolution of various N-(3,5-dinitrobenzoyl)-α-alkylamino alkyl esters and N-(3,5-dinitrobenzoyl)-α-arylalkylamines on the CSP [14]. From the comparison of the reported resolution results on the CSP derived from the 3,5-dinitroanilide derivative of (*S*)-naproxen with those on CSP **5**, we found that the enantioselectivities for resolving N-(3,5-dinitrobenzoyl)-α-arylalkylamines on the CSP derived from the 3,5-dinitroanilide derivative of (*S*)-naproxen are much worse than those on CSP **5** whereas those for resolving N-(3,5-dinitrobenzoyl)-α-alkylamino alkyl esters on the CSP derived from the 3,5-dinitroanilide derivative of (*S*)-naproxen are comparable to those on CSP **5**. These results might be rationalized based on the chiral recognition mechanisms shown in Figs. 3 and 6 as follows. N-(3,5-Dinitrobenzoyl)-α-arylalkylamines which are proposed to be resolved through the effective $\pi-\pi$ complexation between the π-acidic DNP group of the analyte and the π-basic DMP group of CSP **5** as shown in the chiral recognition model in Fig. 6 cannot make an effective $\pi-\pi$ donor–acceptor complex with the CSP derived from the 3,5-dinitroanilide of (*S*)-naproxen because the CSP lacks the DMP group and are resolved very poorly. However, N-(3,5-dinitrobenzoyl)-α-alkylamino alkyl esters, which are expected to be resolved through the effective $\pi-\pi$ complexation between the π-acidic DNP group of the analyte and the π-basic NAPH group of CSP **5** as shown in the chiral recognition model in Fig. 3, can induce an effective $\pi-\pi$ donor–acceptor interaction with the CSP derived from the 3,5 dinitroanilide of (*S*)-naproxen utilizing the 6-alkoxy-2-naphthyl group of the CSP and are resolved well on this CSP. Consequently, these results support the proposed chiral recognition models utilizing different π-basic aromatic

groups of CSP **5** in resolving N-(3,5-dinitrobenzoyl)-α-alkylamino alkyl esters and N-(3,5-dinitrobenzoyl)-α-arylalkylamines shown in Figs. 3 and 6.

In conclusion, we have demonstrated that CSP **5** prepared by immobilizing the 3,5-dimethylanilide of (*S*)-naproxen on silica gel through the 6-methoxy-2-naphthyl functionality of (*S*)-naproxen shows greater enantioselectivities in resolving some π-acidic racemates than the previously reported CSPs prepared by immobilizing an alkylamide of (*S*)-naproxen on silica gel through the alkylamide functionality. From the chromatographic resolution trends and the study based on the CPK molecular models, we proposed two chiral recognition mechanisms, shown in Figs. 3 and 6, which utilize either the NAPH group or the DMP group of the CSP for the enantioselective π–π complexation with the DNP group of the analytes in resolving N-(3,5-dinitrobenzoyl)-α-alkylamino alkyl esters or N-(3,5-dinitrobenzoyl)-α-arylalkylamines, respectively. However, we had some difficulty in clearly portraying three-dimensional structures of the chiral recognition models in two-dimensional representations. Therefore, some parts of the chiral recognition models shown in Figs. 3 and 6 are exaggerated or distorted and readers who wish to see clear three-dimensional structures of the molecular models shown in Figs. 3 and 6 are advised to use CPK molecular models. Finally, we should mention that the chiral recognition models shown in Figs. 3 and 6 might be modified or improved as more spectroscopic and/or crystallographic data for the diastereomeric complex formed between the chiral selector molecule of the CSP and the analyte molecule are collected.

Acknowledgements

This work was supported by grants from the Organic Chemistry Research Centre sponsored by the Korea Science and Engineering Foundation and from the Basic Science Research Program (BSRI-94-3410).

References

[1] W.H. De Camp, in W.J. Lough (Editor), *Chiral Liquid Chromatography*, Blackie, Glasgow, 1989, Ch. 2, p. 14.
[2] S.C. Stinson, *Chem. Engi. News*, September 27 (1993) 38.
[3] S.C. Stinson, *Chem. Engi. News*, September 19 (1994) 38.
[4] S. Ahuja, in S. Ahuja (Editor), *Chiral Separations by Liquid Chromatography* (*ACS Symposium Series*, No. 471), American Chemical Society, Washington, DC, 1991, Ch. 1, p. 1.
[5] S.R. Perrin and W.H. Pirkle, in S. Ahuja (Editor), *Chiral Separations by Liquid Chromatography* (*ACS Symposium Series*, No. 471), American Chemical Society, Washington, DC, 1991, Ch. 3, p. 43.
[6] W.H. Pirkle and T.C. Pochapsky, *Chem. Rev.*, 89 (1989) 347.
[7] M.H. Hyun and W.H. Pirkle, *J. Chromatogr.*, 393 (1987) 357.
[8] M.H. Hyun and M.H. Kim, *J. Liq. Chromatogr.*, 13 (1990) 3229.
[9] T.D. Doyle, C.A. Brunner and E. Smith, *US Pat.*, 4 919 803 (1990).
[10] L. Oliveros, C. Mingullon, B. Desmazieres and P.-L. Desbene, *J. Chromatogr.*, 589 (1992) 53.
[11] W.H. Pirkle, C.J. Welch and B. Lamm, *J. Org. Chem.*, 57 (1992) 3854.
[12] W.H. Pirkle, P.L. Spence, B. Lamm and C.J. Welch, *J. Chromatogr., A*, 659 (1994) 69.
[13] M.H. Hyun, S.-Y. Hwang and J.-J. Ryoo, *Chem. Lett.*, (1994) 1021.
[14] M.H. Hyun, J.S. Jin, J.-J. Ryoo and K.K. Jyung, *Bull. Korean Chem. Soc.*, 15 (1994) 497.
[15] D.A. Nicoll-Griffith, *J. Chromatogr.*, 402 (1987) 179.
[16] W.H. Pirkle and J.M. Finn, *J. Org. Chem.*, 46 (1981) 2935.
[17] M.H. Hyun, I.-K. Baik and W.H. Pirkle, *J. Liq. Chromatogr.*, 11 (1988) 1249.
[18] W.H. Pirkle, P.G. Murray and J.A. Burke, *J. Chromatogr.*, 641 (1993) 21.
[19] M.H. Hyun, S.M. Cho, J.-J. Ryoo and M.S. Kim, *J. Liq. Chromatogr.*, 17 (1994) 317.
[20] W.H. Pirkle, M.H. Hyun and B. Bank, *J. Chromatogr.*, 316 (1984) 585.

ELSEVIER

Journal of Chromatography A, 696 (1995) 185–192

JOURNAL OF CHROMATOGRAPHY A

Effect of sodium dodecyl sulfate as stationary phase on signal intensities of dansylamino acids in microcolumn liquid chromatography with on-column fluorimetric detection

Toyohide Takeuchi*, Tomoo Miwa

Faculty of Engineering, Gifu University, 1-1 Yanagido, Gifu 501-11, Japan

First received 18 October 1994; revised manuscript received 20 December 1994; accepted 20 December 1994

Abstract

The effects of stationary phase and mobile phase additive on fluorescence signal intensities of dansylamino acids were examined in microcolumn liquid chromatography. Sodium dodecyl sulfate (SDS), employed as the mobile phase additive, was dynamically introduced into an anion exchanger, and it worked as a stationary phase in the reversed-phase mode. Signal enhancement was achieved by on-column fluorimetric detection owing to the focusing and environmental effects of the SDS stationary phase.

1. Introduction

Armstrong et al. [1] reported the first known example of micellar enhanced fluorescence detection in liquid chromatography (LC). They demonstrated the separation of aromatic hydrocarbons with a micellar mobile phase, and the benefits of micellar enhanced fluorescence detection in LC were discussed. In spite of the promising features of micellar mobile phases, it seems that there have been few papers that appreciate fluorescence enhancement generated by micelles in LC.

The use of various micellar systems in spectrofluorimetric methods for the determination of dansyl (Dns)-amino acids, drugs and other compounds has been assessed [2–5]. It was shown that fluorescence enhancement due to micelles with factors varying from 8 to 20 was achieved for dansylamino acids in comparison with that in water alone, leading to an improvement in sensitivity [2].

On-column detection, defined as the case when analytes are detected in the presence of a stationary phase, provides increased sensitivity by a factor of $1 + k'$ compared with common detection in the absence of the stationary phase, where k' is the capacity factor of the analyte [6,7]. This is due to the focusing effect of the stationary phase. Takeuchi and Yeung [8] reported a signal enhancement due to both the focusing and environmental effects of the stationary phase in on-column fluorimetric detection in open-tubular capillary LC with an octylmethylsiloxane stationary phase. We [9] reported a signal enhancement of dansylamino acids by on-column fluorimetric detection using cyclodextrin-bonded stationary phases, in which fluorescence enhancement by inclusion complexation into cyclodextrin was demonstrated.

* Corresponding author.

0021-9673/95/$09.50
SSDI 0021-9673(94)01282-2

It is frequently observed in LC that the pH, polarity and temperature of the mobile phase dramatically affect the position of the maximum emission wavelength and emission intensity [10]. Intensity changes of an order of magnitude and large wavelength shifts are sometimes found for molecules that can undergo strong solvent interactions [10]. Therefore, on-column fluorimetric detection is expected to accompany a dramatic effect in both the position of the maximum emission wavelength and emission intensity because analytes interact with the stationary phase when they are detected in the presence of the stationary phase.

It is expected that the on-column detection of dansylamino acids in the presence of micelles in the mobile phase can result in better sensitivity because the signal can be enhanced by both the micellar mobile phase and the focusing and environmental effects of the stationary phase.

This paper describes the effects of sodium dodecyl sulfate (SDS) as the stationary phase and mobile phase additive on the fluorescence intensity of dansylamino acids in LC.

2. Experimental

2.1. Apparatus

A microcolumn liquid chromatograph was assembled from an MF-2 microfeeder (Azumadenki Kogyo, Tokyo, Japan) equipped with a 0.5-ml MS-GAN 050 gas-tight syringe (Ito, Fuji, Japan) as a pump, an ML-522 microvalve injector with an injection volume of 0.11 μl (Jasco, Tokyo, Japan), a 150 × 0.35 mm I.D. microcolumn, an 820-FP fluorimetric detector (Jasco) with a laboratory-made flow cell and a Chromatopac C-R4AX data processor (Shimadzu, Kyoto, Japan). The empty and packed flow cells were prepared from fused-silica tubing of 0.32 mm I.D. (GL Science, Tokyo, Japan) as reported previously [11].

A U-330 bandpass filter (Jasco) was attached to the packed flow cell to prevent the second-order light from reaching the flow cell, and an L-39 cut-off filter (Jasco) was employed to prevent the scattered light from reaching the photomultiplier of the detector. Collection of scattered light for the empty flow cell was simply reduced by tilting the flow cell by ca. 30° [11]. The lengths of the flow cell tubes irradiated by the exciting light were 1.6 and 2.1 mm for the packed and empty flow cells, respectively. The wavelength of excitation was 335 nm. The time constant of the fluorimetric detector was kept at 3.5 s. Fluorescence spectra were also obtained with a model 820-FP fluorimetric detector.

The microcolumn was prepared from fused-silica tubing of 0.35 mm I.D. (GL Science) as reported previously [12], and 5-μm TSKgel IC-Anion SW anion exchanger (Tosoh, Tokyo, Japan) or 5-μm Develosil ODS-5 octadecyl-bonded silica gel (Nomura Chemical, Seto, Japan) was employed as the packing. The flow-rate of the eluent was 2.8 μl min^{-1}. Experiments were carried out at room temperature (ca. 25–30°C).

SDS was introduced dynamically into the anion exchanger by passing aqueous acetonitrile solution (50%, v/v) containing 40–100 m*M* SDS for ca. 1 h at 2.8 μl min^{-1}, followed by conditioning with the mobile phase employed.

2.2. Reagents

Guaranteed reagent-grade solvents and reagents were obtained from Nacalai Tesque (Kyoto, Japan), unless indicated otherwise. These reagents were employed as received. Dansyl derivatives of L-amino acids were purchased from Sigma (St. Louis, MO, USA). Distilled water was of HPLC grade (Nacalai Tesque). Eluents were prepared from the distilled water, acetonitrile, ammonium acetate and SDS.

3. Results and discussion

3.1. Fluorescence enhancement of dansylamino acids by SDS

Fluorescence enhancement was measured by using the 820-FP fluorimetric detector with a flow cell for conventional LC. Table 1 compares the wavelengths that give maximum fluorescence

Table 1
Fluorescence enhancement of Dns-L-amino acids on addition of SDS

Dns-L amino acid	λ_{max}(nm)		Enhancement factor
	Without SDS	With SDS	
αAB[a]	539	531	2.44
Ala	539	533	2.16
Arg[b]	539	527	3.88
Asn	541	533	2.05
Asp	541	539	1.08
Cysteic acid	539	539	1.11
Gln	539	533	2.08
Glu	540	540	1.08
Ile	539	529	3.22
Leu	539	529	3.12
Met	541	532	2.65
NVal	538	529	3.01
Phe	541	531	3.51
Pro	542	533	3.46
Ser	543	535	2.11
Thr[c]	539	535	2.03
Trp[d]	540	531	3.45
Val	539	531	2.65

Analyte solution: 40 μ*M* Dns-L-amino acid dissolved in 40 m*M* ammonium acetate containing 0.8% (v/v) acetonitrile with (pH 6.90) or without 100 m*M* SDS (pH 6.93). Excitation wavelength, 335 nm.
[a] Dansyl-L-α-aminobutyric acid.
[b] α-Dansyl-L-arginine.
[c] N-Dansyl-L-threonine.
[d] N^{α}-Dansyl-L-tryptophan.

intensity and the enhancement factors, defined as the ratio of the fluorescence intensity observed in the presence of SDS to that without SDS. The analyte solution prepared was 40 μ*M* Dns-L-amino acids dissolved in 40 m*M* ammonium acetate containing 0.8% acetonitrile with or without 100 m*M* SDS. The pH of the matrix solution was ca. 6.9. It was found that the largest enhancement factor was achieved for Dns-L-Arg, i.e., 3.88. Enhancement factors between 2 and 3.5 were observed for neutral and basic amino acids, whereas almost no enhancement was observed for acidic amino acids. This may be because SDS is anionic so that the acidic amino acids undergo electrostatic repulsion from the SDS micelle. In addition, the wavelength giving the maximum fluorescence intensity was slightly shifted to shorter wavelengths on addition of SDS. The larger the signal enhancement, the larger was the wavelength shift observed. The largest wavelength shift was observed for Dns-L-Arg, i.e., 12 nm.

3.2. Effect of concentration of acetonitrile and SDS

The enhancement factor was strongly affected by the acetonitrile concentration. Fig. 1 shows the effect of acetonitrile concentration on the signal intensity and the signal enhancement of Dns-L-Phe. The analyte was dissolved in aqueous acetonitrile containing 40 m*M* ammonium acetate (pH 6.9–7.5). In the absence of SDS, the signal intensity increased with increasing acetonitrile concentration. This phenomenon probably results because water quenches the fluorescence of dansylamino acids [13]. On the other hand, when SDS micelles are present in the solution, both the SDS micelles and the solvent effect due to acetonitrile contribute to the fluorescence

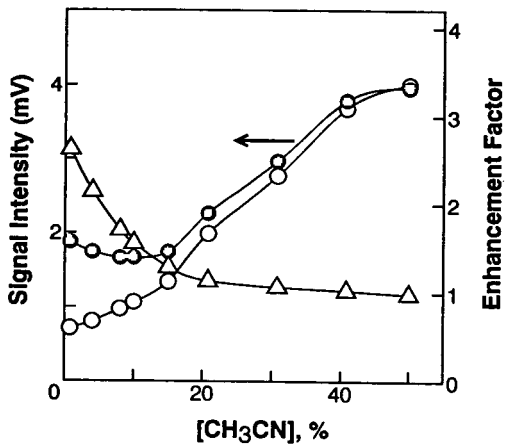

Fig. 1. Effect of acetonitrile concentration on signal intensity and signal enhancement. Analyte solutions, 40 μM Dns-L-Phe dissolved in aqueous acetonitrile in 40 mM ammonium acetate with or without 40 mM SDS (pH 6.9–7.5); excitation wavelength, 335 nm; ● and ○ refer to the signal intensity observed with or without 100 mM SDS, respectively, and △ refers to the signal enhancement.

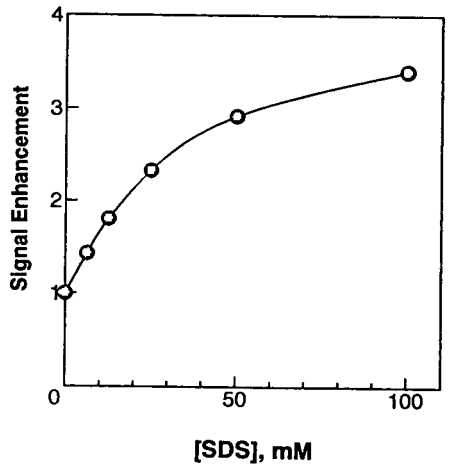

Fig. 2. Signal enhancement as a function of SDS concentration. Solutions, 40 μM Dns-L-Phe dissolved in 0.8% (v/v) acetonitrile containing 40 mM ammonium acetate and SDS as indicated (pH 6.90–6.93); excitation wavelength, 335 nm.

enhancement of dansylamino acids. With increasing acetonitrile concentration, the contribution of the solvent effect due to acetonitrile increases, whereas the signal enhancement due to SDS decreases at higher acetonitrile concentrations. The signal enhancement factor, therefore, decreases with increasing acetonitrile concentration and reaches almost unity at ca. 20% (v/v). In addition, the critical micelle concentration of SDS in water is 8.3 mM, whereas that in 20% acetonitrile solution was estimated to be ca. 30 mM from the measurement of its electrical conductivity.

The signal intensity is expected to increase with increasing SDS concentration. Fig. 2 illustrates the enhancement factor of Dns-L-Phe as a function of SDS concentration at an acetonitrile concentration of 0.8% (v/v). It is found that the enhancement factor increases with increasing SDS concentration. Lower enhancement factors were observed at higher acetonitrile concentrations. These results indicate that only a small signal enhancement of dansylamino acids can be expected when SDS is employed as the mobile phase additive.

3.3. On-column fluorimetric detection of dansylamino acids

In this work, "on-column detection" indicates the case when the analytes are detected in the presence of a stationary phase. On the other hand, when the analytes are detected in the absence of a stationary phase, the term "post-column detection" is utilized. Fig. 3 demonstrates the on-column and post-column fluorimetric detection of Dns-L-amino acids using an anion-exchange column dynamically modified with SDS, in which 0.11 μl of the sample solution containing 0.2 mM of each analyte is injected and the excitation wavelength is 335 nm. The noise levels observed for both detection methods were nearly the same, and better sensitivity was achieved with the on-column detection. Mass detection limits of the analytes at a signal-to-noise ratio of 3 achieved by on-column detection under the conditions in Fig. 3 were 60–130 fmol, which were 5–40 times lower than those achieved by the post-column detection. In addition, SDS micelles are not present in the mobile phase under the conditions in Fig. 3. Laser-based fluorimetric detection will further improve the detection limits.

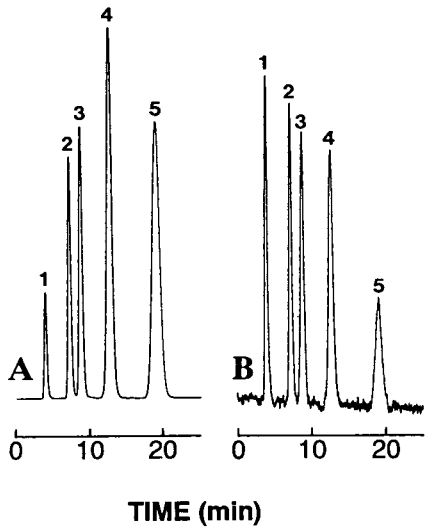

Fig. 3. (A) On-column and (B) post-column fluorimetric detection of dansylamino acids. Column, 150 × 0.35 mm I.D., packed with TSKgel IC-Anion SW; eluent, 15% (v/v) acetonitrile in 40 m*M* ammonium acetate and 5 m*M* SDS (pH 7.07); flow-rate, 2.8 μl min^{-1}; excitation wavelength, 335 nm; emission wavelength, 535 nm; sample, 0.2 m*M* each of dansyl derivatives of (1) L-Glu, (2) L-Ala, (3) L-Val, (4) L-Leu and (5) L-Phe; injection volume, 0.11 μl.

The retention time of the analytes was affected by the concentration of acetonitrile and SDS. When the eluent contained no SDS, the analytes could not be eluted in a reasonable time because SDS introduced into the anion exchanger were gradually eluted from the stationary phase, leading to exposure of bare ion-exchange sites.

Reproducibilities of the retention time, peak height and peak area for on-column detection were calculated for five successive measurements under the same conditions except for the SDS concentration (40 m*M*) as in Fig. 3. The relative standard deviations of the retention time, peak height and peak area were 0.3–0.5, 2.3–3.3 and 2.8–4.0%, respectively.

Takeuchi and Yeung [8] derived an equation that allows the estimation of the environmental effect of the stationary phase by measuring peak heights of analyte solutes as follows:

$$\frac{h_{oi}}{h_{pi}} = \frac{\alpha_o \varepsilon_o I_{om}}{\alpha_p \varepsilon_p I_p} \cdot \left(k_i' \cdot \frac{\varphi_{osi}}{\varphi_{pi}} + 1 \right) \quad (1)$$

where subscripts o, p, s, m and *i* denote on-column detection, post-column detection, the stationary phase, the mobile phase and the analyte component *i*, *h* is peak height, α is a constant, ε is the collection efficiency of fluorescence, *I* is the light intensity, k' is the capacity factor of the analyte and, φ is a factor accounting for the quantum efficiency, selectivity, absorptivity, energy transfer, etc.

The $\varphi_{osi}/\varphi_{pi}$ value represents the environmental effect of the stationary phase. When the value is larger than unity, signal enhancement due to the environmental effect of the stationary phase exists, whereas when it is equal to unity, the focusing effect only contributes to the signal enhancement. On the other hand, when $\varphi_{osi}/\varphi_{pi}$ is smaller than unity, the stationary phase quenches the fluorescence.

When analytes *i* and *j* are detected in a single chromatographic run, Eq. 1, is valid for the component *j*:

$$\frac{h_{oj}}{h_{pj}} = \frac{\alpha_0 \varepsilon_o I_{om}}{\alpha_p \varepsilon_p I_p} \cdot \left(k_j' \cdot \frac{\varphi_{osj}}{\varphi_{pj}} + 1 \right) \quad (2)$$

The ratio of Eq. 1 to Eq. 2 is given by the following equation:

$$\left(\frac{h_{oi}}{h_{pi}}\right) \Big/ \left(\frac{h_{oj}}{h_{pj}}\right) = \left(k_i' \cdot \frac{\varphi_{osi}}{\varphi_{pi}} + 1 \right) \cdot \left(k_j' \cdot \frac{\varphi_{osj}}{\varphi_{pj}} + 1 \right) \quad (3)$$

When k_j' is zero or $\varphi_{osj}/\varphi_{pj}$ is known, $\varphi_{osi}/\varphi_{pi}$ is calculated from the peak-height ratios and the capacity factors of the analytes.

Figs. 4 and 5 illustrate the relationships between the peak height and the capacity factor of the analytes for post-column and on-column detection, respectively, where eluents with different acetronitrile concentrations are employed. With post-column detection, the peak height of the analytes decreases with increasing capacity factor, whereas the dependence of the peak height on the capacity factor is not obviously recognized in on-column detection. In addition, nearly the same levels of baseline noise were observed for both detection methods, indicating that the sensitivity is improved by on-column detection.

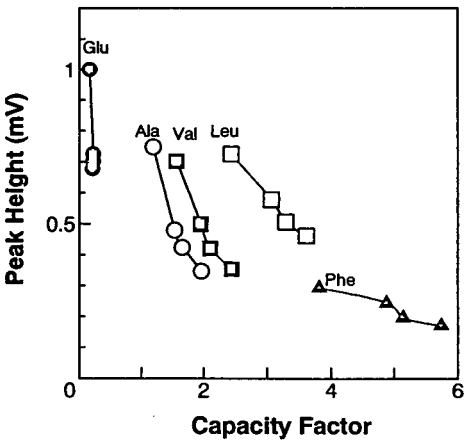

Fig. 4. Relationship between peak height and capacity factor in post-column fluorimetric detection. Mobile phase, 5–15% (v/v) acetonitrile in 40 m*M* ammonium acetate and 40 m*M* SDS (pH 6.98–7.07); other operating conditions as in Fig. 3B.

The ratio of the peak height achieved by on-column detection to that achieved by post-column detection is plotted as a function of the capacity factor in Fig. 6. It is found that the peak-height ratio increases with increasing capacity factor and the on-column detection

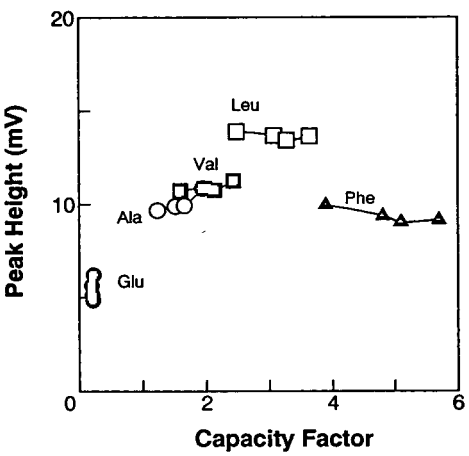

Fig. 5. Relationship between peak height and capacity factor in on-column fluorimetric detection. Mobile phase, 5–15% (v/v) acetonitrile in 40 m*M* ammonium acetate and 40 m*M* SDS (pH 6.98–7.07); other operating conditions as in Fig. 3A.

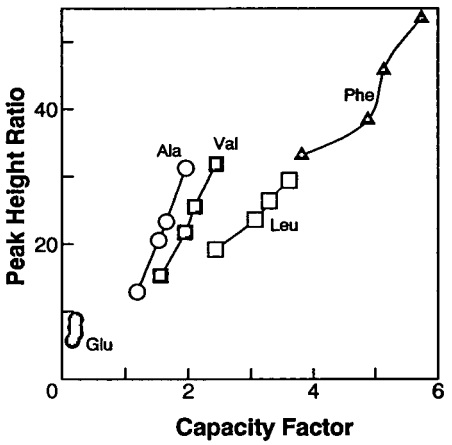

Fig. 6. Ratio of peak height observed in on-column detection to that in post-column detection as a function of capacity factor. Operating conditions as in Figs. 4 and 5.

improves the detection limits by a factor of 5.6–54 under the conditions in Fig. 6.

The concentration of SDS in the mobile phase also affected the retention time of the analytes. The capacity factor decreased slightly with increasing SDS concentration, e.g., the capacity factor of Dns-L-Phe was 5.44 for 5 m*M* SDS and 3.86 for 40 m*M* SDS when aqueous acetonitrile solution (15%, v/v) containing 40 m*M* ammonium acetate was used as the mobile phase. In addition, the peak heights achieved by on-column detection were almost constant, irrespective of the SDS concentration in the region 5–40 m*M*.

Fig. 7 illustrates the fluorescence intensity and signal enhancement for Dns-L-Glu as a function of acetonitrile concentration. It is found that the signal enhancement is not significant and is almost independent of the acetonitrile concentration. This may be because Glu is an acidic amino acid, and its net negative charge makes it difficult to interact with the anionic detergent.

By assuming that $\varphi_{osi}/\varphi_{pi}$ for Dns-L-Glu is unity, $\varphi_{osi}/\varphi_{pi}$ values for other dansylamino acids can be calculated. Table 2 lists the $\varphi_{osi}/\varphi_{pi}$ values under different mobile phase conditions. The mobile phase contained SDS micelles under the conditions in Table 2, and the micelle concentration increased with decreasing acetonitrile

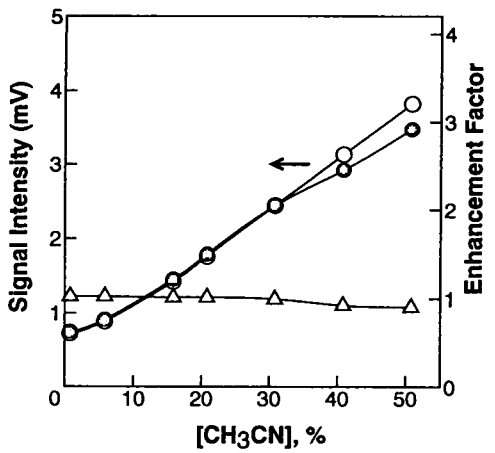

Fig. 7. Fluorescence intensity and signal enhancement for Dns-L-Glu as a function of acetonitrile concentration. Analyte solutions, 40 μM Dns-L-Phe dissolved in aqueous acetonitrile in 40 mM ammonium acetate with or without 40 mM SDS (pH 6.9–7.5); excitation wavelength, 335 nm; ● and ○ refer to the signal intensity observed with or without 40 mM SDS, respectively, and △ refers to the signal enhancement.

concentration. $\varphi_{osi}/\varphi_{pi}$ values smaller than unity were observed for Dns-L-Leu at lower acetonitrile concentrations, indicating that the φ value of Dns-L-Leu in the mobile phase is larger than that in the stationary phase. On the other hand, the largest $\varphi_{osi}/\varphi_{pi}$ values were observed at 10% acetonitrile for Dns-L-Ala and Dns-L-Val.

When octadecyldimethylsilyl-bonded silica (ODS) and an ammonium acetate solution of acetonitrile without SDS were used as the stationary and mobile phase, respectively, $\varphi_{osi}/\varphi_{pi}$ was 2.3–2.4 for dansyl derivatives of Ala, Val, Leu and Phe, indicating that ODS also enhances the fluorescence of the dansylamino acids [14]. Considering these results, there is no evidence supporting the existence of micellar or aggregates of SDS on the stationary phase. In other words, SDS micelles may be present only in the mobile phase even when the SDS concentration is higher than its critical micelle concentration. In addition, the length of alkyl group, the type of modifier and variations in charge on the micelle reagents may affect the fluorescence enhancement. These effects are being investigated.

4. Conclusions

On-column fluorimetric detection with the stationary phase dynamically modified with SDS improved the detection limits of dansylamino acids. The environmental effects of the stationary phase were estimated from the peak heights. Laser-based on-column fluorimetric detection will further improve the detection limits.

Acknowledgement

The authors thank Dr. Kiyokatsu Hibi, Jasco, for his kind gifts of cut-off and band-pass filters employed in this work.

References

[1] D.W. Armstrong, W.L. Hinze, K.H. Bui and H.N. Singh, *Anal. Lett.*, 14 (1981) 1659.

Table 2
Environmental effect ($\varphi_{osi}/\varphi_{pi}$) of SDS stationary phase

Acetontrile (%)	$\varphi_{osi}/\varphi_{pi}$				
	Glu	Ala	Val	Leu	Phe
15	1	1.38	1.38	1.21	1.53
10	1	1.80	1.52	1.08	1.23
8	1	1.66	1.47	0.98	1.23
5	1	1.69	1.39	0.85	1.11

Operating conditions as in Fig. 4 except for the mobile phase: 5–15% acetonitrile containing 40 mM SDS and 40 mM ammonium acetate (pH 7.0–7.1).

[2] H.N. Singh and W.L. Hinze, *Analyst*, 107 (1982) 1073.
[3] O. Jules, S. Scypinski and L.J. Cline Love, *Anal. Chim. Acta*, 169 (1985) 355.
[4] G. Patonay, M.E. Rollie and I.M. Warner, *Anal. Chem.*, 57 (1985) 569.
[5] H. Singh and W.L. Hinze, *Anal. Lett.*, 15 (1982) 221.
[6] E.J. Guthrie and J.W. Jorgenson, *Anal. Chem.*, 56 (1984) 483.
[7] T. Takeuchi and D. Ishii, *J. Chromatogr.*, 435 (1988) 319.
[8] T. Takeuchi and E.S. Yeung, *J. Chromatogr.*, 389 (1987) 3.
[9] T. Takeuchi and T. Miwa, *Chromatographia*, 38 (1994) 555.
[10] C.F. Pool and S.K. Pool, *Chromatography Today*, Elsevier, Amsterdam, 1991, pp. 573–586.
[11] T. Takeuchi, T. Asano and D. Ishii, *J. Chromatogr.*, 471 (1989) 297.
[12] T. Takeuchi and D. Ishii, *J. Chromatogr.*, 213 (1981) 25.
[13] M. Hoshino, M. Imamura, K. Ikehara and Y. Hama, *J. Phys. Chem.*, 85 (1981) 1820.
[14] T. Takeuchi and T. Miwa, , in preparation.

ELSEVIER

Journal of Chromatography A, 696 (1995) 193–199

JOURNAL OF CHROMATOGRAPHY A

Normal-phase high-performance liquid chromatography with relay gradient elution
I. Description of the method

Laszlo R. Treiber

Department of Microbial Chemotherapeutics and Molecular Genetics, Merck & Co., Inc., RY80Y-200, Rahway, NJ 07065, USA

First received 15 December 1994; revised manuscript received 3 January 1995; accepted 16 January 1995

Abstract

The utility of normal-phase HPLC with relay gradient elution covering the entire practical range of polarity from hexane through water is demonstrated. The separations have been carried out on a LiChrospher 100 Diol column. Analytes without appreciable UV absorbance have been detected by means of an evaporative light-scattering detector. The method presented is suitable for the classification of sample components according to their polarity. The potential utility of the technique in programs such as profiling, classification and screening of biological materials, metabolic studies and preparative-scale isolation is discussed.

1. Introduction

Although reversed-phase methods account for the majority of HPLC applications [1], recent developments indicate increasing interest in normal-phase separations. Reversed-phase and normal-phase HPLC frequently find applications for compounds in the range of non-polar to medium polarity. More recently, encouraging results have been reported in the application of normal-phase HPLC for the separation of some very polar compounds. A number of common carbohydrates have been successfully resolved [2] on a LiChrospher Diol column with an acetonitrile–water gradient. The resolution of proteins, peptides, oligonucleotides, carbohydrates, phosphorylated amino acids and underivatized amino acids by means of "hydrophilic-interaction" chromatography on a PolyHydroxyethyl A column [3] has been reported. Several amino acids have also been resolved by means of subcritical fluid chromatography on LiChrospher CN and LiChrospher Diol columns with CO_2 modified with methanol, water, triethylamine and pyridine as mobile phase [4]. An early report [5] presents the theoretical aspects of "incremental gradient elution" capable of resolving mixtures of analytes covering a wide range of polarity. The method has been experimentally demonstrated using a column packed with Bio-Sil A silica gel and a series of twelve solvents to cover the polarity range from *n*-heptane to water in a run stretching over 7 h.

The properties of the common polar bonded-phase columns [6] and highly purified porous silica microspheres [7] have been extensively

0021-9673/95/$09.50
SSDI 0021-9673(95)00070-4

studied and reported. The consistent performance of polar bonded-phase columns well documented for specific separations of compounds throughout a wide polarity range prompted the investigation to determine the possibility of their use in programs such as profiling, classification and screening of biological materials, metabolic studies and preparative-scale isolation. The present study describes a dynamic concept of chromatographic isolation based on normal-phase HPLC method with relay gradient elution suitable for sample constituents covering the entire practical polarity range from extremely non-polar lipophilic compounds through inorganic cations.

2. Experimental

2.1. Instrumentation and methodology

Reversed-phase separation of choline and acetylcholine has been carried out on a Shandon Hypercarb S (150 × 4.6 mm) column (Shandon Scientific, Cheshire, UK). The adsorbent in this column is graphitised carbon. Rainin Microsorb MV C_{18} column (3 μm, 50 × 4.6 mm; Rainin, Woburn, MA, USA) has been used as pre-column.

Normal-phase separations have been performed on an E. Merck LiChrospher 100 Diol column (5 μm, 250 × 4 mm; EM Separations, Gibbstown, NJ, USA) with a modular HPLC instrument consisting of an HP-1050 quaternary solvent-delivery system, an HP 3390A integrator (both from Hewlett-Packard, San Fernando, CA, USA) and a Sédex 55 evaporative light-scattering detection (ELSD) system (Sédéré, Alfortville, France). The resolution of choline, acetylcholine and some inorganic cations by means of normal-phase chromatography has been the specific application in the extremely polar region studied in detail. The results have been obtained by means of binary gradient. For general applications covering the widest polarity range, the mobile phase is designed as a series of consecutive gradients, or relay gradient. The simplest relay gradient is starting with a program from hexane (A) to EtOAc (B) and continuing from EtOAc (B) to 0.1% HCOOH in acetonitrile (C) and finishing from 0.1% HCOOH in acetonitrile (C) to 0.1% HCOOH in water (D). All sequences are linear gradients starting with 100% of the less polar component and changing to 100% of the more polar component. Preconditioning of the column for the next run is carried out by sequential washing the column with the pure solvents in the reverse order going stepwise from the more polar to the less polar solvent. Typically, depending on the solvent, washing for 5–12 min is required. The preconditioning procedure necessary for the column between runs has been empirically determined and is, with additional details of the experimental conditions, provided together with the illustrations in the Results and discussion section below.

2.2. Solvents and chemicals

All chromatographic solvents have been purchased from EM Science (Gibbstown, NJ, USA) and are of OmniSolv quality. Inorganic salts have also been purchased from the same source. Other chemicals have been purchased from Aldrich (Milwaukee, WI, USA) and Sigma (St. Louis, MO, USA). The sample solutions used for reversed-phase chromatography have been dissolved in water. Samples for normal-phase chromatography have been dissolved in *n*-propanol or dimethylformamide both containing 20% of water. The amounts injected have been in the range of 1.5–6 μg per component.

3. Results and discussion

There is ample selection of reversed-phase and normal-phase HPLC methods published in the literature for the separation of compounds of low to medium polarity. Finding generally applicable separation methods for compounds in the polar to extremely polar range has historically been a more difficult problem. It is fair to assume that once a satisfactory general procedure for separating polar classes of compounds had been found, the extension of the method to the

medium to non-polar range would be relatively simple. Ion-exchange chromatography can be ruled out as a general method due to the inherent specificity of resins. The performance of reversed-phase media have limitations particularly in the extremely polar region. The limitations are not only resolution-related. While choline and acetylcholine are completely resolved on a Shandon Hypercarb S column (Fig. 1), the method cannot be used routinely for samples also containing much less polar compounds due to demanding column clean-up procedures specified by Shandon Scientific. The retention of non-polar organic molecules on activated carbon is so strong that column performance can be lost after only a few injections of real (e.g. biological) samples.

On the LiChrospher 100 Diol column, not only is the resolution of acetylcholine and choline complete, but some common inorganic cations are also fully resolved (Fig. 2). This quite remarkable normal-phase column performance in the extremely polar region has never been demonstrated with any reversed-phase system. As a matter of fact, the dynamic range presented here cannot be matched by all known reversed-phase systems combined. It is not surprising at all that the elution profile of the same cations is drastically changing when trifluoroacetic acid (TFA) is substituted with HCOOH (Fig. 3). The characteristics of the counter ion greatly influence the polarity of the ion pair. The non-polar TFA facilitates the elution of cations at much lower water content of the mobile phase and with better resolution than the highly polar

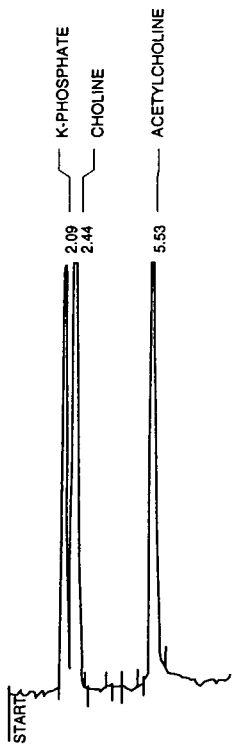

Fig. 1. Separation on a Shandon Hypercarb S column (150 × 4.6 mm) with Rainin Microsorb MV C_{18} column (3 μm, 50 × 4.6 mm) as precolumn. Mobile phase: 0.2% TFA in water. Flow-rate: 0.9 ml/min. In all figures, the numbers at the peaks indicate retention times in min.

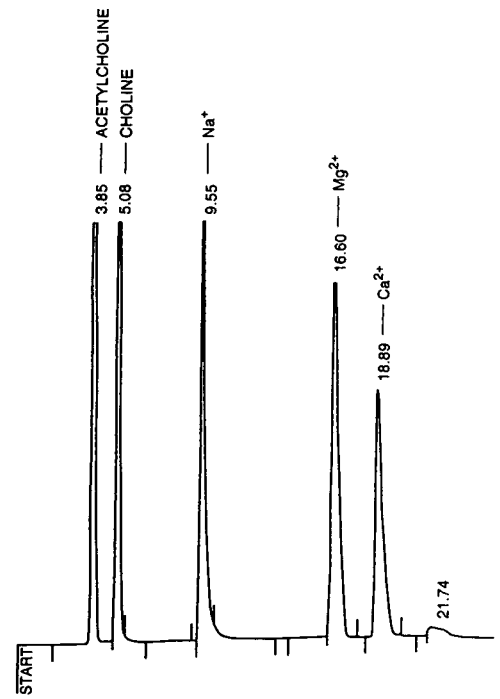

Fig. 2. Separation on an E. Merck LiChrospher 100 Diol column (5 μm, 250 × 4 mm). Gradient elution with solvents 0.1% TFA in MeCN (A) and 0.1% TFA in water (B). The gradient program is as follows: 0–1 min: 10% B; 1–18 min: 10→30% B; 18–20 min: 30→100% B; 20–24.5 min: 100% B. Flow-rate: 0.9 ml/min.

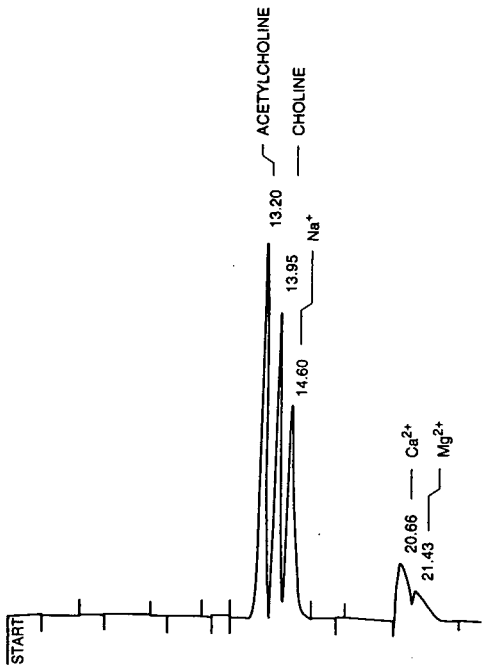

Fig. 3. Separation on the same column as in Fig. 2. Gradient elution with solvents 0.1% HCOOH in MeCN (A) and 0.1% HCOOH in water (B). The gradient program is as follows: 0–1 min: 20% B; 1–15 min: 20→100% B; 15–24.5 min: 100% B. Flow-rate: 0.9 ml/min.

HCOOH does. However, for a general method designed to classify compounds according to their polarity, HCOOH-containing mobile phases are found more suitable than their TFA-containing counterparts. Although the resolution for cationic species is sacrificed to some extent, the relative polarities of the sample components are more realistically represented when the inherent polarity of cations is not suppressed by using a non-polar counter ion. A classification procedure designed with a broad scope in mind necessitates such a sacrifice. This allows the cations to be pushed beyond other polar classes of organic compounds such as carbohydrates and amino acids. Even the most polar quaternary ammonium compounds are still being eluted before the inorganic cations. All cations discussed here were used in the chloride form. During the chromatographic run, Cl^- is displaced by the $HCOO^-$ anion. Cl^- and many other common organic and inorganic anions form volatile acids when protonated and are not detected by ELSD under the conditions used here. Therefore, the separation of anions will be discussed in a separate report.

A mixture of arbitrarily selected solutes used as polarity markers allows the classification of the components of actual samples according to their polarity. A chromatogram of a test mixture obtained by means of a simple relay gradient elution illustrates the wide dynamic range of the method (Fig. 4). The origin of some minor peaks (e.g. at 10.66, 40.44 and 49.65 min) is currently unknown. It may be the result of incomplete equilibria between the stationary and the mobile phases, limited solubility in the mobile phase, etc. Minor peaks are partially eliminated by overlapping the EtOAc to acetonitrile and acetonitrile to aqueous cycles (Fig. 5). This modi-

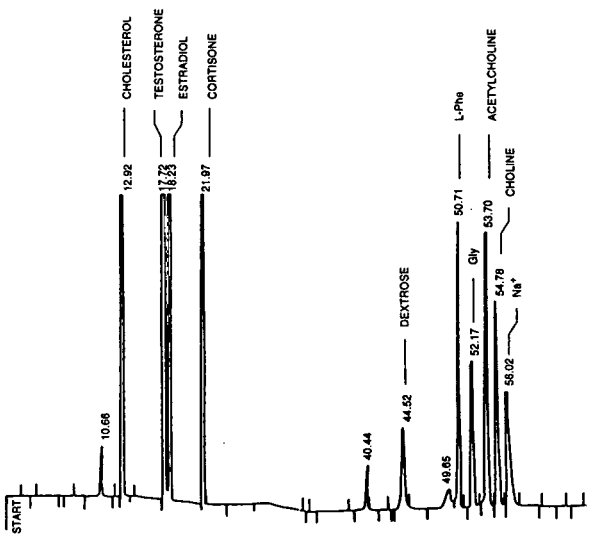

Fig. 4. Separation on the same column as Fig. 2. Relay gradient elution with solvents hexane (A), EtOAc (B), 0.1% HCOOH in MeCN (C) and 0.1% HCOOH in water (D). The gradient program is as follows: 0–5 min: 100% A; 5–20 min: 100→0% A and 0→100% B, 0% C and D; 20–25 min: 100% B; 25–30 min: 100→0% B and 0→100% C, 0% A and D; 30–35 min: 100% C; 35–60 min: 100→0% C and 0→100% D, 0% A and B; 60–65 min: 100% D.

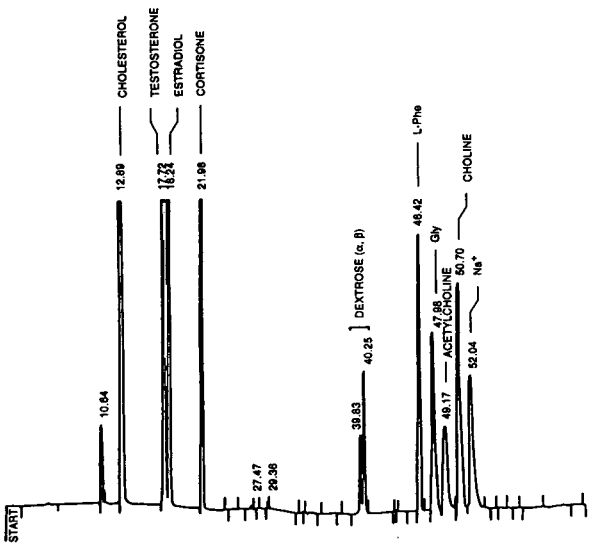

Fig. 5. Separation on the same column as Fig. 2. Relay gradient elution with solvents hexane (A), EtOAc (B), 0.1% HCOOH in MeCN (C) and 0.1% HCOOH in water (D). The gradient program is as follows: 0–5 min: 100% A; 5–20 min: 100→0% A and 0→100% B, 0% C and D; 20–25 min: 100% B; 25–30 min: 100→10% B, 0→80% C, 0→10% D, 0% A; 30–35 min: 10→0% B, 80% C, 10→20% D, 0% A; 35–60 min: 80→0% C, 20→100% D, 0% A and B; 60–65 min: 100% D.

fication also resulted in the resolution of dextrose to its α and β anomers previously accomplished on a Nucleosil OH column (Macherey–Nagel) [2].

The reliability of the method is understandably an important concern. The most relevant measure of reliability in this case being a separation method is the reproducibility of retention times. The prerequisite to acceptable reproducibility of retention times is obviously strict control over the key parameters such as the condition of the column, the quality of the solvents and the accuracy of the gradient program. While some parameters are mostly dependent on the instrumentation chosen, the development of a suitable gradient program and the restoration of the column to a standardized starting condition are completely the operator's responsibility. Assuming that the stationary phase is sufficiently stable, its initial condition at the beginning of a run depends on the pre-equilibration of the column. This is particularly true when following 0.1% aqueous HCOOH as mobile phase, the column has to be prepared for hexane as the initial eluent. For obtaining reproducible retention times, the pre-equilibration consists of washing with MeCN, EtOAc and hexane, in that order, for 10, 5 and 12 min, respectively. Changing the duration of the wash cycles results in predictable changes of the retention times. Shorter wash cycles may cause insufficient displacement of residues of polar solvents from the column leading to significantly shorter retention times and poor resolution. Extending the wash cycles may cause much smaller (less than 1.0%) increase of the retention times. The results of the latter case are still useful for the classification of the fractions according to their polarity, but constitute poor utilization of instrument time. Also predictable is the effect of any polar solvent used for dissolving the samples for injection, particularly in the non-polar portion of the relay gradient. Adherence to standard HPLC practices and the time cycles specified assure reproducibility of retention times comparable to that of any HPLC method as shown by the data summarized in Table 1. The slight discrepancies between long term and short term reproducibilities of the retention times are a good indication of the stability and reliability of both the system and the method. It should be noted, however, that the instrument including the column has been regularly used during the four months for numerous separations, some of them unrelated to this work. In any long-term study, factors such as gradual deterioration of the column packing, contaminants retained, changes in the mechanical properties of the resin, dead space in the column, etc. would readily explain inferior reproducibility compared to the same in short term studies. The results summarized in Table 1 show no evidence of any of these factors.

It has been the experience of this laboratory that after using the column for other methods, a complete cycle of the relay gradient also including the standard pretreatment adequately restores the system to its reliable operating condition. For practical reasons and for reasons of

Table 1
Retention times of the test compounds under the conditions given in Fig. 4

Fraction	t_R (min)		
	Initial values	Five consecutive runs after four months	
		Average	Range
Cholesterol	12.92	13.23	13.22–13.25
Testosterone	17.72	17.71	17.70–17.74
Estradiol	18.23	18.22	18.21–18.26
Cortisone	21.97	21.90	21.88–21.93
Dextrose	44.52	44.46	44.41–44.55
L-Phe	50.71	50.87	50.84–50.92
Gly	52.17	52.37	52.34–52.44
Acetylcholine	53.70	53.94	53.87–53.99
Choline	54.78	55.04	54.99–55.11
Na^+	56.02	56.29	56.23–56.37

assuring standardization of the conditions to the fullest extent possible, the pre-equilibration cycle for every run is included in the gradient program of the previous run. The results of long-term as well as short-term reproducibility summarized in the table fully satisfy if not exceed the criteria of reliability required within the scope of the intended use of the method presented.

The primary goal of this report is to describe the methodology suitable for the initial and general classification of complex mixtures according to the polarity of their components. A detailed analysis of the theoretical aspects and the understanding of the phenomena underlying the method of separation according to polarity require additional studies. However, it appears reasonable to point out similarities and differences between previous studies and the present work. Firstly, one run in the current method is completed in 65 min as opposed to 7 h for the method based on incremental gradient elution [5]. With the re-equilibration time of the column of ca. 30 min in the current method, the total turn-around time is approximately 1.5 h. Furthermore, the polarity range covered appears considerably wider in the present method with only four solvents used as opposed to twelve solvents needed for the incremental gradient elution method. As a matter of fact, Scott and Kucera [5] suggested, that incremental gradient elution would require even more than twelve solvents for additional improvement of resolution. Their projection was based on theoretical considerations using GC with temperature programming as model. The validity of the same model is obviously limited when applied to the interpretation of the results presented here. Considering the stationary and mobile phases used in the present study, the key phenomena responsible for the resolution are more likely to be related to those reported in connection with the concept of hydrophilic-interaction chromatography [3] and with polar bonded phases [6].

ELSD has been found very useful as a general mass detection method [2,4,8–10] particularly with analytes not detectable with spectrophotometric detectors. It also allows the freedom of solvent selection not possible with UV detectors and gradient programs not compatible with refractive index detectors. ELSD certainly has its scope and limitations when used in analytical work, as do all other detection methods. The emphasis in this report is placed on chromatographic performance rather than on examining various aspects of quantitation by means of ELSD.

The technique described here is envisioned to be used primarily as the first step in a series of

classification and preparative isolation methods. The general procedure using the relay gradient elution method covering the entire practical range of polarity facilitates the separation of mixtures into classes defined by the polarity markers. The second steps may then be designed for specific separations within the narrow range of polarity such as non-polar lipids, organic compounds with low to medium polarity, polar organic compounds such as carbohydrates, amino acids, quaternary ammonium ions, etc. One example of a specific separation is shown in Fig. 1 and Fig. 2 involving extremely polar organic and inorganic cations. In this scenario, ELSD fulfils the expectations of the chromatographer by locating the components of the mixtures to be separated. Calibration curves can be established [2] if quantitation is the objective of the work. Reports on applications in specific areas will be published in subsequent papers.

Acknowledgements

The author is pleased to thank Drs. A. Dovletoglou, C.T. Przysiecki, D.K. Roper and R.J. Forsyth for their reviewing the manuscript and offering valuable comments.

References

[1] R.E. Majors, *LC·GC*, 9 (1991) 686.
[2] M. Lafosse, B. Herbreteau, M. Dreux and L. Morin-Allory, *J. Chromatogr.*, 472 (1989) 209.
[3] A.J. Alpert, *J. Chromatogr.*, 499 (1990) 177.
[4] V. Camel, D. Thiébaut and M. Caude, *J. Chromatogr.*, 605 (1992) 95.
[5] R.P.W. Scott and P. Kucera, *Anal. Chem.*, 45 (1973) 749.
[6] A.W. Salotto, E.L. Weiser, K.P. Caffey, R.L. Carty, S.C. Racine and L.R. Snyder, *J. Chromatogr.*, 498 (1990) 55.
[7] J.J. Kirkland, C.H. Dilks, Jr. and J.J. DeStefano, *J. Chromatogr.*, 635 (1993) 19.
[8] P. Carraud, D. Thiebaut, M. Caude, R. Rosset, M. Lafosse and M. Dreux, *J. Chromatogr. Sci.*, 25 (1987) 395.
[9] D. Nizery, D. Thiébaut, M. Caude, R. Rosset, M. Lafosse and M. Dreux, *J. Chromatogr.*, 467 (1989) 49.
[10] M. Dreux and M. Lafosse, *SPECTRA 2000*, 153 (1990) 25.

ELSEVIER

Journal of Chromatography A, 696 (1995) 201–208

JOURNAL OF CHROMATOGRAPHY A

Trace determination of aromatic amines or phenolic compounds in dyestuffs by high-performance liquid chromatography with on-line preconcentration

Chung-Shin Lu, Shang-Da Huang*

Department of Chemistry, National Tsing Hua University, Hsinchu 30043, Taiwan

First received 25 July 1994; revised manuscript received 13 December 1994; accepted 14 December 1994

Abstract

Aromatic amines or phenolic compounds at ppb levels in water were determined by on-line preconcentration with a precolumn followed by high-performance liquid chromatography with UV absorption detection. This method was applied to the determination of aromatic amines or phenolic compounds at ppm levels in commercial dyestuffs. The dyestuff was dissolved in water and precleaned with an SAX cartridge packed with an anion-exchange resin; the effluent was then analysed using the proposed on-line preconcentration and determination method.

1. Introduction

The isolation and identification of phenolic compounds is of great importance owing to their wide applicability in pharmaceuticals, dyes, pesticides and foods. The impact of phenolic compounds on the environment is subject to increasing attention. The US Environmental Protection Agency (EPA) lists eleven substituted phenols as "priority pollutants" [1]. Much research is devoted to these phenolic substances [2–7] and many chromatographic separation and detection systems have been tested; however, the separation and determination of other toxic substituted phenols [8] have received little attention.

The carcinogenic activity of benzidine and several aromatic amines is well known [9]. These compounds were widely used as intermediates in the production of azo dyes and pigments [10,11]. Several methods have been developed for the determination of benzidine and related congeners [12–17]. High-performance liquid chromatography (HPLC) is generally regarded as the best technique for the determination of aromatic amines. A method frequently employed to determine aromatic amines in water-soluble dyes involves extraction of amines with chloroform, followed by diazotization of amines and coupling of diazonium salts with a reagent (R-salt or pyrazolone-T) to form a mixture of coloured products [18–20]. The products are then separated by HPLC and determined with UV absorption detection at 254 and 510 nm. However, the protracted and complicated procedures are not only tedious, which limits the number of samples that can be analysed, but also susceptible to contamination and loss of aromatic amines. Hence a simple and specific method is needed to determine aromatic amines in direct dyes.

In this work, a precolumn was used for the

* Corresponding author.

0021-9673/95/$09.50
SSDI 0021-9673(94)01230-X

on-line enrichment of aromatic amines or phenolic compounds at ppb levels from water, with subsequent determination by HPLC with UV absorption detection. Simple methods for determining aromatic amines or phenolic compounds at ppm levels in dyestuff samples, based on off-line clean-up with an SAX cartridge packed with anion-exchange resin, followed by on-line preconcentration (with a precolumn and the column switching technique) and determination by HPLC were developed.

2. Experimental

2.1. Materials

Analytical-reagent grade 3-diethylaminophenol (DEAP), 2,4-dinitro-1-hydroxynaphthalene (2,4-DNHNA), 5-hydroxy-1,4-naphthoquinone (5-HNQ), 4,4′-dihydroxybiphenyl (4,4′-DHBP) and 4-aminoazobenzene (4-AAB) were obtained from Tokyo Chemical Industry (Tokyo, Japan), 2,7-dihydroxynaphthalene (2,7-DHNA) from Merck (Darmstadt, Germany), 2-hydroxynaphthalene (2-HNA) and 1-hydroxynaphthalene (1-HNA) from Janssen Chimical (Beerse, Belgium) and benzidine (Bz), 3,3′-dimethylbenzidine (DMBz), 4-aminobiphenyl (4-ABP), 3,3′-dichlorobenzidine (DCBz) and 2-naphthaylamine (2-NA) from Sigma (St. Louis, MO, USA) and were used as received. LC-grade sodium acetate and acetonitrile were obtained from Fisher Scientific (Fairlawn, NJ, USA). Deionized water was purified in a Milli-Q filtration system (Millipore, Bedford, MA, USA) to obtain LC-grade water for preparing mobile phases and standard solutions.

2.2. Preparation of standard solutions

Stock standard solutions were prepared by weighing the aromatic amines or the phenolic compounds and dissolving them in methanol. A working composite standard solution was prepared by combining an aliquot of each of the stock standard solutions and diluting the mixture with water. These solutions were stored in dark glass bottles at 4°C.

2.3. Apparatus

The HPLC system, assembled from modular components (Waters), consisted of a Model 600E pump, a Model 486 UV detector and a Model 715 automatic samples. A Millennium workstation (Waters) was utilized to control the system and for acquisition and analysis of data.

2.4. On-line preconcentration of aromatic amines or phenolic compounds from water

For on-line enrichment of aromatic amines, the sample loader (Waters Model 170) was used to introduce the aqueous sample (5 ml) at 0.9 ml/min on to a precolumn (IEC CM-825, 75 mm × 8 mm I.D.) (Showa Denko, Shodex). The packing material of this precolumn was carboxymethyl-bonded silica. The mobile phase, acetonitrile–acetate buffer (pH 4.66) (40:60, v/v) was used to desorb analytes from the precolumn and subsequent separation on the analytical column (Nova-Pak C_{18}, 15 cm × 3.9 mm I.D.) (Waters). The UV detector was set at 280 nm.

For on-line preconcentration of phenolic compounds, the precolumn (LiChrosorb RP-18, 25 mm × 4 mm I.D.) (Merck) and the analytical column (Nova-Pak phenyl, 75 mm × 3.9 mm) (Waters) were used. The mobile phase was acetonitrile–0.1 *M* acetate buffer (pH 4.66) (17:83, v/v). The UV detector was set at 254 nm.

The flow-rate of the mobile phase was kept at 1 ml/min throughout the experiments. Backflushing was used.

2.5. Procedures for the determination of aromatic amines or phenolic compounds in dyestuff samples

Dyestuff samples of four kinds (Direct Blue 6, amaranth, Sunset Yellow FCF and D&C Orange No. 4) were used (Tokyo Chemical Industry). Dyestuff (0.1 g) was weighed into a volumetric flask (100 ml), water (ca. 50 ml) was added and the solid was dissolved completely with ultrasonic vibration. For recovery tests, a suitable aliquot of the standard solution of the aromatic amines or the phenolic compounds was added to the dyestuff solution, the pH was adjusted to 5

(for phenolic compounds) or 6 (for aromatic amines) with 0.01 M HCl and water was added to volume. The solution (exactly 10 ml) was passed through the SAX cartridge and the effluent collected. By this means, whereas aromatic amines or phenolic compounds passed unretained through the SAX cartridge, dyestuff components were adsorbed. To minimize losses of aromatic amines or phenolic compounds caused by partial adsorption on the SAX cartridge, the cartridge was then eluted with 4 ml of 0.1 *M* acetate buffer (pH 4.66) and the eluent was collected in a tube. The effluent and eluent were combined and mixed. An aliquot of the mixed solution (5 ml) was then enriched with an on-line device and analysed in the manner described above.

3. Results and discussion

3.1. On-line preconcentration of aromatic amines from water with a CM-825 precolumn

The recovery data for two concentrations are given in Table 1. Aromatic amines were recovered in the range 87–102%; the recoveries were approximately the same at both spiking levels. A plot of aromatic amine concentration (range 10–100 ng/ml) vs. integrated area gave linear regression lines having correlation coefficients >0.993. The method detection limits for these aromatic amines were 0.1–0.6 ng/ml.

Table 1
Recoveries of selected aromatic amines from water by on-line enrichment on a CM-825 precolumn[a]

Compound	Recovery[b] (%)	
	2 ppb	100 ppb
Bz	89 ± 2	94 ± 1
DMBz	93 ± 6	96 ± 1
2-NA	98 ± 2	101 ± 0
4-ABP	96 ± 6	97 ± 0
DCBz	102 ± 10	87 ± 1
4-AAB	101 ± 5	102 ± 1

[a] Aqueous sample (5 ml) was pumped at 0.9 ml/min through the CM-825 precolumn.
[b] Average value and standard deviation of triplicate runs.

Table 2
Recoveries of selected phenolic compounds from water by on-line enrichment on a LiChrosorb RP-18 precolumn[a]

Compound	Recovery[b] (%)	
	5 ppb	100 ppb
DEAP	89 ± 3	105 ± 3
2,7-DHNA	107 ± 2	100 ± 1
4,4′-DHBP	96 ± 2	98 ± 1
2,4-DNHNA	92 ± 10	98 ± 2
5-HNQ	86 ± 1	103 ± 3
2-HNA	102 ± 4	98 ± 1
1-HNA	99 ± 4	97 ± 3

[a] Aqueous sample (5 ml) was pumped at 0.9 ml/min through the LiChrosorb RP-18 precolumn.
[b] Average value and standard deviation of triplicate runs.

These results are comparable to those obtained using an RP-18 precolumn [21].

3.2. On-line preconcentration of phenolic compounds from water with a LiChrosorb RP-18 precolumn

As shown in Table 2, phenolic compounds were recovered in the range 86–107% for the two concentrations specified; the recoveries were approximately the same at both spiking levels. The linearity of the method was tested by analysing phenolic compound standards at four concentrations in the range 10–100 ng/ml. The

Table 3
Recoveries of selected aromatic amines added to commercial dyes[a]

Compound	Recovery[b] (%)		
	Sunset Yellow FCF		Amaranth 100 μg/g
	10 μg/g	100 μg/g	
Bz	95 ± 7	94 ± 2	99 ± 2
DMBz	83 ± 3	87 ± 3	85 ± 4
2-NA	88 ± 8	93 ± 9	100 ± 1
4-ABP	94 ± 6	91 ± 2	88 ± 2
DCBz	96 ± 5	85 ± 4	101 ± 3
4-AAB	86 ± 3	85 ± 2	81 ± 4

[a] The dyestuff solutions (0.1 g per 100 ml) were processed as described under Experimental.
[b] Average value and standard deviation of triplicate runs.

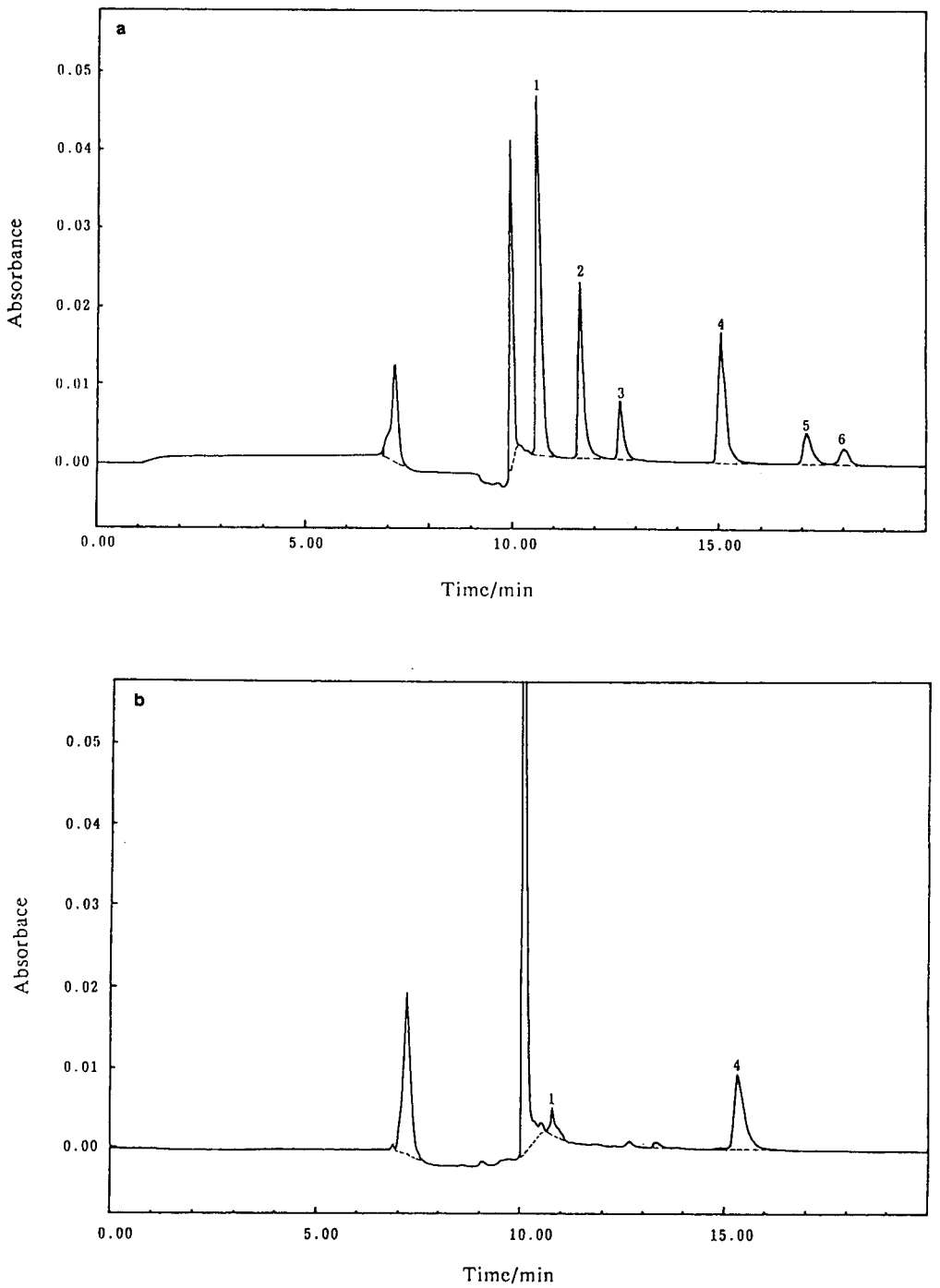

Fig. 1. Chromatograms of (a) a 10 ng/ml aromatic amine standard chromatogram and (b) a dye sample (Direct Blue 6) after clean-up on an SAX cartridge, on-line enrichment with a CM-825 precolumn and separation on a C_{18} column. Mobile phase, acetonitrile–0.1 *M* acetate buffer (pH 4.66) (40:60, v/v). For other experimental conditions, see text. Peaks: 1 = Bz; 2 = DMBz; 3 = 2-NA; 4 = 4-ABP; 5 = DCBz; 6 = 4-AAB.

relationship between peak area and concentration was linear over the entire range for phenolic compounds (the correlation coefficient of the regression lines exceeded 0.998). The method detection limits for these phenolic compounds were 0.1–1.5 ng/ml.

3.3. Determination of aromatic amines in dyestuff samples

A disposable SAX cartridge was used as an off-line clean-up filter, followed by on-line preconcentration (with a CM-825 precolumn) and determination by HPLC. The recovery of aromatic amines from "spiked" dyestuffs was excellent (Sunset Yellow FCF 83–96%, amaranth 81–101%; Table 3). The standard deviation of the mean was less than 9%. No aromatic amine was found in the unspiked dyes.

The method detection limits of this procedure were Bz 0.6, DMBz 0.9, 2-NA 1.8, 4-ABP 0.5, DCBz 1.7 and 4-AAB 1.6 μg/g. The detection limits were measured with a concentration equivalent to three times the standard deviation of replicated measurements ($n = 7$) of the analytes in the dyestuff sample (Sunset Yellow FCF). The Occupational Safety and Health Administration [22] states that the concentrations of these compounds in various matrices to which workers may be exposed must not exceed 0.1%, The content of aromatic amines in synthetic food dyestuffs is limited to 0.01% by European colour additive specifications [23]. Therefore, the proposed method is capable of determining aromatic amines at concentrations much lower than these two regulatory limits.

The utility of the method was demonstrated by the analysis of Direct Blue 6. Representative chromatograms resulting from analysis of the sample and standard (10 μg/l) are shown in Fig. 1a and, b, respectively. The baseline exhibits a slight background because of the efficient removal of co-existing interferents on the SAX cartridge. As the aromatic amines are well isolated from other dyestuff components, the presence of a peak with the retention time of an aromatic amine gave a presumptive test for its presence. The results indicate that certain amounts of carcinogenic aromatic amines may be present in this dye, namely 1.0 ± 0.2 μg/g of benzidine and 6.5 ± 0.2 μg/g of 4-aminobiphenyl. These values were obtained from triplicate determinations according to a calibration graph. The concentrations of benzidine and 4-aminobiphenyl in this dye, determined by the method of standard additions, were 0.9 and 6.6 μg/g, respectively.

3.4. Determination of phenolic compounds in dyestuff samples

A disposable SAX cartridge was found to be suitable as a clean-up filter; it can trap the anionic dyestuff from water without affecting the trace enrichment of phenolic compounds on the LiChrosorbRP-18 column except for 2,4-dinitro-1-hydroxynaphthalene (2,4-DNHNA). After the clean-up step, the dyestuff aqueous samples were processed by on-line preconcentration (with the LiChrosorb RP-18 precolumn) followed by HPLC determination. The recoveries of phenolic compounds added to the dyestuff (Sunset Yellow FCF) at concentrations of 10 and 100 μg/g were excellent (81–102%; Table 4). The standard deviation from the mean was less than 6%. The recoveries of all phenolic compounds indicated that the proposed clean-up and on-line enrichment procedure is highly specific and efficient with no interference from other components of the dyestuff sample.

The method detection limits ($n = 7$) of this

Table 4
Recoveries of selected phenolic compounds added to Sunset Yellow FCF[a]

Compound	Recovery[b] (%)	
	10 μg/g	100 μg/g
DEAP	88 ± 3	93 ± 6
2,7-DHNA	97 ± 6	99 ± 1
4,4′-DHBP	102 ± 3	101 ± 5
5-HNQ	91 ± 1	85 ± 5
2-HNA	99 ± 1	95 ± 4
1-HNA	81 ± 2	84 ± 5

[a] The dyestuff solutions (0.1 g per 100 ml) were processed as described under Experimental.
[b] Average value and standard deviation of triplicate runs.

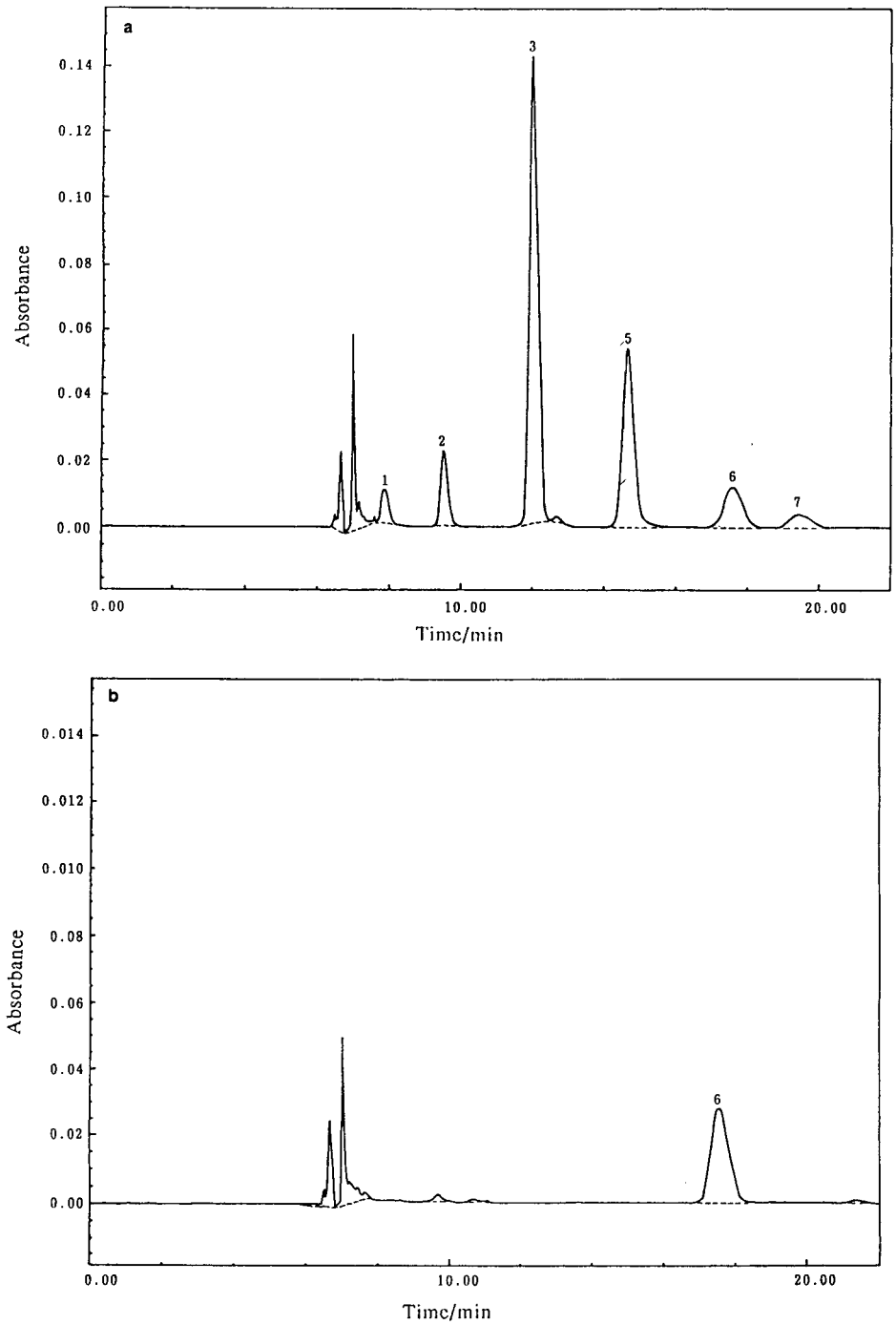

Fig. 2. Chromatograms of (a) a phenolic compound standard (100 ng/ml) and (b) a dye sample (D&C Orange No. 4) after clean-up on an SAX cartridge, on-line enrichment with an RP-18 precolumn and separation with a phenyl column. Mobile phase, acetonitrile–0.1 *M* acetate buffer (pH 4.66) (17:83, v/v). For other experimental conditions, see text. Peaks: 1 = DEAP; 2 = 2,7-DHNA; 3 = 4,4′-DHBP; 5 = 5-HNQ; 6 = 2-HNA; 7 = 1-HNA.

procedure for the individual components were DEAP 1.80, 2,7-DHNA 0.87, 4,4′-DHBP 1.50, 5-HNQ 0.42, 2-HNA 0.90 and 1-HNA 1.26 μg/g. The proportion of phenolic compounds in dyestuffs for drug and cosmetic use is limited to 0.2% according to the USA Code of Federal Regulations [24]. The proposed method is capable of determining phenolic compounds at concentrations of 0.1% of the regulatory limit.

The utility of the method was clarified by the analysis of D&C Orange No. 4. Representative chromatograms obtained from analytes of the sample and a 100 ppb standard are shown in Fig. 2a and b, respectively. The baseline contains a slight background as a consequence of the efficient removal of co-existing interferents left on the SAX cartridge. As phenolic compounds were well isolated from other dyestuff components, the presence of a peak with the retention time of a phenolic compound gave a presumptive test of its presence. The results (using the calibration graph method) indicate that 215 ± 3 μg/g of 2-HNA may be present in this dye. The concentration of 2-HNA in this dye determined by the standard additions method was 216 μg/g, which is identical with the value obtained from the calibration graph.

4. Conclusions

Aromatic amines or phenolic compounds in water at ppb levels can be determined by on-line preconcentration with a small precolumn followed by HPLC with UV absorption detection.

This method was applied to the determination of aromatic amines and phenolic compounds at ppm levels in commercial dyestuffs. Because of the small capacity of the precolumn and the presence of dyestuff components at relatively high concentrations in the commercial dye samples tested, it was necessary to introduce a clean-up step to remove dyestuff compounds from aqueous samples. An anion-exchange cartridge (SAX) was used for the clean-up of aqueous dyestuff samples prior to the on-line preconcentration and determination procedures. The proposed method allows the simple, rapid and efficient clean-up and on-line enrichment and simultaneous determination of aromatic amines and phenolic compounds, and is expected to be suitable for routine analyses for these compounds in commercial dyestuffs.

Acknowledgement

We thank the National Science Council of the Republic of China for grant support (NSC 83-0208-M007-067 and NSC 84-2621-M007-001 ZA).

References

[1] J.E. Longbottom and J.J. Lichtenberg, *Methods for Organic Chemical Analysis of Municipal and Industrial Wastewater*, US EPA, EPA-600/4-82-057, Method 604, 1982.
[2] P.A. Realini, *J. Chromatogr. Sci.*, 19 (1981) 124.
[3] F.P. Bigley and R.L. Grob, *J. Chromatogr.*, 350 (1985) 407.
[4] E. Chladek and R.S. Marano, *J. Chromatogr. Sci.*, 22 (1984) 313.
[5] D.A. Baldwin and J.K. Debowski, *Chromatographia*, 26 (1988) 186.
[6] B. Gawdzik, J. Gawdzik and U. Czerwinska, *J. Chromatogr.*, 509 (1990) 135.
[7] C.B. Borra, AS.D. Corcia and R. Samperi, *Anal. Chem.*, 58 (1986) 2048.
[8] M. Sittig, *Handbook of Toxic and Hazardous Chemicals and Carcinogens*, Noyes Publications, New Jersey, 2nd ed., 1985.
[9] K.H. Ferber, in *Encyclopedia of Chemical Technology*, Vol. 3, Wiley, New York, 3rd ed., 1978, p. 772.
[10] *Colour Index*, Society of Dyers and Colourists, Bradford, 3rd ed., 1971.
[11] J. Szadowski, *J. Dyes Pigments*, 14 (1990) 217.
[12] P. Verma and V.K. Gupta, *Anal. Chim. Acta*, 151 (1983) 261.
[13] M.A. Eldib, *J. Assoc. Off. Anal. Chem.*, 54 (1971) 1383.
[14] M.C. Bowman, J.R. King and C.L. Holder, *Int. J. Environ. Anal. Chem.*, 4 (1976) 205.
[15] V. Concialini, G. Chiavari and P. Vitali, *J. Chromatogr.*, 258 (1983) 244.
[16] G. Chiavari and A.G. Giumanini, *J. Chromatogr.*, 206 (1981) 555.
[17] B. Stavric, R. Klassen and W. Miles, *J. Assoc. Off. Anal. Chem.*, 62 (1979) 1020.
[18] J.E. Bailey, *Anal. Chem.*, 57 (1985) 189.
[19] J.E. Bailey and C.J. Bailey, *Talanta*, 32 (1985) 875.

[20] N.R. Fratz, J.E. Bailey and C.J. Bailey, *J. Chromatogr.*, 331 (1985) 109.
[21] C.W. Whang and L.L. Yang, *J. Chin. Chem. Soc.*, 35 (1988) 109.
[22] J. Schulze, C. Ganz and D. Parkes, *Anal. Chem.*, 50 (1978) 171.
[23] J. Walford, *Devel;opments in Food Colours–2*, Elsevier Applied Science, Barking, 1984.
[24] D.M. Marmion, *Handbook of US Colorants for Foods, Drugs, and Cosmetics*, Wiley, New York, 1979.

ELSEVIER

Journal of Chromatography A, 696 (1995) 209–217

JOURNAL OF CHROMATOGRAPHY A

Separation and identification of hydrophilic peptides in dairy products using FMOC derivatization

J.M. Roturier, D. Le Bars, J.C. Gripon*

Station de Recherches Laitières, Institut National de la Recherche Agronomique, 78352 Jouy-en-Josas cedex, France

First received 11 October 1994; revised manuscript received 14 December 1994; accepted 15 December 1994

Abstract

Small hydrophilic di- and tripeptides from food products are not separated by reversed-phase high-performance liquid chromatography (RP-HPLC). A simple method using precolumn derivatization with 9-fluorenylmethoxycarbonyl chloride (FMOC) of hydrophilic peptides followed by RP-HPLC separation is presented. Peptides can subsequently be identified by Edman degradation after deprotection of the peptide derivatives with piperidine. Fifteen peptides (ten dipeptides, four tripeptides and one tetrapeptide) were sequenced from the water-soluble fraction of an enzyme-modified cheese model. Some synthetic peptides (Ile–Asn, Val–Thr, Ala–Pro, Val–Gln, Thr–Gln and Gly–Gly) corresponding to purified peptides were sensory tested.

1. Introduction

The importance of the non-volatile water-soluble fraction in cheese flavour has been recognized by several workers [1–4]. McGugan *et al.* [1] reported that the water-soluble fraction, containing mainly salts, lactic acid, amino acids and peptides, contributes most to the flavour intensity. Biede and Hammond [2] assigned the brothy–nutty, sweet flavours to the amino acids and dipeptides, whereas bitter and burned flavours were attributed to larger peptides (tri- to hexapeptides). Aston and Creamer [3] also observed that the water-soluble fraction containing peptides is responsible for the taste intensity with bitter and brothy notes.

However, little information is available concerning the structure of these small "savoury" peptides. Mojarro de Guerra et al. [5] purified seven peptides from a Swiss cheese containing proline, namely Gly–Pro–Val–Arg, Arg–Pro, Leu–Pro, Lys–Pro and Tyr–Pro. Roudot-Algaron and co-workers [6,7] isolated three γ-glutamyl dipeptides (γ-Glu–Phe, γ-Glu–Tyr, γ-Glu–Leu) and five diketopiperazines [cyclo(Pro–Pro), cyclo(Pro–Val), cyclo(Pro–Phe), cyclo(Pro–Ala) and cyclo(Pro–Leu)] from Comté cheese. All peptides containing Pro have a bitter taste. The taste of γ-Glu–Phe was described as umami and slightly sour, salty and metallic. The peptide γ-Glu–Tyr was reported as sour and slightly salty. Other peptides isolated from cheese are longer and have been reported to be bitter owing to their hydrophobic properties. Some polar hydrophilic peptides from other food sources were shown to have flavour properties. Glutamyl peptides isolated from proteinase-modified soy bean protein, fish hydrolysate or

* Corresponding author.

0021-9673/95/$09.50
SSDI 0021-9673(94)01234-2

gravy of beef meat have brothy taste properties [8–10].

The aim of this study was to identify such peptides in the non-volatile water-soluble fraction of an enzyme-modified cheese model. Peptides are classically separated by reversed-phase chromatography [11–14]. However, small hydrophilic peptides cannot be studied using this method because they interact poorly with the hydrophobic chains of the stationary phase in reversed-phase chromatography. To overcome this difficulty, we used precolumn derivatization with 9-fluorenylmethoxycarbonyl chloride (FMOC) to allow the separation of hydrophilic peptides on a reversed-phase column. The identification was achieved by Edman degradation after deprotection of the peptide derivatives.

2. Experimental

2.1. Enzyme-modified cheese model

Enzyme-modified cheese model was supplied by SOREDAB (Société de Recherche et Développement Alimentaire Bongrain). This product was the result of the action of lipases, peptidases and proteases on a dairy pasteurized slurry. After 6 days of incubation under aseptic conditions, the product had a strong cheesy flavour and a bitter taste.

2.2. Water-soluble extract

The water-soluble fraction was extracted from an enzyme-modified cheese model with the method described by Aston and Creamer [3] with minor modifications. The enzyme-modified cheese model (16 g) was homogenized in water (30 ml) with an Ultra-Turrax T25 (IKA, Staufen, Germany) for 2 min at room temperature. The resulting slurry was centrifuged at 8650 *g* for 20 min using a JA-21 rotor in a J2-21 centrifuge (Beckman, Palo Alto, CA, USA) at 4°C. The fat and the aqueous layers were collected separately. The pellet was homogenized twice in water (30 ml) and centrifuged. Each time, the fat layer and the water fraction were recovered. The three fat layers were then combined, homogenized in 20 ml of water and centrifuged. The four water fractions were pooled and filtered at 4°C through a Whatman No. 42 paper and a 0.45-μm filter (Millipore, Bedford, MA, USA).

2.3. Gel filtration

The water-soluble fraction was fractionated on a Sephadex G-25 (Pharmacia, Uppsala, Sweden) column (200 cm × 4 cm I.D.). Elution was carried out with water purified with a Milli-Q system (Millipore) at 84 ml/min. Detection was performed at 206 nm and 84-ml fractions were collected for sensory analysis and for purification. The exclusion volume (728 ml) was determined using bovine serum albumin (M_r = 66 000).

2.4. Derivatization

Samples and standards were reacted with FMOC according to the method of Einarsson et al. [15]. A volume of 0.2 ml of gel filtration fraction was dried with a Speed-Vac system (Savant, Farmingdale, USA). The sample was resuspended in 0.2 ml of sodium borate buffer (0.5 *M*, pH 7.8) and 0.2 ml of FMOC reagent (5.8 m*M* in acetone) were added. The vial was vortex mixed and after 45 s the mixture was extracted with 0.4 ml of pentane–ethyl acetate (80:20). The aqueous phase containing the FMOC derivatives was then ready for reversed-phase high-performance liquid chromatography (RP-HPLC).

2.5. HPLC conditions for the separation of non-derivatized peptides

Peptides were separated by RP-HPLC using a Model 600E gradient system (Waters, Bedford, MA, USA) fitted with a Nucleosil C_{18} (5 μm) column (250 mm × 46 mm I.D.) (SFCC, Neuilly Plaisance, France). Peptides were eluted with a linear gradient of solvent A decreasing from 80% to 20% in 30 min at 25°C. Solvent A

consisted of 0.115% trifluoroacetic acid (TFA) in water and solvent B consisted of 0.1% TFA in acetonitrile (ACN)–water (60:40). The flow-rate was 1 ml/min and the absorbance was read at 214 nm.

2.6. HPLC conditions for the separation of FMOC derivatives of peptides and amino acids

The solvent system used for separation consisted of solvent A, ACN–100 m*M* ammonium acetate buffer (pH 3.8) (20:80), and solvent B, ACN–100 m*M* ammonium acetate buffer (pH 4.2) (80:20). Chromatography was carried out at a flow-rate of 1 ml/min at 40°C. Samples were eluted with a gradient from 30 to 80% solvent B in 50 min and isocratic at 100% B for 10 min. The gradient was started 10 min after injection. The absorbance was read at 260 nm.

The main hydrophilic peaks were collected and a second purification step was applied with isocratic elution with ACN–100 m*M* ammonium acetate buffer (pH 3.3) (30:70).

2.7. Deprotection

The peptide derivative collected after RP-HPLC separation was dried with a Speed Vac system. Piperidine (10 μl) was added and the sample was dried again to remove excess of piperidine. The sample was resuspended in 200 μl of 20% TFA and 400 μl of pentane–ethyl acetate (80:20) were added. The aqueous fraction was recovered, extracted again with 400 μl of pentane–ethyl acetate (80:20) and dried. The sample was then ready for sequencing.

2.8. Peptide sequencing

The peptide sequence was determined by automatic Edman degradation using an Applied Biosystems (San-Jose, CA, USA) Model 477A protein sequencer.

2.9. Sensory test

Each fraction (10 ml) from gel filtration was lyophilized, weighed and resuspended in 10 ml of Milli-Q-purified water. The fraction was then evaluated by an eight-member panel, ranging in age from 25 to 35 years. Panellists were selected for their sensitivity to salty, sweet, sour, bitter and umani tastes. Each panellist evaluated the flavour and taste of every sample (1 ml) using a small plastic teaspoon. Between samples they rinsed their mouths with mineral water. Samples were presented to the panellists in random order and not more than four samples were presented at each session.

After identification, some peptides were synthesized by Neosystem (Strasbourg, France), dissolved in Milli-Q-purified water, lyophilized to remove solvent odour and tasted. These synthetic peptides were resuspended in Milli-Q-purified water at a concentration of 5 mg/ml. The panellists were asked to describe each sample for taste and flavour.

3. Results

3.1. Preparation of cheese extract

A total of 4.8 g of lyophilized water-soluble compounds was obtained from 33 g of enzyme-modified cheese model. The amino acid analysis was carried out before (to determine the free amino acid content) and after acid hydrolysis. The difference indicated amino acids involved in peptide linkages. The freeze-dried water-soluble fraction consisted of peptides (35.9%) and free amino acids (6.2%), mainly Glu, Phe, Leu and Lys.

3.2. Gel filtration

Gel filtration was performed in order to fractionnate the extract into less complex fractions. Fig. 1 shows the chromatogram obtained by gel filtration with the water-soluble fraction of the enzyme-modified cheese model. The separation, performed with water as eluent to allow sensory testing, was not strictly on a molecular size basis: aromatic amino acids such as Phe and Tyr were considerably retarded owing to interactions with the Sephadex G-25 matrix.

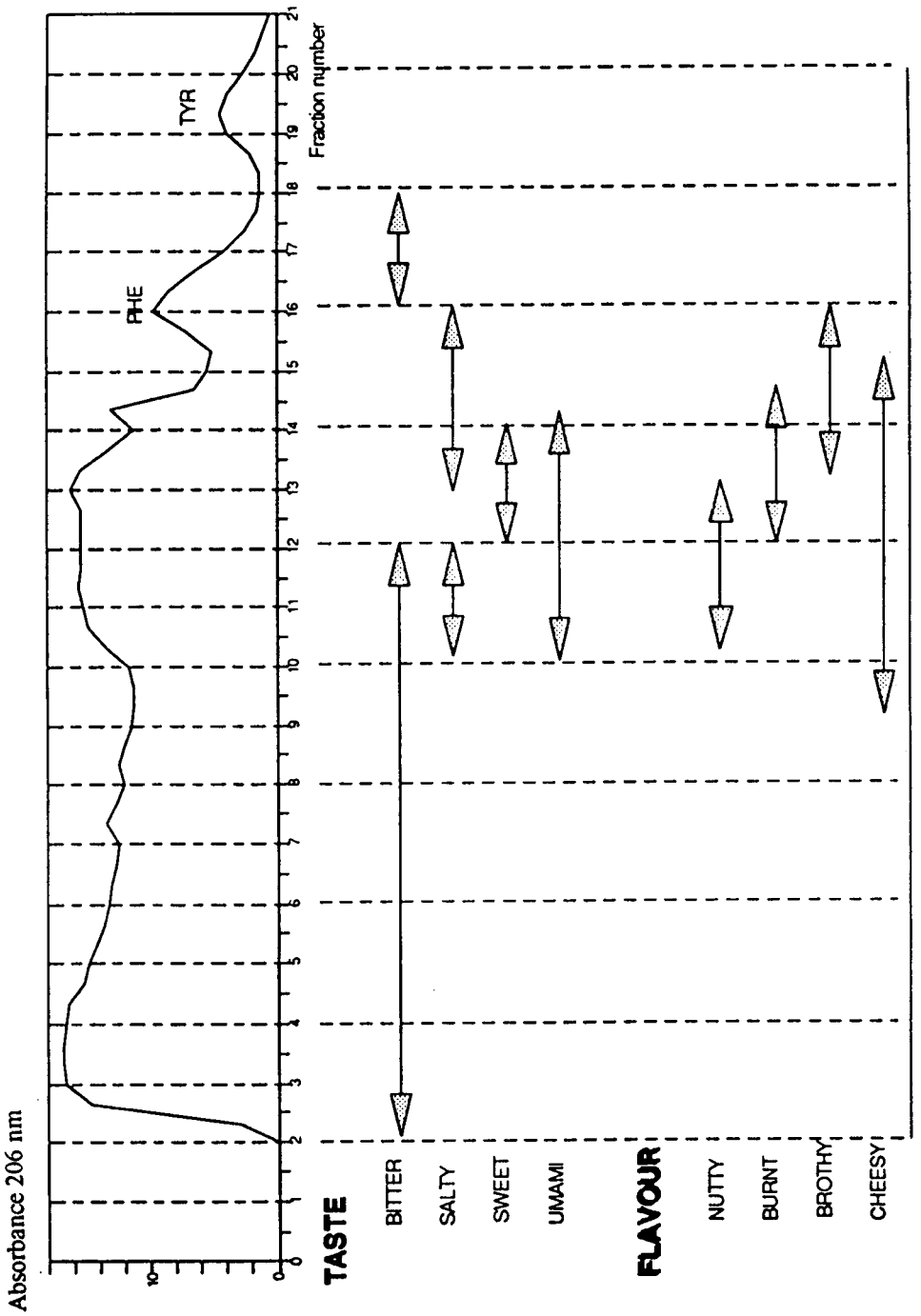

Fig. 1. Gel filtration chromatogram and sensory characterization of the collected fractions.

Fractions were collected and tasted (Fig. 2). Fractions 3–10 were described as bitter. More intense and complex tastes were perceived from fractions 11–14. According to their elution volume, these compounds had low molecular masses.

The comparison of the RP-HPLC traces obtained from each gel filtration fraction revealed that more hydrophilic compounds were present in the later fractions. The separation and identification of short hydrophilic peptides was consequently performed on two of those fractions (12 and 13).

3.3. Separation of peptides derivatives

The separation of peptide derivatives from fractions 12 and 13 is shown in Fig. 4. These chromatograms were compared with a chromatographic profile of amino acid derivatives (Fig. 3) in order to identify the retention times of the amino acid derivatives. Most hydrophilic derivatives were individually collected and dried. Further purification of peptide derivatives was carried out in a second step by decreasing the pH of solvent A from 3.8 to 3.3 (see Experimental). At a lower pH we observed an increase in the retention times of the amino acid and peptide derivatives. A better resolution of most hydrophilic derivatives was also observed. Similar properties had been reported by Einarsson et al. [15] for amino acid derivatives.

3.4. Identification

After deprotection with piperidine as described under Experimental, fifteen peptides (eleven dipeptides and four tripeptides) were sequenced (Table 1) with an automatic Edman degradation sequencer. The retention times of

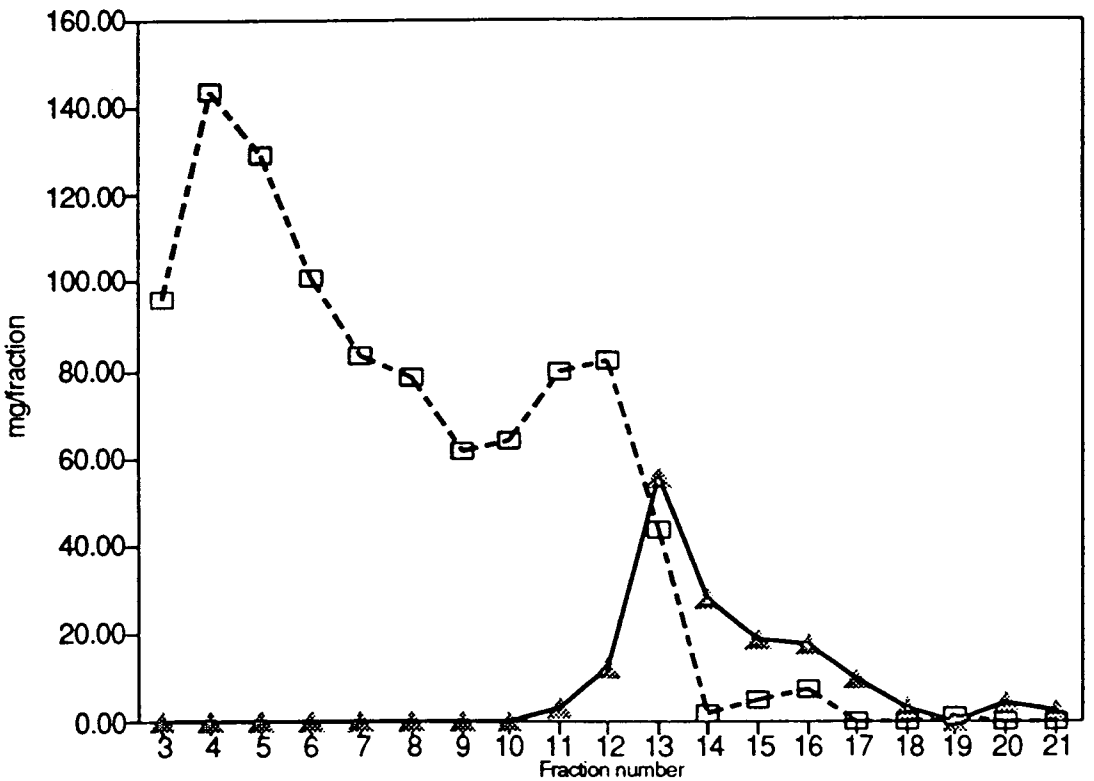

Fig. 2. (▲) Amino acid and (□) peptide concentrations in gel filtration fractions.

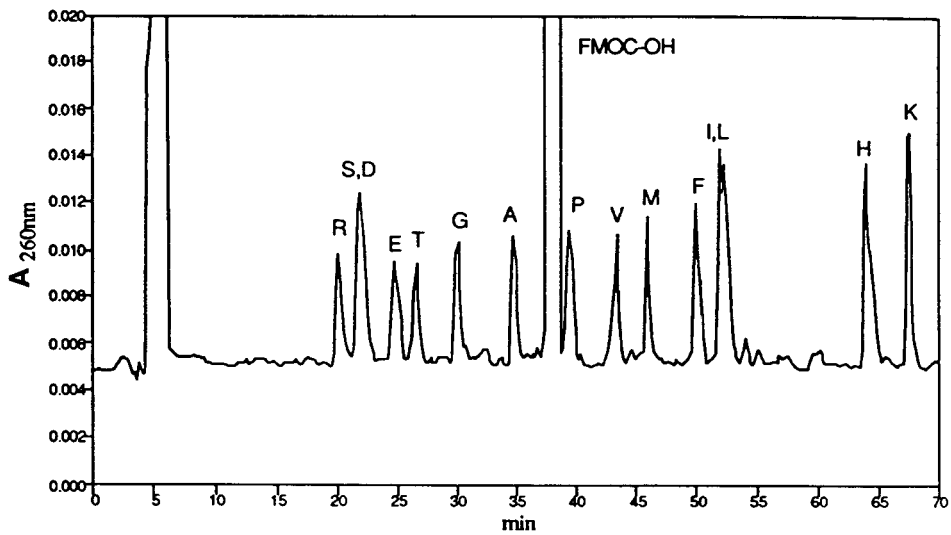

Fig. 3. Separation of derivatized standard mixture of amino acids containing 2.5 μmol of each amino acid. See Experimental for chromatographic conditions.

the purified peptide derivatives were compared with those of synthetic peptides (Fig. 5) (Ile–Asn, Val–Thr, Ala–Pro, Val–Gln, Ala–Gln, Thr–Gln, Gly–Val–Ser and Ala–Gln–Thr) in order to confirm some of the sequences.

3.5. Sensory evaluation of synthetic peptides

Synthetic dipeptides (Ile–Asn, Val–Thr, Ala–Pro, Val–Gln, Ala–Gln and Thr–Gln) were tasted at a concentration of 5 mg/ml. Most of the peptides were described as flat. Only Val–Gln and Ala–Pro were slightly sweet and slightly bitter, respectively. Ala–Gln was tasted at a concentration of 20 mg/ml and was found to be slightly bitter and umami.

4. Discussion

Separations of short hydrophilic peptides were carried out with FMOC derivatization followed by RP-HPLC. This method has certain advantages: FMOC-Cl reacts rapidly with both primary and secondary amino acids to form very stable derivatives [15–18]. Moreover, this acylation is less sensitive to salts than other reagents, e.g., phenyl isothiocyanate (PITC) [18]. In order to identify peptides, we developed a simple method for peptide derivative deprotection with piperidine, classically used in peptide synthesis. Piperidine allows the liberation of peptides by reacting with the methylfluorenyl group of the derivative. However, the resulting molecule leads to an artefact peak during the RP-HPLC step of sequencing. This problem was solved by resuspending the sample in 20% TFA. This procedure induces FMOC-OH formation (detected by RP-HPLC), suggesting cleavage of the molecule formed by reaction of piperidine with the methylfluorenyl group. The FMOC-OH is removed by pentane–ethyl acetate extraction and piperidine is eliminated by drying. One limitation of the FMOC method is the ratio between the amino acid and small peptide concentrations in the extract. A high concentration of amino acid derivatives could mask peptide derivative peaks in RP-HPLC. Prior partial separation of peptides and amino acids must be done by gel permeation.

Using the FMOC method, we were able to identify fifteen peptides. As expected, most of these peptides are particularly hydrophilic owing to their chain length and their amino acid

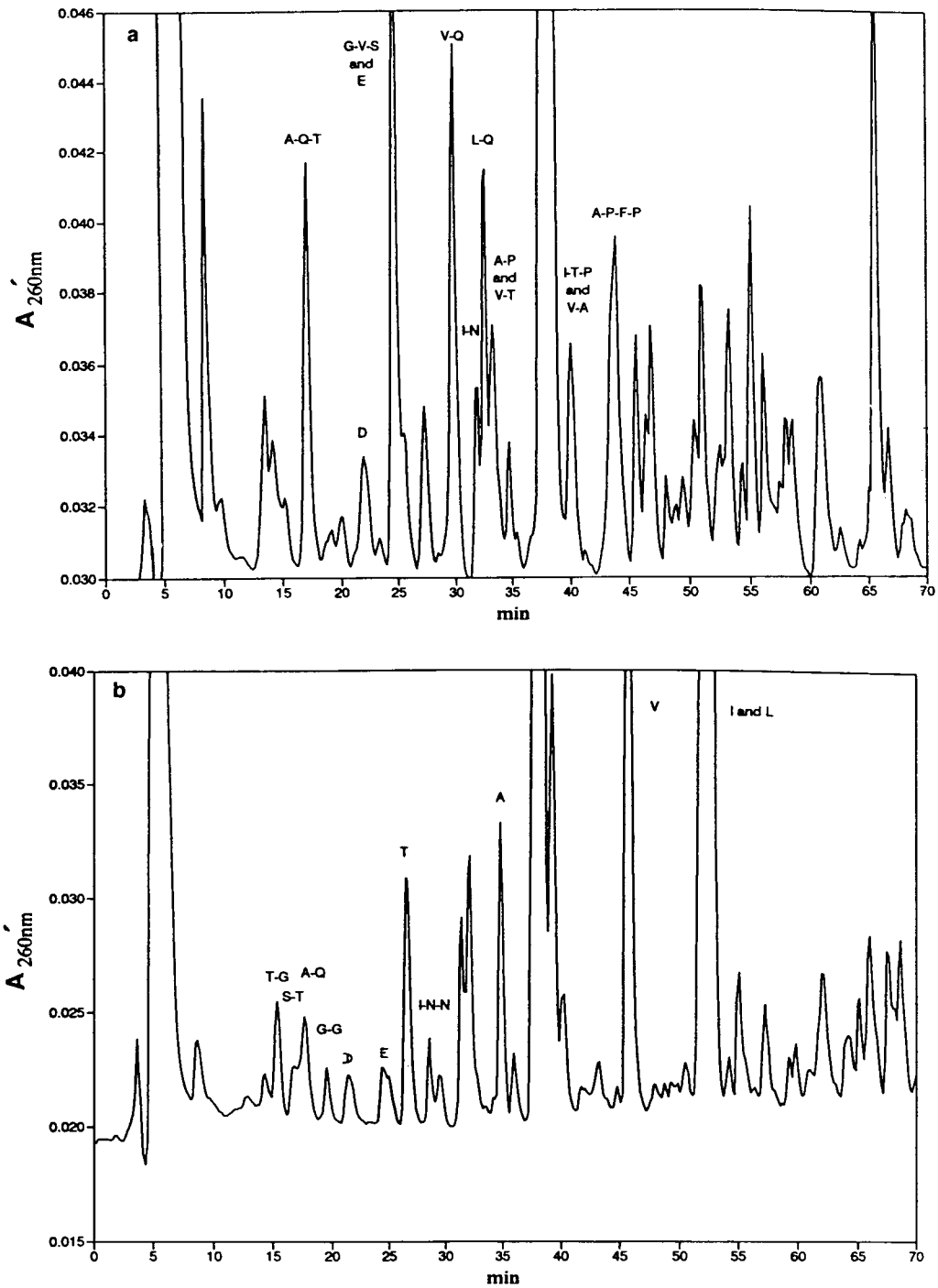

Fig. 4. Separation of peptide derivatives of gel filtration fractions (a) 12 and (b) 13. See Experimental for chromatographic conditions.

Table 1
Amino acid sequence of peptides isolated from gel filtration fractions 12 and 13 and sensory evaluation of some synthetic peptides

Peptide identification	Taste of synthetic peptides	Concentration of synthetic peptides for tasting (mg/ml)
Gly–Gly	Tasteless	5
Thr–Gln	Tasteless	5
Ser–Thr	Tasteless	5
Ala–Gln	Slightly bitter and umami	20
Ala–Gln–Thr		
Gly–Val–Ser		
Val–Gln	Slightly sweet	5
Ile–Asn–Asn		
Val–Thr		
Leu–Gln		
Val–Ala	Tasteless	5
Ile–Asn		
Ala–Pro	Slightly bitter	5
Ile–Thr–Pro		
Ala–Pro–Phe–Pro		

composition. Among these peptides, Ala–Gln–Thr, Gly–Val–Ser, Val–Gln, Val–Thr, Ile–Asn–Asn and Gly–Gly could be assigned to the residues β-casein 53–55, β-casein 94–96, κ-casein 161–162, κ-casein 164–165, κ-casein 51–53 and α-lactabumin 19–20, respectively. The other peptides could originate from several localizations in casein sequences.

None of these peptides contained glutamic acid in their sequence. This is surprising as caseins are particularly rich in glutamic acid and potentially could liberate numerous small glutamic peptides. On the other hand, eight peptides contained Gln or Asn residues. As far as we know, no information is available concerning the taste of these peptides. As mentioned, Ile–Asn, Ala–Gln and Thr–Gln were tasted and described as flat. Val–Gln is slightly sweet. The concentration of the peptides (estimated by amino acid analysis of peptide derivatives after the first step of purification) was lower than 0.1 mg/ml in the tasted samples. This indicates that these peptides individually could

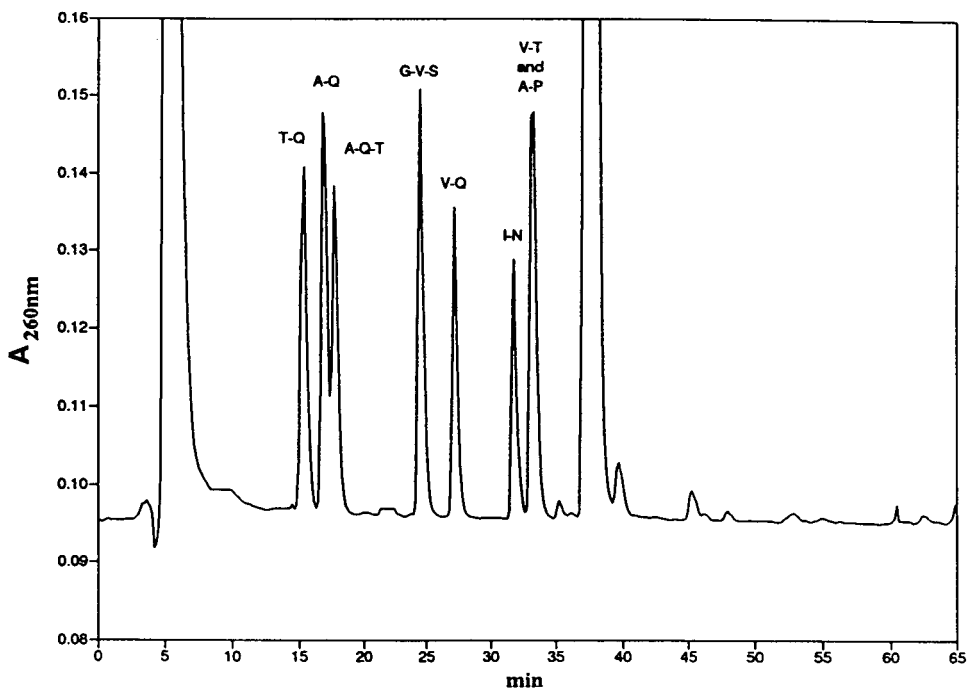

Fig. 5. Separation of synthetic peptide derivatives (T–Q, A–Q, A–Q–T, G–V–S, V–Q, I–N, V–T, A–P). See Experimental for chromatographic conditions.

not explain the enzyme-modified cheese model flavour. If they play a role in flavour, synergic effects or interaction phenomena must occur.

Hydrophobic proline peptides (Ala–Pro, Ile–Thr–Pro and Ala–Pro–Phe–Pro) were also identified. The last two peptides could be assigned to the residues α_{s1}-casein 119–121 and α_{s1}-casein 26–29. Ala–Pro, previously described as bitter by Shiraishi *et al.* [19], was also found to be bitter by our panel. Ile–Thr–Pro and Ala–Pro–Phe–Pro are probably bitter owing to their high hydrophobicity.

5. Conclusions

We have demonstrated that the FMOC method permits the separation and identification of very hydrophilic peptides in a complex medium such as cheese water-soluble extract. Such a technique could be applied in combination with RP-HPLC to follow and understand protein hydrolysis mechanisms during the maturation of cheese, meat or any protein hydrolysate used in the food industry.

Acknowledgements

This work was supported by the Ministère de la Recherche et de la Technologie, Décision d'Aide No. 90 G 0429. We acknowledge Michèle Dame of the Société de Recherche et Développement Alimentaire Bongrain for helpful discussions and for supplying enzyme-modified cheese model. We are grateful to Annick Bouroche for her assistance with the preparation of the manuscript.

References

[1] W.A. McGugan, D.B. Emmons and E. Larmond, *J. Dairy Sci.*, 62 (1979) 398.
[2] S.L. Biede and E.G. Hammond, *J. Dairy Sci.*, 62 (1979) 227.
[3] J.W. Aston and L.K. Creamer, *N.Z.J. Dairy Sci. Technol.*, 21 (1986) 229.
[4] J. Kowaleska, H. Zelakowska, A. Babochowski, E.G. Hammond and F. Ross, *J. Dairy Sci.*, 68 (1985) 2165.
[5] S.H. Mojarro de Guerra, R. Amado, E. Arrigoni and J. Solms, *J. Food. Sci.*, 56 (1991) 943.
[6] F. Roudot-Algaron, L. Kerhoas, D. Le Bars, J. Einhorn and J.C. Gripon, *J. Dairy Sci.*, 77 (1994) 1161.
[7] F. Roudot-Algaron, D. Le Bars, J. Einhorn, J. Adda and J.C. Gripon, *J. Food Sci.*, 58 (1993) 1005.
[8] J. Kirimura, A. Shimizu, A. Kimizuka, T. Ninomiya and N. Katsuya, *J. Agric. Food Chem.*, 17 (1969) 689.
[9] M. Fujimaki, S. Arai, M. Yamashita, H. Kato, and M. Noguchi, *Agric. Biol. Chem.*, 37 (1973) 2891.
[10] M. Tamura, T. Nakatsuka, M. Tada, Y. Kawasaki, E. Kikuchi and H. Okai, *Agric. Biol. Chem.*, 53 (1989) 319.
[11] H.M. Champion, and D.W. Stanley, *Can. Inst. Food Sci. Technol. J.*, 15 (1982) 283.
[12] M.P. Polo, D.G. De Llano and M. Ramos, in L.M.L. Nollet (Editor), *Food Analysis by HPLC*, Marcel Dekker, New York, 1992, pp. 117–139.
[13] D.G. De Llano, M.C. Polo and M. Ramos, *J. Dairy Res.*, 58 (1991) 363.
[14] K.F. Kaiser, H.D. Belitz and R.J. Fritsch, *Z. Lebensm.-Unters.-Forsch.*, 195 (1992) 8.
[15] S. Einarsson, B. Josefsson and S. Lagerkvist, *J. Chromatogr.*, 282 (1983) 609.
[16] I. Betner and P. Foldi, *LC · GC Int.* 3 (1988) 12.
[17] J.H. Kunte, A.E. Galnski and H.G. Truper, *J. Microbiol. Methods*, 17 (1993) 129.
[18] R. Cunico, A.G. Mayer, T. Wehr and T.L. Sheenan, *Biochromatography*, 1 (1986) 7.
[19] H.S. Shiraishi, K. Okuda, Y. Sato, N. Yamaoka and K. Tuzimura, *Agric. Biol. Chem.*, 37 (1973) 2427.

ELSEVIER

Journal of Chromatography A, 696 (1995) 219–225

JOURNAL OF CHROMATOGRAPHY A

Purification of antigenized immunoglobulins derivatized with monomethoxypolyethylene glycol

T.-D. Brumeanu, H. Zaghouani[1], C. Bona*

Department of Microbiology, Mount Sinai School of Medicine, Box 1124, New York, NY 10029, USA

First received 15 August 1994; revised manuscript received 19 December 1994; accepted 20 December 1994

Abstract

Genetically engineered immunoglobulins (Igs) carrying viral B or T cell peptides in the CDR3 loop, function as efficient delivery system of the defined viral epitopes. Two of these antigenized Igs (AIgs) were derivatized with 2-O-monomethoxypolyethylene glycol-4,6-dichloro-*s*-triazine (mPEG). Herein, we describe a two-step strategy to purify mPEG-derivatized AIgs (AIgs–mPEG). Unreacted mPEG polymers were removed by size-exclusion chromatography using ammonium hydrogencarbonate as a buffer system. Mildly PEGylated AIgs were isolated from free and highly derivatized AIgs by anion-exchange chromatography. Electrophoretic analysis indicated that the AIgs–mPEG preparation contained less than $4 \cdot 10^{-4}$ *M* unreacted mPEG. This strategy may be applied to other mPEG-derivatized monoclonal antibodies.

1. Introduction

Polyethylene glycol (PEG) is non-toxic, non-immunogenic, and is approved by the US Food and Drug Administration (FDA) for internal use in humans. PEG is commonly used as additive to food and drugs. PEGylated proteins preserve their biologic activity to various extends depending on the degree of PEGylation. Bovine serum catalase derivatized with 2-O-monomethoxypolyethylene glycol-4,6-dichloro-*s*-triazine (mPEG) at low ratio retained full enzymatic activity and it was more stable and soluble in aqueous solutions [1,2]. Derivatization of 7–14% of the primary amines of proteins, significantly increased the half life in blood circulation without loss of biologic activity [3]. Highly mPEG-derivatized immunoglobulins (18–25%) exhibited tolerogenic effect in mice [4]. Administration of PEGylated self peptides to mice with experimental autoimmune myasthenia Gravis suppressed the production of acetylcholine receptor specific autoantibodies [5].

The increase in half life of proteins modified with mPEG was correlated with high resistance to enzymatic degradation and low clearance rate through the kidneys [6]. Based on these observations many of the mPEG-derivatized enzymes, cytokines and monoclonal antibodies entered clinical trials as substitutes or immunotherapeutic agents [7–11].

Genetically engineered Ig molecules carrying viral B or T cell epitopes in the CDR3 loop can

* Corresponding author.

[1] Present address: University of Tennessee, Department of Microbiology, M409 Walters Life Science, Knoxville, TN 37996, USA.

0021-9673/95/$09.50
SSDI 0021-9673(94)01275-X

prime animals for the induction of specific immune responses [12–16]. Ig-HA is a BALB/c IgG2b antibody expressing in the CDR3 loop a T cell epitope (HA110–120) from the hemagglutinin of PR8 influenza virus [13]. Ig-HA was able to prime BALB/c mice and to mount virus-specific T helper response [13]. Ig-V_3C is a mouse variable-human γ_1/k constant regions, expressing within the heavy-chain CDR3 loop a B cell epitope from the V_3 cysteine bridged loop of the envelope protein of HIV-1. Ig-V_3C was able to induce virus-specific antibody response in baboons [16]. Herein we derivatized Ig-HA and Ig-V_3C with mPEG 5000 and attempted to purify the antigenized Igs (AIgs)–mPEG conjugates.

During the PEGylation process, various degrees of derivatization may occur as a consequence of the micro heterogeneity of the protein, the distribution of both the number and the position of attachment of PEG units, the inherent polydispersity of PEG polymers, and microenvironmental conditions of the reaction. In addition, dioxy-PEG that can cross-link proteins maybe present in commercial preparation as a result of hydrolysis of the ethylene oxide monomers during polymerization process [17,18]. Thus, protein–mPEG preparations may contain species of highly PEGylated and/or cross-linked proteins in addition to unreacted materials. Purification of the conjugates is therefore required prior to their use in biological systems. Purification of protein–PEG conjugates has always relayed on a single-step chromatographic removal of free PEG polymers [3,6,19,20]. Herein, we describe a two step-procedure able to remove free mPEG, free AIgs and heavily PEGylated AIgs leading to a relatively pure population of mildly PEGylated AIgs.

2. Experimental

2.1. Chemicals

AIgs (Ig-HA and Ig-V_3C) were generated in our laboratory as previously described [12–16]. PhastSystem electrophoresis apparatus, PhastGels 4–15% gradient of polyacrylamide and cyanogen bromide-activated Sepharose CL-4B were purchased from Pharmacia-LKB. Ultrogel AcA-44 and dialysis bags of 75 000 MWCO (molecular weight cut-off) were from Spectrum. Ultra concentrators of 100 000 MWCO (molecular weight cut-off) (Centrex UF-2, 2 ml volume) were from Schleicher & Schuell. Rat hybridoma cells secreting monoclonal anti-murine k chain antibodies and HP6053 mouse hybridoma producing anti-human k chain antibodies were from ATCC. The Q300 HPLC column (250 × 4.6 mm, 300 μm particle size) was from Rainin. Nessler's reagent and 2,4,6-trichloro-*s*-triazine-activated monomethoxypolyethylene glycol MWCO 5000 (mPEG 5000) were from Sigma. The agarose gels (Titan gel high-resolution protein kit) were from Helena Labs.

3.2. Purification of AIgs

Ig-HA and Ig-V_3C were affinity purified on a rat anti-murine k chain and mouse anti-human k chain antibody-Sepharose columns, respectively. Affinity purified AIgs were equilibrated in 0.1 *M* sodium tetraborate, pH 9.6 and concentrated to 1 mg/ml by ultracentrifugation using tubes of 100 000 MWCO.

3.3. Derivatization of AIgs with mPEG

A 10-mg amount of each AIg was derivatized with 2,4,6-trichloro-*s*-triazine-activated mPEG 5000 as described [20]. Briefly, a 50 times molar excess of mPEG was added to 10 mg AIgs in 10 ml of 0.1 *M* tetraborate buffer, pH 9.6. The mixture was stirred vigorously for 4 h at room temperature. The conjugate preparations were concentrated to 1.5 ml in tubes of 100 000 MWCO and further purified.

3.4. Chromatographic purification of AIg–mPEG conjugates

AIg–mPEG preparations were applied on an Ultrogel AcA-44 gel filtration column (80 × 1.6 cm) equilibrated with 0.1 *M* NH_4HCO_3, pH 8.5 and flow-rate of 0.4 ml/min. Fractions were collected at 4-min intervals, dried by speed vacuum centrifugation and resuspended in 0.5 ml

of 5 m*M* sodium acetate, pH 5. Each fraction was then analyzed for protein content by Biuret micro assay, and for the presence of free hydrolyzed mPEG by Nessler's reagent as described [4]. Fractions of the conjugates free of hydrolyzed mPEG were then rechromatographed on a Q300 anion-exchange HPLC column equilibrated with 5 m*M* sodium acetate, pH 5 using a 45-min linear gradient from 5 to 500 m*M* sodium acetate, pH 5, and flow-rate of 0.5 ml/min. Fractions from Q300 column were dialyzed in Spectrapor bags with 75 000 MWCO against phosphate-buffered saline (PBS) and concentrated in Centrex UF-2 tubes.

3.5. Electrophoretic analyses of AIg–mPEG conjugates

The purity of AIg–mPEG conjugate was analyzed by sodium dodecyl sulfate–polyacrylamide gel electrophoresis (SDS-PAGE) and mPEG was detected by electrophoresis on agarose gels. The SDS-PAGE was performed under non-reducing conditions as described by Laemmli [21]. Briefly, samples (5 μg) were resuspended in 5 μl of sample buffer (0.1% SDS, 0.1 *M* Tris–HCl, 6 *M* urea, pH 8.5) and incubated at 37°C for 2 h. Samples were run on 4–15% gradient PhastGel (Pharmacia) at 250 V and 5 W for 45 min at 15°C. The gel was then fixed and silver stained. Electrophoresis on agarose Titan gels was carried out according to the manufacture's instructions. Samples (10 μg in 5 μl barbital buffer) were run at 250 V for 30 min on duplicate gels. One gel was stained with a mixture of 0.1% Coomassie Blue R-250 and 1% Ponceau S, and the second gel was immersed in 20% trichloroacetic acid (TCA) in water for 30 s and immediately photo-scanned.

3.6. Fluorescamine assay

Graded amounts (1, 0.5 and 0.25 μg) of AIg–mPEG or AIgs in 25 μl of PBS were mixed with equal volume of fresh fluorescamine in acetone (150 mg/ml) and incubated for 5 min at room temperature. Samples were then brought to 1 ml with PBS and fluorescent intensity was measured at 475 nm emission versus 390 nm excitation. The percent of PEGylated primary amines was estimated according to the following formula $1 - (A_{475}$ AIgs–mPEG$/A_{475}$ AIgs$) \times 100$ [22].

4. Results and conclusions

4.1. Derivatization of AIgs with mPEG

Conjugation of proteins with mPEG increase the half life, solubility, and stability of the proteins. The biological activity may be reduced depending on the degree of PEGylation [1,2,6,7]. Igs engineered to carry viral peptides in the CDR3 loop are efficient delivery systems of viral epitopes to the immune system and induce virus-specific responses [12–16].

Preliminary experiments indicated that derivatization of 6–8% of the primary amines of AIgs with mPEG requires 50-fold molar excess of mPEG. Following the derivatization procedure described in the Experimental section, we PEGylated 10 mg of both Ig-HA and Ig-V_3C with mPEG. The chemical events involved in this PEGylation process are described in Fig. 1. mPEG has an active chlorine that can be substituted with the ϵ amino group of lysine residues at 18°C and pH 9.6. Since hydrolysis is faster than aminolysis, an excess of mPEG is required to achieve optimal coupling. A significant amount of hydrolyzed mPEG is thus generated. The reactivity of commercial mPEG 5000 varies from batch to batch, leading to different degrees of PEGylation. Preliminary experiments of PEGylation of bovine γ-globulins with the batch used in these studies indicated that the molar ratio Ig/mPEG of 1 to 50 was optimal to achieve 6 to 8% substitution of the primary amines.

Each of the AIg–mPEG preparation contained excess of free hydrolyzed PEG, unconjugated AIg, mildly and heavily conjugated AIgs. Only mildly PEGylated AIgs were of interest for our immunological studies. Thus, all other compounds had to be removed in order to perform pertaining evaluation of the effect of mild PEGylation on the immunogenicity of viral peptides grafted in the Igs.

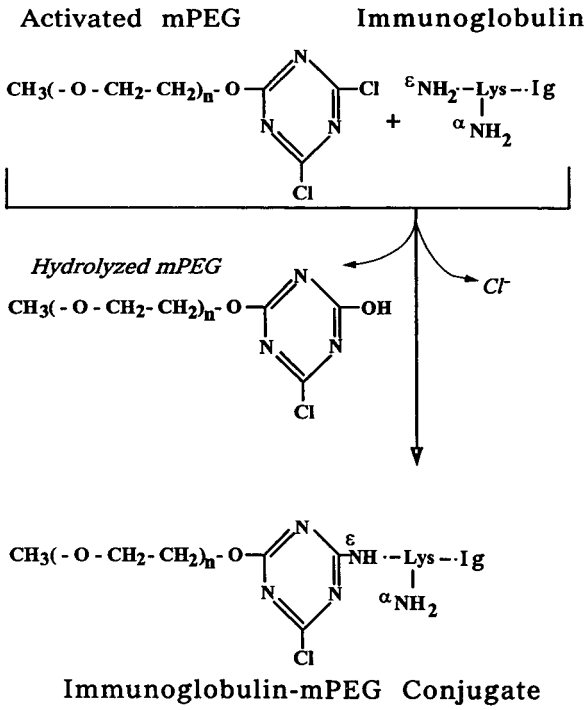

Fig. 1. Chemical reactions for the attachment of mPEG to AIgs.

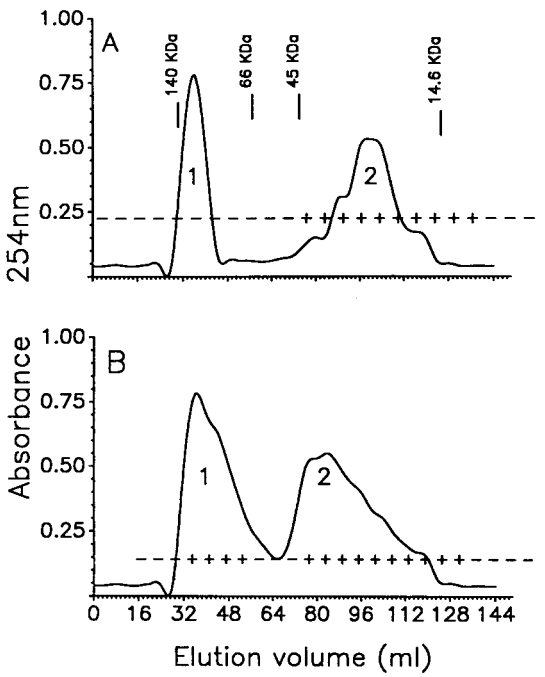

Fig. 2. Removal of hydrolyzed mPEG from AIg-mPEG preparation by size-exclusion chromatography. Ultrogel AcA-44 column (80 × 1.6 cm) was calibrated at 0.4 ml/min flow-rate with molecular mass markers (Pharmacia-LKB) and then loaded with 10 mg of Ig-HA–mPEG preparation. The column was equilibrated with either 0.1 *M* NH_4HCO_3 (A) or PBS (B). Peak 1 contained the conjugates and peak 2 corresponds to free mPEG. A plus sign indicates the presence of free polymer as detected by Nessler's test. KDa = kilodalton.

4.2. Chromatographic removal of free mPEG from AIg–mPEG preparations

During the conjugation process significant amounts of hydrolyzed mPEG are generated. Removal of excess of free mPEG is the foremost step for purification of AIgs–mPEG conjugates. To this aim, samples were applied on Ultrogel AcA-44 equilibrated in ammonium hydrogencarbonate. AIg–mPEG conjugates were eluted in the exclusion volume and were tested for the presence of free PEG using Nessler's reagent. As indicated in Fig. 2, AIgs–mPEG as well as unconjugated AIgs are eluted in the exclusion volume (peak 1). Free hydrolyzed mPEG eluted in later fractions (peak 2). It should be noted that free mPEG which is of M_r 5000 has an unusual elution profile between M_r 15 000–45 000 in agreement with previous observations [17,23]. Equilibration of the column with ammonium hydrogencarbonate allowed for a better removal of free mPEG than the equilibration with PBS, as indicated by Nessler's test. The improved resolution obtained with ammonium hydrogencarbonate maybe related to better neutralization of the active charges on gel matrix and therefore lower interactions between free mPEG polymer and the matrix.

4.3. Removal of the unreacted compounds from AIg–mPEG conjugates

Because no one-step procedure for the separation of protein–mPEG conjugates from unreacted compounds is described, we chose a method that includes a first-step removal of hydrolyzed mPEG and a subsequent step that

removes underivatized and highly derivatized AIgs. Since the size-exclusion limit of the Ultrogel AcA-44 column is 140 000 kDa, hydrolyzed mPEG can be removed but the underivatized AIgs can not. The removal of excess mPEG is required because it could interfere with the isolation of the conjugates in the subsequent anion-exchange chromatography step. Preliminary experiments performed on anion-exchange HPLC columns as a single step of purification, showed poor resolution and low yields even if minimal amounts of sample were applied on the column. In fact, the conjugates showed a broad elution profile as a result of the presence of excess of free polymers which interfere strongly with the binding of conjugates to the anion-exchange matrix. Poor resolution of PEGylated proteins was also described when conjugates were separated by charge-reversal capillary zone electrophoresis without previous removal of free PEG [19,23]. The authors concluded that it is of great importance to remove free polymers from the conjugate preparation in order to obtain good resolution in different separating media.

To isolate mildly PEGylated AIgs with 6–8% degree of PEGylation, we rechromatographed the conjugates on anion-exchange HPLC column under optimized conditions as described in the Experimental section. Fig. 3 shows the elution profiles of Ig-HA–mPEG (Fig. 3a) and free Ig-HA (Fig. 3b). In the case of Ig-HA–mPEG, three major peaks were eluted from the column and labeled 1, 2 and 3 (Fig. 3a). Peak 3 represents free Ig-HA since it elutes at the same salt concentration as the unconjugated control Ig-HA. The material of peak 1 may represents highly PEGylated AIgs that could not bind to the matrix. Peak 2 seems to contain mildly PEGylated Ig-HA as revealed by SDS-PAGE analysis.

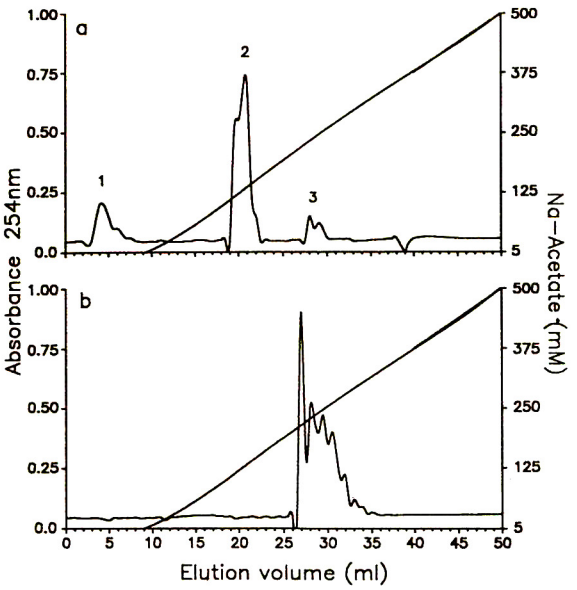

Fig. 3. Removal of un-PEGylated AIgs from AIg–mPEG preparations by anion-exchange HPLC. The material of peak 1 in Fig. 2, presumably Ig-HA–mPEG and other materials (a) and un-PEGylated Ig-HA preparation (b) were loaded onto Q300 anion-exchange HPLC column and chromatographed as described in the Experimental section.

4.4. Analysis of the purity of AIg–mPEG conjugates

The purity of AIgs–mPEG preparations was further analyzed for the presence of traces of free mPEG and unconjugated AIgs by electrophoresis on agarose and polyacrylamide gels, respectively. Although purification of AIgs–mPEG conjugates followed one-step purification by size exclusion chromatography, small amounts of free mPEG that could not be detected by Nessler's test may be present in the conjugate preparations. To trace small amounts of free PEG that could interfere with the immunogenicity of the AIgs–mPEG we developed an original, sensitive electrophoretic technique able to detect μM of free mPEG. Based on the observation that mPEG migrate on agarose to the cathode and can be visualized by TCA precipitation but not by protein dyes, we attempted to trace free mPEG in our preparation by electrophoresis on Titan gel followed by TCA precipitation. As can be seen in Fig. 4, left panel, Ig-HA–mPEG preparation obtained from the second chromatographic purification (lane 1) like un-PEGylated Ig-HA preparation (lane 2), did not show detectable amount of free hydrolyzed mPEG while the preparation collected from the first chromatographic purification con-

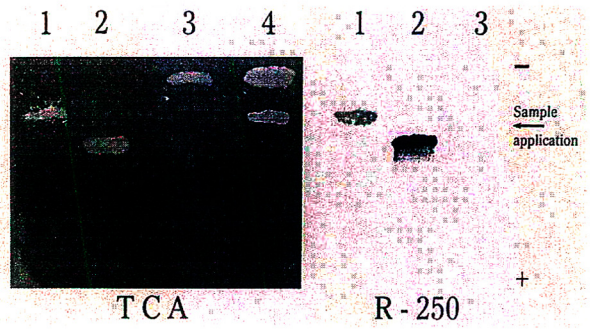

Fig. 4. Detection of residual mPEG in AIgs–mPEG preparations by electrophoresis on Titan agarose gel. Samples collected at various steps of purification were run on duplicate Titan gels and either stained with Coomassie/Ponceau (R250) or precipitated with TCA. Lanes: 1 = Ig-HA–mPEG conjugate after purification on anion-exchange HPLC; 2 = un-PEGylated Ig-HA; 3 = mPEG 5000 ($4 \cdot 10^{-4}$ *M*); 4 = Ig-HA–mPEG conjugate after first step of purification by gel filtration on AcA-44 (not done in Coomassie staining).

tained residual free PEG (lane 4). The amount of free residual mPEG, if any, in the final Ig-HA–mPEG preparation (lane 1) should be lower than $4 \cdot 10^{-4}$ *M*. Calibration experiments indicated that as little as $4 \cdot 10^{-4}$ *M* of mPEG 5000 can be detected using this technique (lane 3).

When a duplicate gel was stained with Coomassie/Ponceau (Fig. 4, right panel), only Ig-HA and Ig-HA–mPEG conjugates were revealed (lanes 1 and 2, respectively) but not free hydrolyzed mPEG (lane 3). Interestingly, PEGylated Ig-HA showed better staining with Ponceau S than un-PEGylated Ig-HA. The differential staining maybe attributed to different ability of the two dyes to access their specific sites on the native protein versus the PEGylated one.

Using this assay, we were also able to trace free mPEG polymers in preparations of chicken egg ovalbumin–mPEG, bovine serum albumin–mPEG and bovine γ-globulin–mPEG conjugates (not shown). Although our electrophoretic technique shows a sensitivity of detection for mPEG similar to that of Childs' assay [24] or the test of Schiavon et al. [25], it has the advantage of distinguishing free PEG from PEG attached to proteins.

To investigate the extend to which AIgs–mPEG preparations were depleted of free and highly PEGylated AIgs, we analyzed the Ig-HA–mPEG and Ig-V_3C–mPEG conjugates by SDS-PAGE on 4–15% gradient gels (PhastGels, Pharmacia) under non-reducing conditions. The results in Fig. 5 show that the final Ig-HA–mPEG and Ig-V_3C–mPEG preparation (peak 2 in Fig. 3) were pure (second and fourth lanes, respectively) and did not contain un-PEGylated Ig-HA and Ig-V_3C. They also did not contain highly PEGylated AIgs. Since the 4–15% gradient gels offer a high resolution for proteins within the range of M_r 50 000–350 000, it is possible to distinguish mild (6–8%) from heavily (15% up) PEGylated AIgs. In Fig. 5, lanes 3 and 6 show the presence of material with $M_r > 250\,000$, indicating that high PEGylation can still take place at a low ratio of 1:50. After anion-exchange HPLC purification, two major populations of Ig-HA–mPEG conjugates migrating

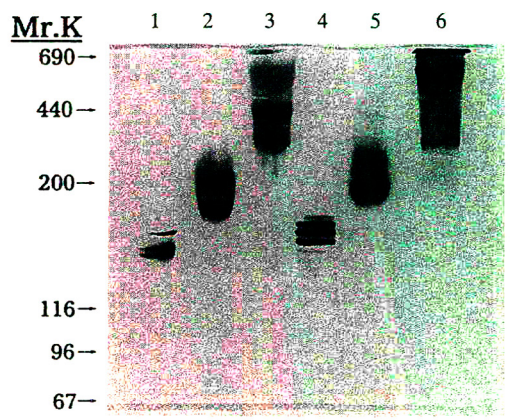

Fig. 5. Analysis of the purity of AIg–mPEG preparations by SDS-PAGE. Samples collected subsequent to purification on anion-exchange HPLC were analyzed on 4–15% polyacrylamide gradient PhastGels (Pharmacia) under non-reducing conditions. First and fourth lanes = un-PEGylated Ig-HA and Ig-V_3C, respectively; second and fifth lanes = Ig-HA–mPEG and Ig-V_3C–mPEG, respectively (content of peak 2 in Fig. 3); and third and sixth lanes = highly derivatized Ig-HA and Ig-V_3C (content of peak 1 in Fig. 3).

between M_r 200 000 and 250 000 (lane 2) were revealed, indicating a mild PEGylation. The degree of PEGylation of these populations was 6–8% according to fluorescamine assay.

The sensitivity of detection of un-PEGylated AIgs corresponds to the limit of detection of silver staining that is approximately 0.05 μg of free AIg. Considering that 5 μg of conjugate were loaded on the SDS-PAGE gels, the preparation contains 1% of free AIgs but 99% of conjugated AIgs.

In summary, we were able to isolate relatively pure populations of AIg–mPEG with 6–8% degree of derivatization as indicated by the electrophoretic and fluorescamine assays. Mildly PEGylated Ig-HA showed a long half life in blood circulation and induced strong T cell activation in vivo. Also mildly PEGylated Ig-V_3C–mPEG was able to elicit anti-V_3C antibody response in mice [26]. Derivatization of the AIgs with mPEG may increase their half life and therefore their efficacy in delivering the viral peptides to the immunocompetent cells.

Acknowledgements

We thank Dr. B. Leveugle, G.M. Lang and E. Siden for helpful discussion.

References

[1] A. Abuchowski, T. van Es, N.C. Palczuk and F.F. Davis, *J. Biol. Chem.*, 252 (1977) 3578–3581.
[2] A. Abuchowski, J.R. McCoy, N.C. Palczuk, T. van Es and F.F. Davis, *J. Biol. Chem.*, 252 (1977) 3582–3586.
[3] K. Kitamura, T. Takahashi, T. Yamaguchi, A. Noguchi, K. Takasina, H. Tsurumi, M. Inagake, T. Toyokuni and S. Hakomori, *Cancer Res.*, 51 (1991) 4310–4315.
[4] I. Wilkinson, C.J.C. Jackson, G.M. Lang, V. Strevens-Holford, and A.H. Sehon, *Immunol. Lett.*, 15 (1987) 17–22.
[5] M.Z. Atassi, K.H. Ruan, K. Jinnai, M. Oshima and T. Ashizawa, *Proc. Natl. Acad. Sci. U.S.A.*, 89 (1992) 5852–5856.
[6] R.A. Cunningham, Z. Zhou, B. Griffith and J.J. Keenan, *Immunol. Methods*, 152 (1992) 177–190.
[7] K. Kawashima, H. Takeshima, Y. Higashi, M. Hamaguchi, H. Sugie, I. Imamura and H. Wada, *Leuk. Res.*, 15 (1991) 525–530.
[8] N.V. Katre, M.J. Knauf and W.J. Laird, *Proc. Natl. Acad. Sci. U.S.A.*,, 84 (1987) 1487–1491.
[9] C. Caliceti, O. Schiavon, A. Mocali and F.M. Veronese, *Farmaco*, 44 (1989) 711–720.
[10] K. Nho, D. Glower, S. Bredehoeft, H. Shankar, R. Shorr and A. Abuchowski, *Biomater. Artif. Cells Immobilization Biotechnol.*, 20 (1992) 511–524.
[11] P.L. Lisi, T. van Es, A. Abuchowski, N.C. Palczuk and F.F.J. Davis, *Appl. Biochem.*, 4 (1982) 19–33.
[12] H. Zaghouani, M. Krystal, H. Kuzu, T. Moran, H. Shah. Y. Kuzu, J. Schulman and C. Bona, *J. Immunol.*, 148 (1992) 3604.
[13] H. Zaghouani, R. Steinman, R. Nonacs, R. Shah, W. Gerhard, and C. Bona, *Science*, 259 (1993) 224.
[14] H. Zaghouani, Y. Kuzu, H. Kuzu, T.-D. Brumeanu, W.J. Swiggard, R.M. Steinman and C. Bona, *Eur. J. Immunol.*, 23 (1993) 2746–2750.
[15] T.D. Brumeanu, W.J. Swiggard, R.M. Steinman, C.A. Bona and H. Zaghouani, *J. Exp. Med.*, 178 (1993) 1795–1799.
[16] H. Zaghouani et al., *Proc. Natl. Acad. Sci. U.S.A.*, in press.
[17] B. Selisko, C. Delgado, D. Fisher and R. Ehwald, *J. Chromatogr.*, 641 (1993) 71–79.
[18] J.M. Harris and M. Yalpani, in D.E. Brooks and D. Fisher (Editors), *Partitioning in Aqueous Two-Phase Systems*, Academic Press, Orlando, FL, 1985, p. 593.
[19] J. Snider, C. Neville, L.-C. Yan and J. Bullock, *J. Chromatogr.*, 599 (1992) 141–155.
[20] C.-J.C. Jackson, J.L. Charlton, K. Kuzminski, M.G. Land, and A.H. Sehon, *Anal. Biochem.*, 165 (1987) 114–127.
[21] U.K. Laemmli, *Nature (London)*, 227 (1970) 680–685.
[22] C.J. Neville, J.L. Snider, J. Bullock and L.-C. Yuan, presented at the *6th Annual Meeting of the American Association of Pharmaceutical Scientists, Washington, DC, 17–21 November 1991.*
[23] P. McGoff, A.C. Baziotis and R. Maskiewicz, *Chem. Pharm. Bull.*, 36 (1988) 3079.
[24] C.E. Childs, *Microchem. J.*, 20 (1975) 190–192.
[25] O. Schiavon, L. Sartore, P. Caliceti and F.M. Veronese, *Farmaco*, 45 (1990) 791–795.
[26] T.-D. Brumeanu et al., *J. Immunol.*, (1995) in press.

ELSEVIER

Journal of Chromatography A, 696 (1995) 227–234

JOURNAL OF CHROMATOGRAPHY A

Limitations of ion chromatography with post-column reaction for determination of heavy metals in waters containing strong chelating agents

M. Teresa Vasconcelos*, Carlos A.R. Gomes

LAQUIPAI, Chemistry Department, Faculty of Science of Oporto, P-4000 Porto, Portugal

First received 20 July 1944; revised manuscript received 15 December 1994; accepted 23 December 1994

Abstract

A published method for the determination of heavy metals was applied to the determination of Cu(II), Ni(II), Zn(II) and Mn(II) in synthetic solutions that contained one of the following ligands (L): citrate, nitrilotriacetate (NTA), ethylenediaminetetraacetate acid (EDTA) and cyclohexylenediaminetetraacetate (CDTA). The method involves on-column derivatization with 2,6-pyridinedicarboxylic acid (PDCA) and ion-exchange separation, followed by post-column reaction with 4-(2-pyridylazo)resorcinol (PAR) to form metal–PAR chelates, which can be sensitively monitored by spectrophotometric detection at 520 nm. Solutions with 12.6 μmol/l of Cu(II), Ni(II), Zn(II) and Mn(II) and 12.6 or 25.2 μmol/l of L were analysed. A 100% recovery was obtained for all metals with citrate or NTA, for Cu(II), Zn(II) and Mn(II) with EDTA and only for Mn(II) with CDTA. The recoveries in further cases were Ni(II)–EDTA $\leq$68%, Ni–CDTA $\leq$80%, Cu(II)–CDTA $\leq$20% and Zn(II)–CDTA $\leq$87%. To interpret these results, simpler solutions with 12.6 or 6.3 μmol/l Cu(II) and Cu:L ratios (R) in the range 4.2–0.26 were analysed. For both citrate and NTA an almost 100% recovery of Cu(II) was found for all values of R. For EDTA, 100% recovery was only observed for $R \geq 1.0$. For CDTA the recoveries were between 76% ($R = 4.2$) and 0% ($R \leq 0.52$). Speciation calculations showed that only kinetic factors were responsible for the inefficiency of both the on-column and the post-column derivatizations. Analytical implications of the results are discussed.

1. Introduction

One of the most satisfactory methods for the determination of transition metals by high-performance liquid chromatography (HPLC) involves a cation-exchange (or a mixed cation- and anion-exchange) separation followed by post-column complexation with 4-(2-pyridylazo)resorcinol (PAR), to form chelates which can be sensitively monitored by spectrophotometric detection [1]. To facilitate transition metal separation without the need for concentrated eluent solutions, complexing agents are also included in the mobile phase to provide on-column (or in situ) derivatization. 2,6-Pyridinedicarboxylic acid (PDCA) is one of the most commonly used reagents for this purpose.

When a sample solution which contains metal ions in free (hydrated) form is injected into a flow of eluent which contains PDCA, metal

* Corresponding author.

0021-9673/95/$09.50
SSDI 0021-9673(94)01295-4

complexes are formed (electric charges were omitted for the sake of simplicity):

$$M + PDCA \rightleftharpoons M\text{–}PDCA \quad (1)$$

Anion exchange in the column, conditioned by the relative affinity of the complexes to the resin, is responsible by the separation of the different complexes:

$$M\text{–}PDCA + resin\text{–}PDCA \rightleftharpoons resin\text{–}(M\text{–}PDCA) + PDCA \quad (2)$$

After elution, the complexes with PDCA are converted into coloured complexes in the post-column reaction system, by reaction with PAR, and detected by spectrophotometry at 520 nm:

$$M\text{–}PDCA + PAR \rightleftharpoons M\text{–}PAR + PDCA \quad (3)$$

The suitability of this method depends on the following chemical factors: (i) high thermodynamic stability of the complexes formed in reactions 1 and 3, and (ii) rapid kinetics of ligand substitution in both reactions. PDCA and PAR, which are used in very large excess relative to the metal, satisfy these requirements.

One of the main fields of application of this ion chromatographic (IC) method is the determination of heavy metals in natural or residual waters. In the case of industrial effluents, the waters may contain aminopolycarboxylic acids, e.g., nitrilotriacetic acid (NTA) and ethylenediaminetetraacetic acid (EDTA), which are widely used in industrial processes and as additives in detergents [2–4]. These chelating agents produce complexes of high thermodynamic stability and low rate of dissociation. However, little attention has been paid to establishing whether strong chelating agents such as these in the sample interfere in the IC method.

The purpose of this work was to evaluate the interference of citrate (Cit), nitrilotriacetic acid (NTA), ethylenediaminetetraacetic acid (EDTA) and cyclohexylenediaminetetraacetic acid (CDTA) in a procedure recommended by Dionex to be performed with their equipment [5], which involves on-column (with PDCA) and post-column (with PAR) derivatizations. These ligands (L) were selected because they form complexes with very diverse stability constants. First, the method was applied to a mixture of Cu(II), Ni(II), Zn(II) and Mn(II) and severe interferences of EDTA and CDTA were found. As the interpretation of the results was very difficult, owing to the complexity of the chemical system, a more detailed study was performed only for copper(II), selected because in the Irving–Williams series it is the metal that forms the most stable complexes.

The efficiencies of (i) the overall procedure, e.g., on-column plus post-column reactions, and (ii) of only the post-column derivatization were studied. For the latter purpose, the set of separation columns were replaced by a simple tube which transports quickly and without separation the sample from the injection loop to the post-column reaction system. The interpretation of the experimental results is based on both thermodynamic and kinetic considerations. For this purpose, speciation calculations based on stoichiometric stability constants from the literature were performed for the systems Cu–PDCA–L or Cu–PAR–L in the ranges of concentrations used in the study. Further, kinetic measurements were carried out to estimate the rate of dissociation of the Cu–L complexes in the chromatographic system. Some important consequences of the results are discussed.

2. Experimental

2.1. Reagents, solutions and apparatus

All reagents were of analytical-reagent grade. All solutions were prepared with deionized water with conductivity <0.1 μS/cm. Standard solutions of metallic cations were in the nitrate form. The compositions of the buffer solutions used for the several types of experiments are given in Table 1.

A DX 300 IC system from Dionex was used. The system included a 50-μl loop, an IonPac CG5 guard column (50 × 4 mm I.D.), an IonPac CS5 analytical column (250 × 4 mm I.D.) and a post-column reaction (PCR) system composed of a DQP-1 isocratic peristaltic pump and a mem-

Table 1
Buffer solutions

Buffer	Composition	pH
T1	5 mmol/l NaOAc–5 mmol/l HOAc	4.5
T2	6 mmol/l PDCA–50 mmol/l NaOAc–50 mmol/l HOAc	4.4
R1	0.2 mmol/l PAR–3 mol/l NH_3–1 mol/l HOAc	10.4
R2	0.2 mmol/l PAR–50 mmol/l NaOAc–50 mmol/l HOAc	4.6

brane reactor (MR). After the membrane reactor, a reaction coil of length 234 mm was used. A Model 204 UV–Vis detector from Konik with a 9-μl cell was used.

2.2. Separation and detection

The following two IC configurations were used: IC(A), Dionex columns for separation and T2 buffer solution (Table 1) as mobile phase; IC(B), similar to IC(A) but the columns were replaced with a 450 mm × 0.25 mm I.D. polyether ether ketone tube. Four standard solutions with metal concentrations between 3 and 16 μmol/l prepared in buffer T1 were used for calibration.

2.3. Kinetics

To determine the rate constant of the Cu–L dissociation (see discussion below), 500 μl of a pre-equilibrated 1:1 Cu–L solution which was 400 μmol/l in copper(II) were mixed with stirring with 20 ml of buffer R1 (Table 1) to attain a final solution with [Cu–L]/[PAR] ratios $\geq$1:20. This solution was immediately ($t = 0$ s) injected into the spectrophotometer cell with stopped flow, and the rate of appearance of Cu–PAR at 508 nm (absorbance maximum of that complex) was measured with time (t) at constant ln t intervals. The data were collected in a PC and stored to be processed later. For the calculation of the rate constant of the reaction under study, the absorbance of the $Cu(PAR)_2$ after each period of time (A_t) was subtracted from the final absorbance (A_∞). The experiments were repeated for solutions in which buffer R1 had been replaced with buffer R2 (Table 1) to study the influence of both the pH and solution composition on the kinetic behaviour.

3. Results and discussion

3.1. Heavy metal determination

A widely used procedure [5–7] [IC(A) configuration] was applied to determine total heavy metal concentrations in synthetic solutions with and without L at pH 4.5. Results were obtained for solution containing a pre-equilibrated mixture of 12.6 μmol/l each of Cu(II), Ni(II), Zn(II) and Mn(II) and 12.6 or 25.2 μmol/l of L (L = CDTA, EDTA, NTA, Cit). For Cit and NTA, 100% recoveries were found for all the metals at both L concentrations. However, as Fig. 1 shows, for EDTA low recoveries were observed for Ni(II) viz., 68% and 36% for 12.6 and 25.2 μmol/l, respectively. For CDTA, low recoveries occurred for Cu(II) (19% and 0%, respectively), Ni(II) (83% and 68%) and Zn(II) (87% and 51%), but not for Mn(II). The complexity of the sample, where competition of several chemical equilibria takes place, rendered the interpretation of the results very difficult.

Therefore, simpler solutions containing copper(II) only and Cu:L ratios (R) between 4.2 and 0.26 were used as synthetic samples for a more detailed study. A single chromatographic peak for a retention time (t_r) of 7.86 ± 0.02 min ($n = 58$, $P = 0.05$) was observed for both "samples" and standards, which indicates that the peak corresponds to the metal that was retained in the separation column (hydrated form plus labile complex on the time-scale of the chromatographic separation). The recoveries of cop-

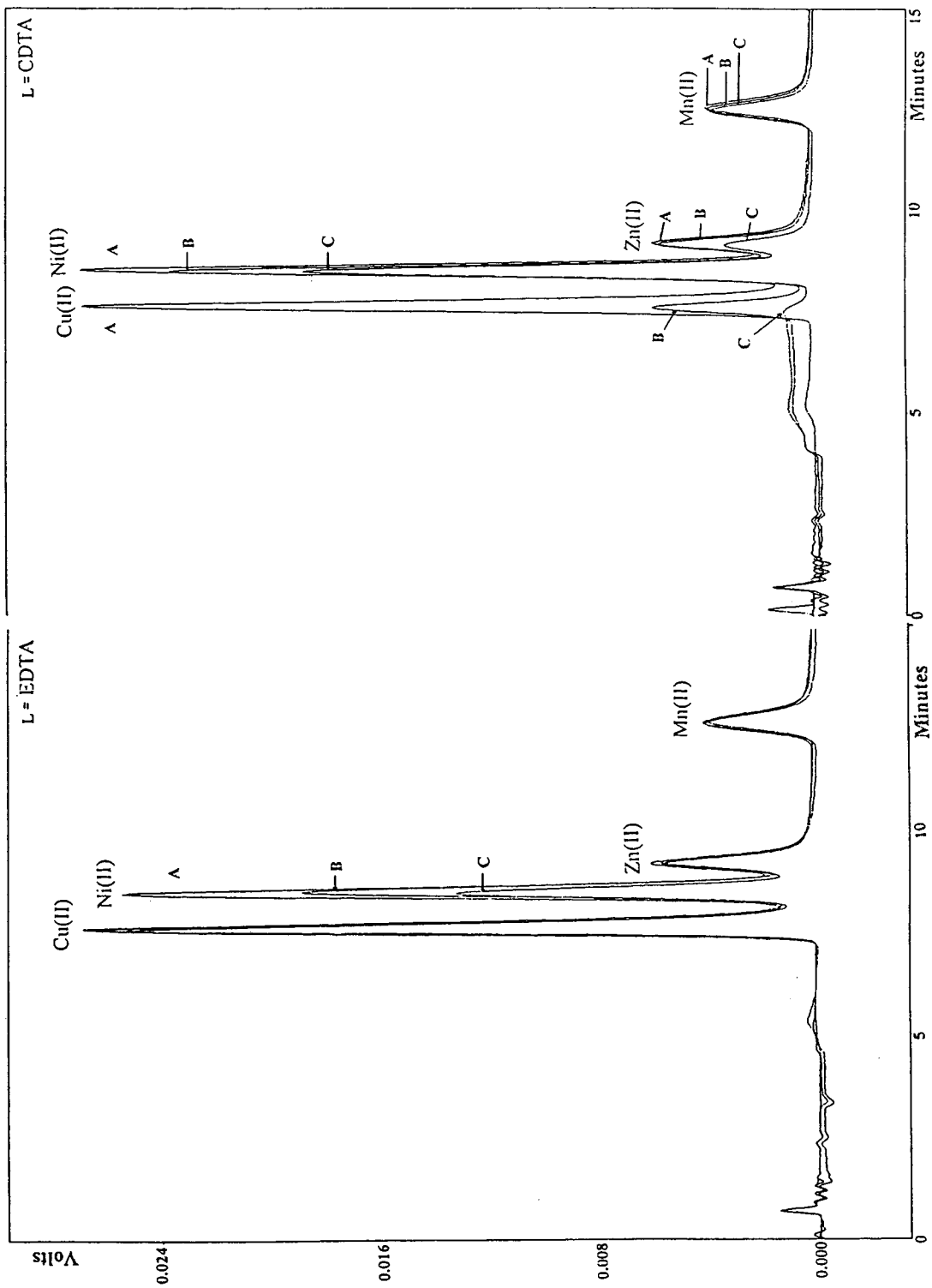

Fig. 1. Overlapping of typical chromatograms obtained with the IC(A) configuration for a mixture of 12.6 μmol/l of heavy metals (A) without and with (B) 12.6 μmol/l and (C) 25.2 μmol/l EDTA (left) or CDTA (right), prepared in buffer T1 (pH 4.5). Eluent, 6 mmol/l PDCA–50 mmol/l sodium acetate–50 mmol/l acetic acid; flow-rate of eluent, 1 ml/min; separation column, IonPac CG5 + IonPac CS5; post-column reagent, 0.2 mmol/l PAR–3 mol/l NH_3–1 mol/l acetic acid; flow-rate of post-column reagent, 0.71 ml/min; loop volume, 50 μl.

Table 2
Copper recovery (%) obtained with procedure IC(A)

Cu(II)[a]:L	CDTA		EDTA		NTA		Cit
	T1	T2	T1	T2	T1	T2	T1
4.20	74.6 ± 5.2		100.3 ± 1.1		104.5 ± 1.1		99.7 ± 5.7
2.10	71.4 ± 2.0		100.5 ± 1.1		103.7 ± 1.1		101.9 ± 10.1
1.05	12.7 ± 2.0		100.3 ± 5.0		99.7 ± 8.0		102.9 ± 9.9
0.53	ND[b]		92.1 ± 5.2		99.7 ± 8.2		102.4 ± 9.9
0.26	ND	99.9 ± 0.75	89.7 ± 5.2	101.4 ± 3.8	102.4 ± 12.0	101.1 ± 1.2	100.0 ± 10.4

Mean values and confidence limits ($P = 0.05$, $n = 3$) are given.
[a] [Cu(II)] = 12.6 μmol/l.
[b] ND = Not detected.

per(II) are presented in Table 2, which shows that no inferences of Cit or NTA were found even when the concentration of any of these was about four times higher than that of the metal. Interference of EDTA was observed when $R \leq 0.5$, and marked interference of CDTA was found even with a ligand deficiency: for instance, for $R = 4.2$, the copper(II) recovery was 76% and total suppression of the chromatographic peak occurred for $R < 0.5$. Similar results were obtained for 6.3 μmol/l Cu(II) and an identical R range.

These results are a consequence of the fact that when the analyte is in the form of a very stable complex in the "sample", the reaction which takes place on-column is not that in Eq. (1) but

$$M\text{–}L + PDCA \rightleftharpoons M\text{–}PDCA + L \quad (4)$$

The extension of the ligand substitution on the time-scale of the chromatographic procedure depends on the thermodynamic and kinetic factors.

Speciation calculations (performed by the program SPECIATE, Microsoft Basic V7 version, developed according the COMPLEX [8] algorithm program) based on stoichiometric stability constants from the literature [9–11] were performed for the different chemical Cu–PDCA–L systems (and also for the other metals used in this study) as pH 4.5 for the ranges of concentrations used. For all types of L and all values of R, the Cu–PDCA complexes predominate under equilibrium conditions. These results show that the low copper(II) recoveries observed were mainly due to kinetic factors. Indeed, when PDCA was added to the sample before the analysis, e.g., when buffer T1 was replaced with buffer T2 (see Table 1), the copper(II) recovery became virtually 100% in all cases (Table 2). Instead of the batch inclusion of PDCA in the sample, on-line precolumn derivatization with PDCA (in a coil of length 234 mm) was also carried out, but although the efficiency increased, low Cu(II) recoveries were still found: for instance, for $R = 0.26$, the recovery was only 91.01 ± 0.91% (confidence limits, $P = 0.05$, $n = 3$) for EDTA and 1.63 ± 0.25% for CDTA. Longer precolumn reaction coils were not used, because they induce dispersion of the analyte in the eluent and broadening of the peaks, which reduces the efficiency of the process.

3.2. Performance of the detection system

The occurrence of a single chromatographic peak, which appeared for a t_r identical with that for the standard solutions [all the copper(II) in the hydrated form], indicate that the copper(II) fraction in the Cu–L (L = EDTA or CDTA) form not substituted on-column was not detected. Therefore, the replacement of L by PAR in the post-column reactor:

$$Cu\text{–}L + PAR \rightleftharpoons Cu\text{–}PAR + L \quad (5)$$

also did not occur, again for kinetic reasons. Indeed, speciation calculations [8] similar to those mentioned above for Cu–PAR–L systems showed that virtually 100% of the copper was in the Cu–PAR form when equilibrium conditions were attained.

The efficiency of the post-column reaction system to provide complete conversion of Cu–L to Cu–PAR (Eq. 5) was also evaluated separately. For this purpose, the separation column was replaced with a simple tube [IC(B) configuration] to ensure that all the copper(II) from the sample (independently of its chemical form) reached the detection system at virtually the same time. Experiments were performed for Cu–EDTA solutions with R between 4.12 and 0.26. It was found that when EDTA was in excess relative to the metal, the recovery of copper(II) was much lower than 100% (78.5% for $R = 0.52$ and 65.4% for $R = 0.26$), corresponding to incomplete replacement of EDTA by PAR.

3.3. Kinetic aspects

Another set of experiments was carried out to obtain information about the rate of dissociation of the different Cu–L complexes. Cu–L solutions (1:1) (e.g., with $R = 1$) were mixed with a solution of PAR, with a large excess relative to L ([PAR] = 20[L]), and the absorbance of Cu–PAR in the mixture was measured with time (experimental details as above). If pseudo-first-order kinetics relative to Cu–L are assumed, the rate of formation of the Cu–PAR complex, d[Cu–PAR]/dt, is given by

$$\frac{\mathrm{d[Cu\text{–}PAR]}}{\mathrm{d}t} = {}^{*}k_{\mathrm{d}}[\mathrm{Cu\text{–}L}] \qquad (6)$$

where ${}^{*}k_{\mathrm{d}}$ is the pseudo-first-order rate constant of reaction 5.

The formation of the Cu–PAR complex is almost instantaneous [12], hence it can be assumed that the rate-determining step of reaction 5 is the dissociation of the Cu–L complex [12,13]:

$$\mathrm{Cu - L} \xrightarrow{k_{-1}} \mathrm{Cu + L} \qquad (7)$$

Therefore, if PAR is in large excess, the determination of the rate constant of reaction 5, ${}^{*}k_{\mathrm{d}}$, will provide an estimate of the rate constant of reaction 7, k_{-1}.

Kinetic experiments were performed at two pH values: 10.4 (buffer solution R1), and 4.6 (buffer solution R2). The pH of 10.4 was that used in the post-column reagent in the chromatographic determinations. However, as the mobile phase in procedure IC(A) had a pH of 4.4 (buffer T2), measurements at a similar pH (buffer R_2, pH 4.6) could provide an estimate of the on-column (Eq. 4) dissociation rate of Cu–L.

The rate constant of reaction 5 could not be determined for Cu–NTA and Cu–Cit because the reactions were too fast to allow the measurement of A_t with the rudimentary device used in this work. In fact, A_∞ (e.g., for stabilized signal) had already been attained when the solution arrived at the detector cell. Therefore, it was concluded that ${}^{*}k_{-1} > 0.2\ \mathrm{s}^{-1}$ (calculated assuming that the equilibrium position was attained for $t = 30$ s). For Cu–EDTA at pH 10.4, although slower than for the Cu–NTA and Cu–Cit complexes, reaction 5 was still too fast to allow accurate results. However, for Cu–EDTA at pH 4.6 and especially for Cu–CDTA at both pH values, the reaction was sufficiently slow for measurement.

Fig. 2 illustrates the results obtained for Cu–CDTA (for Cu–EDTA similar behaviour was observed). The function $\ln(A_\infty - A_t) = f(t)$ was almost linear (correlation coefficient of the adjustment by least squares >0.99), which suggests that pseudo-first-order kinetics describe reaction 5 and, therefore, reaction 7. From the slopes, k_{-1} values were calculated (Table 3). The k_{-1} values are lower for Cu–CDTA than for Cu–EDTA at both pH values, and are compatible with the results obtained by the IC(A) procedure. The rigid and voluminous cage structure of CDTA, which causes steric hindrance, prevents direct attack of the metallic centre of Cu–CDTA by PAR.

Table 3 also shows that ${}^{*}k_{\mathrm{d}}$ is about one order of magnitude higher at pH 10.4 than at pH 4.6 for Cu–EDTA, whereas for Cu–CDTA ${}^{*}k_{\mathrm{d}}$ is similar at both pH values. This is probably due to the presence of 3 mol/l of ammonia in the R2 buffer solution (pH 10.4). Reactions with am-

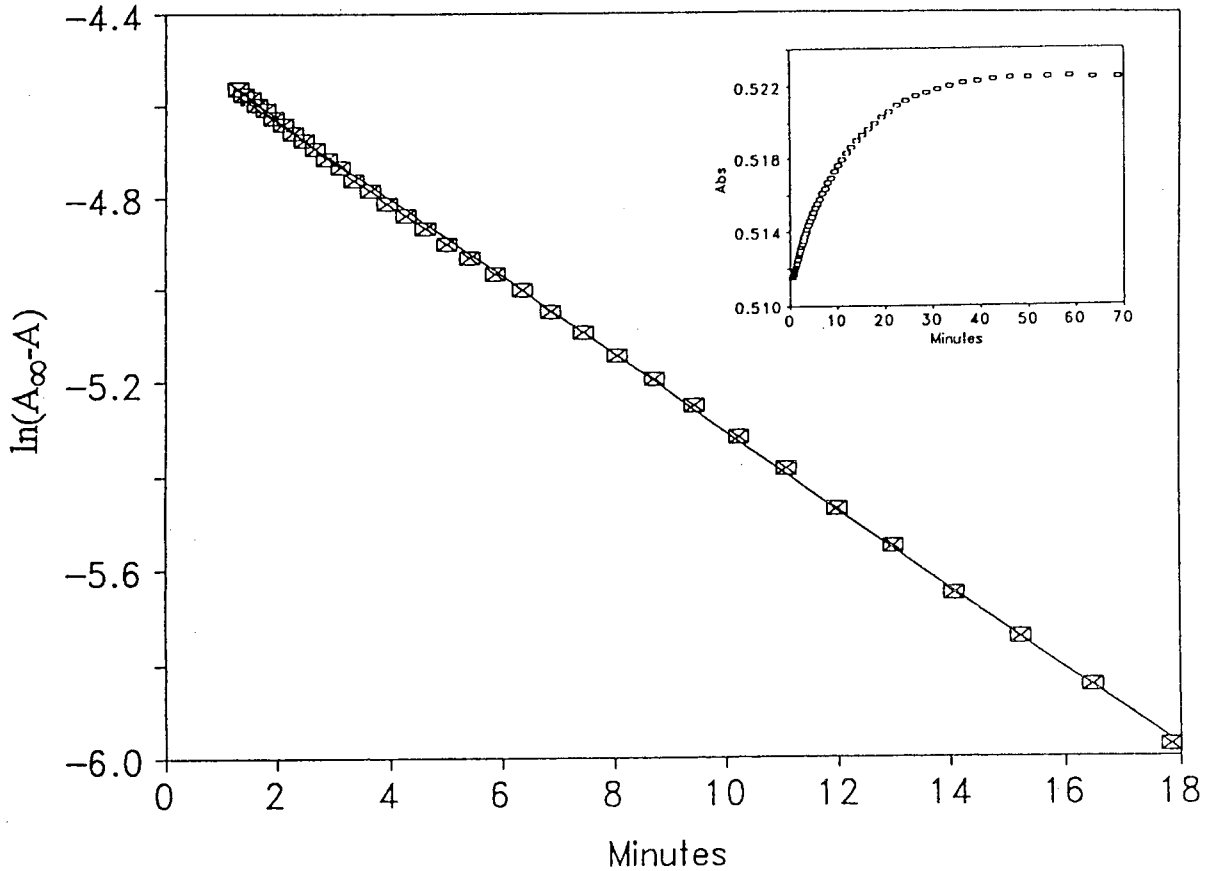

Fig. 2. Kinetic curves for the reaction of replacement of CDTA by PAR (Eq. 5) obtained for [Cu] = 9.8 μmol/l, [Cu]:[CDTA]:[PAR] = 1:1:20 and pH 4.6 (buffer R2). Regression parameters: $\ln(A_\infty - A_t) = -1.40 \cdot 10^{-3}\ (\pm 1 \cdot 10^{-5})t - 4.47\ (\pm 5 \cdot 10^{-3})$, $R = 0.9998$, $n = 34$ (confidence limits, $P = 0.05$ are given).

monia (and polyamines) are much faster for Cu–EDTA than for Cu–CDTA [14]. Ammonia can complex with copper without displacing the EDTA or the CDTA, and the mixed complexes formed [14] are probably intermediate species in reaction 5. The more basic nitrogen atoms and cage-like structure of CDTA contribute to a smaller rate constant, because both stabilize the Cu–CDTA complex but not the transition state [14].

Table 3
Pseudo-first-order rate constants [$*k_d$ (s^{-1})] calculated for ligand substitution reaction (Eq. 5)

Ligand	pH	
	4.6	10.4
EDTA	$(6.1 \pm 5.1) \cdot 10^{-2}$ ($n = 3$)	>0.2
CDTA	$(1.40 \pm 0.13) \cdot 10^{-3}$ ($n = 4$)	$(1.29 \pm 0.49) \cdot 10^{-3}$ ($n = 4$)

Mean values and confidence limits ($P = 0.05$) are given.

4. Conclusions

IC with on-column derivatization with PDCA followed by post-column reaction with PAR and spectrophotometric detection [5–7] was applied to heavy metal determination. It was found that in samples which contain very stable (both

thermodynamically and kinetically) complexes, interferences in the determination of the metals may occur. For instance, for Cu(II), an EDTA interference was observed when this was in excess relative to the metal, and for CDTA even when it was deficient. For Ni(II), severe EDTA interference was found even with a ligand deficiency. The low metal recoveries are mainly due to kinetic factors, which prevent complete replacement of L by PDCA in the mobile phase or by PAR at the post-column reactor. Low metal recoveries are also expected for other metals not included in this work, e.g., Co(III) (d^3) and Cr(III) (diamagnetic d^6), due to the large crystal field activation energies for the substitution reactions [15]. Therefore, when strong chelating agents are suspected to be present in the sample, a batch derivatization with PDCA should be performed before the analysis. Alternatively, digestion of the sample (e.g., in acid or using UV irradiation) to destroy the ligand can be used.

However, these procedures are time consuming and not easily compatible with, for instance, automated on-line analysis, which are frequently used in industrial plant operation and control [16]. Even with more acuity, these procedures preclude the use of a concentration column for collecting a ppb-level sample in the field and returning it to the laboratory for analysis [17]. In such cases the development of instrumentation and procedures for on-line metal collection and/or the determination of heavy metals free of interferences is required. The results in this paper may be helpful for this purpose.

Acknowledgements

The authors thank JNICT(Lisbon)–PROGRAMA CIÊNCIA, project M-27/9/20, for financial support for acquisition of the Dionex ion chromatograph and the Konik detector. Professor A.A.S.C. Machado. (Chemistry Department, Faculty of Science, University of Oporto, Oporto, Portugal) is thanked for helpful discussions.

References

[1] B.D. Karcher and I.S. Krull, in I.S. Krull (Editor), *Trace Metal Analysis and Speciation*, Elsevier, Amsterdam, 1991.
[2] W. Buchberger, P.R. Haddad and P.W. Alexander, *J. Chromatogr.*, 558 (1991) 181.
[3] W. Buchberger, P.R. Haddad and P.W. Alexander, *J. Chromatogr.*, 546 (1991) 311.
[4] R.P. Schneider, F. Zurcher, T. Egli and G. Hames, *J. Chromatogr.*, 462 (1989) 293.
[5] *Determination of Transition Metals by Ion Chromatography*, TN10, Dionex, Sunnyvale, CA, 1987.
[6] C.O. Moses, A.T. Herlihy, J.S. Herman and A. Mills, *Talanta*, 35 (1988) 15.
[7] N.T. Basta and M.A. Tabatabai, *Soil Sci. Soc. Am. J.*, 54 (1990) 1289.
[8] G. Ginzburg, *Talanta*, 23 (1976) 149.
[9] L.G. Síllén and A.E. Martell, *Stability Constants of Metal Ion Complexes (Special Publication No. 17)*, Chemical Society, London, 1964.
[10] L.G. Síllén and A.E. Martell, *Stability Constants of Metal Ion Complexes (Special Publication No. 25)*, Chemical Society, London, 1971.
[11] D.D. Perrin, *Stability Constants of Metal Ion Complexes, Part B: Organic Ligands*, Pergamon Press, Oxford, 1979.
[12] D.L. Olson and M.S. Shuman, *Anal. Chem.*, 55 (1983) 1103.
[13] D.W. Margerum, J.B. Pausch, G.A. Nyssen and G.F. Smith, *Anal. Chem.*, 41 (1969) 233.
[14] J.D. Carr, R.A. Libby and D.W. Margerum, *Inorg. Chem.*, 6 (1967) 1083.
[15] T. Yotsujanagi, R. Yamashita and K. Aomura, *Anal. Chem.*, 44 (1972) 1091.
[16] I.S. Krull and W. Childress, in I.S. Krull (Editor), *Trace Metal Analysis and Speciation*, Elsevier, Amsterdam, 1991.
[17] G.H. Mansfield, in J.D. Mulik and E. Sawick (Editors), *Ion Chromatographic Analysis of Environmental Pollutants*, Vol. 2, Ann Arbor Sci. Publ., Ann Arbor, MI, 1979.

ELSEVIER

Journal of Chromatography A, 696 (1995) 235–244

JOURNAL OF CHROMATOGRAPHY A

Dual vapor and liquid injector for gas chromatography

Labib Ghaoui*, L. Shayne Green

Analytical Sciences, Building 1897B, The Dow Chemical Company, Midland, MI 48667, USA

First received 11 October 1994; revised manuscript received 2 December 1994; accepted 5 December 1994

Abstract

Binary vapor–liquid equilibrium (VLE) data are used in designing process equipment for distillation, extraction, stripping, or decantation. Experimental determinations of VLE data require analyses of vapor and liquid from a binary liquid mixture equilibrated at a specific temperature. A large amount of reliable VLE data can be obtained by using a headspace analyzer with a gas chromatograph. The headspace analyzer is rugged and reproducible, and the analyzer automatically samples the gas phase. The liquid phase is most often manually sampled by insertion of a needle into a heated headspace vial's septum followed by collection of the liquid in a syringe. Representative liquid samples must be collected and analyzed, and safety precautions must be used whenever sampling hot, toxic samples.

A dual sampling system has been developed to automatically sample and inject both headspace and liquid phases from a binary mixture. The system is based on a modification to a Hewlett-Packard 19395A headspace analyzer. The instrument was evaluated with a standard binary VLE system of cyclohexane–*n*-heptane and the data were found to be consistent with data obtained with a Hewlett-Packard headspace analyzer using conventional procedures.

1. Introduction

A significant amount of process engineering involves designing separation processes such as distillation, extraction, stripping, or decantation. Process engineers avoid any undersizing and oversizing of the process equipment by using phase equilibria data for binary or multicomponent mixtures. Both undersizing and oversizing can be costly for a separation process. One of the most common process separations of liquid mixtures is through distillation. Quantitative understanding of vapor–liquid equilibria in multicomponent mixtures is required for distillation and can be obtained from liquid-phase activity coefficients as a function of liquid concentration and temperature. Equipment design can thus be optimized using vapor–liquid equilibrium (VLE) data. A comprehensive description of the thermodynamic equation and parameters and the mathematical relationships among these equations have been previously described [1–3]. The relative volatility or separation factor of a binary mixture is calculated from the vapor and liquid concentration data of a binary mixture and related back to activity

* Corresponding author.

SSDI 0021-9673(94)01203-2

coefficients. The equation used to calculate relative volatility is

$$RV = \frac{Y_1/Y_2}{X_1/X_2} \quad (1)$$

where RV is the relative volatility, Y_1 is the mol fraction of the light component in the vapor, Y_2 is the mol fraction of the heavy component in the vapor, X_1 is the mol fraction of the light component in the liquid and X_2 is the mol fraction of the heavy component in the liquid. This equation estimates the ability to separate the components in the mixture.

Several techniques [4] have been developed for obtaining experimental VLE data. A common technique used is headspace gas chromatography (GC), which was suggested by Wichterle and Hala [5]. VLE studies of binary mixtures using static headspace gas chromatography are carried out by preparing various concentrations of the binary mixture in sealed fixed-capacity containers and equilibrating the mixtures at a predetermined temperature. After equilibration, the vapor phase is then sampled either manually or through an automated headspace analyzer and then analyzed by GC. After all the vapor samples have been analyzed, the liquid phase is then sampled while the mixtures are at their equilibration temperature. The liquid samples are analyzed off-line using GC conditions that are similar to the vapor conditions. A more thorough description of static headspace is described in Refs. [1,6–9]. Calculation of mol percent from the prepared mass percent will be adequate in most cases. However, there are certain examples where the liquid concentrations will change because of the relative volatility of the components of interest and the liquid analysis will give the most accurate data.

Sampling of the vapor phase and GC analysis are fully automated using commercially available headspace analyzers in conjunction with a gas chromatograph. Although the injection and analysis of the liquid phase by GC are automated through the use of liquid autosamplers, the liquid sample collection is not automated. The liquid phase must be transferred into liquid autosampler vials, while still at an elevated temperature. Manually transferring of the hot chemical mixture subjects the analyst to potential exposure of volatile chemicals. Also, sampling of the liquid could be a source of error in the VLE data. In some instances, sampling may result in a non-representative sample being collected because of disturbances in the equilibrium and loss of vapor from the previous vapor sampling due to an unsealed septum. The sample composition and homogeneity can also change in the syringe by crystallization or flash evaporation of a component. All these factors could result in collection of a non-representative liquid sample.

In order to completely automate the experimental part of the VLE studies, a dual injector capable of simultaneously injecting vapor and liquid phases from the same vial into two equivalent columns has been constructed. The new system has all the advantage described earlier. In addition, the analysis time is reduced by more than half, because the data for the vapor and liquid phase are generated at the same time and there is no sample transfer operation.

2. Experimental

2.1. Instrumentation

The automated dual injection system is based upon a modification of an HP19395A headspace analyzer. The device is programmed through a data system (PE Nelson, Access*Chrom Data System) as well as the headspace analyzer to synchronize the dual injection. A schematic diagram of the system is shown in Fig. 1. The original air cylinder that is responsible for the needle movement was replaced by another air cylinder (A) that has a longer shaft (2 cm longer than the original one). The air cylinder was obtained from Lyn-Act Manufacturing Corp., IL, USA, and was mounted on the original bracket with longer spacers (25 mm long). The cylinder was controlled using the original electronics of the headspace analyzer. A modified needle joint (B) was constructed with two internal grooves to fit two needles of different

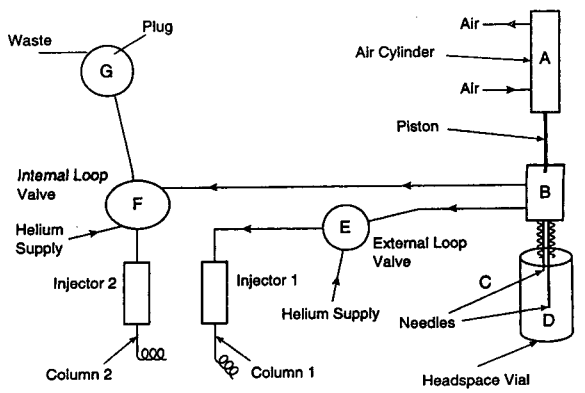

Fig. 1. Schematic diagram of the dual-needle injector.

lengths. One needle allows for vapor sampling and vial pressurizing (C), and the other allows for liquid sampling (D). Fig. 2 illustrates the sampling set-up at an expanded scale. The two needles were housed in a stainless-steel cylinder similar to the original one, but with a larger hole to accommodate the two needles. The needles were obtained in 30 cm long from Hamilton, Reno, NV, USA. The short needle (C) is a 20-gauge side-port needle with a length of 71 mm from the needle joint (B). The longer needle

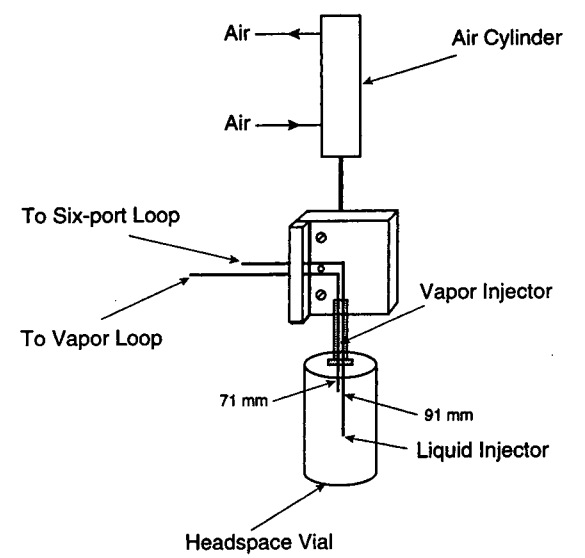

Fig. 2. Blow-up diagram of the vapor and liquid sampling set-up.

(D) is a 22-gauge sharp point needle with 91 mm length from the needle joint (B). The needle used in vapor sampling was connected via a PTFE tube to the headspace unit's original sampling valve (E), which, in turn, was connected to injector 1. This PTFE connection was changed later to a low dead volume connection from Valco, Houston, TX, USA. The needle used in liquid sampling was connected to a heated transfer line, via a low-dead-volume connector. The transfer line was connected to the sample port of an internal 4-port sampling valve (F) with 0.5-μl volume internal loop. Heating of the transfer line was achieved by passing it through a 60 cm length of copper tube that was wrapped with heat tape and insulation. The temperatures of the transfer line and sampling valve were electronically controlled and monitored with thermocouples. The liquid transfer line, sampling valve, and oil bath for heating the sample vial can be independently controlled at the same or different temperatures up to 150°C. The column port of the sampling valve was connected to the injector with a short length of stainless-steel needle, and the carrier gas port was connected to a helium supply line. The carrier gas flow was controlled by a flow controller. The waste port of the sampling valve was connected to a 6-port switching valve (G). One port of the switching valve was used to plug the waste line and the other was used for collection of liquid in a waste container. The sampling and switching valves were air actuated and electronically controlled using the PE Nelson data acquisition system.

Vapor sampling was controlled by the headspace analyzer's electronics. Sampling of the vapor was performed prior to liquid sampling. During vapor sampling, the waste line of the sampling valve (F) was plugged by the 6-port switching valve (G). After the vapor was injected, the headspace instrument was programmed to pressurize the vial. Simultaneously, the external valve (G) was switched to allow liquid to flow through the sample loop and into the waste container. When a representative liquid sample had been collected, the sample loop was switched into the carrier gas stream, which

transferred the sample to the injector. After the liquid was injected, the waste line was plugged (G), the sample loop switched back into the collect position (F), and the needles were removed by the air cylinder (A) from the sample bottle. The sampling system was ready for the next sample analysis.

The gas chromatograph was an HP5890 series II equipped with flame ionization detection (FID) and thermal conductivity detection (TCD) system. FID was used with the liquid injection and TCD was used with the vapor injection. Two different detectors were used because of the GC configuration we had at the time and not because of any technical merits. Two identical detectors will give similar performance. Two 30 m × 0.32 mm I.D., 5 μm 5% CP-SIL-8CB columns (Chrompack) were installed in the two injectors of the gas chromatograph. The sample was introduced into a split injector (injector 1) on column 1. The liquid sample was introduced into the split injector (injector 2) on column 2.

Table 1
Sequence of events for the headspace analyzer

Method 1	Equilibration time	20 min
	Vent	70 s
	Equilibrate	5 s
	Pressurize	60 s
	Equilibrate	30 s
	Vent	70 s
	Pressurize	60 s
Method 2	Equilibration time	20 min
	Vent	5 s
	Equilibrate	5 s
	Vent	5 s
	Equilibrate	5 s
	Inject	60 s
	Pressurize	62 s
Bath temperature		75°C
Loop/valve temperature	Vapor loop	95°C
	Liquid loop	75°C
Loop volume	Vapor loop	1 ml
	Liquid loop	0.5 μl
Transfer line temperature	Vapor	150°C
	Liquid	75°C

2.2. VLE studies

Eight binary mixtures were prepared from HPLC-grade cyclohexane and heptane (Fisher Scientific) with % (w/w) values that ranged from 5 to 95% cyclohexane. Results were obtained as area% values and were assumed to be equivalent to % (w/w) values. Calibration curves were generated for both components. The GC oven was programmed from 100 to 150°C at 3°C/min with an initial hold of 1 min. Both injectors and detectors were held at 250 and 280°C, respectively. Similar flow-rates were allowed into both columns. Split flows from the liquid and vapor injections were 50 and 200 ml/min, respectively. The range for both signals, TCD and FID, was set to 6. The sequence of events for the headspace analyzer during the sampling and injection process are shown in Table 1.

3. Results and discussion

The quality of experimental VLE data is very dependent on the proper use of the headspace equipment and the manual collection of a representative liquid sample for off-line GC analysis. An automated dual injection headspace VLE system was constructed with one short needle and one long needle to perform vapor and liquid injections from the same vial (Fig. 1) to overcome the problems described in the Introduction section about sampling vapor and liquid phases. The dual injector automatically samples the liquid phase after the vapor phase sampling is complete, eliminates manual sampling of hot solutions, and decreases the analysis time by more than half. The system is limited to liquids of low viscosity because the liquid solution is transferred to the valve injector through a transfer line. The current design requires sample sizes of approximately 4–5 ml. This is not a problem for typical VLE studies because we most often study binary mixtures that consist of commercially available reagents or the components are available in large quantities. Because of the design of the sampling system, liquid injection

occurs 1–2 min after the vapor injection. This does not pose any problem with isothermal separations. The temperature program can be modified with a 2–3-min initial hold time to reduce or eliminate any problems that might occur with programmed runs. Evaluation of the dual sampling system involved a chromatographic evaluation of the performance of liquid injection and determination of VLE data for a standard binary mixture.

3.1. Evaluation of liquid sampling system

Liquid injections using a loop injector are used routinely in on-line analysis where feed material from reactors is transferred to a loop injector and fed into the column directly. The combination of this injection technique with the vapor injection technique makes this a unique system for situations where the data from the vapor phase and liquid phase are needed. Due to the 90-cm transfer line and the valve injection of liquid samples, carry-over effects from consecutive runs was an important aspect of the evaluation. A wash solvent can be used between injections or a 2-ml aliquot of the sample can purge the transfer line and the loop injector before the sample is injected. This requires a large sample size. The length of the needles and the vial size restricted use of a smaller sample size. Fig. 3 shows the difference in carry-over effect noticed for an acetonitrile–chlorobenzene sample subjected to different helium purging times. The 0.75- and 1-min purging times (corresponding to 1.5 and 2 ml) of the sample showed no carry-over effect. A 0.5-min purge (1 ml),

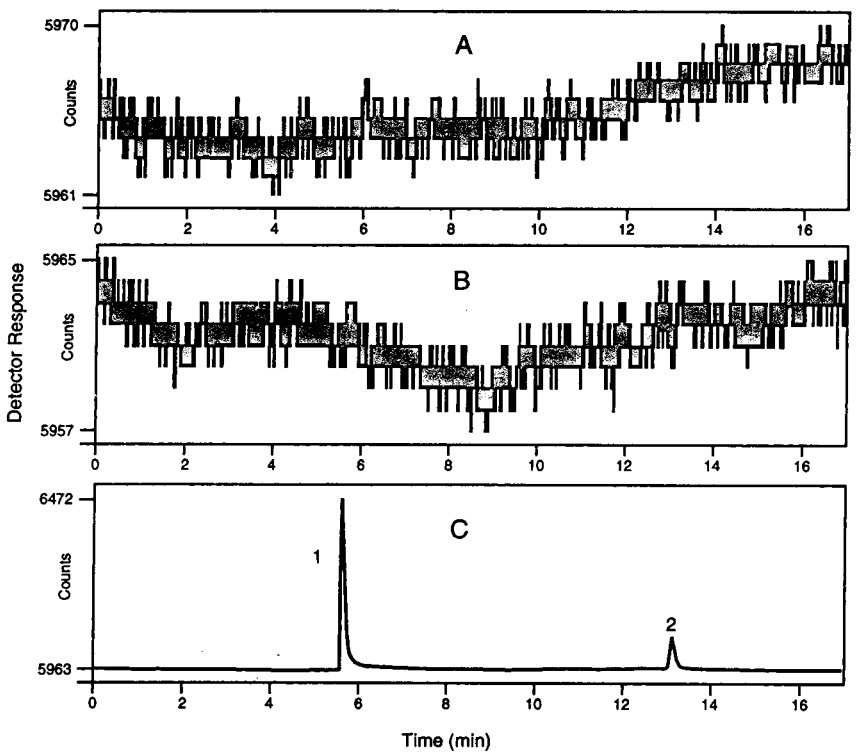

Fig. 3. Carry-over effect. (A) Purge volume 2 ml, (B) purge volume 1.5 ml, (C) purge volume 1 ml. Peaks: 1 = acetonitrile; 2 = chlorobenzene.

however, showed carry-over at a moderate level. A 2-ml wash sample was used for all subsequent studies. Carry-over effect is a matrix-dependent phenomenon related to the volatility and functional groups present. Fig. 4 shows a comparison of chromatograms for *n*-propylbenzene. Fig. 4A is a chromatogram obtained for a liquid injection of *n*-propylbenzene. Fig. 4B is a chromatogram obtained for a blank injection from an empty vial directly after the *n*-propylbenzene injection. Fig. 4C and D are chromatograms for *n*-propylbenzene and for an acetonitrile sample injected after the *n*-propylbenzene. There is a minimum carry-over effect (ca. 40 ppm) for this matrix. That effect did not pose any problem for neat liquid injection with percent concentrations. The oven temperature program was 100°C and programmed to 200°C at 6°C/min. The transfer line and the valve temperature were held at 75 and 95°C, respectively. All other conditions are the same as described in the Experimental section.

The valving system prior to the split injector may be operated at different temperatures. No noticeable peak broadening was observed with the acetonitrile–chlorobenzene test solutions under the conditions described above because the liquid sample from the loop injector was transferred into a regular split injector. This reduced any problem from the loop injector. The valve and transfer line temperature may need to be heated or optimized for certain solutes. Two alcohols, 3-methyl-2-butanol and 4-methyl-2-pentanol, were tested at different valve temperatures for chromatographic performance. Resolution degraded at the low valve temperature for

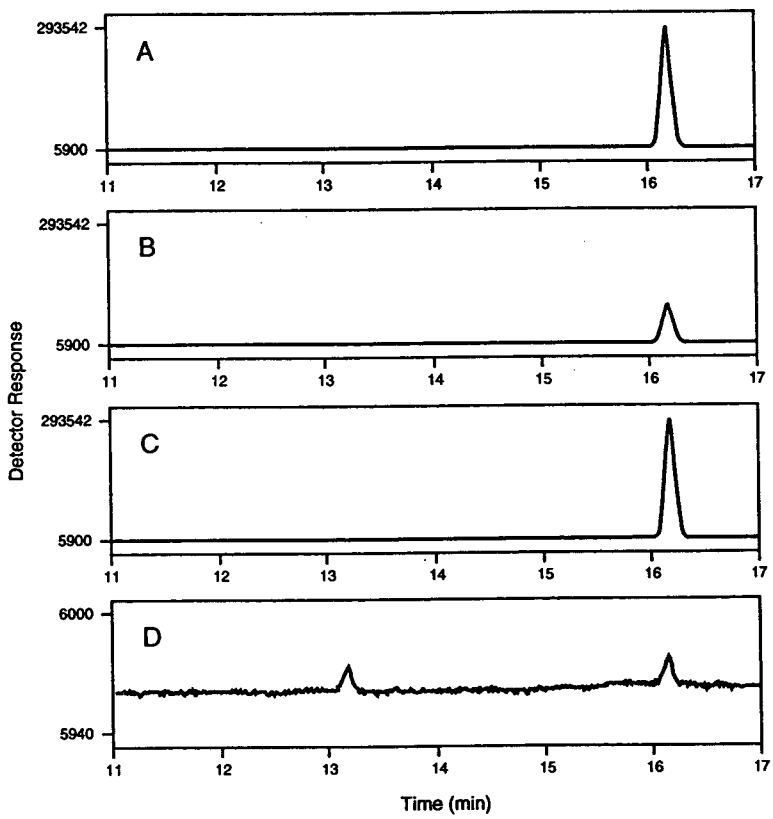

Fig. 4. Carry-over effect. (A) *n*-Propylbenzene; (B) blank injection, no solvent, no sample; (C) *n*-propylbenzene; (D) acetonitrile injection, different scale.

several peaks. The high-temperature analysis showed good chromatographic performance. A comparison of the performance of the dual injection system, at a valve temperature of 95°C, with manual liquid injection is shown in Fig. 5 for 3-methyl-2-butanol. No comparison was done using an autosampler because the instrumental setup prevented the use of an autosampler. No significant difference is noticed in the chromatograms. The peak width of the peak at 5.4 min in the dual injection mode was 3.48 s. The peak width of the corresponding peak in the manual injection was 3.42 s. Other matrices injected, such as N,N-dimethylformamide and N,N-dimethylacetamide, also gave good chromatographic performance with the dual injector.

A reproducibility study of the dual injection system was performed for the liquid sample injection using 15% (v/v) chlorobenzene in acetonitrile. The relative precision at the 95% confidence level (2.78 s) using absolute area counts was determined to be 2.9 and 2.6%, respectively. The modifications on the sampling system did not affect the vapor injections. The system gave good results for both vapor and liquid injections. More than 200 injections were performed by the system without any mechanical failure.

3.2. Evaluation using a standard VLE study

A standard test system of a binary mixture of cyclohexane–*n*-heptane was chosen based on the availability of the components in high purity and the availability of high-quality VLE data from the literature and from data previously collected using a Hewlett-Packard headspace analyzer. This mixture is one of the standards chosen by Fractionation Research, Inc. for evaluation of distillation tray efficiency. Fig. 6 presents representative chromatograms of the liquid and vapor samples. Fig. 7 illustrates the calibration curves

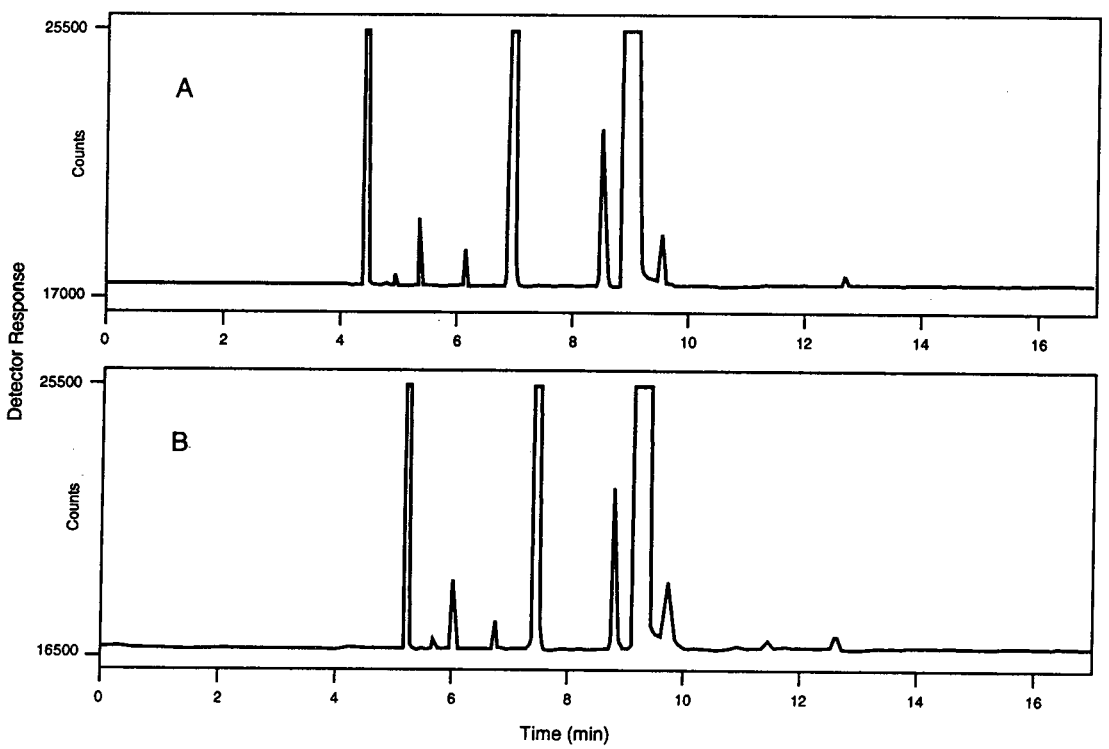

Fig. 5. Comparison for liquid injection of 3-methyl-2-butanol. (A) Manual injection, (B) dual-needle injection.

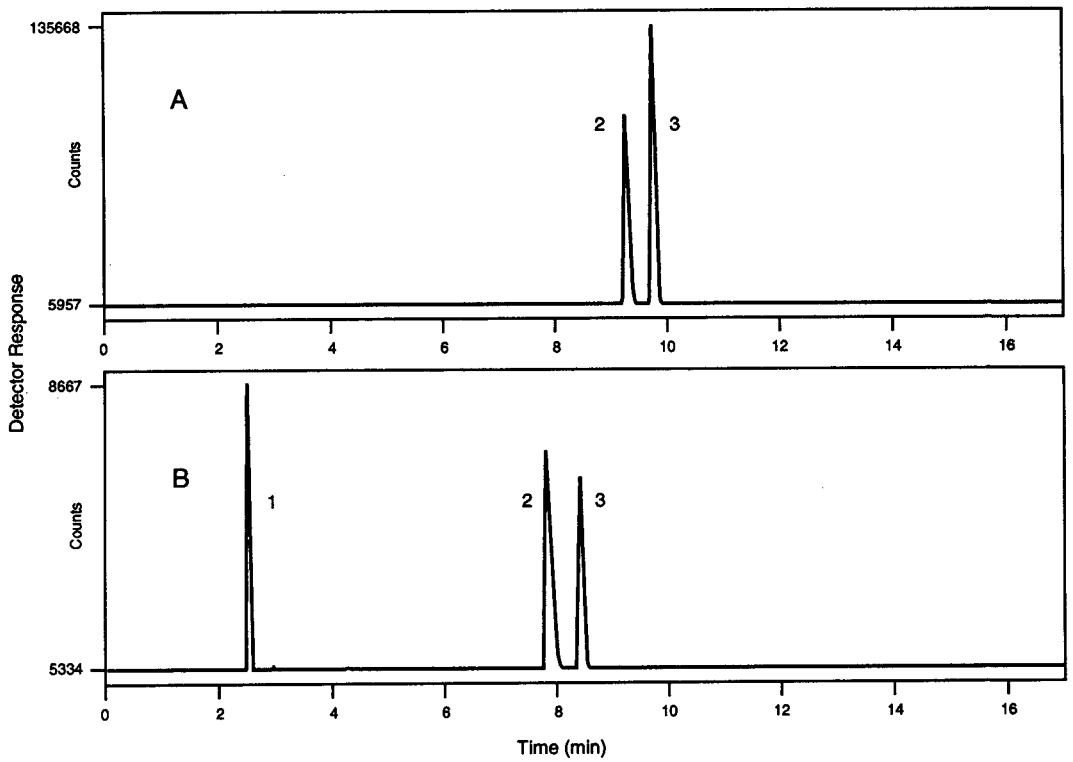

Fig. 6. Liquid and vapor injection of cylcohexane–heptane mixture. (A) Liquid injection, FID; (B) vapor injection, TCD. Peaks: 1 = air; 2 = cyclohexane; 3 = *n*-heptane.

for cyclohexane and *n*-heptane. The calibration curves show a good fit with the data over the sample concentration range. The relative volatility results are reported in Table 2. The experimental data were regressed using the Scatchard and Wilson [10] model for liquid phase non-idealities. Fig. 8 illustrates the plots of the mass fraction in the liquid versus the mass fraction in the vapor and the mol fraction in the liquid versus the relative volatility for the binary systems. In Fig. 8A, the dashed curve represents the ideal curve using vapor pressure data for the mixture and the solid straight line in Fig. 8B represents the ideal line, which is the ratio of the components vapor pressure. The solid curves in Fig. 8A and B represent a regression of the data using the Scatchard and Wilson model (the solid straight line in Fig. 8A is used to relate the actual data to positive and negative deviations from Raoult's Law). In Fig. 8A and B the data lie about the ideal line; thus, as expected, the binary mixture is an ideal system. The dual injection system's results were consistent with the experimental data determined earlier using the conventional headspace system.

4. Conclusions

The dual-needle injector was found to give good performance for VLE studies; it reduced the analysis time by more than half because the GC data from the vapor and liquid injections were generated at the same time, and handling hot chemicals was eliminated thus reducing the potential of chemical exposure. The dual-needle

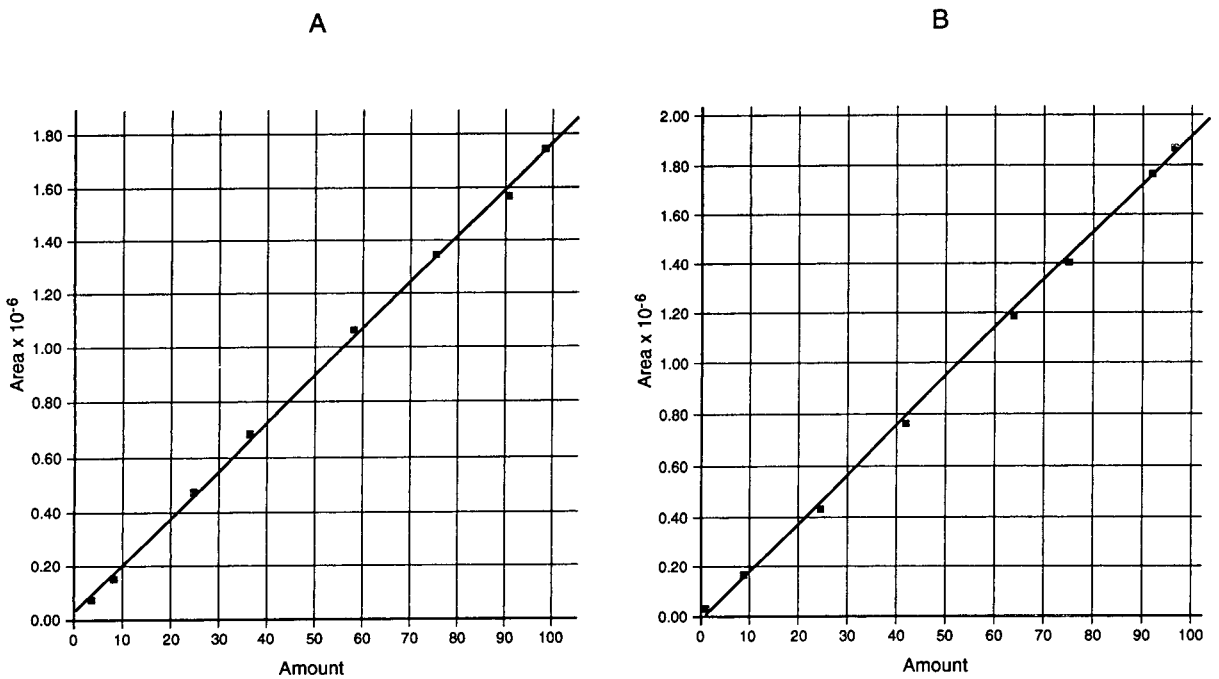

Fig. 7. Calibration curves for (A) *n*-heptane and (B) cyclohexane using absolute area counts.

instrument allows collection of representative vapor and liquid samples. Without using this system, liquid samples may be non-representative because of disturbances in the equilibrium, loss of vapor from vial after vapor sampling, and crystallization or flash evaporation of a component in the syringe. Several other applications were either considered or evaluated, such as liquid–liquid equilibrium studies, high-temperature injections for samples that are insoluble at

Table 2
Relative volatility results for cyclohexane–*n*-heptane at 75°C

Liquid (%, w/w)		Vapor (%, w/w)		Relative volatility
Cyclohexane	*n*-Heptane	Cyclohexane	*n*-Heptane	
1.69	98.31	2.94	97.06	1.76
9.51	90.49	15.03	84.97	1.68
25.10	74.90	37.00	63.00	1.75
42.16	57.84	56.91	43.09	1.81
63.82	36.18	77.12	22.88	1.91
75.19	24.81	85.29	14.71	1.91
92.04	7.96	95.84	4.16	1.99
96.28	3.72	98.18	1.82	2.09

Relative volality = [% (w/w) $\text{vapor}_{\text{cyclohexane}}$/% (w/w) $\text{vapor}_{n\text{-heptane}}$]/[% (w/w) $\text{liquid}_{\text{cyclohexane}}$/% (w/w) $\text{liquid}_{n\text{-heptane}}$].

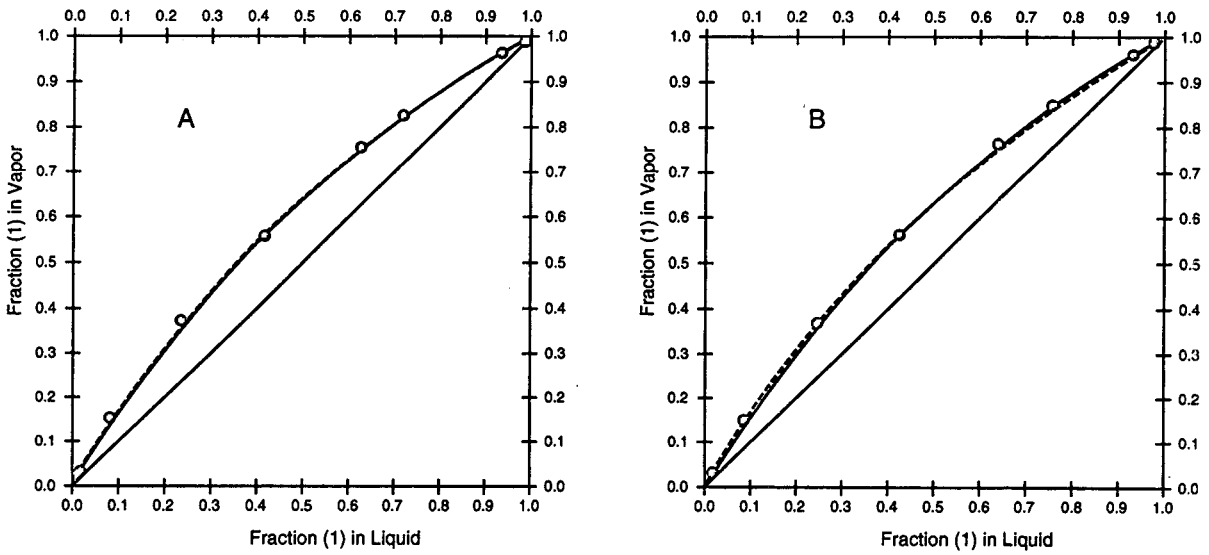

Fig. 8. VLE plots of cyclohexane–*n*-heptane at 75°C. Components: 1 = cyclohexane, 2 = *n*-heptane. Broken line, ideal solution at 75°C; solid line, Scatchard and Wilson [10] model at 75°C, V1 = 115.9000, V2 = 157.8700; O = experimental data, TXY, Obj Fct = A. (A) Conventional, Scatchard and Wilson parameters: U12 = 13.982, U21 = 47.074. (B) Dual injection system, Scatchard and Wilson parameters: U12 = − 126.056, U21 = 143.379. All axes: mass fractions.

room temperature, and implementation on other commercial headspace analyzers.

References

[1] H. Hachenberg and A.O. Schmidt, *Gas Chromatographic Head Space Analysis*, Heyden, London, 1977.
[2] J. Gmehling, U. Dnken and W. Arlt, *Vapor–Liquid Equilibirium Data Collection*, Schon & Wetzer, Frankfurt/Main, Germany, 1981.
[3] M. Hirata, S. Ohe and K. Nagahama, *Computer Aided Data of Vapor–Liquid Equilibirium*, Kodansha, Tokyo, 1975.
[4] E. Hala, J. Pick, V. Fried and O. Vilim, *Vapor–Liquid Equilibrium*, Pergamon, Oxford, 1976.
[5] I. Wichterle and E. Hala, *Ind. Eng. Chem. Fundam.*, 2 (1963) 155.
[6] B.V. Ioff and A.G. Vitenberg, *Head-Space Analysis and Related Methods in Gas Chromatography*, Wiley, New York, 1982.
[7] C. Poole and S. Schuette, *Contemporarty Practice of Chromatography*, Elsevier, Amsterdam, New York, 1984, pp. 463–469.
[8] H. Binder, *J. Chromatogr.*, 25 (1966) 189.
[9] K. Kolb, *J. Chromatogr.*, 112 (1975) 287.
[10] G. Scatchard and G.M. Wilson, *J. Am. Chem. Soc.*, 86 (1964) 125.

ELSEVIER

Journal of Chromatography A, 696 (1995) 245–256

JOURNAL OF CHROMATOGRAPHY A

Mechanism of sulfur emission quenching in flame photometric detectors

Lev Kalontarov, Hongwu Jing, Aviv Amirav, Sergey Cheskis*

School of Chemistry, Sackler Faculty of Exact Sciences, Tel Aviv University, Ramat Aviv, Tel Aviv 69978, Israel

First received 5 October 1994; revised manuscript received 19 December 1994; accepted 20 December 1994

Abstract

The effect of sulfur emission quenching by CH_4, CO, CO_2 and octane was studied using pulsed flame photometric detection (PFPD). It was established that quenching is more efficient at the long time delayed emission. The dependence of quenching efficiency on quencher concentration was found to be similar for all of the above compounds when it was normalized to the concentration of carbon atoms. It is proposed that the dominant reaction leading to sulfur emission quenching is $CO + S = COS$ whereas CO is probably the main product of hydrocarbon combustion in a hydrogen-rich hydrogen–air flame. The experiments and model calculation indicate that CO-induced catalytic hydrogen recombination also promotes quenching and thus quenching is a universal phenomenon in FPD. A quenching-free dynamic range is defined; it is 10^5 for pulsed FPD. It is shown how quenching is identified and largely reduced with pulsed FPD.

1. Introduction

One of the most important aspects which limits the application of flame photometric detection (FPD) in the determination of sulfur-containing compounds is the sulfur emission quenching by co-eluting organic compounds [1–11]. The decrease in sulfur response with addition of hydrocarbons has been found for all existing types of FPD instruments: continuous FPD monitors [1], gas chromatographic (GC)-based FPD [2–11], supercritical fluid chromatography (SFC) FPD [12] and pulsed FPD (PFPD) [13]. It is difficult to draw a complete picture of the phenomenon based on the results of the work cited. Rupprecht and Phillips [2] demonstrated that if mixtures of sulfur compounds and hydrocarbons are subsequently injected into a flame photometric detector, the sulfur response is less than for an equivalent amount of sulfur admixed with nitrogen. An increase in hydrocarbon concentration yields smaller responses, leading eventually to complete suppression of the signal. An increase in the carbon number of the diluting gas in the order ethane, propane, butane also diminished the signal. When the diluent gas was carbon dioxide, interference was much less and complete suppression was not observed. Fredriksson and Cedergren [3,4] have also shown that carbon monoxide is an efficient quencher of sulfur emission and carbon dioxide has lower efficiency. They found that quenching depends on the stoichiometry of the flame, i.e., in leaner hydrogen–air mixtures the degree of quenching is reduced. Unlike these workers [2–4], Weber et

* Corresponding author.

0021-9673/95/$09.50
SSDI 0021-9673(94)01273-3

al. [1] established that carbon dioxide is very effective in inducing quenching, leading to complete suppression of the sulfur signal at about 3000 ppm of CO_2. Moreover, they have shown that the interference with the emission is independent of the concentration of the sulfur-containing compound. The same result had been obtained earlier by Sugiyama et al. [8] for hydrocarbon quenching agents. Sugiyama et al. [8] also found that the quenching efficiency increases exponentially with increase in the quencher concentration. It has been shown by Maruyama and Kakemoto [11] that the extent of quenching varies inversely with the concentration of the sulfur compound. However, the reverse dependence has been found by Olesik et al. [12] for hydrogen–oxygen flames.

The above brief review shows that there are contradictions in the literature on the phenomenology of sulfur emission quenching. The quenching efficiency depends on the type of FPD instrument, the method of mixing reacting gases and the composition of the flame. Nevertheless, it is commonly agreed that even minute amounts of hydrocarbons, if present in the flame, cause the quenching effect which hampers the accurate determination of sulfur compounds. This problem is further exacerbated by uncertainty about the existence of quenching and hydrocarbon-related emission signal due to the limited FPD selectivity. This aspect of the problem has been solved to some extent in PFPD [13]. The concept of PFPD is based [13–15] on a flame propagating in the detector from the igniter to the fuel gas source. The rate of fuel–oxidant gas flow is made insufficient for continuous flame operation, and therefore the propagating flame is observed in a pulsed periodic manner. The most important feature of the pulsed flame is the ability to obtain kinetic information about the processes involved. In particular, it has been shown [13,15] that there is a time delay between sulfur emission and the emission from the propagating flame front. The temporal profile of the sulfur response depends on the presence of quenchers, i.e., both the intensity and the kinetics of the emission are sensitive to quenching, which facilitates its discovery, while hydrocarbon residual emission is filtered also in time.

Considerable efforts have been devoted to overcoming quenching [3,4,9] and it has been claimed that this problem can be minimized in a dual-flame photometric detector [2,16,17]. In this FPD design, the first flame serves for oxidizing the hydrocarbon samples and sulfur emission is then generated and detected in the second hydrogen-rich flame. Some positive results with respect to quenching have also been reported using furnace/single-flame detectors [3,4] and in supercritical fluid chromatography–FPD [12].

The greatest confusion and contradictions are associated with the mechanism of sulfur emission quenching. Several possible reasons for quenching have been proposed [8–10,12,18,19]: (a) collisional deactivation of the S_2^* excited state by hydrocarbons or their oxidation products [8,18], (b) absorption of sulfur emission by a quencher [18], (c) the chemical reaction of hydrocarbons or their products with sulfur atoms and/or hydrogen atoms [8,13], (d) the hydrocarbon-induced temperature variations of the flame [19], (e) collisional deactivation governed by the diffusional quenching constant [10] and (f) quencher induced deactivation of some other excited flame species [10].

A new approach to the study of quenching has appeared with the development of PFPD. A model for sulfur emission in PFPD has been developed [20] and it has been proposed that the quenching is concerned with the reaction of sulfur atoms with carbon monoxide. Based on computer simulation [20], it was shown that CO is the main product of hydrocarbon combustion in hydrogen rich flames. In this paper, we present new experimental and computational results on sulfur emission quenching in PFPD induced by octane, methane, CO and CO_2, and a quenching mechanism is discussed.

2. Experimental

We used two types of PFPD instruments for the study of quenching. Octane-induced quenching has been investigated by means of a PFPD instrument mounted on a gas chromatograph. Its construction has been described in detail previously [13]. In brief, the combustible gases H_2

and air are mixed together in a small quartz combustor flame chamber (quartz tube, 12 mm × 3 mm I.D.) and flow to a continuously heated igniter (Kanthal AF 0.25 mm wire). The ignited flame then propagates back to the gas source, where it is extinguished until the next portion of gases fills the chamber and a new act of ignition occurs. This detector was mounted on a Varian Model 3600 gas chromatograph with a laboratory-made mount. The mount included a separate entrance for controlling the vaporization rate of liquids [tetrahydrothiophene (THT) in a small glass tube]. Typical gas flow-rates were 10 ml/min of hydrogen and 18 ml/min of air with pulse repetition rate of 3 Hz. In these experiments a constant sulfur background injected in the form of THT was quenched by a variable and known amount of octane eluting from the GC column.

Quenching by CH_4, CO and CO_2 was studied in a similar PFPD instrument that is able to measure the flame emission in two positions. Fig. 1 shows a schematic diagram of this detector. The hydrogen, air and nitrogen containing 100 ppm of SO_2 (Matheson) were mixed together using an Omega FL-6GP gas mixer. Their flow-rates could be regulated from 1.0 to 100 ml/min. The flow of the gas quencher was separately supplied to a gas line connected to the PFPD where it was mixed with the fuel–oxidant gas mixture and N_2–SO_2. Then the mixture entered the combustor (Pyrex tube, 80 mm × 4 mm I.D.) and the cycles of pulsed flame propagation took place as described above. The total gas flow-rate

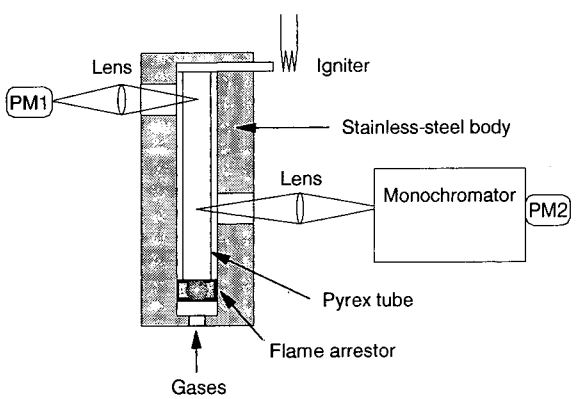

Fig. 1. Schematic diagram of the pulsed FPD instrument. PM1 and PM2 are photomultipliers.

was about 120–130 ml/min. The flow of the gas quencher was regulated from 0.07 to 10 ml/min by an Omega FL-310 flow meter and its concentration was calculated in parts per million (ppm) of the total gas flow (H_2 + air + SO_2–N_2 + quencher). The flow of SO_2–N_2 was about 1% of the total flow (1 ppm SO_2). The typical flow-rates of fuel–oxidant gases were 65 ml/min H_2 and 55 ml/min air.

The design of this PFPD system allows the measurement of flame emission at two points (A and B in Fig. 1). Such an arrangement permits the direct measurement of the flame front velocity. The light emission at point A was collected by a quartz lens (F = 30 mm) and detected by a photomultiplier. A Spex 270 M monochromator was used for the analysis of the light emitted from point B and for the selection of the sulfur emission at 395 nm. Two Hamamatsu R 269 photomultipliers were employed for the emission detection. The signals from the photomultipliers were analysed by a LeCroy 9310 digital oscilloscope–averager and then transferred to a computer for additional processing.

3. Analysis of existing mechanisms for sulfur emission quenching

The mechanisms cited in the Introduction for sulfur emission quenching can be divided into two large groups according to the possible physical or chemical character of the quenching process. Of all the physical concepts, only the mechanisms concerned with collisional deactivation of excited sulfur species by hydrocarbons or their products are of some interest. As has already been noted by Olesik et al. [12], the concentration of hydrocarbon intermediates and the optical path length in FPD are too small to screen the emitted light from sulfur species. Also, combustion of a small amount ($\leq$1% of the hydrogen) of introduced hydrocarbons cannot increase the temperature of the flame and thus reduce the sulfur response; moreover, it has a larger heat capacity than the flame gases. Thus only concepts based on collisional deactivation and chemical interactions between quencher and

sulfur and/or hydrogen atoms seem like likely candidates for S_2^* emission quenching in FPD.

Fig. 2 shows typical kinetic experimental curves of sulfur emission measured by PFPD as presented in Fig. 1 and its quenching time dependence. Note that similar results were obtained for all the quenchers studied (CH_4, CO_2 and CO) and we shall discuss them below. These curves illustrate the kinetics of the formation and consumption of S_2^* excited molecules after the flame front has passed the observation zone. As can be seen in Fig. 2, the addition of quencher can result in a total decrease in sulfur signal and a shift of the emission maximum to shorter times. Further, the decrease in the sulfur response is asymmetric in time. The signal at long times is more dramatically reduced than that at short times. The main conclusions emerging from Fig. 2 are that quenching becomes dominant at quencher concentrations of about 500–1000 ppm (0.4–0.8 Torr) and its kinetics exhibit

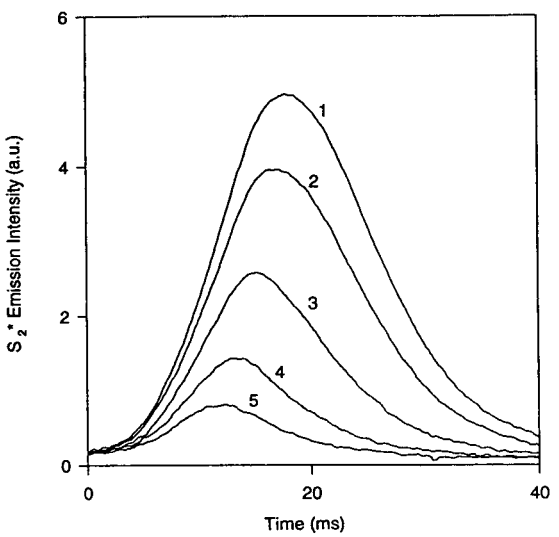

Fig. 2. Kinetic curves of sulfur emission in H_2–air pulsed flame at various concentrations of carbon dioxide obtained at 395 nm through a monochromator. Zero time corresponds to the beginning of the emission from the propagating flame front, which is caused mainly by OH* molecules. Flow-rates were 65 and 55 ml/min for H_2 and air, respectively. The detector body temperature was 160°C. The CO_2 concentrations were (1) 0, (2) 650, (3) 1480, (4) 2800 and (5) 4600 ppm.

time asymmetry. We note that the first of these observations has been established in a large number of previous studies (e.g., Refs. [9] and [10] and references cited therein).

Note that the collisional quenching concept is in disagreement with this experimental evidence. Indeed, it is well established [21–23] that the radiative lifetimes of the $S_2^*(B^3\Sigma_u^-)$ excited state are in the region of 20–40 ns. The addition of quenching gases leads to complex fluorescence decay with a maximum lifetime of about 100–300 ns [23]. If we propose that collisional deactivation plays the dominant role in quenching, we have to draw the conclusion that it must not depend on the emission kinetics of sulfur because characteristic times of energy transfer (nanoseconds) are much shorter than those of the formation of S_2 (milliseconds in Fig. 2) unless the observed kinetics is of the quencher itself, which is highly unreasonable. This conclusion is in contradiction with the experimental asymmetry of quenching. Thus the time dependence of quenching shown in Fig. 2 serves as strong evidence both against the collisional quenching mechanism and in favour of the chemical nature of quenching. This conclusion seems true for other mechanisms of physical quenching, e.g., a diffusional model and deactivation of some other excited flame species. Since physical concepts are unable to explain the experimental observations, it is necessary to search for a quenching mechanism in the chemistry of the sulfur species involved.

4. Chemistry of hydrogen–air flame seeded with hydrocarbons

In order to enhance our understanding of hydrocarbon chemistry in rich H_2–air flames, we carried out model calculations using the Chemkin code for a constant-pressure explosion problem [24]. To make this model more realistic we incorporated exponential heat losses into the model and fitted its time constant to provide the best agreement between the observed sulfur emission time domain and our model calculations [20]. The general scheme of flame calcula-

tions has been divided into two subsystems: one hydrogen–oxygen reaction as has been done by Kee et al. [24] and a methane combustion subsystem with rate constants according to Westbrook [25]. Because of the low concentration of carbon-containing molecules, we did not consider reactions including more than one such molecule. The analysis of the calculation results shows that methane and its products undergo strong atomic pyrolysis by hydrogen atoms in rich H_2–air flames. Reactions with OH radicals are responsible, converting virtually all the methane into CO and CO_2 where the CO/CO_2 ratio is governed by the fast equilibrium reaction $OH + CO = H + CO_2$.

Fig. 3 shows the results of our calculations when 5000 ppm of CH_4 was added to the hydrogen–air system. It is seen that during ca. 0.2 ms all the hydrocarbon molecules are converted into CO and CO_2 with negligibly small concentrations of other molecules. Similar calculated results were obtained when 5000 ppm of CO and CO_2 were added; after combustion, all three systems give almost the same amounts of CO and CO_2 in less than 1 ms. The similarity of the results is even more conclusive at lower concentrations of quencher. Hence the results of our calculations show that any memory about the origin of the quencher is lost after a very short initial time and then all the processes in the system are determined by the equilibrium between CO and CO_2. A change in this equilibrium with decrease in temperature produces an increase in the CO_2/CO ratio, as can be seen in Fig. 3 at time 1–2 ms. The final CO_2/CO ratio strongly depends on an equivalence ratio defined as the molar ratio of fuel to oxidant divided by the stoichiometric ratio. Fig. 4 shows such a dependence as the fraction of final CO in comparison with the hydrocarbon concentration which was initially added to the system.

According to our calculations, the addition of CH_4, CO or CO_2 to the hydrogen–air flame at a concentration lower than 5000 ppm hardly affects the fuel–oxidant combustion during its first 5 ms (Fig. 5). However, at longer times the additive dramatically decreases the hydrogen atom concentration. Since the concentrations of other reactive species, such as O and OH, are connected by equilibrium reactions, their con-

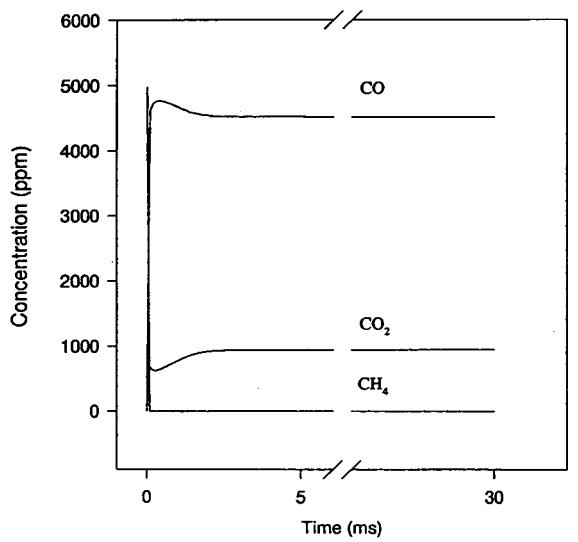

Fig. 3. Calculated kinetic curves of CH_4, CO and CO_2 concentrations during the pulsed flame combustion of 5000 ppm of methane in a hydrogen-rich H_2–air flame.

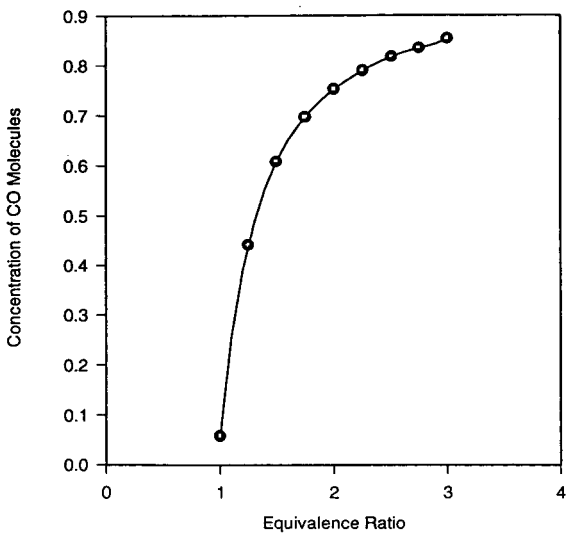

Fig. 4. Calculated dependence of the stationary long time concentration of carbon monoxide (expressed as a fraction of the initial methane concentration) on the equivalence ratio in a hydrogen–air flame after the combustion of 5000 ppm of CH_4.

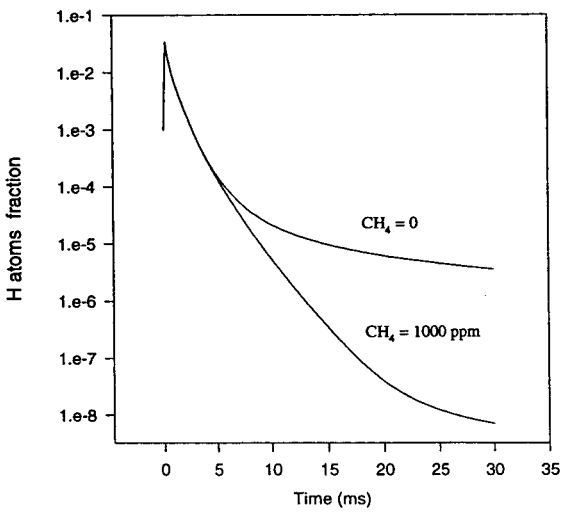

Fig. 5. Calculated kinetic curves of the concentration of hydrogen atoms in a hydrogen–air pulsed flame with and without the addition of methane.

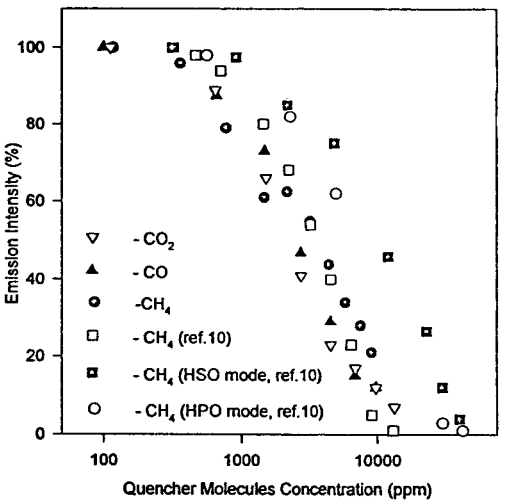

Fig. 6. Dependence of the relative sulfur emission intensity (expressed as a percentage relative to the emission intensity without quencher) on the concentration of quencher molecules. HSO and HPO emission dependences are added from Ref. [10].

centrations are also drastically reduced. The reason for such a decrease is the reaction

$$H + CO + M = HCO + M$$

followed by the fast reaction

$$H + HCO = H_2 + CO$$

These two reactions produce a net effect of H atom recombination: $H + H = H_2$.

5. Results

Based on the conclusion regarding the chemical nature of quenching and computational results of hydrocarbon combustion, one of the principal questions is the type of molecule that is responsible for the quenching effect. There are three possibilities: (1) the hydrocarbons introduced into the flame; (2) their short-lived intermediate products of combustion and (3) the final products, mainly CO and CO_2. To clarify this problem, we measured the quenching efficiency of CH_4, CO and CO_2.

Fig. 6 shows the dependence of the sulfur response on quencher concentration. It also includes literature quenching data on the linear sulfur detection via HSO emission [10] and phosphorus HPO quenching [10]. The sulfur response is defined as the ratio of the intensity of sulfur emission in the presence of quencher to that without quencher multiplied by 100. As can be seen, within the accuracy of our measurements and ability to regulate very small flows of gas-quencher (±20%) there is a universal dependence of the sulfur signal on the quencher concentration for CH_4, CO and CO_2 regardless of the chemical identity of the quencher. Moreover, the data on methane-induced quenching obtained in continuous GC–FPD by Aue and Sun [10] fit our quenching curve well. The latter testifies to the same nature of quenching for both types of detectors. Further, although the data on HSO and phosphorus quenching seem to indicate a lower degree of quenching, when these points are raised to the second power to simulate the sulfur quadratic response, they fall above but close to our points within the uncertainty of our accuracy.

It should be noted that the main kinetic regularities were also the same for all quenchers, i.e., the shift of the maximum of the kinetic curve to shorter times and more effective

quenching at the long time edge (Fig. 2) are characteristic for all quenching gases. The universal dependence of quenching efficiency and the similar kinetic phenomenology serve as strong evidence to support the idea that the final products of hydrocarbon combustion provide the main contribution to sulfur emission quenching. This conclusion is confirmed by the comparison of characteristic times for CH_4 combustion (Fig. 3) and sulfur formation (Fig. 2). Fig 3 shows that all intermediate processes of hydrocarbon combustion end after ca. 0.3 ms whereas the sulfur emission and its quenching begin at much longer times ($\geq$5 ms) when only CO and CO_2 are present at the flame in noticeable amounts.

Fig. 7 illustrates the above-mentioned kinetic asymmetry of sulfur quenching. The CO_2 concentration necessary for sulfur emission intensity is halved; $[Q]_{1/2}$ is 1200 ppm at $t = 25$ ms and 3400 ppm at $t = 12$ ms. In Fig. 7 the data are presented on semi-logarithmic coordinates [log-(sulfur signal) versus quencher concentration], showing an exponential decrease of the sulfur signal with rise in quencher concentration.

The results of octane-induced quenching studies by GC–PFPD are presented in Fig. 8. These plots also show that the S_2 emission

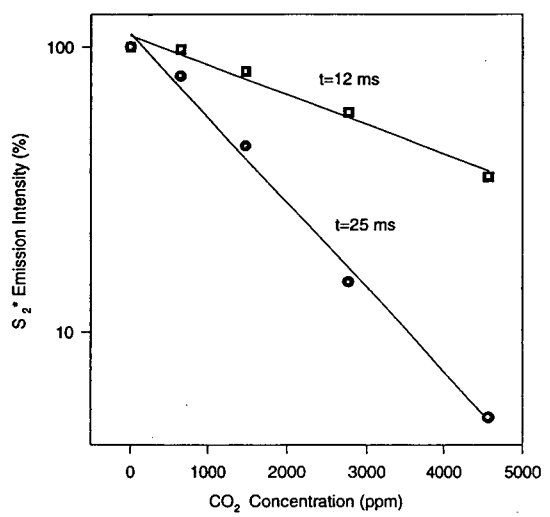

Fig. 7. Dependence of the relative S_2^* emission intensity on the carbon dioxide concentration measured at different times of the kinetic curve of sulfur emission.

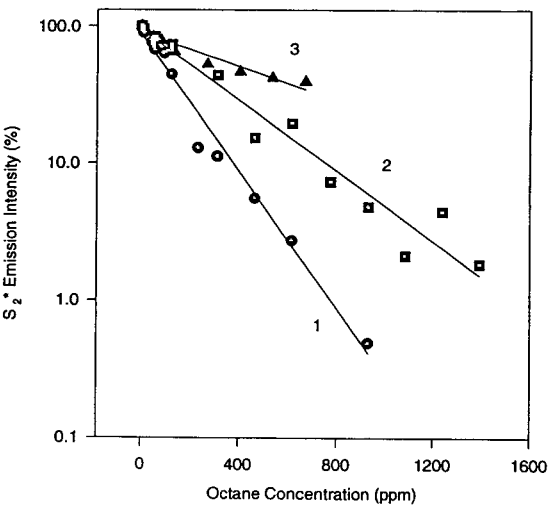

Fig. 8. Dependence of the relative sulfur emission intensity on the octane concentration. (1) Sulfur emission signal integrated over the whole kinetic curve of the sulfur emission (full gate) in a hydrogen-rich H_2–air pulsed flame; (2) sulfur signal measured at the short time edge of the kinetic curve (narrow gate) in a hydrogen-rich H_2–air pulsed flame; (3) sulfur signal measured with full time integral in a hydrogen medium-concentration H_2–air pulsed flame.

quenching by octane conform to the same regularities as quenching by CO, CO_2 and CH_4 studied spectroscopically. However, the quenching efficiency of octane is much higher, $[Q]_{1/2} =$ 110 ppm for full gate and $[Q]_{1/2} = 240$ ppm for narrow gate observation. The full gate denotes that the sulfur signal was measured as the integral over the entire kinetic curve of the S_2 response and the narrow gate is the signal integrated at the short time edge. It is seen that octane-induced quenching is reduced upon transition to the field of short times. The higher quenching efficiency of octane is easily understandable in terms of the approach we presented. Indeed, the combustion of octane, whose molecule contains eight carbon atoms, results in the formation of eight molecules of CO or CO_2, whereas the combustion of the other quenchers gives only one molecule of CO or CO_2 per quencher molecule. Accordingly, the quenching efficiency of octane has to be higher by a factor of eight than that for CH_4, CO and CO_2. The observed disagreement by a factor of two

($[Q]_{1/2} \approx 2000$ ppm for CO_2 and 1000 ppm for octane) is small considering the difference in the methods of registration of quenching and the use of two different experimental set-ups.

A comparison of curves 1 and 3 in Fig. 8 shows that the change in the stoichiometry of the flame gases (equivalence ratio) influences the quenching efficiency, i.e., under conditions of a leaner mixture the quenching becomes weaker. This indicates that carbon monoxide plays the dominant role in quenching, because the reduction of hydrogen in the flame leads to a shift of the CO_2/CO equilibrium to the predominant formation of carbon dioxide (Fig. 4). It should be noted that the transition to lean mixtures results not only in a decrease in quenching but also in a shift of the sulfur emission time response to short times and also in a reduced emission intensity which sharply decreases near the stoichiometric mixture.

6. Mechanism of quenching

The major conclusions emerging from the above results and discussion are that (1) the hydrocarbon-induced sulfur quenching takes place through the chemical interactions of the quencher with sulfur-related chemical species and (2) carbon monoxide, which is the principle product of hydrocarbon combustion in the rich flame, is the direct reason for quenching.

There are two main possibilities for the influence of carbon monoxide on sulfur-related chemistry in flames, depending on the mechanism of sulfur emission. If S_2^* excited dimers are formed through the following reaction [9]:

$$H + H + S_2 = H_2 + S_2^* \quad (1)$$

CO can react with hydrogen atoms according to the scheme described in Section 4, and which would reduce the sulfur emission. In the case of sulfur atoms, recombination is a dominant mechanism of the formation of S_2^* [9]:

$$S + S + M \rightarrow S_2^* + M \quad (2)$$

Both the reaction of CO with H atoms and the reaction between CO and S,

$$CO + S + M \rightarrow COS + M \quad (3)$$

can cause the quenching effect. Indeed, the sulfur atom production includes many steps in which hydrogen atoms are involved. The most important steps are

$$H + H_2S \rightarrow SH + H_2$$

$$H + SH \rightarrow S + H_2$$

Hence the decrease in H atom concentration on addition of hydrocarbons to the flame (as seen in Fig. 5) will result in a decrease in sulfur atom production.

The proposed mechanism of sulfur emission [20] showed that reaction 2 describes the observed PFPD time delay of sulfur emission and its temporal profile much better. Therefore, to model quenching we carried out numerical calculations based on three subsystems. The first subsystem describes the basic hydrogen–oxygen flame reactions, the second is due to hydrocarbon combustion and the third is concerned with sulfur-related chemistry with the mechanism of sulfur-excited dimer formation according to reaction 2. To simulate the interaction between the sulfur and hydrocarbon subsystems, the following reactions were added to the flame:

$$S + CO = COS + M \quad (4)$$

$$H + COS = CO + SH \quad (5)$$

The rate constant for reaction 5 was used according to Lee et al. [26] [$k_5 = 9.06 \cdot 10^{-12} \exp(-3.85/RT)$ cm^3 molecule^{-1} s^{-1}]. Unfortunately, we could not find the rate constants for reaction 3, so we used the rate constant for the analogous reaction between oxygen and CO [27] [$1.7 \cdot 10^{-32} \exp(-4100/RT)$].

The calculated kinetic curves of sulfur emission with the addition of methane are shown in Fig. 9. There is excellent qualitative agreement between the calculated and measured experimental data (Fig. 2). Our calculations show that without reaction 3, quenching hardly occurs. This means that the CO–hydrogen interaction contributes minimally to the quenching process. This is not surprising because Fig. 5 shows that the number of hydrogen atoms begins to de-

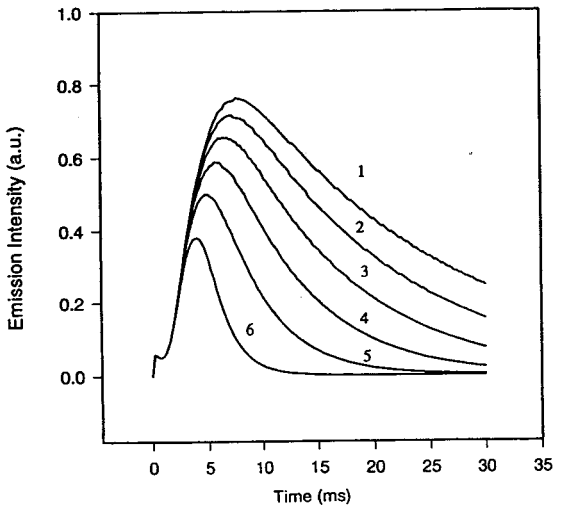

Fig. 9. Calculated kinetic curves of sulfur emission in a hydrogen–air rich pulsed flame at various concentrations of CH_4: (1) 0; (2) 200; (3) 500; (4) 1000; (5) 2000; (6) 5000 ppm.

crease after 5 ms, when the accumulation of sulfur is already finished (Fig. 9). Fig. 10 presents the calculated and experimental dependences of the sulfur response on the quencher concentration at long times of the kinetic curves.

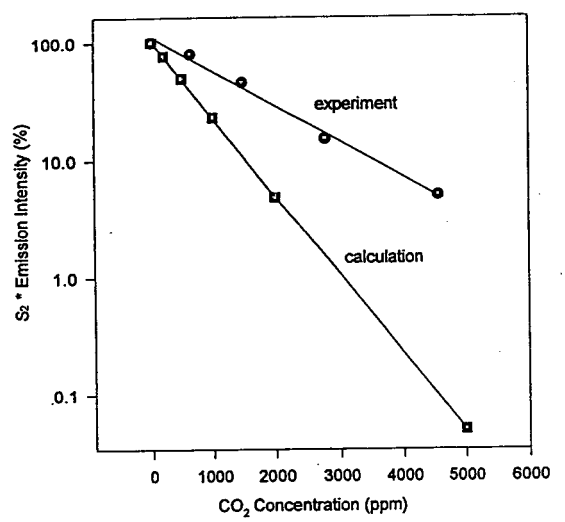

Fig. 10. Dependence of the relative sulfur emission intensity on the carbon dioxide concentration measured at long times of the kinetic curves of sulfur emission. Experimental data are taken from Fig. 2 and calculation results from Fig. 9.

The slope of the calculated line is twice that of the experimental line and full coincidence can be obtained with a halved rate constant for reaction 3. Taking into account the large uncertainty in our knowledge of this rate constant, the obtained agreement of experimental and calculated results seems adequate. In its turn, such agreement serves as indirect evidence for the rationality of the previously developed mechanism of sulfur emission [20].

While our study indicates reaction 4 as the most important sulfur-scavenging reaction, the catalytic destruction of atomic hydrogen by CO will result in a universal response change (usually quenching) of all elements in all the flame and combustion-based chemical detectors. This mechanism is expected to be important at hydrocarbon concentrations above 1000 ppm.

7. Quenching and its reduction using the pulsed FPD with gas chromatography

The emerging general conclusion from this study and based on Fig. 6 is that response quenching is a general phenomenon that exists in all the flame photometers as it depends on basic combustion and flame chemical reactions. This conjectured conclusion can be further generalized into claiming that quenching is a universal phenomenon in the detection of any element in all types of detectors that employ flame and combustion. Note that 1% CH_4 in a 50% air flame can lower the available relative amount of oxygen by 40% through its combustion, whereas octane at this level can extinguish the flame itself.

While quenching is well established in sulfur detection with FPD, it also exists in several other elements in FPD [10]. In addition, it also seems to exist in the flame chemiluminescence detector [28], where a massive decrease in response is observed (Ref. [28], Fig. 4) at the time of solvent elution. Based on this paper, it is clear that the scavenging reaction CO + S = COS is a universal sulfur-quenching mechanism which affects its detection through S_2 emission or HSO emission [10,13] or SO plus ozone chemi-

lumenescence [28]. CO can also affect other species such as ozone decomposition or induce hydrogen recombination. Thus, in attempting to assess a quantitative factor that will specify quenching, one should establish an acceptable parameter that will quantify the effect of quenching.

We have shown above that the degree of response quenching depends only on the final carbon concentration in the flame and on its stoichiometry. Thus quenching exists in all FPD instruments and its magnitude is similar if it is normalized to the total gas flow-rate. Accordingly, dual FPD is the least subjected to quenching among the various FPD designs, not because of its dual flame design [16,17] but rather owing to its highest total flow, which dilutes the CO and sulfur species (also owing to its wide flame nozzle, which dilutes the flame species). It was shown above that the prior combustion of hydrocarbons into CO_2 in the first flame has virtually no effect on quenching as the quenching induced by CO_2 is identical with that induced by CH_4. On the other hand, different FPD designs result in different detection sensitivities. Lower detection limits permit the injection of smaller sample amounts into the GC column and thus results in decreased quenching. We define here a new term to quantify quenching, namely the "quenching free dynamic range (QFDR)", which is the ratio of maximum allowed amount of co-eluting hydrocarbon that results in response quenching of less than 10% divided by the minimum detected amount of sulfur in that particular detector.

The PFPD instrument has a QFDR of 10^5 as the onset of 10% quenching under normal conditions is at 20 ng C/s, while its sulfur MDA is 0.2 pg S/s [13]. In comparison, the dual FPD instrument [16,17] has a higher overall gas flow-rate by a factor of 20 and MDA [13] by a factor of 100. Thus the PFPD instrument is assumed to have a higher QFDR by a factor of 5 than the dual FPD instrument. Note, however, that the dual FPD instrument can accept 0.4 μg C/s without quenching, and this level is beyond the level that is normally encountered in capillary GC and so it can be considered as a quenching-free FPD system for practical applications, while care should be exercised when using PFPD although it has a higher QFDR.

PFPD offers two additional advantages in comparison with FPD in attempt to reduce the effects of response quenching on quantitative measurements: (a) the time gating of sulfur emission eliminates the hydrocarbon contribution to the flame emission through increased selectivity; and (b) the existence of quenching can be observed, identified and corrected for through its unique effect on the sulfur emission time response.

This identification can be achieved by the observation of the pulsed flame emission on an oscilloscope. Alternatively, we have used a double-gated amplifier for automatic quenching identification and correction. One gate was used to collect and time integrate all the sulfur-emitted light and the other gate was time delayed by 10 ms to amplify the effect of quenching as shown in Fig. 2. The gas chromatogram of sulfur compounds was then monitored with the two gates simultaneously using a double-gated amplifier. From the two chromatograms obtained, the various sulfur compound responses of the delayed gate chromatogram were divided by that of the normal gate chromatogram to obtain the gate response ratio (GRR). The gate response ratio was normalized to 1 for a sulfur compound peak that has no quenching. Any decrease in the GRR now automatically indicated response quenching, and the GRR was monotonically decreased with increased degree of quenching. Fig. 11 shows a calibration graph for the GRR plotted against the degree of quenching in the normal gate. The plot depends on the gate delays and width and also on the H_2–air stoichiometry, but once these parameters are fixed, Fig. 11 can be very useful for introducing correction factors to correct for quenching. The data in Fig. 11 were obtained by measurement of the effect of hydrocarbon elution from the GC column on a background of sulfur in the PFPD instrument. Note that the magnitude of quenching is independent of the amount of sulfur (pseudo-first-order kinetics). The data in Fig. 11

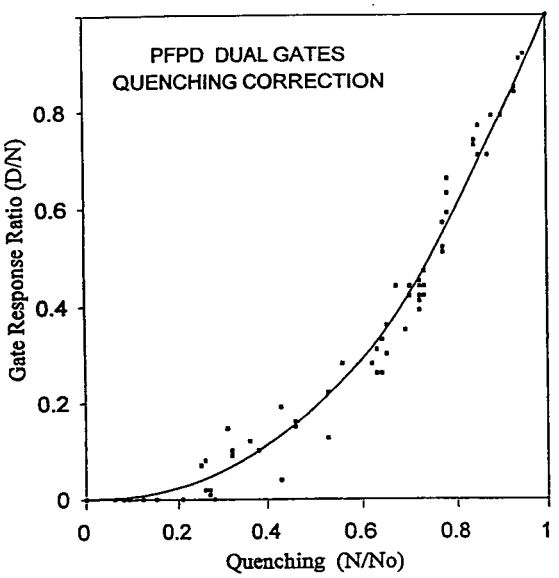

Fig. 11. Calibration graph of the gate response ratio (GRR) versus the degree of quenching at fixed gate delay and H_2–air stoichiometry. The gate response ratio is normalized to unity for a compound that has no quenching.

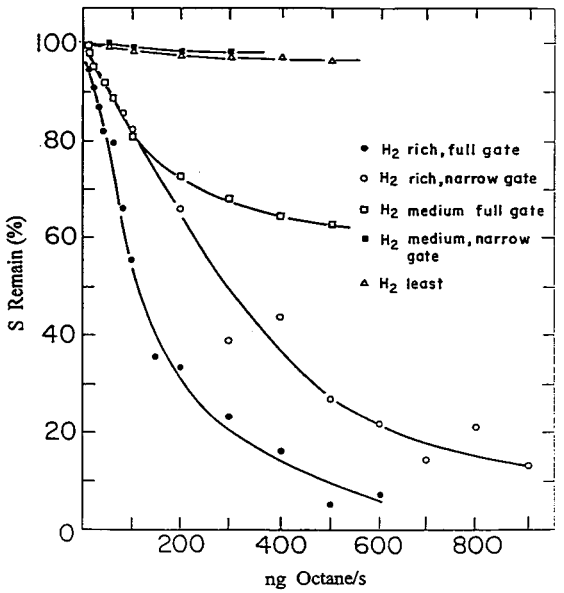

Fig. 12. Dependence of the sulfur response quenching on the amount of co-eluting octane. A PFPD instrument mounted on a gas chromatograph was continuously fed with tetrahydrothiophene and its response under octane elution was measured. The remaining sulfur is defined here as the square root of the sulfur signal to indicate the effective reduction in the extrapolated amount of sulfur. The relative hydrogen concentrations are as follows: H_2 rich is 2.7 equivalence ratio, H_2 medium is 2.1 equivalence ratio and H_2 least is 1.7 equivalence ratio.

can also be obtained by other standard GC methods for the creation of overlapping hydrocarbon and sulfur compound peaks [29].

The use of PFPD also offers other ways to overcome quenching at the expense of a lower detection sensitivity. Fig. 12 shows the sulfur response quenching versus the amount of co-eluting octane under different conditions: (a) normal operation conditions; (b) normal hydrogen-rich conditions as in (a), but using a shorter gate; the sulfur response was decreased 3.3-fold but the quenching level was also decreased; note that decrease in response by a factor of 3.3 means that the MDA increase by a factor of less than 1.8 owing to the sulfur quadratic response, and a lower noise level with a shorter gate; (c) the amount of air was increased and even though a full gate was used, the response was decreased by a factor of 14 and the MDA was increased by a factor of 3.7; (d) stoichiometry as in (c), but with a short gate; under these conditions, quenching was eliminated in the range of practical applicability of using capillary GC; the trade-off is a factor of 30 in the sulfur response and an increase by a factor of ca. 5.5 in the MDA to the level of about 1–2 pg S/s; (e) a further increase in the air level eliminates quenching even with full gate but the MDA is reduced by a factor 9; we note that while the same trade-off of sensitivity-reduced quenching can be achieved with continuous FPD, the penalty of a further reduction in selectivity by one or two orders of magnitude seems unacceptable with FPD, in contrast to PFPD.

In conclusion, either the use of the gate response ratio for quenching identification and correction or the use of increased air and a

shorter gate can decrease, eliminate or correct the sulfur response quenching and increase its QFDR by another order of magnitude to 10^6.

Acknowledgements

This research was partially supported by a grant from the Israel Ministry for Science and Technology, by the James Franck Germany–Israel Binational Program in Laser Matter Interaction and by a grant from the Israel National Science Fund administered by the Israel Academy of Sciences and Humanities.

References

[1] D. Weber, K.B. Olsen and J.D. Ludwick, *Talanta*, 27 (1980) 665.
[2] W.E. Rupprecht and T.R. Phillips, *Anal. Chim. Acta*, 47 (1969) 439.
[3] S. Fredriksson and A. Cedergren, *Anal. Chem.*, 53 (1981) 614.
[4] S. Fredriksson and A. Cedergren, *Anal. Chim. Acta*, 100 (1978) 429.
[5] D.A. Clay, C.H. Rogers and R.H. Jungers, *Anal. Chem.*, 49 (1977) 126.
[6] D.A. Ferguson and L.A. Luke, *Chromatographia*, 12 (1979) 197.
[7] E. Mangani, F. Bruner and N. Penna, *Anal. Chem.*, 55 (1983) 2193.
[8] T. Sugiyama, Y. Suzuki and T. Takeuchi, *J. Chromatogr.*, 80 (1973) 61.
[9] S.O. Farwell and C.J. Barinaga, *J. Chromatogr. Sci.*, 24 (1986) 483.
[10] W.A. Aue and X.-Y. Sun, *J. Chromatogr.*, 641 (1993) 291.
[11] M. Maruyama and M. Kakemoto, *J. Chromatogr. Sci.*, 16 (1978) 1.
[12] S.V. Olesik, L.A. Pekay and E.A. Paliwoda, *Anal. Chem.*, 61 (1989) 58.
[13] S. Cheskis, E. Atar and A. Amirav, *Anal. Chem.*, 65 (1993) 539.
[14] A. Amirav, *Isr. Pat.*, 95617 (1990); *US Pat.*, 5153673 (1992).
[15] E. Atar, S. Cheskis and A. Amirav, *Anal. Chem.*, 63 (1991) 2061.
[16] P.L. Patterson, R.L. Howe and A. Abu-Shumays, *Anal. Chem.*, 50 (1978) 339.
[17] P.L. Patterson, *Anal. Chem.*, 50 (1978) 345.
[18] R. Buffington and M.K. Wilson, *Detectors for Gas Chromatography—A Practical Primer*, Hewlett-Packard, Palo Alto, CA, 1987.
[19] V.L. McGuffin and M. Novotny, *Anal. Chem.*, 53 (1981) 946.
[20] S. Cheskis, *Combust. Flame*, in press.
[21] K.A. Meyer and D.R. Crosley, *J. Chem. Phys.*, 59 (1973) 1933.
[22] T.H. McGee and R.E. Weston, *Chem. Phys. Lett.*, 47 (1977) 352.
[23] T.H. McGee and R.E. Weston, *J. Chem. Phys.*, 68 (1978) 1736.
[24] R.J. Kee, F.M. Rupley and J.A. Miller, *Sandia National Laboratory Report*, SAND89-8009, 1991.
[25] C.K. Westbrook, *Combust. Sci. Technol.*, 20 (1979) 5.
[26] J.H. Lee, L.J. Stief and R.B. Timmons, *J. Chem. Phys.*, 67 (1977) 1705.
[27] B. Lewis and G. Elbe, *Combustion, Flames and Explosions of Gases*, Academic Press, New York, 1987, p. 102.
[28] R.L. Stearer, *Anal. Chem.*, 64 (1992) 2192.
[29] J. Efer, T. Maurer and W. Engewald, *Chromatographia*, 29 (1990) 115.

ELSEVIER

Journal of Chromatography A, 696 (1995) 257–263

JOURNAL OF CHROMATOGRAPHY A

Extraction–gas chromatographic method for the determination of organophosphorus compounds as lubricating oil additives

Albertine E. Habboush*, Sabri M. Farroha, Hussain I. Khalaf

Chemistry Department, College of Science, University of Baghdad, Baghdad, Iraq

First received 16 March 1994; revised manuscript received 17 October 1994; accepted 18 October 1994

Abstract

A direct solvent extraction–gas chromatographic method was developed for the determination of organophosphorus compounds as additives in lubricating oil for control purposes. Ethanol (95%) was used as an extractant and Varian GC-Vista 6000 gas chromatograph with a 3% OV-17 column and dual flame photometric detector was used for the measurements under the optimum experimental conditions. The accuracy and precision of the method were determined by preparing model samples of different types of engine lubricating base oils blended with different amounts of triphenyl phosphate or *p*-tricresyl phosphate ranging from 0.002 to 1.0% (w/w), which correspond to 2.12–955 ppm of phosphorus. The results showed errors ranging from 0.40 to 2.96% and the relative standard deviation did not exceed 3%. This method was applied successfully to the determination of phosphorus compounds in different types of lubricating oils. Each sample requires 20 min for analysis and 72 samples can be analysed per 8-h day. The effect of storage on the amount of phosphorus as an additive in lubricating oils was also considered.

1. Introduction

An important industrial use of phosphorus is as organophosphorus additives in lubricating oils because of their oxidation-inhibiting, corrosion-inhibiting, anti-wear and extreme-pressure characteristics [1–3]. Lubricant additives are based on various organic and inorganic chemicals and the proportion of organophosphorus is 6–10% of the total additive content [2]. Limitations on the amount of phosphorus compounds is important when petroleum products are blended with additives. Hence an accurate, simple, rapid and reproducible method of analysis for control purposes in blending or for performance testing on field samples taken during customer use is required. Chemical methods usually require the phosphorus in the sample first to be converted into inorganic orthophosphate, which is usually done by oxidation and/or hydrolysis of the sample [4–6]. The most popular chemical method seems to be spectrophotometry [7], but completeness of combustion and burning a sufficient amount of sample are common problems. Photometric titration for the determination of disubstituted dithiophosphates in lubricating oils was described by Płaza [8]. The method is simple and rapid and samples do not require separation or other preliminary stages prior to their analysis, but the method is specific for this type of

* Corresponding author.

0021-9673/95/$09.50
SSDI 0021-9673(94)01008-0

additive and only at concentrations above 0.01%.

Emission spectroscopic methods [9] are also widely used. Their main advantage is the wide concentration range of additives that can be determined, but the disadvantages are poor precision (5–10%) and slowness and also HPO flame emission suffers from interferences from organic solvents which can affect the emission intensity of species to be detected [10].

Atomic absorption spectrometry (AAS) has also been used to determine phosphorus additives in lubricating oils [11,12]. The electrothermal AAS determination of phosphorus additive in lubricating oils and related products was reported by Russeva and Rhavezov [13]. The phosphorus content of the samples analysed ranged from 0.003% to 7%. Interference from inorganic phosphorus can be expected in this method.

Gas chromatography with flame photometric detection (GC–FPD) has been used to determine some organophosphorus compounds [14,15]. However, very little has been published on the use of GC for the determination of organophosphorus compounds as additives in lubricating oils or other petroleum products. Pospisilova et al. [16], determined tricresyl phosphate in lubricating oils using GC with nitrogen–phosphorus detection. The phosphorus content of the samples analysed varied from 0.049% to 0.093% with a relative error of 5–10%.

Habboush et al. [17] developed a direct GC method for the determination of organophosphorus compounds as gasoline additives. The phosphorus content of the samples analysed ranged from 0.84 to 13.4 ppm with an error ranging from 1×10^{-4} to 7×10^{-4}% (w/w) and a relative standard deviation not exceeding 4.2%.

This work was aimed at developing a method for the determination of organophosphorus compounds as additives in lubricating oils by direct extraction of the additive from the sample in a suitable organic solvent and analysis by GC–FPD. Triphenyl phosphate and *p*-tricresyl phosphate were used as models for the organophosphorus additives in lubricating oils.

2. Experimental

2.1. Apparatus

A Varian GC-Vista 6000 gas chromatograph equipped with both a flame photometric detector and a flame ionization detector. The FDP was used during this work. Nitrogen of 99.99% purity was used as the carrier gas with an optimum volume flow-rate of 30 ml/min. The optimum volume flow-rates of the other gases were hydrogen 140 ml/min, and air-I 80 ml/min and air-II 170 ml/min. The detector and column inlet temperatures were set at 20°C above the column temperature. Isothermal column temperatures between 200 and 280°C were applied (Table 1) and 260°C was the most suitable for selective separation (Fig. 1). All the optimum conditions found during this work were fixed throughout the analysis. A linear 1200 paper recorder with capacity 1 mV and chart speed 1

Table 1
Retention times of organophosphorus compounds dissolved in 95% ethanol on 3% OV-17 at different column temperatures

Compounds	Retention time (min)								
	200°C	210°C	220°C	230°C	240°C	250°C	260°C	270°C	280°C
Triphenyl phosphate	17.6	12.2	7.91	5.33	3.77	2.62	1.88	1.49	1.01
p-Tricresyl	43.0	39.8	20.6	14.4	9.43	5.34	4.39	3.01	2.12

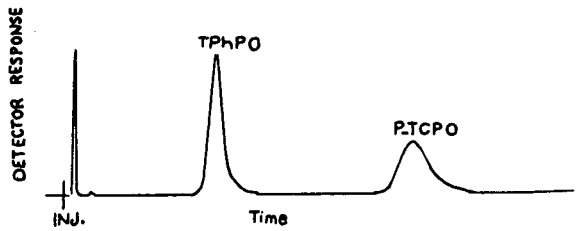

Fig. 1. Chromatogram of a mixture of triphenyl phosphate and *p*-tricresyl phosphate in gasoline engine lubricating oil obtained on a 3% OV-17 column with FPD at 260°C.

cm/min was used. Columns were made of stainless-steel tubing (2 m × 3.25 mm O.D. and 2.4 mm I.D.). They were packed with different percentages of different polysiloxane liquid stationary phases on Chromosorb W DMCS (80–100 mesh). The most selective for the analysis was found to be 3% OV-17 (50% phenylmethylpolysiloxane).

2.2. Materials

All compounds were of high purity purchased from Fluka and BDH and no further purification was needed. Engine lubricating oils (base and improvement treated oil) were obtained from the Al-Dora Refinery, Baghdad, Iraq.

2.3. Preparation of samples

Samples of different types of engine lubricating oils were blended with different amounts of triphenyl phosphate ranging from 0.002 to 1.0% (w/w), which correspond to 2.12–955 ppm phosphorus; this range was selected based on the literature [2]. The preparation was done by weighing 1 g of triphenyl phosphate accurately and blending it with 100 g of oil by heating at 40°C for 1 min with shaking. Approximately 1 g of this sample was weighed accurately in a conical flask, then 20 ml of 95% ethanol were added, the mixture was shaken well and transferred into a 25-ml separating funnel, shaken vigorously for 1 min and then allowed to settle for 5 min and the ethanol layer (upper) was transferred into a 100-ml volumetric flask. The extraction with 95% ethanol was repeated five times to ensure completeness of extraction and 95% ethanol was used to complete the volume to 100 ml. The same procedure of blending and extraction was followed for *p*-tricresyl phosphate.

Table 2
Accuracy and precision of the determination of triphenyl phosphate as an additive in gasoline engine lubricating oils

Sample	Phosphorus added (ppm)	Phosphorus found[a] (ppm)	Error (%)	R.S.D. (%)	Recovery (%)
Base gasoline engine lubricating oil	951	944	−0.70	1.70	99.30
	92.5	91.5	−1.08	0.10	98.92
	9.24	9.11	−1.40	1.05	98.60
	4.65	4.55	−2.08	2.31	97.92
	2.10	2.04	−2.87	1.70	97.13
Treated gasoline lubricating oil[b]	952	941	−1.15	1.33	98.89
	92.0	91.0	−1.09	0.61	98.99
	9.09	8.95	−1.50	0.72	98.50
	4.58	4.50	−1.80	2.23	98.20
	2.12	2.05	−2.40	2.28	97.60

[a] Mean of six values.
[b] Gasoline engine lubricating oil treated with an improvement additive in the refinery.

Table 3
Accuracy and precision of the determination of triphenyl phosphate as an additive in diesel engine lubricating oils

Sample	Phosphorus added (ppm)	Phosphorus found[a] (ppm)	Error (%)	R.S.D. (%)	Recovery (%)
Base diesel engine lubricating oil	955	940	−1.57	0.58	99.47
	92.3	91.8	−0.54	0.35	98.41
	9.20	9.11	−0.98	0.59	99.02
	4.45	4.33	−2.62	1.76	97.38
	2.40	2.34	−2.36	2.42	97.64
Treated diesel engine lubricating oil[b]	949	939	−1.05	0.35	98.96
	95.6	94.2	−1.50	1.34	98.50
	9.11	9.02	−1.01	0.60	98.99
	4.55	4.43	−2.64	1.93	97.36
	2.50	2.44	−2.27	1.65	97.73

[a,b] See Table 2.

2.4. Analysis

A 1-μl volume of the extractant was injected into the gas chromatograph under the optimum experimental conditions found during this work. The calibration graph method was used to determine the amount of organophosphorus compound as an additive in lubricating oils. Therefore, a series concentrations of these additives containing phosphorus ranging from 1.0 to 1000 ppm was prepared in 95% ethanol and 1 μl of each sample was injected into the gas chromatograph.

Samples were prepared in 15-ml Quickfit stoppered, dark-glass tubes. The injections of all samples were made with a 1-μl Hamilton syringe

Table 4
Accuracy and precision of the determination of *p*-tricresyl phosphate as an additive in gasoline engine lubricating oils

Sample	Phosphorus added (ppm)	Phosphorus found[a] (ppm)	Error (%)	R.S.D. (%)	Recovery (%)
Base gasoline engine lubricating oil	850	842	−0.61	0.61	99.03
	85.1	84.2	−1.08	0.30	98.92
	8.56	8.45	−1.32	0.65	98.68
	4.60	4.53	−1.45	1.11	98.55
	2.25	2.21	−1.96	1.40	98.04
Treated gasoline lubricating oil[b]	850	839	−1.29	0.23	98.69
	85.5	84.5	−1.16	0.56	98.84
	8.45	8.45	0.66	0.59	99.44
	4.35	4.45	2.25	1.42	97.75
	2.30	2.27	1.31	1.53	98.70

[a,b] See Table 2.

Table 5
Accuracy and precision of the determination of *p*-tricresyl phosphate as an additive in diesel engine lubricating oils

Sample	Phosphorus added (ppm)	Phosphorus found[a] (ppm)	Error (%)	R.S.D. (%)	Recovery (%)
Base diesel engine lubricating oil	850	843	−0.92	1.25	99.15
	85.5	84.2	−1.52	0.42	98.44
	8.45	8.41	−0.40	1.72	99.60
	4.50	4.36	−2.96	2.07	97.04
	2.30	2.28	−0.73	2.80	99.27
Treated diesel engine lubricating oil[b]	855	845	−1.17	0.59	98.88
	86.6	85.1	−1.73	0.51	98.23
	8.55	8.38	−1.99	0.60	98.01
	4.44	4.35	−2.03	1.15	97.97
	2.60	2.55	−1.93	4.96	98.07

[a,b] See Table 2.

and the value of each determination was the mean of six analyses. The results are given in Tables 2–5.

Samples of different types of engine lubricating oils blended with different amounts of *p*-tricresyl phosphate as an additive were stored for 1 month in the ambient atmosphere and the same procedures were followed for extraction and analysis. The results are given in Tables 6 and 7.

3. Results and discussion

Triphenyl phosphate and *p*-tricresyl phosphate were used as models of organophosphorus addi-

Table 6
Effect of storage of *p*-tricresyl phosphate as an additive in gasoline engine lubricating oils

Sample	Mean value before storage (ppm)	Mean value after storage[a] (ppm)	*t* Value[b]	Significance[c]
Base oil (gasoline)	842	840	0.10	N.S.
	84.2	84.2	0.15	N.S.
	8.44	8.44	0.00	N.S.
	4.35	4.58	0.11	N.S.
	2.20	2.20	0.34	N.S.
Treated oil[d]	839	837	0.78	N.S.
	84.5	84.5	0.02	N.S.
	8.45	8.48	1.16	N.S.
	4.24	4.25	0.26	N.S.
	2.27	2.26	0.43	N.S.

[a] Storage for 30 days.
[b] Data were analysed statistically by using the *t*-test.
[c] N.S. = Not significant.
[d] See footnote B in Table 2.

Table 7
Effect of storage of *p*-tricresyl phosphate as an additive in diesel engine lubricating oils

Sample	Mean value before storage (ppm)	Mean value after storage[a] (ppm)	*t* Value[b]	Significance[c]
Base oil (diesel)	843	843	0.00	N.S.
	84.2	84.2	0.00	N.S.
	8.41	8.41	0.00	N.S.
	4.36	4.37	0.00	N.S.
	2.28	2.34	1.02	N.S.
Treated oil[d]	845	846	0.15	N.S.
	85.1	85.0	0.18	N.S.
	8.38	8.41	0.93	N.S.
	4.35	4.40	1.54	N.S.
	2.55	2.56	0.29	N.S.

[a–d] See Table 6.

tives in lubricating oils. Ethanol was chosen the extraction solvent because of its high polarity, so it extracts the polar components particularly well, and also it is not toxic and easy to work with. The base oil consisted of 70–85% *n*-alkanes (C_{24}–C_{35}) and 15–30% naphthenes, which are not soluble in ethanol, so the expected negative peak interference from alkanes with FPD can be prevented [14,18].

A 3% OV-17 column was utilized for the separation of organophosphorus compounds according to the results obtained previously in our laboratory [19], and a dual flame photometric detector was used for the determination because of its high selectivity, linearity and sensitivity [20].

In order to examine the accuracy, sensitivity and precision of the method, 2.12 ppm was the minimum and 955 ppm the maximum amounts of phosphorus blended with engine lubricating oil as triphenyl phosphate or *p*-tricresyl phosphate.

Tables 2 and 3, for triphenyl-phosphate blended with gasoline and diesel engine lubricating oils, respectively, show errors ranging from 0.70 to 2.80% with relative standard deviations not exceeding 2.4%. Tables 4 and 5, for *p*-tricresyl phosphate blended with gasoline and diesel engine lubricating oils, respectively, show errors ranging from 0.4 to 2.96% with relative standard deviations not exceeding 2.80%.

Tables 6 and 7 indicate that storage for 30 days in an ambient atmosphere of different types of lubricating oils containing phosphorus with concentrations ranging from 2.20 to 845 ppm as *p*-tricresyl phosphate has no effect on the concentration of phosphorus additives in all samples. Finally, the developed method proved to be rapid, since the analysis of each sample requires 20 min and 72 samples can be analyzed per 8-hr day.

References

[1] J.R. Van Wazer, *Phosphorus and Its Compounds*, Vol. II, Interscience Publishers, New York, NY, 1961, Ch. 31.
[2] W.C. Gergel, *Lubricant Additive Chemicals*, Report No. C-9331, Lubrizol, Cleveland, OH, 1987.
[3] E.S. Forbes, *Tribology*, August (1970) 145.
[4] J.E. Barney, II, J.G. Bergmann and W.G. Tuskan, *Anal. Chem.*, 31 (1959) 1394.
[5] *ASTM Standards on Petroleum Products and Lubricants*, American Society for Testing and Materials, Philadelphia, PA, 1958, Method D 1091-58T.
[6] A. Pietrogrande, M. Zancato and G. Bontempelli, *Analyst*, 100 (1985) 993.
[7] S.J. Gedanky, J.E. Bowen and O.I. Milner, *Anal. Chem.*, 32 (1960) 1447.
[8] S. Płaza, Analyst, 109 (1984) 1313.
[9] W.N. Elliot, C. Heathcote and R.A. Mostyn, *Talanta*, 19 (1972) 359.

[10] B.G. Julin, H.W. Vanderborn and J.J. Kirkland, *J. Chromatogr.*, 112 (1975) 443.
[11] P. Tittarelli and A. Mascherpa, *Anal. Chem.*, 53 (1981) 1466.
[12] A. Prevot and M. Gente Janniaux, *At. Absorpt. Newsl.*, 17 (1978) 1.
[13] E. Russeva and I. Rhavezov, *Izv. Akad. Nauk SSSR, Ser. Khim.*, 19 (1986) 422.
[14] C.R. Vogt and S. Kapilla, *J. Chromatogr. Sci.*, 17 (1979) 546.
[15] S. Sass and G.A. Parker, *J. Chromatogr.*, 189 (1980) 331.
[16] K. Pospisilova, J. Senkyrova, J. Paryzkova and Z. Jelinek, *Chem. Prum.*, 38 (1988) 484; *C.A.*, 109 (1988) 233839q.
[17] A.E. Habboush, S.M. Farroha and L.S. Umar, *Abstr. PITTCON 1990,* p. 321, New York.
[18] S.O. Abdelrahman and L.N. Kvitkovski, *Izv. Vyssh. Uchebn. Zaved. Neft Gaz*, 12 (1987) 49; *Ca.*, 108 (1988) 189509k.
[19] H.I. Khalaf, *M.Sc. Thesis*, College of Science, University of Baghdad, Baghdad, 1989.
[20] P.L. Patterson, R.L. Howe and A. Abu-Shumays, *Anal. Chem.*, 50 (1978) 345.

ELSEVIER

Journal of Chromatography A, 696 (1995) 265–272

JOURNAL OF CHROMATOGRAPHY A

Binding of anticancer drugs to human serum albumin studied by reversed-phase chromatography

Esther Forgács*, Tibor Cserháti

Central Research Institute for Chemistry, Hungarian Academy of Sciences, P.O. Box 17, 1525 Budapest, Hungary

First received 2 November 1994; revised manuscript received 6 December 1994; accepted 16 December 1994

Abstract

The interaction of eight commercial anticancer drugs with human serum albumin (HSA) was studied by charge-transfer reversed-phase thin-layer chromatography in neutral, acidic, basic and ionic environments (NaCl and $CaCl_2$) and the relative strength of interaction was calculated. Each drug interacted with HSA in a neutral environment, and the pH and the presence of mono- and divalent cations markedly affected the strength of interaction. The capacity of anticancer drugs to interact with HSA depended considerably on their molecular structure. Various multivariate statistical methods such as principal component analysis and cluster analysis indicated that the steric parameters of anticancer drugs have a considerable impact on their capacity to bind to HSA. The influence of electronic parameters on the HSA–drug interaction was of secondary importance.

1. Introduction

Much effort has been devoted to the elucidation of the mode of action of various anticancer drugs. It has been established that they can bind to different biomolecules such as model and native membranes [1], DNAs [2,3] and various proteins [4]. The binding of anticancer drugs to proteins may modify the protein structure [5] and can increase or decrease the enzyme activity [6,7], resulting in modified biological efficiency of the drugs [8].

Until now, mainly reversed-phase high performance liquid chromatography was used for the study of the interaction of various drugs with proteins [9], because the mobility of proteins is very low on traditional reversed-phase thin-layer chromatographic (RP-TLC) plates. However, it has been found that serum albumins show adequate mobility on recently developed reversed-phase (RP-18W/UV_{254}) plates. This effect has been exploited for the enantiomeric separation of various compounds by adding bovine serum albumin at a concentration of 3–6% to aqueous eluents [10]. The same reversed-phase plates have been used for the successful enantiomeric separation of dansylated amino acids [11].

Charge-transfer chromatography carried out on RP-TLC layers has previously been applied to study the interaction between taxol and other anticancer drugs with acetyl-β-cyclodextrin [12] and hydroxypropyl-β-cyclodextrin [13]. To elucidate the role of individual amino acids in the binding of anticancer drugs to proteins, the interaction of amino acids with anticancer drugs has also been studied by this method and the involvement of hydrophilic forces in the drug–amino acid interaction has been stressed [14].

* Corresponding author.

0021-9673/95/$09.50
SSDI 0021-9673(94)01264-4

Principal component analysis (PCA) and cluster analysis (CA) have frequently been used to extract maximum information from retention data matrices of considerable dimensions [15,16]. The advantages of the application of PCA is that it allows a reduction in the number of variables whilst maintaining most of information content. PCA is suitable not only for calculations of two–two variables relationships, but also for the simultaneous study of all-variables relationships. For the easier visualization of the multi-dimensional results of PCA, the two-dimensional nonlinear map [17] and cluster analysis (CA) [18] can be applied.

The objectives of this work were to study the interaction of some anticancer drugs with human serum albumin (HSA) by means of charge-transfer chromatography, to study the effect of various environmental conditions (pH, NaCl and $CaCl_2$), to determine the relative strength of interaction and to elucidate the role of various molecular parameters of drugs that influence their binding to HSA. The use of various additives was motivated by the fact that the pH of the environment and the presence of various salts considerably influence the strength of interaction between bioactive molecules [19].

2. Experimental

RP-18W/UV_{254} plates were purchased from Macherey–Nagel (Düren, Germany) and used as received. HSA (electrophoretic purity over 95%) was purchased from Reanal (Budapest, Hungary) and used as received. The IUPAC and common names and the structures of anticancer drugs are shown in Table 1 and Fig. 1, respectively.

The drugs were dissolved in methanol at a concentration of 3 mg/ml and 2-μl volumes of the solutions were spotted separately on the plates. The eluent systems were aqueous solutions containing HSA in the concentration range 0–50 mg/ml. Owing to the relatively high molecular mass, higher concentrations of HSA could be used because the eluent became extremely viscous, resulting in a very low mobility of the eluent front. As the object was to study the binding of drugs to HSA and not to study the effect of HSA on the separation of anticancer drugs, the drugs were separately spotted on the plates. In this way the HSA: drug ratio was the same for each drug. Developments were carried out in sandwich chambers ($22 \times 22 \times 3$ cm) at room temperature, the distance of development being about 16 cm. After development, the plates were dried at 105°C and the spots of anticancer drugs were revealed by their UV adsorption and with iodine vapour. Each determination was run in quadruplicate. To study the effect of pH and the presence of salts, each experiment was run also in eluents containing 0.16 *M* sodium acetate, acetic acid, NaCl and $CaCl_2$ (the pH of the $CaCl_2$ solution was set at 7).

The R_M value characterizing molecular lipophilicity in RP-TLC was calculated from the equation by $R_M = \log(1/R_F - 1)$ separately for each drug and eluent system. The dependence of the R_M value of each drug on the concentration of HSA was calculated by the following equation:

$$R_M = R_{M0} + bc \quad (1)$$

where R_M is the R_M value for a drug determined at a given HSA concentration, R_{M0} is the R_M value extrapolated to zero HSA concentration b is the decrease in the R_M value caused by a unit change in HSA concentration in the eluent (related to the strength of HSA–drug interaction) and C is the concentration of HSA in the eluent (m*M*).

To find the similarities and dissimilarities between the relative strength of HSA–drug interactions determined in neutral, basic, acidic and ionic environments and the physico-chemical parameters of the drugs, PCA was applied. The slope (b) value in Eq. 1 and the various physico-chemical parameters of drugs were the variables (fourteen altogether) and the drugs were the observations. The total variance explained was set to 99%. The physico-chemical parameters included in the calculation were π = Hansch–Fujita substituent constant characterizing hydrophobicity, *H-Ac* and *H-Do* = indicator variables

Table 1
IUPAC names of anticancer drugs

No.	Common name	Systematic name	Provenance
1	Ftorafur	N-(2-Furanidyl)-5-fluorouracil	Medexport (Russia)
2	Bicnu	N,N-Bis(2-chloroethyl)-N-nitrosourea	Laboratoire Bristol (France)
3	Vumon	4′-O-Demethyl-1-O-(4,6-O-2-thenylidene-β-D-glucopyranosyl)epipodophyllotoxin	Bristol-Arzneimittel (Germany)
4	Natulan	N-(1-Methylethyl)4-[(2-methylhydrazino)methyl]benzamide	Roche (Switzerland)
5	Alexan	4-Amino-1-β-D-arabifuranosyl-2(14)-pyrimidine	Mack (Germany)
6	Mitomycin C	[1-a*R*]-6-Amino-8-[(aminocarbonyl)oxymethyl]-1, 1a, 2, 8, 8a, 8b-hexahydro-8a-methoxy-5-methylazirino[2′,3′:3,4]pyrrolo[1,1*a*]indole-4,7-dione	Kyowa (Japan)
7	Deticene	5-(3,3-Dimethyl-1-triazenyl)-1-*H*-imidazole-4-carboxamide	Rhône-Poulenc (France)
8	Metotrexate	2,4-Diamino-10-methylpteroylglutamic acid	Lachema (Czech Republic)

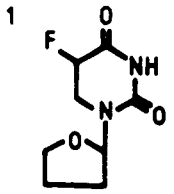

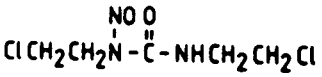

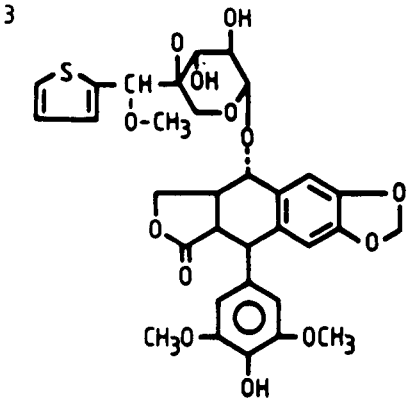

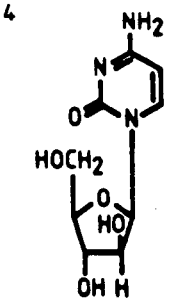

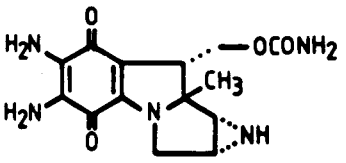

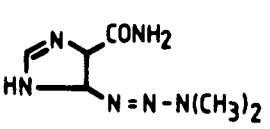

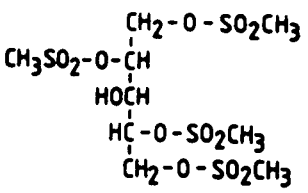

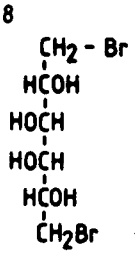

Fig. 1. Structures of anticancer drugs.

for proton acceptor and proton donor properties, respectively, *M-RE* = molar refractivity, *F* and *R* = Swain–Lupton electronic parameters characterizing the inductive and resonance effect, respectively, σ = Hammett's constant, characterizing the electron-withdrawing power of the substituent, *Es* = Taft's constant, characterizing steric effects of the substituent, and B_1 and B_4 = Sterimol width parameters determined by the distance of substituents at their maximum point perpendicular to attachment.

Both two-dimensional non-linear mapping and CA were applied to the PC loadings and PC variables to visualize the multi-dimensional results of PCA and to compare their information content.

3. Results and discussion

In most instances the R_M value of the anticancer drugs decreased with increasing concentration of HSA in the eluent. This result indicates the binding of drugs to HSA; the more hydrophilic HSA makes the drugs less lipophilic by interacting with them. The direct binding of the drugs to HSA may modify the concentration of free drugs in the blood, their mobility, accessibility to the target organ or organs, their distribution between the hydrophobic and hydrophilic compartments of the cell, etc.

The parameters of Eq. 1 are compiled in Table 2. Each anticancer drug showed an interaction with HSA. Eq. 1 fits the experimental data well, the significance level being over 95%. Eq. 1 accounted for 60.12–98.23% of the total variance, suggesting that HSA has a significant impact on the hydrophobicity parameters of the drugs. The relative strength of interaction (*b*) shows a high divergence depending both on the type of drug and on the pH and salts. This finding supports the supposition that not only the molecular structure but also the physiological conditions of the environment may have a significant influence on the binding of anticancer drugs to HSA. The interaction strength of drugs containing basic –NH– or $-NH_2$ groups was higher in the presence of $CaCl_2$ than in an ion-free neutral environment. It is probable that with these drugs the formation of salt bridges between the corresponding substructures of HSA and the drugs contribute to the binding.

The results of PCA are given in Table 3. Five principal components were sufficient to explain most of the variance (96.29%), which means that the original fourteen variables can be substituted by five background (imaginary) variables without a considerable loss of information. Unfortunately, PCA does not define these five background variables as concrete physico-chemical entities, it only indicates their mathematical possibility. Except for the interactive forces determined in the presence of $CaCl_2$, the other interactive forces, the steric (*Es*, B_1, *M-RE* and B_4) characteristics and electronic (*R*) parameter of the drugs have high loadings in the first principal component, indicating that these physico-chemical parameters may have a marked impact on the HSA–drug interaction. This result can be explained by the supposition that steric parameters of the drugs influence the accessibility of the active centers on the surface of the HSA molecule. These active centers are probably hydrophilic, and the direct binding of drugs to HSA occurs by hydrophilic forces (probably hydrogen bond formation). The conclusions drawn from the two-dimensional non-linear map (Fig. 2) and cluster dendogram of PC loadings (Fig. 3) entirely support our previous conclusions: the relative strengths of interaction determined in neutral, acidic, basic and NaCl-containing environments form a cluster with steric parameters of drugs. We must stress that other physico-chemical parameters of anticancer drugs not included in the calculations may also have some influence on the HSA–drug interactions and our conclusions are valid only for the parameters included in these calculations.

The two-dimensional non-linear map and cluster dendogram of PC variables are shown in Figs. 4 and 5, respectively. Anticancer drugs do not form distinct clusters on these maps. However, drugs with a basic substructure (compounds **3**, **6** and **8**) are slightly separated from the other. This again indicates the possible role of hydrophilic forces in the HSA–drug interactions. It

Table 2
Parameters of the linear correlation between the retention (R_M) of anticancer drugs and the concentration of human serum albumin (C mM) in the mobile phase ($R_M = R_{M0} + bc$)

Eluent	Compound[a]	R_{M0}	$-b \cdot 10$	$S_b \cdot 10$	r_{calc}
Neutral					
	1	0.85	1.34	0.93	0.9356
	2	2.55	10.10	0.96	0.9911
	3	1.74	4.11	1.49	0.7772
	4	2.07	6.78	2.26	0.8021
	5	0.44	6.22	1.41	0.9746
	6	2.15	6.32	1.98	0.8803
	7	1.19	3.30	1.11	0.8278
	8	1.66	13.71	2.43	0.9293
0.16 *M* acetic acid end concentration					
	1	0.73	3.17	0.83	0.8844
	2	2.26	6.57	1.75	0.8825
	3	1.64	3.82	1.39	0.7754
	4		Not significant		
	5		Not significant		
	6	2.02	3.83	1.43	0.7674
	7	1.06	4.84	1.16	0.9007
	8	1.85	8.62	2.02	0.9049
0.16 *M* sodium acetate end concentration					
	1		Not significant		
	2	2.15	6.35	2.16	0.8268
	3	1.71	3.41	1.18	0.7890
	4		Not significant		
	5		Not significant		
	6	1.96	5.36	0.55	0.9897
	7	1.07	4.29	0.91	0.9199
	8	1.73	10.97	1.50	0.9562
0.16 *M* NaCl end concentration					
	1	0.21	0.71	0.02	0.7878
	2	2.01	2.55	0.37	0.9501
	3	1.91	5.05	1.12	0.7932
	4		Not significant		
	5	0.12	2.77	0.58	0.9218
	6	1.65	2.86	0.34	0.9865
	7	0.99	7.76	1.04	0.9657
	8	1.86	14.49	4.32	0.9320
0.16 *M* $CaCl_2$ end concentration					
	1	1.15	6.37	1.20	0.9588
	2	2.18	4.94	1.04	0.8998
	3	1.75	3.87	0.89	0.8974
	4		Not significant		
	5	0.10	4.45	1.23	0.9583
	6	2.16	10.92	1.11	0.9080
	7	0.79	6.65	1.78	0.8096
	8		Not significant		

[a] See Table 1.

Table 3
Relationship between the retention parameters and physico-chemical parameters of anticancer drugs: results of principal component analysis

No. of PC	Eigenvalue	Variance explained (%)	Total variance explained (%)
1	6.18	44.18	44.18
2	2.63	18.82	63.00
3	1.94	13.93	76.92
4	1.45	10.38	87.30
5	1.26	8.99	96.29

Parameter		Principal component loadings			
		1	2	3	4,5
π	−0.21	0.68	−0.26	0.38	0.47
H-Do	0.36	−0.33	−0.11	−0.13	0.78
M-Re	0.54	0.45	−0.68	0.01	−0.01
F	−0.34	0.90	0.12	−0.11	0.12
R	−0.86	−0.05	0.26	0.28	0.25
σ	0.10	0.83	0.46	−0.19	0.03
Es	−0.93	−0.08	0.33	−0.05	0.01
B_1	0.98	0.03	0.01	−0.09	−0.15
B_4	0.88	0.14	−0.42	−0.07	0.04
b_{H_2O}	0.72	−0.38	0.39	−0.18	0.28
$b_{H\text{-}Ac}$	0.64	0.12	0.48	0.56	0.07
$b_{Na\text{-}Ac}$	0.82	−0.12	0.32	0.41	0.19
b_{NaCl}	0.70	0.25	0.38	0.20	−0.39
b_{CaCl_2}	−0.33	−0.23	−0.40	0.75	−0.17

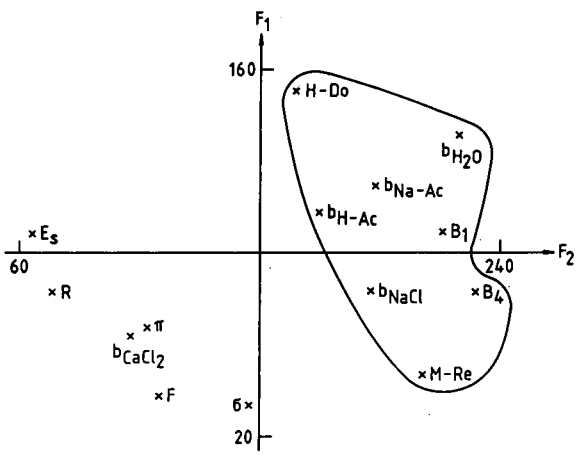

Fig. 2. Two-dimensional non-linear map of principal component loadings. Number of iterations, 77; maximum error, $4.54 \cdot 10^{-2}$. For symbols, see Experimental.

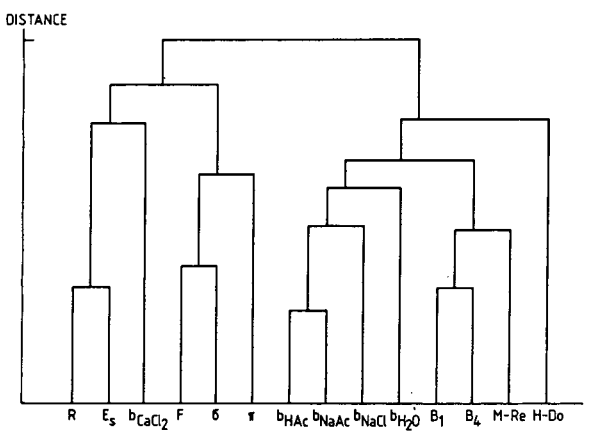

Fig. 3. Cluster dendogram of principal component loadings. For symbols, see Experimental.

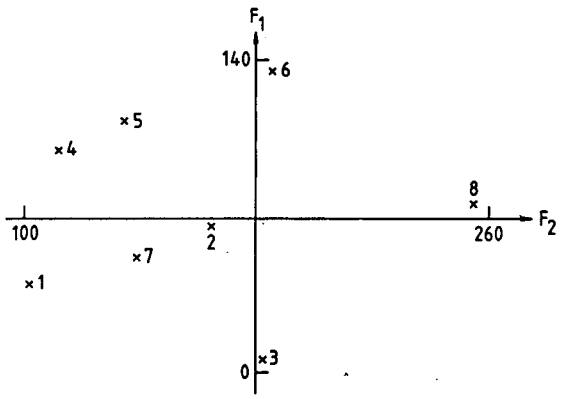

Fig. 4. Two-dimensional non-linear map of principal component variables. Number of iterations, 87; maximum error, $3.67 \cdot 10^{-2}$. Numbers refer to anticancer drugs in Fig. 1 and Table 1.

can be assumed that these basic structures can bind to secondary carboxyl groups of dicarboxyamino acids in HSA, contributing to the stability of the HSA–drug binding.

It can be concluded from the data that the anticancer drugs can bind to HSA, the strength of interaction depending on the pH and on the presence of dissociable salts. Multivariate mathematical statistical calculations indicated that the steric and electronic parameters of anticancer drugs have a marked impact on their capacity to interact with HSA. It is probable that the steric conditions govern the accessibility of polar binding centers on the HSA surface whereas hydrophilic forces (possibly hydrogen bonding) are the decisive factors in the formation of the various HSA–drug associates.

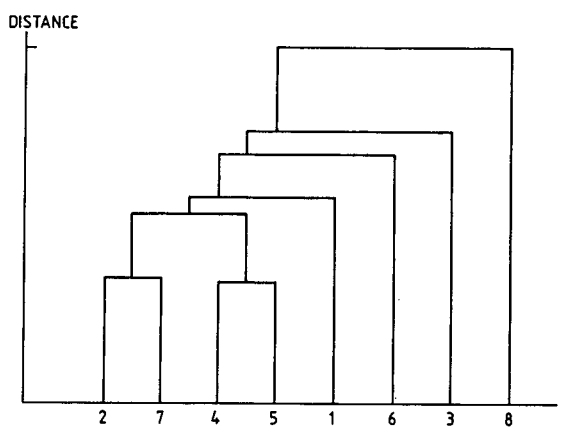

Fig. 5. Cluster dendogram of principal component variables. Numbers refer to anticancer drugs in Fig. 1 and Table 1.

Acknowledgement

This work was supported by a grant (OTKA T7340) from the Hungarian Academy of Sciences.

References

[1] J.B.A. Custodio, L.M. Almeida and V.M.C. Madeira, *Biochim. Biophys. Acta*, 1150 (1993) 123.
[2] T. Araka, T. Kusakabe, J. Kuwahara, M. Otsuka and Y. Sugiura, *Biochem. Biophys. Res. Commun.*, 190 (1993) 362.
[3] G.J. Finlay, E. Marshall, J.H.L. Matthews, K.D. Paull and B.C. Baguley, *Cancer Chemother Pharmacol.*, 31 (1993) 401.
[4] M. Kimura, *Yakugaku Zasshi*, 112 (1992) 914.
[5] J.A. Broomhead, L.M. Rendina and L.K. Webster, *J. Inorg. Biochem.*, 49 (1993) 221.
[6] D.W. Fry, T.J. Boritzki, R.C. Jackson, P.D. Cook and W.R. Leopold, *Mol. Pharmacol.*, 44 (1993) 479.
[7] C. Leguellec, B. Lacarelle, J. Catalin and A. Durand, *Cancer Chemother. Pharmacol.*, 32 (1993) 491.
[8] G.N. Kumar, U.K. Walle, K.N. Bhalla and T. Walle, *Res. Commun. Chem. Pathol. Pharmacol.*, 80 (1993) 337.
[9] T. Cserháti and K. Valkó, *Chromatographic Determination of Molecular Interactions*, CRC Press, Boca Raton, FL, 1994.
[10] L. Lepri, V. Coas, G. Desideri and L. Pettini, *J. Planar Chromatogr.*, 6 (1993) 100.
[11] L. Lepri, P. Desideri and D. Santianni, *Chromatographia*, 36 (1993) 297.
[12] T. Cserháti, *Fresenius' J. Anal. Chem.*, 349 (1994) 751.
[13] T. Cserháti and J. Holló, *Int. J. Pharm.*, 108 (1994) 69.
[14] T. Cserháti and J. Holló, *Biochem. Mol. Biol. Internat.*, 32 (1994) 201.
[15] K.V. Mardia, J.T. Kent and J.M. Bibby, *Multivariate Analysis*, Academic Press, London, 1979.
[16] J.R. Llinas and J.M. Ruiz, in G. Vernin and M. Chanon (Editors), *Computer Aids to Chemistry*, Ellis Horwood, Chichester, 1985, p. 200.
[17] J.W. Sammon, Jr., *IEEE Trans. Comput.*, C18 (1969) 401.
[18] W.R. Dillon, *Multivariate Analysis*, Wiley, New York, 1984, p. 157.
[19] J. Turkova, *Bioaffinity Chromatography*, Elsevier, Amsterdam, 1993, p. 328.

ELSEVIER

Journal of Chromatography A, 696 (1995) 273–284

JOURNAL OF CHROMATOGRAPHY A

Parameters controlling the elution window and retention factors in micellar electrokinetic capillary chromatography

P.G.H.M. Muijselaar*, H.A. Claessens, C.A. Cramers

Laboratory of Instrumental Analysis, Eindhoven University of Technology, P.O. Box 513, 5600 MB Eindhoven, Netherlands

First received 24 August 1994; revised manuscript received 15 December 1994; accepted 23 December 1994

Abstract

The resolution of uncharged compounds in micellar electrokinetic capillary chromatography (MECC) is influenced by both the elution window and the retention factors of the compounds. The influence of the electroosmotic mobility and the effective mobility of the micelles on the elution window is treated theoretically and the effect of different experimental conditions on the elution window and the retention factors is determined. Although these variables cannot be controlled independently in many cases, the resolution in MECC can be improved by adjusting the composition of the applied electrolyte system. This is demonstrated for several electrolyte systems with different pH values, ionic strengths, surfactant concentrations and organic modifier contents. Further, the influence of the applied field strength, capillary surface modifications and the alkyl chain length of the surfactant are evaluated.

1. Introduction

Micellar electrokinetic capillary chromatography (MECC), has proved to be a highly efficient separation method for the determination of neutral compounds. Applying the same instrumentation as in capillary zone electrophoresis, in MECC uncharged compounds can be separated based on differences in their partitioning between two phases, just as in chromatographic techniques. Since the introduction of MECC by Terabe et al. [1,2], several authors have paid attention to the fundamental characteristics of this separation method [3,4] and to the effect of different separation parameters on the migration behavior [5–11]. Also the theoretical [12,13] and practical [14,15] aspects of resolution optimization have been well described.

1.1. Elution window and migration modes

The separation mechanism of neutral compounds in MECC is based on their partitioning between two moving phases, viz. an electroosmotically pumped aqueous mobile phase and a pseudostationary micellar phase. The distribution between these two phases is expressed by the retention factor, k, which can be calculated according to [1,2]:

$$k = \frac{\eta_{MC}}{\eta_{AQ}} = \frac{t_S - t_{EOF}}{t_{EOF}\left(1 - \frac{t_S}{t_{MC}}\right)} \quad (1)$$

where η_{MC} and η_{AQ} are the numbers of moles of

* Corresponding author.

0021-9673/95/$09.50
SSDI 0021-9673(94)01293-8

the solute in the micellar and the aqueous phase, and t_S, t_{EOF} and t_{MC} are the migration times of the solute, the electroosmotic flow (EOF) and the micelles, respectively. All neutral compounds will migrate with an overall linear velocity, v_S, according to:

$$v_S = \frac{1 + \frac{t_{EOF}}{t_{MC}} k}{1 + k} m_{EOF} E \quad (2)$$

where m_{EOF} and E are the electroosmotic mobility and the applied field strength, respectively. They will be detected within the time interval between t_{EOF} and t_{MC} [2], which is called the elution window. Under conditions of a constant field strength, the elution window is determined by the electroosmotic mobility, m_{EOF}, and the effective mobility of the micelles, m_{MC}, according to:

$$\frac{t_{MC}}{t_{EOF}} = \frac{m_{EOF}}{m_{EOF} + m_{MC}} \quad (3)$$

The elution window, i.e. t_{MC}/t_{EOF}, can be increased by increasing $|m_{MC}|$ or by decreasing m_{EOF}. If the absolute value of the effective mobility of the micelles exceeds the electroosmotic mobility, the elution window becomes negative.

As described by Vindevogel and Sandra [4], three different migration modes can be distinguished. If $t_{MC}/t_{EOF} > 0$, all compounds will migrate to the detector, which is called the normal mode. If $t_{MC}/t_{EOF} < 0$, only compounds for which holds $k < -(t_{MC}/t_{EOF})$ will migrate to the detector. This mode is called the restricted elution mode. Compounds for which holds $k > -(t_{MC}/t_{EOF})$ will migrate in the opposite direction. In order to detect these compounds a reversed polarity will have to be applied, which is called the reversed direction mode.

1.2. Resolution equation

The basic resolution equation for the resolution, R_S, between two closely eluting peaks (assuming $k \approx k_1 \approx k_2$) in MECC is given by [2,4]:

$$R_s = \frac{\sqrt{N}}{4} \frac{\alpha - 1}{\alpha} \frac{k}{1 + k} \frac{1 - \frac{t_{EOF}}{t_{MC}}}{1 + \frac{t_{EOF}}{t_{MC}} k} \quad (4)$$

where N and α are the number of theoretical plates and the separation factor k_2/k_1, respectively. The last term in Eqn. (5) reflects the specific resolution characteristics in MECC. The influence of the retention factor on the resolution is described by the retention term $f(k)$, formed by the product of the last two terms in Eqn. (4):

$$f(k) = \frac{k}{1 + k} \frac{1 - \frac{t_{EOF}}{t_{MC}}}{1 + \frac{t_{EOF}}{t_{MC}} k} \quad (5)$$

Graphs of $f(k)$ versus k in the normal mode show that increasing the elution window with a given retention factor leads to a higher value of $f(k)$ [2]. For each value of the elution window, the optimum retention factor, k_{opt}, can be calculated by differentiating Eqn. (5) with respect to k [12,16]:

$$k_{opt} = \sqrt{t_{MC}/t_{EOF}} \quad (6)$$

In the restricted elution mode and in the reversed direction mode the contribution of $f(k)$ to the resolution can reach much higher values than in the normal mode. However, this will lead to long analysis times, especially for compounds with a retention factor close to $-(t_{MC}/t_{EOF})$ [6].

Thus, assuming a constant efficiency and the selectivity being determined by the nature of the surfactant system, the resolution is mainly influenced by the elution window and the retention factors of the sample compounds. Therefore a good understanding of the effects of different experimental conditions on both these variables is important for the development of MECC analyses and for resolution optimization strategies. In this work, we studied the influence of the applied field strength, buffer pH, ionic strength, capillary surface modifications, alkyl chain length of the surfactant, surfactant concentration and organic modifier content on the elution window

and the retention factors of uncharged compounds in MECC.

2. Experimental

2.1. Instrumentation and separation conditions

All experiments were carried out on a BioFocus 3000 Capillary Electrophoresis System (BioRad, Hercules, CA, USA) at a constant temperature of 25°C. The wavelength of the detector was set at 200 nm. Pressure injection was carried out with an injection constant of 2 psi.s. All experiments were carried out with a constant voltage, with the anode placed at the inlet side and the cathode at the outlet side of the capillary, respectively. Two different fused-silica capillaries of 50 μm I.D. were applied; an original BioRad standard capillary, total length 50.0 cm, distance between injection and detection 45.5 cm, and a capillary from Supelco (Bellefonte, PA, USA), total length 70.0 cm, distance between injection and detection 65.4 cm. For some of the experiments several different coated fused-silica capillaries of 50 μm I.D. were applied; a C_{18} coated capillary from Supelco (CElect-H250, Bellefonte, PA, USA), a methyl silicone coated capillary and a polyethylene glycol coated capillary, both from Chrompack (Middelburg, The Netherlands), all with total length 70.0 cm, distance between injection and detection 65.4 cm. All experiments with the BioRad standard capillary were carried out three times, except for the experiments with the organic modifiers, which were carried out two times. The reported values are the average values.

2.2. Samples and solutions

All chemicals were of analytical-reagent grade. In Table 1 the compositions of the background electrolytes at different pH values are listed. To these buffer solutions 50 m*M* sodium dodecyl sulphate (SDS) was added, unless otherwise noted. Eight aromatic compounds were selected as sample compounds, covering a wide range of hydrophobicity. All sample compounds were dissolved at a final concentration of about 0.0005 *M* in a 50 m*M* SDS solution. Formamide was used as a neutral EOF marker and Sudan III as a micelle marker to measure t_{EOF} and t_{MC}, respectively.

Table 1
Composition of background electrolytes at different pHs

Cation[a] (0.01 *M*)	Buffering counter species[a]	pH
TRIS	Acetic acid	4.9
TRIS	MES	6.2
TRIS	o-Phosphoric acid	7.0
TEA	MOPS	7.0
TEA	HEPES	7.5
TRIS	MOPS	7.9
TRIS	MOPS	8.2
TRIS	Acetic acid	8.2
TRIS	Boric acid	8.5

[a] TRIS = tris(hydroxymethyl)aminomethane; TEA = triethanolamine; MES = 2-(N-morpholino)ethanesulphonic acid; MOPS = morpholinopropanesulphonic acid; HEPES = 4-(2-hydroxyethyl)-1-piperazineethanesulfonic acid.

3. Results and discussion

3.1. Applied field strength

According to Eqn. (2) the velocity of the sample compounds is linearly related to the applied field strength. Although a linear relationship was obtained at low field strengths, a positive deviation was observed at field strengths above ca. 200 V/cm. At a higher field strength the generated electric power will increase. Due to Joule heating, the mean temperature in the capillary will increase, which in turn will result in a decrease of the viscosity of the electrolyte solution. Both the electroosmotic mobility and the effective mobility of the micelles are inversely proportional to the viscosity.

The specific conductivity of the electrolyte solution, κ, can be calculated by Ohm's law:

$$V = \frac{1}{\pi r^2 \kappa} I \qquad (7)$$

where V is the applied voltage, l and r are the length and the radius of the capillary, respectively, and I is the measured electric current. Since the specific conductivity is inversely proportional to the viscosity, the electric current will proportionally increase if the viscosity decreases at a higher field strength. Therefore, a linear relationship was obtained for field strengths up to 400 V/cm between the velocity of the sample compounds and the measured electric current with regression correlation coefficients larger than 0.999. In Table 2 the measured electric current, the calculated specific conductivity, the electroosmotic mobility, the effective mobility of the micelles and the corresponding values for the elution window are listed for the different applied voltages.

3.2. Buffer pH and ionic strength

In fused-silica capillaries, the EOF originates from the dissociation of the surface silanol groups of the capillary wall. Therefore the electroosmotic mobility is dependent on the pH of the background electrolyte and, according to the double layer theory, also on the ionic strength. In Fig. 1 the pH dependence of the EOF is illustrated for phosphate buffers. As expected, a sigmoidal curve was obtained for m_{EOF} versus pH, also for the phosphate buffers containing 50 mM SDS. The lower m_{EOF} obtained with the buffers containing 50 mM SDS at high and intermediate pHs is due to an increase in viscosity and ionic strength of the electrolyte systems.

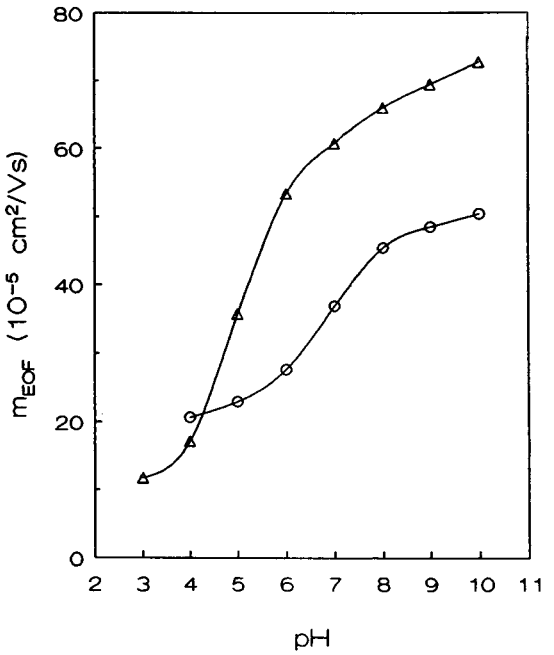

Fig. 1. Dependence of the electroosmotic mobility, m_{EOF}, on the pH for phosphate buffers, containing (△) 0 and (○) 50 mM SDS. The phosphate buffers were prepared by adding o-phosphoric acid to a 10 mM KOH solution until the desired pH was reached. Capillary from Chrompack. Applied voltage, 20 kV.

The more slightly decrease observed at lower pHs is due to adsorption of SDS on the inner wall of the capillary. For a given surfactant, the effective mobility of the micelles can be expected to be almost independent of pH [6]. In order to examine the influence of buffer pH and ionic

Table 2
Applied voltage, V (kV), measured electric current, I (μA), specific conductivity, κ (S/m), electroosmotic mobility, m_{EOF} (10^{-5} cm²/Vs), effective mobility of the micelles, m_{MC} (10^{-5} cm²/Vs), and values for the elution window, t_{MC}/t_{EOF}, for different applied field strengths. BioRad standard capillary. Background electrolyte, 10 mM TRIS–acetic acid at pH 8.2.

V	I	κ	m_{EOF}	m_{MC}	t_{MC}/t_{EOF}
3	3.0	0.255	61.96	−40.71	2.92
6	6.0	0.255	62.20	−40.54	2.87
9	9.2	0.260	63.48	−41.21	2.85
12	12.7	0.270	65.69	−42.47	2.83
15	16.7	0.284	68.50	−44.21	2.82
18	21.3	0.301	71.25	−45.88	2.81
20	24.3	0.309	73.39	−47.18	2.80

strength on the elution window and the retention factors in MECC, experiments were carried out with the electrolyte systems given in Table 1, containing 50 m*M* SDS. In addition, experiments were carried out with electrolyte systems containing 0.02 *M* of the cation and 100 m*M* SDS. In Table 3 all calculated electroosmotic mobilities, effective mobilities of the micelles, corresponding values of the elution window and retention factors of the eight sample compounds are listed. As can be seen from these results the electroosmotic mobility is dependent on pH and ionic strength, whereas the effective mobility of the micelles and the retention factors of the compounds are virtually constant for a given surfactant concentration. Of course this only applies for uncharged compounds in MECC. For charged compounds, the degree of dissociation and hence the retention factor may be strongly influenced by the pH of the electrolyte system [17]. The retention factors obtained with 100 m*M* SDS are less than twice those obtained with 50 m*M* SDS for all compounds, which is inconsistent with theory. Due to a higher electric current with the 100 m*M* SDS electrolyte system, the mean temperature in the capillary will increase. This will cause a decrease of distribution constants and retention factors of the sample

Table 3
Electroosmotic mobility, m_{EOF} (10^{-5} cm^2/Vs), effective mobility of the micelles, m_{MC} (10^{-5} cm^2/Vs), values for the elution window, t_{MC}/t_{EOF}, and retention factors, k, for (1) resorcinol, (2) phenol, (3) *p*-nitroaniline, (4) *p*-cresol, (5) 2,6-xylenol, (6) toluene, (7) 1,2-xylol and (8) propylbenzene, in two background electrolytes at different pHs. BioRad standard capillary. Applied voltage, 15 kV

pH	m_{EOF}	m_{MC}	t_{MC}/t_{EOF}	k							
				1	2	3	4	5	6	7	8
Cation concentration 10 mM, containing 50 mM SDS											
6.2	58.07	−44.31	4.22	0.22	0.52	1.14	1.47	2.87	3.33	8.24	24.79
7.0[a]	56.43	−43.97	4.53	0.25	0.56	1.22	1.55	2.82	3.22	7.94	24.27
7.5	61.26	−44.34	3.62	0.25	0.56	1.23	1.56	2.82	3.20	7.84	23.67
7.9	64.59	−44.68	3.24	0.27	0.56	1.19	1.51	2.60	3.10	7.66	23.32
8.2[b]	66.46	−44.95	3.09	0.28	0.56	1.19	1.51	2.74	3.12	7.62	23.06
8.2[c]	65.94	−44.00	3.00	0.24	0.51	1.11	1.42	2.63	3.02	7.46	22.48
8.5	66.75	−44.18	2.96	0.27	0.53	1.14	1.45	2.68	3.23	7.49	22.92
Average		−44.35		0.25	0.54	1.17	1.50	2.74	3.17	7.75	23.50
Standard deviation		0.33		0.02	0.02	0.04	0.05	0.10	0.09	0.26	0.75
Cation concentration 20 mM, containing 100 mM SDS											
7.5	52.88	−44.29	6.02	0.36	0.95	1.90	2.61	4.70	5.92	14.29	43.40
7.9	56.42	−44.45	4.72	0.35	0.91	1.81	2.49	4.54	5.76	13.95	42.40
8.2[d]	57.98	−44.32	4.24	0.37	0.93	1.87	2.56	4.64	5.83	14.02	42.83
8.2[e]	59.90	−45.09	4.05	0.38	0.93	1.86	2.55	4.66	5.84	14.20	43.02
8.5	60.14	−44.90	3.95	0.41	0.97	1.94	2.65	4.83	6.01	14.48	43.99
Average		−44.61		0.37	0.94	1.88	2.57	4.67	5.87	14.20	43.13
Standard deviation		0.32		0.02	0.02	0.04	0.05	0.09	0.09	0.18	0.54

[a] 0.01 *M* TEA–MOPS.
[b] 0.01 *M* TRIS–MOPS.
[c] 0.01 *M* TRIS–acetic acid.
[d] 0.02 *M* TRIS–MOPS.
[e] 0.02 *M* TRIS–acetic acid.

compounds [18,19]. In Fig. 2 the relationship between t_{MC}/t_{EOF} and m_{EOF} for the experiments, listed in Table 3, is illustrated.

From the foregoing it can be concluded that for a given separation of neutral species with a specific surfactant, the pH of the electrolyte system can be used to optimize the elution window in MECC. This is demonstrated in Fig. 3, where the electrokinetic chromatograms are shown for the separation of the sample mixture in an electrolyte system of 0.01 *M* TRIS–boric acid at pH 8.5 and 0.01 *M* TRIS–acetic acid at pH 4.9, respectively. In order to determine the effective mobility of the micelles and to be able to calculate retention factors with the low m_{EOF} at pH 4.9, Sudan III was injected at the outlet side of the capillary by electrokinetic injection with 10 kV for 10 s, after the hydrodynamic

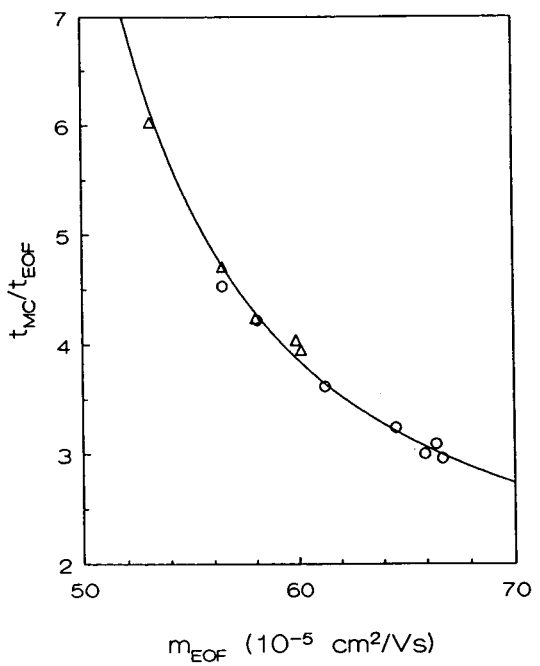

Fig. 2. Relationship between elution window and electroosmotic mobility for the electrolyte systems at different pHs with (○) a cation concentration of 0.01 *M*, containing 50 m*M* SDS and (△) a cation concentration of 0.02 *M*, containing 100 m*M* SDS. The drawn line represents the theoretical curve for an m_{MC} of $-44.46 \cdot 10^{-5}$ cm²/Vs. BioRad standard capillary. Applied voltage, 15 kV.

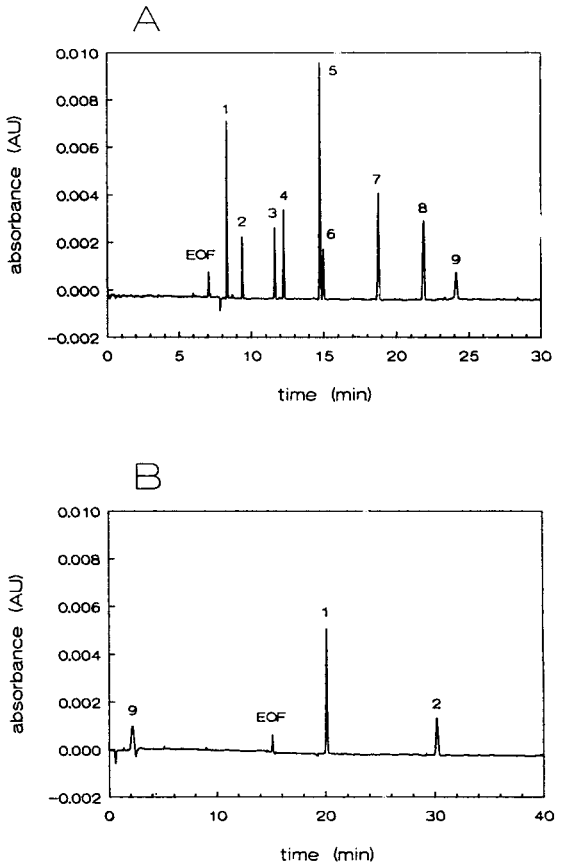

Fig. 3. Electrokinetic chromatograms of the separation of (1) resorcinol, (2) phenol, (3) *p*-nitroaniline, (4) *p*-cresol, (5) 2,6-xylenol, (6) toluene, (7) 1,2-xylol, (8) propylbenzene and (9) Sudan III in a background electrolyte of (A) 10 m*M* TRIS–boric acid at pH 8.5 and (B) 10 m*M* TRIS–acetic acid at pH 4.9. Capillary from Supelco. Applied voltage, 20 kV. For further explanation, see text.

injection of the sample mixture at the inlet side of the capillary. In Table 4 all measured migration times and calculated retention factors are listed. From these results it can be calculated that a change in t_{MC}/t_{EOF} is obtained from 3.43 to −2.08 if the pH of the electrolyte system is lowered from 8.5 to 4.9. Consequently a higher resolution is obtained, however, at the cost of a longer analysis time. Notice that in Fig. 3A all compounds are migrating in the normal mode. In Fig. 3B resorcinol and phenol are migrating in

Table 4
Migration times, t (min), and retention factors, k, with standard deviations (in parentheses), and theoretical plate numbers, N, in two background electrolytes. Capillary from Supelco. Applied voltage, 20 kV. ($n = 5$)

Compound	t	k	$N \cdot 10^{-5}$
10 mM TRIS–boric acid at pH 8.5			
EOF	7.01 (0.04)	0	–
Resorcinol	8.26 (0.05)	0.272 (0.001)	1.35
Phenol	9.35 (0.03)	0.547 (0.005)	1.52
p-Nitroaniline	11.64 (0.03)	1.283 (0.024)	1.69
p-Cresol	12.27 (0.02)	1.538 (0.029)	1.87
2,6-Xylenol	14.78 (0.02)	2.889 (0.053)	2.24
Toluene	15.03 (0.02)	3.061 (0.059)	2.32
1,2-Xylol	18.77 (0.03)	7.702 (0.142)	2.24
Propylbenzene	21.82 (0.07)	23.172 (0.449)	1.75
Sudan III	24.01 (0.11)	∞	1.73
10 mM TRIS–acetic acid at pH 4.9			
EOF	15.11 (0.07)	0	–
Resorcinol	19.98 (0.13)	0.197 (0.001)	1.64
Phenol	29.77 (0.31)	0.499 (0.007)	1.31
Sudan III[a]	2.21 (0.04)	∞	–

[a] Note that the length from injection to detection is only 4.6 cm for Sudan III. For further explanation, see text.

the restricted elution mode, whereas Sudan III is migrating in the reversed direction mode.

3.3. Capillary surface modifications

Besides the composition of the electrolyte system, the electroosmotic mobility can be controlled by modification of the capillary surface [20–22]. To investigate the influence of several surface modifications in MECC, the sample mixture was analysed with one uncoated and three different coated fused-silica capillaries in a 0.01 *M* TRIS–phosphoric acid electrolyte system at pH 7.0. In Fig. 4 all electrokinetic chromatograms are shown. The C_{18} and the polyethylene glycol coated capillaries showed a decrease in m_{EOF}, resulting in a larger elution window. However, also a decrease in efficiency was observed, probably due to solute–wall interactions. The methyl silicone coated capillary showed an increase in m_{EOF}, resulting in a smaller elution window. Toluene, 1,2-xylol, propylbenzene and Sudan III could not be detected, owing to adsorption of these compounds on the polymer coating. These results suggest that only for a limited number of compounds the application of coated capillaries in MECC may be advantageous.

3.4. Alkyl chain length of the surfactant

For micelles, the effective mobility will be strongly dependent on the nature of the surfactant. A shorter alkyl chain will lead to a reduced aggregation number and consequently to a reduced effective charge, but also to a reduced micelle size [23]. Both these factors influence the m_{MC} in an opposite way. Moreover, the m_{EOF} is also influenced by the nature of the surfactant. At equal surfactant concentrations, the phase ratio will decrease if a surfactant with a shorter alkyl chain is applied, due to an increase in the critical micelle concentration and a decrease in the partial molar volume of the micelles (see Eqn. 9), resulting in a decrease of the retention factors. Therefore the elution window and the retention factors cannot independently being

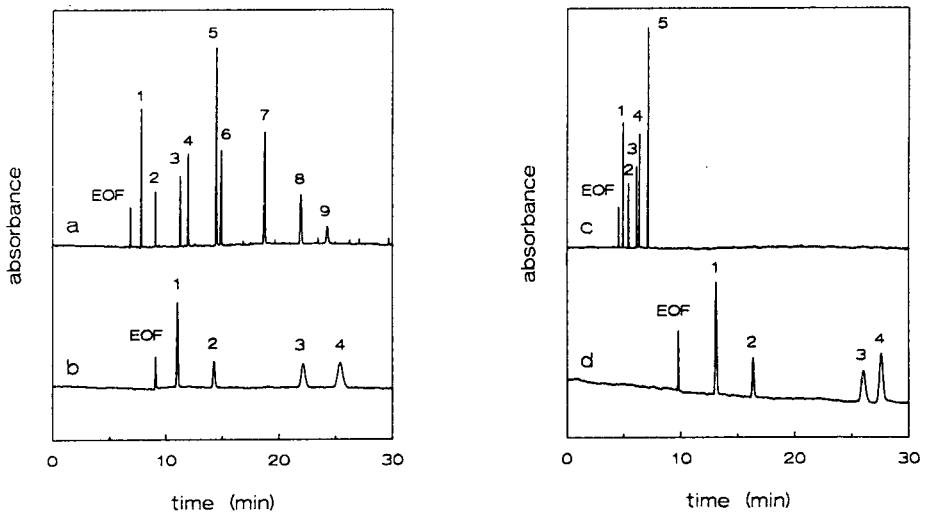

Fig. 4. Electrokinetic chromatograms of the sample mixture obtained with capillaries with different surface modifications: (a) untreated fused-silica capillary from Supelco, (b) C_{18} coated capillary from Supelco, (c) methyl silicone coated capillary from Chrompack and (d) polyethylene glycol coated capillary from Chrompack. Background electrolyte, 10 m*M* TRIS–phosphoric acid at pH 7.0. Applied voltage, 20 kV. See the legend of Fig. 3 for the names of the compounds.

optimized by changing the alkyl chain length of the surfactant.

3.5. Surfactant concentration

The retention factor is related to the distribution constant, K_c, and the phase ratio, β, according to:

$$K_c = k\,\beta \tag{8}$$

The phase ratio can be calculated according to:

$$\beta = \frac{V_{AQ}}{V_{MC}} = \frac{1 - \bar{v}\,(C_{SF} - CMC)}{\bar{v}\,(C_{SF} - CMC)} \tag{9}$$

where V_{AQ} and V_{MC} are the volume of the aqueous phase and the micellar phase, respectively, $\bar{v}$ is the partial molar volume of the micelles, C_{SF} is the surfactant concentration and *CMC* is the critical micelle concentration. Under normal MECC conditions the numerator of Eqn. (9) is approximately equal to 1, leading to:

$$k = K_c\,\bar{v}\,(C_{SF} - CMC) \tag{10}$$

Thus the retention factor is linearly related to the surfactant concentration [2].

To investigate the influence of the phase ratio on the retention factors and the elution window, experiments were carried out with an electrolyte system of 0.01 *M* TRIS–MOPS at pH 8.2, containing different concentrations SDS, ranging from 30 m*M* to 100 m*M*. For the retention factors versus concentration SDS linear graphs were obtained with regression correlation coefficients larger than 0.997. As can be seen from the results, listed in Table 5, both m_{EOF} and $|m_{MC}|$ decrease with increasing surfactant concentration, due to changes in viscosity and ionic strength. The increase in viscosity will be partly compensated by Joule heating with a higher electric current (see also section 3.1., *Applied field strength*). Here it should be noted that in capillary electrophoretic techniques a distinction can be made between bulk viscosity (important for m_{MC}) and wall–surface viscosity (important for m_{EOF}) [24]. We assume that bulk viscosity will be more influenced by Joule heating than wall surface viscosity. As a result, a small increase of the elution window is observed at higher surfactant concentrations as also reported by others [4,25]. Terabe et al. [20], however, reported a small decrease of the elution window,

Table 5
Electroosmotic mobility, m_{EOF} (10^{-5} cm^2/Vs), effective mobility of the micelles, m_{MC} (10^{-5} cm^2/Vs), values for the elution window, t_{MC}/t_{EOF}, and measured electric current, I (μA), at different SDS concentrations, C_{SDS} (mM). BioRad standard capillary. Background electrolyte, 10 mM TRIS–MOPS at pH 8.2. Applied voltage, 15 kV

C_{SDS}	m_{EOF}	m_{MC}	t_{MC}/t_{EOF}	I
30	60.62	−43.18	3.47	11.1
40	59.48	−43.93	3.60	13.7
50	58.38	−42.53	3.69	16.7
60	58.29	−42.50	3.69	19.7
70	57.93	−42.34	3.72	22.7
80	57.49	−42.49	3.83	25.8
90	57.49	−42.76	3.91	29.6
100	57.15	−42.47	3.89	33.4

which may be due to differences in thermoregulating the capillary.

In Fig. 5 the effect of the surfactant concentration on the function $f(k)$ is demonstrated. For weakly hydrophobic compounds with $k < k_{opt}$ like resorcinol and phenol, an increase in $f(k)$ is observed with increasing surfactant concentration, whereas for strongly hydrophobic compounds with $k > k_{opt}$ like 1,2-xylol a decrease in $f(k)$ is observed. For moderately hydrophobic compounds like p-cresol only a small influence of the surfactant concentration on $f(k)$ is observed.

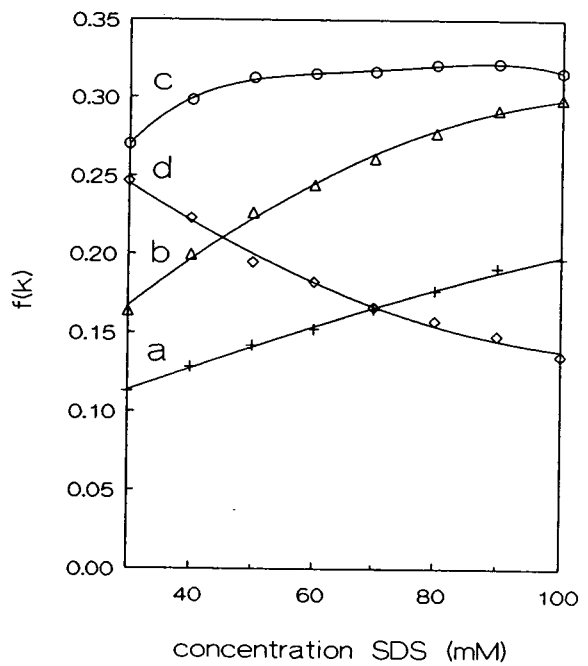

Fig. 5. Relationship between $f(k)$ and concentration SDS for (a) resorcinol, (b) phenol, (c) p-cresol and (d) 1,2-xylol. BioRad standard capillary. Background electrolyte, 10 mM TRIS–MOPS at pH 8.2. Applied voltage, 15 kV.

3.6. Organic modifiers

Generally in MECC hydrophobic compounds show retention factors much larger than k_{opt}. The separation of these compounds can be improved by the addition of an organic modifier to the background electrolyte in order to decrease their retention factors to more favourable values. Moreover, the elution window will be extended by the addition of organic modifiers [10,11]. To study the influence of different organic modifiers in MECC, experiments were carried out with an electrolyte system of 0.01 M TRIS–boric acid at pH 8.5, containing different amounts of methanol, acetonitrile or urea. The migration times of the micelles for these experiments were calculated by an iteration procedure, applying the migration data of a homologous series of alkylbenzenes [19,26]. In Table 6 all calculated values for the electroosmotic mobility, the effective mobility of the micelles and the corresponding elution windows are summarized. At a methanol concentration above 20% (v/v) the restricted elution mode was obtained and t_{MC} could no longer be determined. A decrease in m_{EOF} and $|m_{MC}|$ is observed at increasing modi-

Table 6
Electroosmotic mobility, m_{EOF} (10^{-5} cm^2/Vs), effective mobility of the micelles,m_{MC} (10^{-5} cm^2/Vs), and values for the elution window, t_{MC}/t_{EOF}, at different concentrations of methanol (%(v/v)), acetonitrile (%(v/v)) and urea (M). Background electrolyte, 10 mM TRIS–boric acid at pH 8.5. BioRad standard capillary. Applied voltage, 15 kV

Methanol				Acetonitrile				Urea			
%(v/v)	m_{EOF}	m_{MC}	t_{MC}/t_{EOF}	%(v/v)	m_{EOF}	m_{MC}	t_{MC}/t_{EOF}	M	m_{EOF}	m_{MC}	t_{MC}/t_{EOF}
0	67.14	−44.21	2.93	0	63.75	−44.11	3.25	0	58.40	−43.12	3.82
5	56.68	−39.18	3.24	5	58.86	−42.58	3.62	1	56.19	−41.99	3.96
10	48.90	−35.62	3.68	10	56.74	−42.41	3.96	2	54.97	−40.49	3.80
15	41.72	−31.96	4.28	15	52.78	−40.96	4.46	3	53.73	−41.03	4.23
20	36.64	−29.41	5.06	20	50.72	−42.08	5.87	4	52.88	−40.26	4.19
25	32.84	–	–	25	49.04	−41.47	6.48	5	51.43	−40.11	4.55
30	29.76	–	–	30	47.21	−41.45	8.22	6	50.71	−39.26	4.43
								7	49.04	−38.65	4.73

fier concentrations, due to changes in the viscosity and the dielectric constant of the electrolyte systems. Moreover, the micelle structure and hence m_{MC} will be influenced by the addition of an organic modifier. As a result, an increase in the elution window is observed with increasing concentrations of methanol, acetonitrile or urea.

In reversed-phase high-performance liquid chromatography it has been shown that the variation of the retention factor, k, with the volume fraction of organic solvent in the aqueous–organic mobile phase, ϕ, is reasonably well described by [27]:

$$\ln k = A + B\phi + C\phi^2 \quad (11)$$

where A, B and C are constants for a specific solute and eluent combination. For a small range of solvent compositions Eqn. (11) can be approximated by

$$\ln k = A + B\phi \quad (12)$$

Although in MECC small changes in the phase ratio may occur, due to the influence of organic modifiers on micelle structures, for methanol and urea a linear relationship was obtained between the logarithm of the retention factor and the concentration modifier in the background electrolyte, as shown in Fig. 6. For acetonitrile a 2nd order relationship was obtained. From Fig. 6 and Table 6 it can be concluded that with an increase in modifier concentration a decrease in retention factors as well as an increase in elution window is obtained, resulting in a better resolution for hydrophobic compounds. As an example in Fig. 7 parts of the electrokinetic chromatograms are shown of the separation of alkylbenzenes with different amounts of methanol. As can be clearly seen a better resolution is obtained for strongly hydrophobic compounds migrating near t_{MC} at higher concentrations methanol, due to both a decrease in retention factor and an increase in elution window.

4. Conclusions

The overall linear velocity of neutral sample compounds was shown to be linearly related to the measured electric current. According to the resolution equation both the elution window and the retention factor influence the resolution in micellar electrokinetic capillary chromatography. These variables are often simultaneously affected by the experimental conditions and hence they cannot be controlled independently in many cases. The results demonstrate that the resolution of uncharged compounds can be improved by adjusting different separation parameters. The elution window can be increased by decreasing the pH of the electrolyte system, whereas the retention factors of the compounds remain fairly

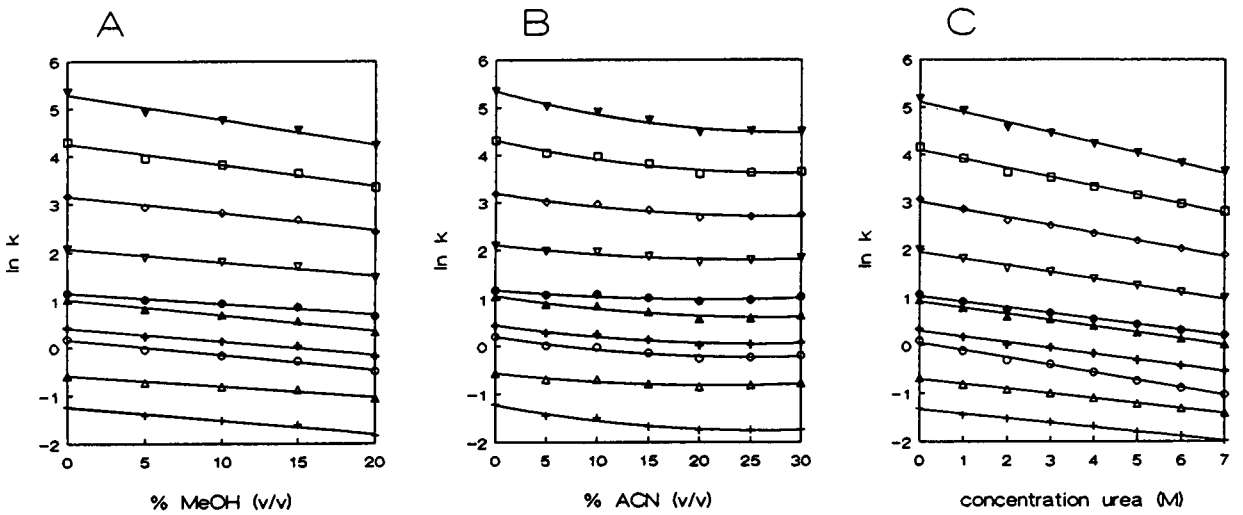

Fig. 6. Logarithm of retention factor versus concentration modifier for (A) methanol (%, v/v), (B) acetonitrile (%, v/v) and (C) urea (*M*) . BioRad standard capillary. Background electrolyte, 10 m*M* TRIS–boric acid at pH 8.5, containing different amounts of organic modifier. Applied voltage, 15 kV.

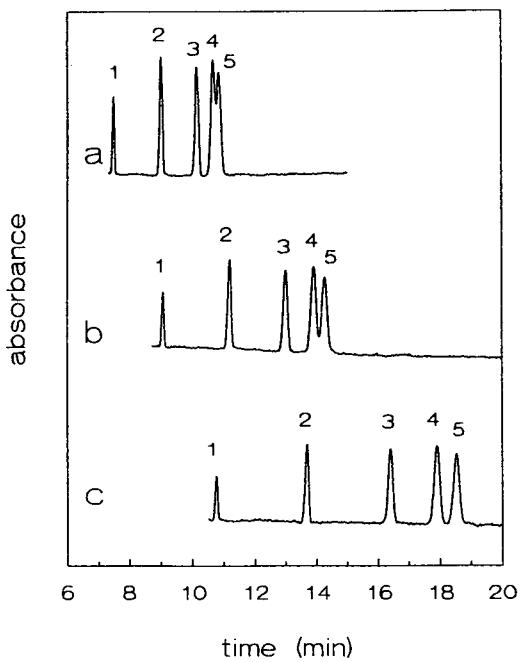

Fig. 7. Electrokinetic chromatograms of the separation of the alkylbenzenes (1) benzene, (2) toluene, (3) ethylbenzene, (4) propylbenzene and (5) butylbenzene in a background electrolyte of 10 m*M* TRIS–boric acid at pH 8.5, containing (a) 0%, (b) 5% and (c) 10% (v/v) methanol. BioRad standard capillary. Applied voltage, 15 kV.

constant. With a low electroosmotic flow at low pH values, the restricted elution mode can be obtained, resulting in a better resolution for weakly hydrophobic compounds. The use of coated capillaries was shown to be of limited value in MECC. The retention factor can be optimized in order to increase the function $f(k)$ by changing the surfactant concentration. An increase in elution window as well as a decrease in retention factors can be obtained by the addition of an organic modifier to the background electrolyte, resulting in a better resolution for strongly hydrophobic compounds. For methanol and urea a linear relationship is obtained between the logarithm of the retention factor and the modifier concentration whereas for acetonitrile a 2nd order relationship is obtained.

Acknowledgement

The authors express their gratitude to the Foundation for Chemical Research in the Netherlands (SON) for financial support of this investigation.

References

[1] S. Terabe, K. Otsuka, K. Ichikawa, A. Tsuchiya and T. Ando, *Anal. Chem.*, 56 (1984) 111.

[2] S. Terabe, K. Otsuka and T. Ando, *Anal. Chem.*, 57 (1985) 834.

[3] S. Terabe, K. Otsuka and T. Ando, *Anal. Chem.*, 61 (1989) 251.

[4] J. Vindevogel and P. Sandra, *Introduction to Micellar Electrokinetic Chromatography*, Hüthig, Heidelberg, 1992.

[5] M.J. Sepaniak and R.O. Cole, *Anal. Chem.*, 59 (1987) 472.

[6] K. Otsuka and S. Terabe, *J. Microcol. Sep.*, 1 (1989) 150.

[7] H.T. Rasmussen and H.M. McNair, *J. High Resol. Chromatogr.*, 12 (1989) 635.

[8] J. Vindevogel and P. Sandra, *J. Chromatogr.*, 541 (1991) 483.

[9] A.T. Balchanus and M.J. Sepaniak, *Anal. Chem.*, 60 (1988) 617.

[10] J. Gorse, A.T. Balchanus, D.F. Swaile and M.J. Sepaniak, *J. High Resol. Chromatogr. Chromatogr. Commun.*, 11 (1988) 554.

[11] S. Terabe, Y. Ishihama, H. Nishi, T. Fukuyama and K. Otsuka, *J. Chromatogr.*, 545 (1991) 359.

[12] J.P. Foley, *Anal. Chem.*, 62 (1990) 1302.

[13] K. Ghowsi, J.P. Foley and R.J. Gale, *Anal. Chem.*, 62 (1990) 2714.

[14] J. Vindevogel and P. Sandra, *Anal. Chem.*, 63 (1991) 1530.

[15] E.L. Little and J.P. Foley, *J. Microcol. Sep.*, 4 (1992) 145.

[16] H. Nishi, T. Fukuyama, M. Matsuo and S. Terabe, *J. Microcol. Sep.*, 1 (1989) 234.

[17] M.G. Khaledi, S.C. Smith and J.K. Strasters, *Anal. Chem.*, 63 (1991) 1820.

[18] S. Terabe, T. Katsura, Y. Okada, Y. Ishihama and K. Otsuka, *J. Microcolumn Sep.*, 5 (1993) 23.

[19] P.G.H.M. Muijselaar, H.A. Claessens and C.A. Cramers, *Anal. Chem.*, 66 (1994) 635.

[20] S. Terabe, H. Utsumi, K. Otsuka, T. Ando, T. Inomata, S. Kuze and Y. Hanaoka, *J. High Resol. Chromatogr. Chromatogr. Commun.*, 9 (1986) 666.

[21] A.T. Balchanus and M.J. Sepaniak, *Anal. Chem.*, 59 (1987) 1466.

[22] J.A. Lux, H. Yin and G. Schomburg, *J. High Resol. Chromatogr.*, 13 (1990) 145.

[23] B. Lindman and H. Wennerström in F.L. Boschke (Editor), *Micelles (Topics in Current Chemistry*, Vol. 87), Springer, Berlin, 1980, p. 61.

[24] J.C. Reijenga, G.V.A. Aben, Th.P.E.M. Verheggen and F.M. Everaerts, *J. Chromatogr.*, 260 (1983) 241.

[25] H.T. Rasmussen, L.K. Goebel and H.M. McNair, *J. Chromatogr.*, 517 (1990) 549.

[26] M.M. Bushey and J. Jorgenson, *Anal. Chem.*, 61 (1989) 491.

[27] C.F. Poole and S.K. Poole, *Chromatography Today*, Elsevier, Amsterdam, 1991, p. 396.

ELSEVIER

Journal of Chromatography A, 696 (1995) 285–294

JOURNAL OF CHROMATOGRAPHY A

Calculation of the composition of sample zones in capillary zone electrophoresis
II. Simulated electropherograms

J.L. Beckers

Eindhoven University of Technology, Laboratory of Instrumental Analysis, P.O. Box 513, 5600 MB Eindhoven, Netherlands

Received 1 November 1994; accepted 27 December 1994

Abstract

Non-steady-state zone electrophoretic processes can be treated by repeated application of a steady-state mathematical model. Based on this principle, a computer program was set up for the simulation of electropherograms on a temporal basis. Because all parameters of the sample zones can be calculated, all possible detector traces can be simulated. Simulated electropherograms were compared with experimentally determined electropherograms to establish the ability of the mathematical model in qualitative respects. It appears that with this model the fronting and tailing character of sample peaks can be predicted and the reversal of the fronting/tailing character at the point where the mobility of the sample ions equals that of the co-ions. It was remarkable that for strong sample ionic species and applying weak co-ions, the originally tailing character did not change into a fronting character when the mobility of the sample ions exceeded that of the co-ions. Also, the appearance of peaks and dips for the distinguished cases in indirect and direct UV detection can be predicted by the model.

1. Introduction

In Part I [1], a mathematical model was described with which all parameters in sample zones in capillary zone electrophoresis (CZE) can be calculated. The basis of this model is that sample peaks in CZE are divided into small segments with varying sample component concentrations and all parameters of a segment can be calculated from the parameters of the preceding segment with a steady-state model, based on the mass balances of the co- and counter ions, the electroneutrality equation and the modified Ohm's law [2]. In this way, non-steady-state electrophoretic processes can be treated by repeated application of a steady-state model. This model is only usable if electrodispersive effects predominate because other peak-broadening effects, such as diffusion and the influence of the temperature, are neglected. Calculations with this model showed that nearly linear relationships exist between the parameters in the sample peaks, such as the pH, the concentrations of co- and counter ions, the electric field strength and the concentration of the sample component. Although in this model various parameters affecting the electrophoretic separation process are not taken into account, this model gives an insight into the separation process because the changes in all parameters in the sample zones can be calculated.

Electropherograms are generally measured on

0021-9673/95/$09.50
SSDI 0021-9673(94)01297-0

a temporal basis and in order to compare measured and simulated electropherograms, to check the above-mentioned mathematical model, in this work this model was applied for the simulation of electropherograms on a temporal basis. Measured and simulated electropherograms were compared with respect to peak shape, the fronting and tailing character of sample peaks and the question of peaks or dips [3].

2. Theory

Electropherograms are generally measured on a temporal basis, i.e., that at the detector position the trace of a specific parameter is registered. For the simulation of electropherograms this means that it must be calculated how a specific parameter changes in time at the position of the detector. For a UV detector, where the total absorbance of the system is registered, generally concentration profiles of the UV-absorbing components have to be calculated, corrected for differences in molar absorptivities for the different components. For a conductivity detector the trace of the specific conductivity must be calculated.

Calculations with the mathematical model, described in Part I [1], show that different segments of a sample peak, with a different sample component concentration, migrate with different apparent mobilities by the combined effect of differences in the local electric field strength and the effective mobility of the component owing to a change in ionic strength and pH. The apparent velocity of a peak segment i, $v_{app,i}$, is the product of the apparent mobility, $m_{app,i}$, and the electric field strength in the background electrolyte (BGE), E_{BGE}. The apparent mobility is determined by the local effective mobility, $m_{eff,i}$, of the sample component in the peak segment i and the local electric field strength, E_i, and the overall mobility of the electroosmotic flow, m_{EOF}:

$$v_{app,i} = m_{app,i} E_{BGE} = \left(m_{eff,i} \cdot \frac{E_i}{E_{BGE}} + m_{EOF} \right) E_{BGE} \quad (1)$$

According to this model, the different segments of the sample peak migrate with different velocities and pass the detector at different times, causing the typical triangular sample peaks in CZE. If the mobility of the sample component is higher than that of the co-ions, the velocity of segments with increasing sample component concentrations decrease, through which fronting peaks are obtained. If the mobilities of the sample components are lower than those of the co-ions, tailing peaks are the result. What this means for the development of a sample peak in time and space can be seen in Fig. 1, where the calculated positions of the concentration profiles in the separation capillary are given on a spatial basis for a potassium peak (amount injected $1 \cdot 10^{-11}$ mols) at different times applying a BGE of 0.01 M histidine adjusted to pH 5 by adding acetic acid. The mobilities at infinite dilution and the pK values of all ionic species used in the simulations and experiments are given in Table 1. It can be clearly seen that in course of time (in experiments often after a sample stacking procedure) peaks elute whereby the peaks become broader and the peak heights decrease owing to the electrodispersive character. This means that a sample peak is in dynamic equilibrium. The shape of a sample peak changes in time and a mass transport takes place continuously over all

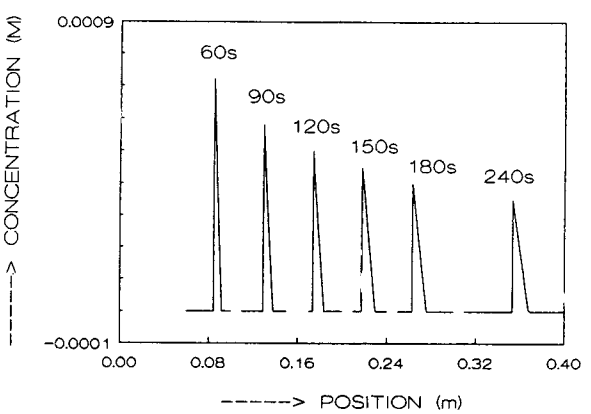

Fig. 1. Development of concentration profiles of a sample peak of potassium (injected amount $1 \cdot 10^{-11}$ mol) in space and time on a spatial basis, applying a BGE of 0.01 M histidine adjusted to pH 5 by adding acetic acid. The numbers refer to the migration times.

Table 1
Ionic mobilities at infinite dilution, m ($m^2/V \cdot s$), and pK values for ionic species used in the simulations and experiments

Ionic species[a]	$m \times 10^9$	pK
Acetic acid	−42.4	4.76
Benzoic acid	−33.6	4.203
Butyric acid	−33.8	4.82
Caproic acid	−30.2	4.857
Formic acid	−56.6	3.75
Histidine	29.7	6.03
Hydrochloric acid	−79.1	−2.0
Imidazole	50.4	6.953
Lithium	40.1	14.0
MES	−28.0	6.095
Sodium	51.9	14.0
Potassium	76.2	14.0
TEA	32.5	>9.0
TMA	43.4	>9.0
Tris	29.5	8.10

[a] MES = 2-(N-Morpholino)ethanesulphonic acid; TEA = tetraethylammonium; TMA = tetramethylammonium; Tris = tris(hydroxymethyl)aminomethane.

peak segments. What this means for the detection of the sample peaks at a specific detector position is illustrated schematically in Fig. 2, where the spatial positions of a peak are shown at times I and II. At time I, the segment with a

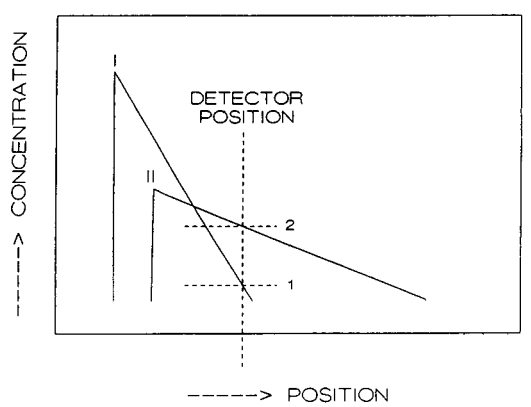

Fig. 2. Concentration profiles of a sample peak at two different times I and II. At time I the peak segment with a concentration 1 is detected whereas at time II the segment with a concentration 2 has reached the detector position. During the time interval I–II the shape of the sample peak changes, i.e., during detection a mass transport takes place continuously over the peak segments.

concentration 1 has reached the detector position. At time II, the segment with a concentration 2 has reached the detector position. During the time interval I–II the shape of the sample peak is changed and in order to know the amount of sample component that has passed the detector at time II, the amount of sample component present in the sample peak beyond the detector position has to be calculated at time II on a spatial basis. The effect of shape deformation is exaggerated in Fig. 2 in order to illustrate this effect.

The calculation of simulated electropherograms on a temporal basis is therefore as follows. First, the relationships between the concentrations of a sample component in a peak segment and various parameters, such as the apparent mobility, concentration of co- and counter ions, electric field strength and specific conductivity, are calculated. In the apparent mobility, deviations in electric field strength are included. Then the velocities of the segments of a sample peak are calculated by applying Eq. 1, starting from the diffuse side of the sample peak. For each time it can be calculated which concentration segment passes the detector position and at that time the amount of sample component Q that already has passed the detector on a spatial basis can be calculated, according to

$$Q = \sum_i A \Delta x_i c_i \qquad (2)$$

with A is the capillary area, Δx_i is the length of the peak segment i and c_i is the concentration of the sample peak in segment i. This procedure is repeated until the sample amount that has passed the detector is equal to the injected amount. The back or front sides of the component peaks are assumed to be sharp. For simulated electropherograms a specific parameter is given in time, dependent on the detector chosen. This procedure can be followed for both fronting and tailing peaks.

3. Experimental

For all CZE experiments a P/ACE System 2000 HPCE apparatus (Beckman, Fullerton,

CA, USA) was used. All experiments were carried out with Beckman eCAP capillary tubing (75 μm I.D.) with a total length of 46.7 cm and a distance between injection and detection of 40.0 cm. The wavelength of the UV detector was set at 214 nm. All experiments were carried out in the cationic mode applying a constant voltage of 10 kV, unless stated otherwise, and the operating temperature was 25°C. Sample introduction was performed by applying pressure injection, where a 1-s pressure injection represents an injected volume of ca. 6 nl and an injected length of 0.136 cm. Data analysis was performed using the laboratory-written data analysis program CAESAR. If experimentally obtained electropherograms are compared with simulated electropherograms, identical values for apparatus parameters are assumed in the simulations. The simulation conditions were as follows: capillary length, 0.467 m; distance between injection and detection, 0.4 m; applied voltage, 10 kV; and capillary diameter, 75 μm.

4. Results and discussion

The mathematical model and the simulation model resting on it must be able to predict both qualitative and quantitative aspects of CZE experiments in order to be useful. The model must be able to predict whether a sample peak will be fronting or tailing, and for weak bases and acids fronting peaks must change into tailing peaks at a specific pH where the effective mobility of the sample ions equals that of the co-ions of the BGE. Sometimes, sample components can be present in electropherograms as a peak or as a dip [3] and the model must be able to predict these effects. Also, quantitative aspects such as the start and end times of the sample peaks, concentrations of the sample component and co- and counter ions, pH, electric field strength and peak area have to be calculated. A problem in the comparison of simulated and calculated values is that calculated values are often based on concentrations, whereas in practice often a UV detector is used, measuring the total UV absorbance of all ionic species. Measured UV absorbances have to be recalculated to concentrations. If only one UV-absorbing component is present, this can easily be done [4]. In the first instance we shall compare calculated and measured electropherograms, focusing on the ability of the model to predict qualitative aspects.

4.1. Peak shape

According to the calculations, the slopes of the concentration profiles of the sample component peaks are independent of, e.g., the concentration of the sample component in the sample solution and sample stacking and/or other concentration procedures. Of course, the maximum concentration in a sample peak cannot exceed the original concentration of the sample component in the sample solution without a sample stacking procedure. To illustrate these effects and to test the model, in Fig. 3 the simulated electropherograms are given for the peaks of the sample components potassium, sodium and lithium applying BGEs consisting of (A) 0.01 *M* histidine and (B) 0.01 *M* imidazole adjusted to pH 5 by adding acetic acid for different injected amounts. Both (1) the concentrations of the co-ions (a measure of the indirect UV signal) and (2) the concentrations of the sample components (a measure of the direct UV signal) are given. Because the mobilities of all sample ions are higher than that of the co-ions histidine, all peaks are fronting and because of the large difference between the mobilities of the sample components and co-ions of the BGE, the effect of electrodispersive effects is great and sample peaks are broad in Fig. 3A. For increasing injected amounts, the diffuse sides of the sample peaks start at the same side. Applying imidazole acetate as the BGE (the mobility of imidazole is just slightly lower than that of sodium), potassium shows a fronting peak and lithium a sharp, tailing peak. For sodium the peak is much steeper and higher, because the electrodispersive character is very small and the diffusion is neglected in the model. Also, the potassium and lithium peaks are narrower and higher than in the case of histidine acetate because the differences between the mobilities of sample ions and

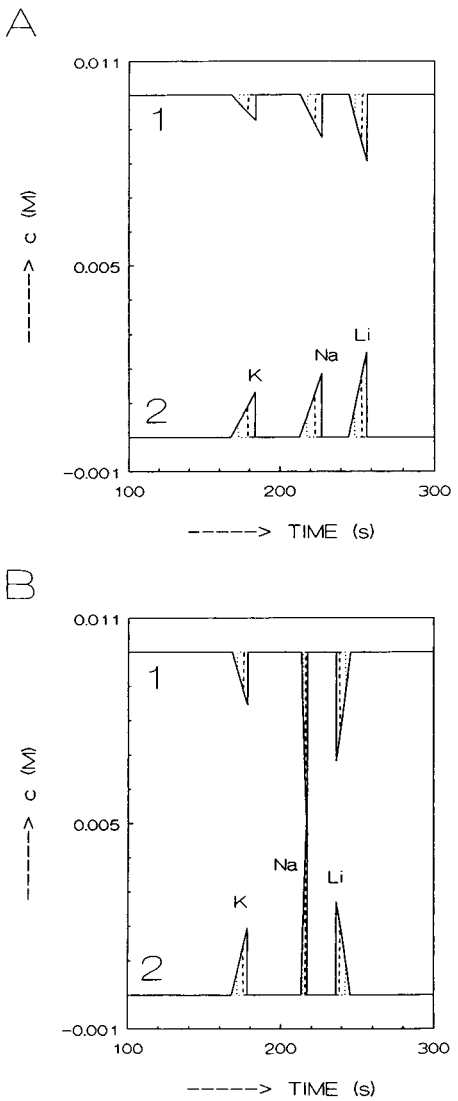

Fig. 3. Simulated electropherograms on a temporal basis for the separation of potassium, sodium and lithium applying BGEs of (A) 0.01 *M* histidine and (B) 0.01 *M* imidazole adjusted to pH 5 by adding acetic acid for injected amounts of (dotted line) $1.1 \cdot 10^{-11}$, (dashed line) $5.5 \cdot 10^{-11}$ and (solid line) $11 \cdot 10^{-11}$ mol. Electropherograms indicated with the number 1 represent the total concentration of the co-ions and gives information about the detector signal applying the indirect UV mode, whereas those indicated with the number 2 represent the total concentrations of the sample components and give an impression of the signal in the direct UV mode. For components with a mobility higher than that of the co-ions fronting peaks are obtained, otherwise tailing peaks. Sample peaks are broader if the mobilities of the components differ much from those of the co-ions.

co-ions are much smaller. In the simulation the m_{EOF} is assumed to be $40 \cdot 10^{-9}$ $m^2/V \cdot s$ arbitrarily and the applied voltage is 10 kV. In the simulations the injected amounts for all components are $1.1 \cdot 10^{-11}$, $5.5 \cdot 10^{-11}$ and $11 \cdot 10^{-11}$ mol, respectively. As can be seen in Fig. 3, the slopes of the sample concentration profiles are always identical for different amounts of sample injected and the diffuse sides start at the same time both for fronting and tailing peaks. To check these aspects experimentally, the potassium peaks were measured carefully, applying a BGE consisting of 0.01 *M* histidine adjusted to pH 5 by adding acetic acid and injecting several different amounts of potassium, dissolved both in water and in BGE. In Fig. 4A the electropherograms are given for (a) the 5-s pressure injection of $1 \cdot 10^{-4}$ *M* and the 10-s pressure injections of (b) $5 \cdot 10^{-4}$ *M* and (c) $1 \cdot 10^{-3}$ *M* solutions of potassium in water. In Fig. 4B the electropherograms are given for 10-s pressure injections of (a) $5 \cdot 10^{-4}$ *M* and (b) $1 \cdot 10^{-3}$ *M* potassium in BGE and 20-s pressure injections of (c) $1 \cdot 10^{-3}$ *M* potassium in BGE and (d) $1 \cdot 10^{-3}$ *M* potassium in water. It can be clearly seen that the slopes of the diffuse sides in all peaks of Fig. 4 are fairly equal. In aqueous solutions the peak height increases, although not linearly, with increasing injected amounts, whereas applying solutions of potassium in BGE a maximum peak height is obtained (Fig. 4B, c) depending on the concentration of potassium in the sample solution. The positions of the diffuse sides can vary owing to a change in mobility of the EOF and a different length of the injection plug.

To check whether the model can predict the change from a fronting peak into a tailing peak, simulations and experiments were carried out for the sample component imidazole in BGEs consisting of 0.01 *M* Tris adjusted to pH 5, 7, 7.5 and 8 by adding acetic acid. In Fig. 5A the measured electropherograms are given for 10-s pressure injections of $5 \cdot 10^{-4}$ *M* imidazole in 10% BGE solution. At a BGE pH of 5 imidazole is fronting whereas the fronting character is changed into a tailing character at pH 7. In Fig. 5B the simulated electropherograms are given for the same cases. For the simulations the m_{EOF}

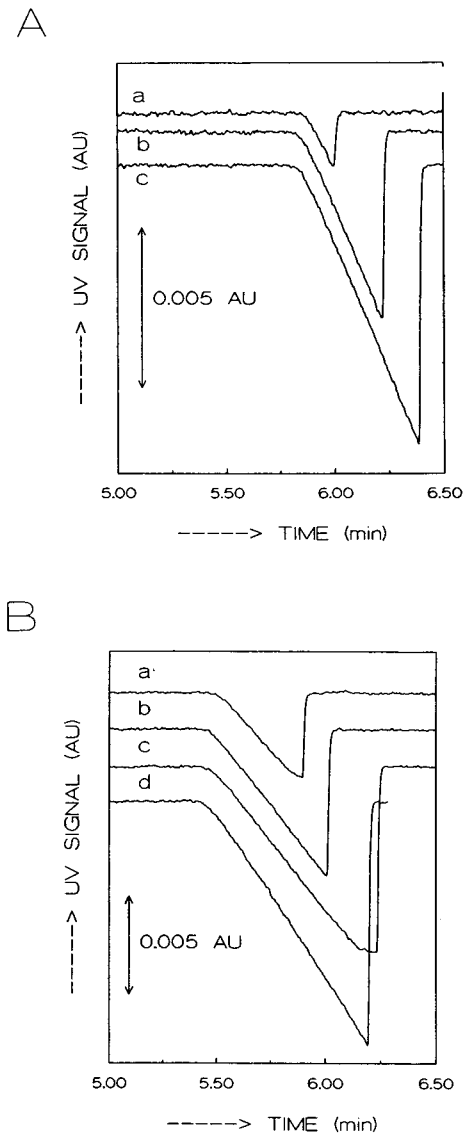

Fig. 4. (A) Electropherograms for (a) 5-s pressure injection of a solution of $1 \cdot 10^{-4}$ *M* potassium ions and 10-s pressure injections of a solution of potassium ions of (b) $5 \cdot 10^{-4}$ and (c) $1 \cdot 10^{-3}$ *M*. The slopes of the concentration profiles of the sample components are equal in all cases. The BGE was 0.01 *M* histidine acetate at pH 5. Applied voltage, 5 kV. (B) Electropherograms for 10-s pressure injections of a solution of potassium ions in BGE for (a) $5 \cdot 10^{-4}$ and (b) $1 \cdot 10^{-3}$ *M* and for 20-s pressure injection of a solution of $1 \cdot 10^{-3}$ *M* potassium ions in (c) BGE and (d) water. The BGE was 0.01 *M* histidine acetate at pH 5. Applied voltage, 5 kV. The slopes of the concentration profiles of the sample component are equal in all cases, for solutions both in water and in BGE.

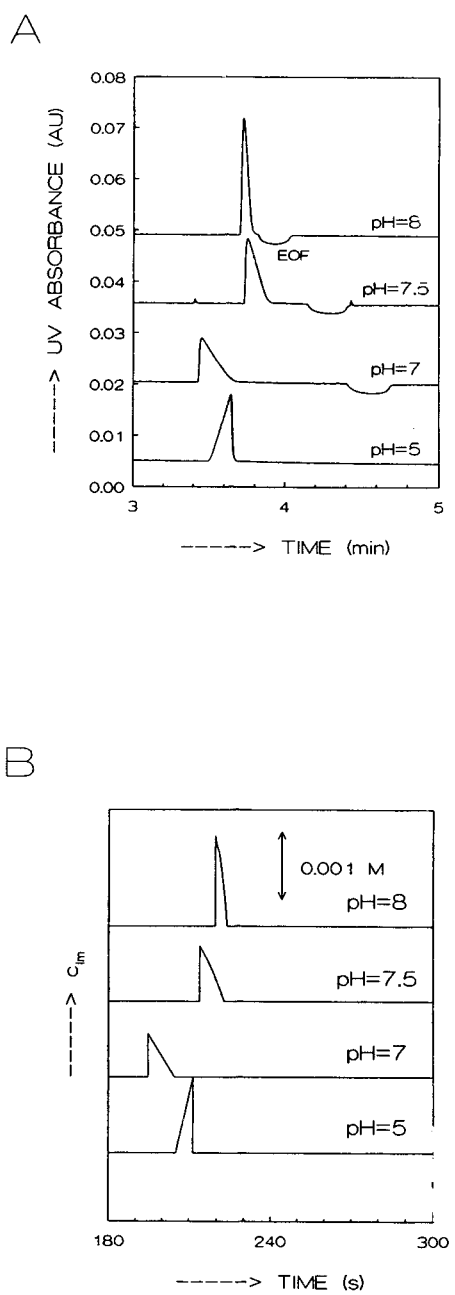

Fig. 5. (A) Measured and (B) simulated electropherograms for 10-s pressure injections of a $5 \cdot 10^{-4}$ *M* solution of imidazole dissolved in 10% BGE solution, applying BGE solution of 0.01 *M* Tris adjusted to different pHs by adding acetic acid. Between pH 5 and 7 the fronting character of the imidazole peaks changes to a tailing character in both the measured and simulated electropherograms. For further information, see text.

values are used as obtained from the experiments. The simulated electropherograms strongly resemble the experimentally obtained electropherograms, although the measured values are based on the direct UV signal whereas in the simulated electropherograms the concentrations of the sample component imidazole are given. The calculated values for the start time of the peaks are generally slightly too small and can be caused because the breakthrough time according to Ref. [5] is not taken into account or from the fact that at $t = 0$ the voltage is not immediately put across the electrodes. This phenomenon is often observed [6].

As a next check on the mathematical model, the sample peak of lithium was calculated applying BGEs consisting of 0.01 *M* imidazole adjusted to different pHs by adding acetic acid. At pH 5, imidazole can be considered as to be fully protonated and its effective mobility will be higher than that of lithium. The lithium peak will be tailing. At pH 7 and higher, the effective mobility of imidazole will decrease and it can be expected that the lithium peak will change into a fronting peak. Surprisingly, in the calculations, the lithium peak maintains a tailing character. The calculated concentration profiles of imidazole (a measure of the UV signal in the indirect UV mode) are given in the simulated electropherograms of Fig. 6A. In the simulations the values of the mobility of the EOF obtained from the measured electropherograms were used. In Fig. 6B the relationships between the calculated apparent mobilities and the pH and the total concentrations of the sample ions in the segments are given for the BGEs 0.01 *M* imidazole acetate at pH 5 and 7. For the BGE of pH 5, the calculated pH (line 4) decreases for an increasing concentration of the sample component and the calculated apparent mobilities (line 2) increase causing tailing sample peaks. For the BGE of pH 7, in first instance the apparent mobilities increased (line 1) with increasing concentration of the sample component, i.e., a peak sharp at the front side and with tailing can be expected, although the effective mobility of the lithium zone is much larger than that of the co-ions in the BGE. At higher concentrations of the sam-

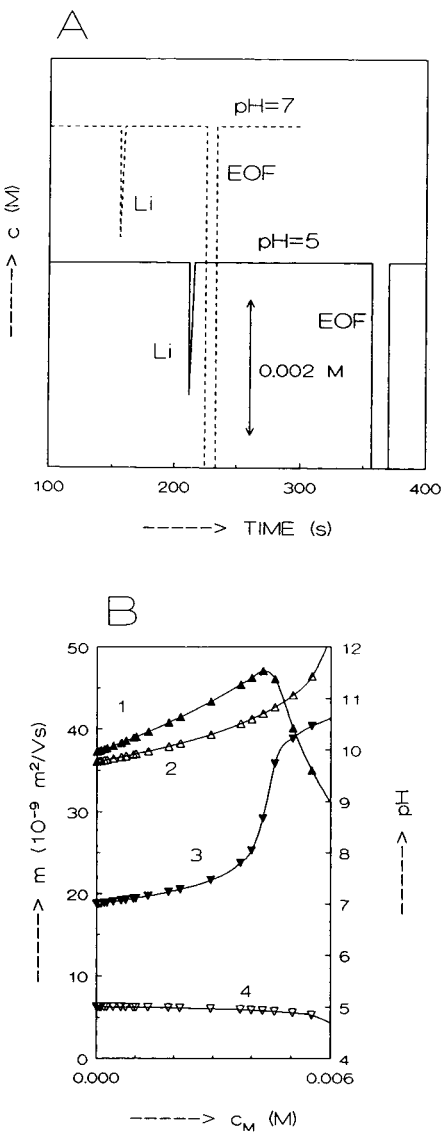

Fig. 6. (A) Simulated electropherograms for lithium applying a BGE of 0.01 *M* imidazole adjusted to pH 5 and 7 by adding acetic acid. Because Li will be measured in the indirect UV mode, the concentration of the co-ions imidazole is given on the electropherograms. In the simulations the Li peaks are tailing in both systems, although the effective mobilities of the co-ions are higher and lower than that of Li at pH 5 and 7, respectively. (B) Calculated relationships between (1, 2) apparent mobilities (left-hand scale) and (3, 4) pH (right-hand scale) of different peak segments in the sample zones and the concentrations of the sample component in the peak segments, for a BGE of imidazole acetate adjusted to (2, 4) pH 5 and (1, 3) pH 7 by adding acetic acid. For further information, see text.

ple component the apparent mobility decreases again, however. For the BGE of pH 7, the pH in the sample zone increase until unrealistic values are reached. What this means in practice is shown in Fig. 7, where the measured electropherograms are given for different injected amounts of lithium applying BGEs consisting of 0.01 *M* imidazole adjusted to a pH of (A) 5 and (B) 7 by adding acetic acid. At both pHs lithium shows a tailing peak. At pH 5 all sample peaks are triangular for different injected amounts of lithium. At pH 7 all peaks are tailing and triangular for not too high injected amounts. On injecting large amounts of sample component, anomalies are obtained. It appears that the sample peak is tailing until a specific concentration is reached, whereas for larger amounts of sample component it migrates as a sharp plug in front of the tailing peak.

4.2. *Peaks or dips?*

Recently, Beckers [3] applied the Kohlrausch regulating function (KRF) and distinguished eight cases in the direct and indirect UV detection modes for fully ionized monovalent ions, assuming identical molar absorptivities for all UV-absorbing ionic species. In several of the cases both UV-transparent and UV-absorbing components could give both peaks and dips, depending on the mobilities of components and co-ions. The mathematical model described must also decisively answer the question of whether peaks or dips can be obtained for all cases, even for weak acids and bases. We therefore simulated and measured electropherograms for some interesting cases. As a first example, the (A) measured and (B) simulated electropherograms are given in Fig. 8 for the separation of a 15-s pressure injection of (1) potassium, (2) sodium, (3) TMA, (4) TEA, (6) caproate, (7) butyrate, (8) acetate and (9) formate ions applying a BGE of 0.01 *M* imidazole adjusted to pH 7 by adding benzoic acid. The concentrations of all sample ions were $2 \cdot 10^{-4}$ *M*, except sodium ($8 \cdot 10^{-4}$ *M*). Because both co- and counter ions are UV absorbing, all sample components are measured in the classical indirect UV mode and therefore the sum of the total concentrations of co- and counter ions is given in the simulated electropherogram. In the measured electropherogram the EOF peak (5) is split and a system peak S is

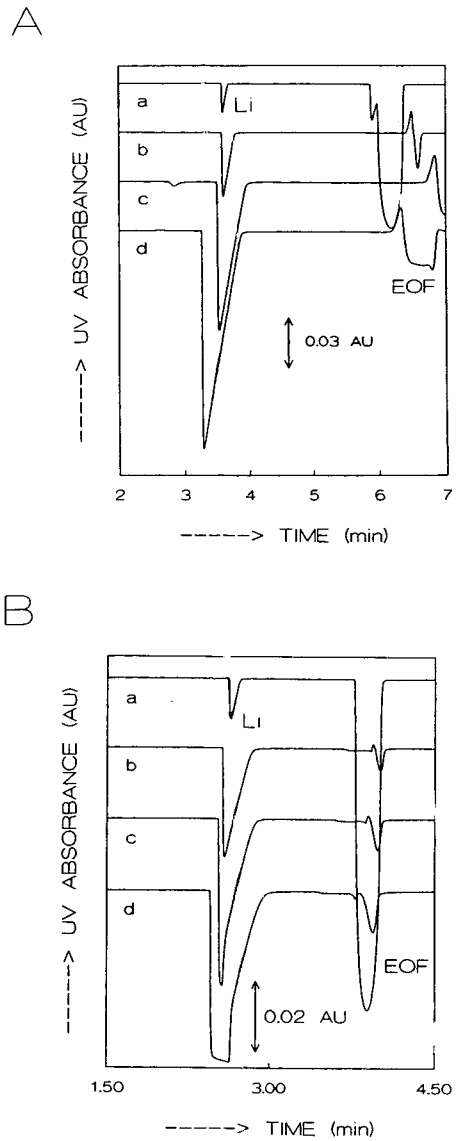

Fig. 7. Measured electropherograms for different amounts of lithium injected applying BGEs of 0.01 *M* imidazole adjusted to pH (A) 5 and (B) 7 by adding acetic acid. The pressure injection times and lithium concentrations were, respectively, (A) (a) 10 s and $5 \cdot 10^{-4}$ *M*, (b) 2 s and $1 \cdot 10^{-2}$ *M*, (c) 10 s and $1 \cdot 10^{-2}$ *M* and (d) 20 s and $1 \cdot 10^{-2}$ *M* and (B) (a) 10 s and $5 \cdot 10^{-4}$ *M*, (b) 3 s and $1 \cdot 10^{-2}$ *M*, (C) 5 s and $1 \cdot 10^{-2}$ *M* and (d) 10 s and $1 \cdot 10^{-2}$ *M*. Applied voltage, 10 kV. For further information, see text.

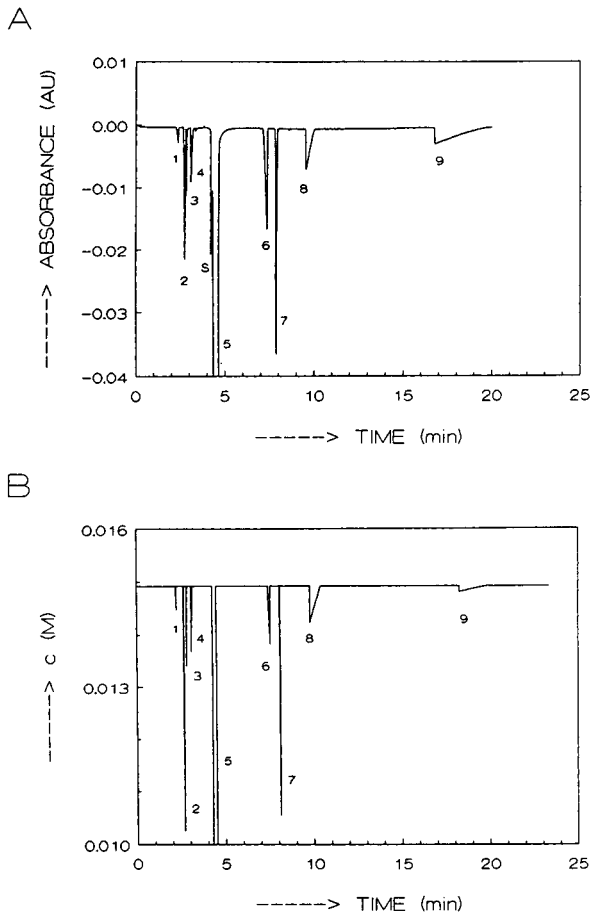

Fig. 8. (A) Measured and (B) simulated electropherograms for the separation of a 15-s pressure injection of (1) potassium, (2) sodium, (3) TMA, (4) TEA, (6) caproate, (7) butyrate, (8) acetate and (9) formate ions applying a BGE of 0.01 *M* imidazole adjusted to pH 7 by adding benzoic acid. The concentrations for all sample ions were $2 \cdot 10^{-4}$ *M*, except for sodium ($8 \cdot 10^{-4}$ *M*). Because both co- and counter ions are UV absorbing, all sample components are measured in the classical indirect UV mode. In the simulated electropherogram the sum of the total concentrations of co- and counter-ions is given. The EOF peak (5) is split and a system peak S is present on the measured electropherogram. For further information, see text.

present [1]. The applied voltage was 10 kV in both the simulated and measured electropherograms. In the simulations the value of the mobility of the EOF obtained from the measured electropherogram was used. In both the measured and simulated electropherograms the sample peaks for the cations and anions with mobilities close to those of the cation (imidazole) and anion (benzoic acid) of the BGE are very sharp and a minimum electrodispersive effect can be observed for these sample components, although this aspect is overestimated in the simulated electropherogram because the diffusion term is neglected in the mathematical model. The very broad peak of formate migrating in the upstream mode, the difference between the mobilities of the sample component and co-ions is large, is remarkable. For all peaks the fronting and tailing character agree in the simulated and measured electropherograms and even the peak shapes and migration times agree well. In Fig. 9 the electropherograms for the separation of the same sample ions are shown, applying a BGE consisting of 0.01 *M* imidazole adjusted to pH 7 by adding acetic acid. In this case the cations are measured in the normal classical indirect UV mode whereby measured peaks resemble the peaks in Fig. 8A. Because the anions of the BGE are UV transparent, in the simulation the concentration of imidazole is given because the UV absorbance will be proportional to this concentration. Again, the EOF peak is split and a system peak S is present in the measured electropherogram. For anions with a mobility higher than that of the co-ions of the BGE, the ionic strength in the sample peak will increase, because the transfer ratio is smaller than one [7], through which also the concentration of imidazole increases, causing an increase in UV absorbance for a UV-transparent component [3]. For this reason, formate is present as a peak in the chromatograms, whereas caproate and butyrate are present as dips. Acetate can not be observed in the electropherogram, because it is present in the BGE.

5. Conclusions

With a simulation model based on a mathematical model described in Part I [1], realistic simulations can be obtained for zone electrophoretic processes whereby the electrodispersive character is the dominant peak-broadening mechanism. All qualitative aspects concerning the peak shape, such as the fronting and tailing

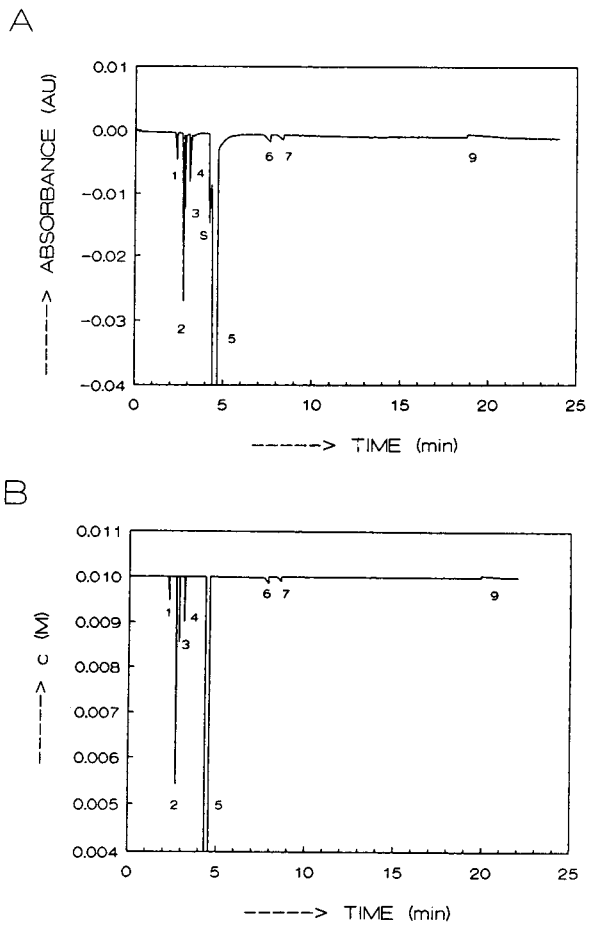

Fig. 9. (A) Measured and (B) simulated electropherograms for the separation of a 15-s pressure injection of (1) potassium, (2) sodium, (3) TMA, (4) TEA, (6) caproate, (7) butyrate, (8) acetate and (9) formate ions applying a BGE of 0.01 *M* imidazole adjusted to pH 7 by adding acetic acid. The concentrations for all sample ions were $2 \cdot 10^{-4}$ *M*, except for sodium ($8 \cdot 10^{-4}$ *M*). Because only the positive ions of the BGE are UV absorbing, all positive ions are measured in the classical indirect UV mode. In the simulated electropherogram the concentration of imidazole is given. In sample peaks of negative ions, with a mobility higher than that of acetate, the ionic strength increases, through which the concentration of imidazole increases, giving an increase in UV absorbance. The EOF peak (5) is split and a system peak S is present on the measured electropherogram. For further information, see text.

character of peaks and the question of peaks and dips, can be predicted. Even anomalies such as the deviating behaviour of lithium in the BGE of imidazole acetate can be seen. Further, all other parameters in the sample peak can be calculated, including concentrations of all constituents, pH and electric field strength. This is in contrast to many other simulation programs or mathematical models. Models based on the KRF [5,8,9] can predict all peak shapes, but generally cannot calculate, e.g., the pH and anomalies in peak shape and baseline disturbances [4]. Also, a recently presented instrument simulator [10,11] for fast graphic illustration of the effect of a large number of variables on the shape of the electropherogram includes many factors but assumes the presence of a BGE, constant in composition, and cannot calculate the various possible UV traces in UV detection.

Quantitative aspects of the mathematical model, such as peak area, peak height and migration times, are currently under investigation.

References

[1] J.L. Beckers, *J. Chromatogr.*, 693 (1995) 347.
[2] J.L. Beckers and F.M. Everaerts, *J. Chromatogr.*, 480 (1989) 69.
[3] J.L. Beckers, *J. Chromatogr. A*, 679 (1994) 153.
[4] J.L. Beckers, *J. Chromatogr. A*, 662 (1994) 153.
[5] F.E.P. Mikkers, *Thesis*, University of Technology, Eindhoven, 1980.
[6] S.V. Ermakov and P.G. Righetti, *J. Chromatogr. A*, 667 (1994) 257.
[7] M.W.F. Nielen, *J. Chromatogr.*, 588 (1991) 321.
[8] E.V. Dose and G.A. Guiochon, *Anal. Chem.*, 63 (1991) 1063.
[9] W. Thormann, *Electrophoresis*, 4 (1983) 383.
[10] J.C. Reijenga and E. Kenddler, *J. Chromatogr. A*, 659 (1994) 403.
[11] J.C. Reijenga and E. Kenddler, *J. Chromatogr. A*, 659 (1994) 417.

ELSEVIER

Journal of Chromatography A, 696 (1995) 295–305

JOURNAL OF CHROMATOGRAPHY A

Determination of hyaluronan and galactosaminoglycan disaccharides by high-performance capillary electrophoresis at the attomole level. Applications to analyses of tissue and cell culture proteoglycans

Nikos K. Karamanos[a,1], Susanna Axelsson[b], Peter Vanky[c], George N. Tzanakakis[c], Anders Hjerpe[c,*]

[a]*Section of Organic Chemistry, Biochemistry and Natural Products, Department of Chemistry, University of Patras, 26110 Patras, Greece*

[b]*Department of Clinical Oral Physiology, Huddinge University Hospital, Karolinska Institute S-141 86 Stockholm, Sweden*

[c]*Department of Immunology, Microbiology, Pathology and Infectious Diseases, Division of Pathology, Huddinge University Hospital, Karolinska Institute F-42, S-141 86 Stockholm, Sweden*

First received 23 June 1994; revised manuscript received 12 December 1994; accepted 23 December 1994

Abstract

A rapid, highly sensitive and reproducible HPCE method is described for the determination of all non- and variously sulphated disaccharides present in hyaluronan and vertebrate chondroitin sulphates and dermatan sulphates. Following chondroitinase digestion of glycosaminoglycans or proteoglycans, the non-, di- and trisulphated Δ-disaccharides are completely separated and readily determined within 14 min on a fused-silica capillary in 15 m*M* sodium dihydrogen orthophosphate, pH 3.00, using reversed polarity at 20 kV and detection at 232 nm. The determination of the various Δ-disaccharides derived from either glucuronic or iduronic acid and the presence of glucuronic and iduronic clustered structures in dermatan sulphate can also easily be made, using digests with chondroitinase AC or B. A linear detector response was obtained for the entire interval tested (up to 10 mg/l of Δ-disaccharides). Concentrations as small as 32, 65, 100 and 250 pmol/l (22, 38, 50 and 98 ng/l) of tri-, di- and nonsulphated Δ-disaccharides, respectively, can be reliably detected.

1. Introduction

Hyaluronan (HA) and the galactosaminoglycans (GalAGs), chondroitin sulphate (CS) and dermatan sulphate (DS), are components of connective tissues and they are susceptible to digestion with chondroitinase. GalAGs are covalently bound to a protein core, forming proteoglycans (PGs), whereas HA is a polysaccharide not found to be an integral constituent of PG molecules. HA, however, forms large aggregates with the monomeric PG [1]. The GalAGs and HA are composed of repeating disaccharide

* Corresponding author.

[1] Present address: Department of Immunology, Microbiology, Pathology and Infectious Diseases, Division of Pathology, Huddinge University Hospital, Karolinska Institute F-42, S-141 86 Stockholm, Sweden.

0021-9673/95/$09.50
SSDI 0021-9673(94)01294-6

units which generally contain a uronic acid glycosidically linked to hexosamine. The sulphated GalAGs are highly charged polymers and their physiological characteristics depend to a large extent on the sulphate position [2–3]. HA is non-sulphated and difficult to separate from CS or DS of low sulphate content. The latter GalAGs of vertebrate origin are mainly sulphated at C-4 and C-6 of the galactosamine moiety and in some cases at C-2 of the uronic acid. Various types of di- and trisulphated disaccharide units may be formed by combining of these sulphation positions.

Analysis of the glycosaminoglycan (GAGs) disaccharides depends on the susceptibility of GAGs to various enzymes with or without simultaneous digestion with chondro-4- or -6-sulphatases [4–8], or to chemical degradation by nitrous acid [9]. The structure of disaccharides obtained after chondroitinase digestion is demonstrated in Fig. 1. Analyses of some of these disaccharides using modern separation and highly sensitive detection techniques have been performed by HPLC [10–21] and capillary zone electrophoresis [22–24].

Although the HPLC methods have been widely and successfully used to analyse GAGs disaccharides, capillary electrophoresis is a powerful technique which may provide extremely high resolution and sensitivity. During recent years HPCE has been used for the analysis and structural characterisation of various types of glycoconjugates (for an excellent review see Ref. 25). The analysis of GalAGs and HA-derived Δ-disaccharides by HPCE facilitated the detection of fmol levels of these polysaccharide constituents. However, the separation between 2 - acetamido - 2 - deoxy - 3 - O - (4 - deoxy - α - L - *threo* - hex - 4 - enopyranosyluronic acid) - D - glucose (Δdi-nonS_{HA}) and 2 - acetamido - 2 - deoxy - 3 - O - (4 - deoxy - α - L - *threo* - hex - 4 - enopyranosyluronic acid) - D - galactose (Δdi-nonS_{CS}), 2 - acetamido - 2 - deoxy - 3 - O - (4 - deoxy - α - L - *threo* - hex - 4 - enopyranosyluronic acid) - 4 - O - sulpho - D - galactose (Δdi-mono4S) and 2 - acetamido - 2 - deoxy - 3 - O - (4 - deoxy - α - L - *threo* - hex - 4 - enopyranosyluronic acid) - 6 - O - sulpho - D - galactose (Δdi-mono6S), as well as between the three types of disulphated disaccharides is incomplete, and various operating buffers are needed to determine each one of these Δ-disaccharides. HPCE analytical protocols using normal polarity have been previously reported by Ampofo et al. [24], Al-Hakim and Linhardt [22] and Carney and Osborne [23]. By these protocols the fractionation of the variously sulphated Δ-disaccharides has been achieved using multiple buffer systems, resulting in poor peak symmetry and peak tailing. The reversed polarity system used by Pervin et al. [26] improved the resolution and peak symmetry and especially the separation between disulphated Δ-disaccharides. However, the later protocol a period as long as 50–60 min was required for a complete electrophoregram, a fact which reduces the sensitivity of the method. Δ-disaccharides derived from iduronic acid (IdoA)-containing disaccharides have not been determined directly by any of the previous HPCE methods. Such Δ-disaccharides can easily be analysed using separate digestions with chondroitinases ABC, AC or B. Chondroitinase ABC cleaves the $1\beta \rightarrow 4$ glycosidic bonds between the galactosamine and the uronic acids, either GlcA

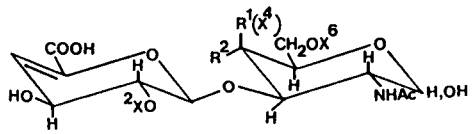

R^1 = H, R^2 = OH	R^1 = OH, R^2 = H
1: X^2, X^4, X^6 = H	2: X^2,X^4,X^6 = H
	3: X^4,X^6 = H, X^2 = SO_3H
	4: X^2,X^6 = H, X^4 = SO_3H
	5: X^2,X^4 = H, X^6 = SO_3H
	6: X^4 = H, X^2,X^6 = SO_3H
	7: X^6 = H, X^2,X^4 = SO_3H
	8: X^2 = H, X^4,X^6 = SO_3H
	9: X^2,X^4,X^6 = SO_3H

Fig. 1. Structures of the non-sulphated and sulphated Δ-disaccharides of hyaluronan, (1) and chondroitin sulphate and/or dermatan sulphate, (2 through 9), produced by chondroitinase digestion.

or IdoA, whereas chondroitinases AC cleave only those to GlcA and chondroitinase B those to IdoA [27].

In this paper we describe an HPCE method of reversed polarity, by which the various disaccharide types present in pure or cell-secreted HA, CS, DS and in PGs can be determined as their Δ-disaccharide derivatives following digestions with chondroitinases. The separation and determination are performed within 14 min with high sensitivity and accuracy.

2. Experimental

2.1. Chemicals

CSA from whale cartilage, CSC from shark cartilage, CSB from porcine skin and HA from human umbilical cord were obtained from the Sigma Chemical Co. (St. Louis, MO, USA). CS-E was isolated from squid cranial cartilage [28,29]. The nonsulphated CS (chondroitin), monosulphated CS and oversulphated CS fractions of GAGs from squid skin were prepared as previously described by Karamanos et al. [30–33]. Shark fin cartilage, CS, was kindly provided by Dr. Atti-La Dahlgren (Institute for Socio-Medical Research, Areuse, Switzerland). Standard preparations of Δdi-nonS_{HA}, Δdi-nonS_{CS}, Δdi-mono4S, Δdi-mono6S, 2 - acetamido - 2 - deoxy - 3 - O - (4 - deoxy - 2 - O - sulpho - α - L - *threo* - hex - 4 - enopyranosyluronic acid) - D - glucose (Δdi - mono2S), 2 - acetamido - 2 - deoxy - 3 - O - (4 - deoxy - 2 - O - sulpho - α - L - *threo* - hex - 4 - enopyranosyluronic acid) - 4 - O - sulpho - D - galactose [Δdi-(2,4)diS or Δdi-diS_B], 2 - acetamido - 2 - deoxy - 3 - O - (4 - deoxy - 2 - O - sulpho - α - L - *threo* - hex - 4 - enopyranosyluronic acid) - 6 - O - sulpho - D - galactose [Δdi-(2,6)diS or Δdi-diS_D], 2 - acetamido - 2 - deoxy - 3 - O - (4 - deoxy - α - L - *threo* - hex - 4 - enopyranosyluronic acid) - (4,6) - di - O - sulpho - D - galactose [Δdi-(4,6)diS or Δdi-diS_E] and 2 - acetamido - 2 - deoxy - 3 - O - (4 - deoxy - 2 - 0 - sulpho - α - L - *threo* - hex - 4 - enopyranosyluronic acid) - (4,6) - di - O - sulpho - D - galactose [Δdi-(2,4,6)triS or Δdi-triS] were purchased from the Seikagaku Kogyo Co. (Tokyo, Japan). Chondroitinases AC, ABC and B were also obtained from Seikagaku. Membrane filters (0.2 μm) were purchased from Millipore (Waters, Milford, MA, USA). All other chemicals used were of analytical reagent grade.

2.2. Enzymic degradation of GAGs

Digestions of the GAGs with chondroitinase AC or ABC and chondro-4- and 6-sulphatases were performed at 37°C for 90 min in 50 m*M* Tris–HCl, pH 7.5 (4–6), using 0.01 units per 10 μg of uronic acid and 10–100 μl of solution. Digestion with chondroitinase B was performed at 37°C for 60 min in 50–100 μl of 50 m*M* Tris–HCl, pH 8.0, using 0.01 units per 40 μg of uronic acid [27]. The digestions were terminated by heating in a boiling water bath for 1 min, whereafter the mixtures were centrifuged in a Microfuge at 10 000 *g* for 5 min. Aliquots were then taken for direct HPCE analysis of non-, mono-, di- and trisulphated Δ-disaccharides.

2.3. High-performance capillary electrophoresis

Capillary electrophoresis was performed on a Beckman HPCE instrument (P/AGE system 5510) equipped with a diode array detector with a window of 100 × 800 μm set at 232 nm for detection of eluted peaks and at 200 to 600 nm for recording the spectrum of these peaks. Separation and analysis were carried out on an uncoated fused-silica capillary tube (75 μm I.D., 55 cm total length and 50 cm from the injection point to the detector) at 25°C. Before each run, the capillary tube was washed with 0.1 *M* NaOH for 1 min, and then with the operating buffer (various sodium orthophosphate buffers at pH ranging from 2.55 to 5.00) for 4 min. The samples to be analysed were injected automatically, using the pressure injection mode, in which the sample is pressurised for 10 s. The injection volume can be calculated with the Poiseuille equation as proposed by the manufacturer (Beckman), giving an estimated volume of

6 nl per second of injection time. For optimal separation, the electrophoresis was performed at 20 kV using 15 m*M* sodium orthophosphate buffer at pH 3.00 and reversing the electrodes so that the constituents to be analysed would migrate from the negative (cathode) to the positive (anode) electrode by electrophoretic mobility (EM) and against the electroosmotic flow (EOF) of the buffer. Peak heights and areas were recorded and evaluated using the Beckman software system Gold V810. Quantitation of Δ-disaccharide contents in samples was performed using an external standard mixture of commercially available disaccharides, diluted with the chondroitinase digestion buffer to a concentration similar to that of the samples. The operating buffer used was degassed by vacuum filtration through a 0.2 μm membrane filter, followed by agitation in an ultrasonic bath.

2.4. Linearity and detection sensitivity

In order to test the linearity of the detector response, precisely known amounts of all Δ-disaccharides were dissolved in chondroitinase digestion buffer to give stock solutions of 10 mg/l and 10 ng/l each. Standard Δ-disaccharide solutions of 0.1 1.0, 10, 50 and 100 ng/l and 0.5, 10, 25, 50 and 100 μg/l were then prepared by dilutions of the stock solutions. A specified injection time of 10 s was used for the analysis, corresponding to an injection volume of 60 nl. The calibration graphs were constructed by plotting the peak heights of Δ-disaccharide signals against their concentration. The detection limits were estimated as the quantity of the Δ-disaccharides producing a signal of the peak height twice the baseline noise.

2.5. Other analytical assays

Total uronic acid was determined by the carbazole method of Bitter and Muir [34] and the IdoA/GlcA ratios obtained by comparing different digests were verified chromatographically, using the HPLC procedure described by Karamanos et al. [35].

2.6. Applications

Analysis of GAGs secreted by cultured cells

We tested the applicability and sensitivity of the proposed HPCE method by using it to analyse the extracellular medium of two human malignant mesothelioma cell lines secreting GAGs, the quantitation of which can be used as an important test in the diagnosis of this tumour [36–37]. In brief, the medium was clarified by centrifugation at 3000 *g* for 15 min and the macromolecules secreted into the medium were precipitated with 4 volumes of ethanol. The GAGs were then liberated from their PGs with papain digestion [38] and purified by a two-step precipitation procedure [39]. The first precipitation was obtained with 1% (w/v) cetyl pyridinium chloride and the second by 90% (v/v) ethanol, containing 2.5% (w/v) sodium acetate. Two sublines were tested, one with the epithelial phenotype obtained through culture in 10% (v/v) human AB serum, and one with a fibroblast-like morphology, obtained in 10% (v/v) fetal calf serum [40]. The isolated GaGs were degraded with a mixture containing chondroitinases ABC and AC and chondro-4- and -6-sulphatases. The chondroitinase-resistant GAGs were then precipitated with 4 volumes of 90% (v/v) ethanol containing 2.5% (w/v) sodium acetate. The supernatant, containing the Δ-disaccharides from the chondroitinase-susceptible GAGs, was dried, dissolved in distilled water and taken for the HPCE analysis.

2.7. Analysis of PGs and GAGs isolated from tissues

To test the applicability of the HPCE method described, PGs were extracted from squid skin, corresponding to 95% of the total content of PGs in this tissue, and analysed. In brief, powdered tissues (5 mg) were extracted with 5 ml of 4 *M* guanidine hydrochloride–50 m*M* sodium acetate, pH 5.8, containing proteinase inhibitors [31–32] and the extract was precipitated twice with 4 volumes of ethanol. The precipitates were dissolved in distilled water and aliquots were taken for digestion with both chondroitinases

ABC and AC. To these digests, 4 volumes of ethanol were added and, after centrifugation at 10 000 *g* for 10 min, the supernatant was analysed for Δ-disaccharides.

Another aliquot of the PG preparation was digested with papain [38] and the liberated GAGs were separated by chromatography on DEAE-Sephacel eluted with a linear NaCl gradient (0.1 to 1.0 *M*), as previously described [32]. The fractions that were positive with the borate–carbazole reaction [34] were pooled to give three different GAG preparations: nonsulphated CS (chondroitin) eluted with 0.2 *M*, monosulphated CS eluted with 0.6 *M* and oversulphated CS, obtained with 0.9 *M* NaCl. The isolated GAGs were then digested with both chondroitinases ABC and AC and analysed by HPCE.

3. Results and discussion

3.1. Resolution of Δ-disaccharides

The determination of HA is based on an analysis of Δdi-nonS_{HA} produced by digestion with chondroitinases ABC and/or AC, and the separation of Δdi-nonS_{CS} and Δdi-nonS_{HA} is therefore essential for the HA analysis. This separation is preferably performed by HPLC, using a primary amino column eluted with sodium dihydrogen orthophosphate at pH 2.55 [16,19]. The HPLC separation requires that the pH of the eluent be kept slightly below the pK_a (3.1–3.2) of the carboxyl groups, giving a separation based on ion suppression, the separation being obtained only in a narrow pH interval. On the other hand, the HPLC separation of oversulphated Δ-disaccharides on an amino column requires a higher pH (pH 5.0) and salt concentration. Using a pH of 2.55 in the HPCE buffer and concentrations of the phosphate buffer varying between 15 and 50 m*M*, the nonsulphated Δ-disaccharides were not observed within 30 min in either normal or reversed-polarity electrophoresis. At this pH, however, oversulphated and monosulphated Δ-disaccharides were completely resolved within 15 min, using reversed polarity (Fig. 2A).

These anionic sulphated Δ-disaccharides will show only limited interactions with the similarly charged silanol groups of the capillary wall, and their migration is thus mainly influenced by the EM and the EOF. At this low pH, the EM of sulphated Δ-disaccharides is much larger than the EOF which, with reversed polarity, is directed against the migration of the carbohydrates. The nonsulphated Δ-disaccharides, however, are anionic only at about 20% of the time, which means that the active charge per disaccharide is only about 0.2. This is obviously not sufficient to overwhelm the EOF. Both of these factors, EOF and EM, are comparatively low and of similar magnitude, since these substances were detected neither with normal nor with reversed polarity within a 30-minute period.

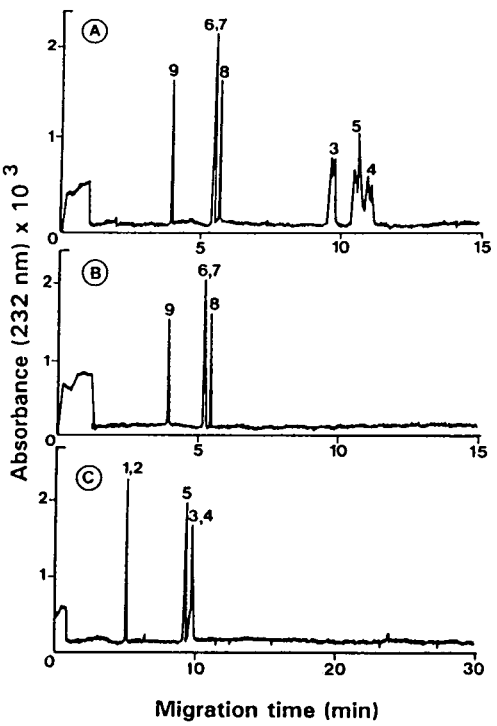

Fig. 2. HPCE profiles of non-sulphated and variously sulphated Δ-disaccharides obtained (A) at pH 2.55, using reversed polarity and (B, C) at pH 5.00, using reversed and normal polarity, respectively. Peaks as indicated in Fig. 1.

Increasing the pH from 2.55 to 5.00 increases both the EOF and the EM. The magnitude of the increase in EM depends on the number of active charges and has very different effects on migration times (Fig. 2A and B). At pH 5.0, the EMs of di- and trisulphated Δ-disaccharides were larger than the EOF, allowing the separation of these structures by reversed polarity, the various types of disulphated Δ-disaccharides migrating similarly (Fig. 2B). The EMs of non- and monosulphated Δ-disaccharides, however, were insufficient to overcome the counter-current EOF, and normal polarity was required to migrate them. Here the separation obtained depended mainly on the number of sulphate groups, with only a poor separation of the different monosulphated types (Fig. 2C).

Better separations were obtained when the pH values between those referred to above were used. At pH 3.00, all Δ-disaccharides tested showed baseline separation (Fig. 3A and B). The double peaks obtained for Δdi-mono4S and Δdi-nonS are well explained by the anomeric forms of the hexosamines present in the reducing terminal of these disaccharides. An increase in the concentration of the operating orthophosphate buffer, pH 3.00, from 15 to 25 and 50 m*M* caused only small differences in the migration times of over- and monosulphated Δ-disaccharides. This pH at a concentration of 15 m*M* was found to be optimal as an operating buffer, since it gave the lowest current value (42 mA) that ensures the best performance of the instrument. At pH 3.50, the separation between non-, mono- and oversulphated Δ-disaccharides was still sufficient, but the resolution between Δdi-(2,4)diS and Δdi-(2,6)diS, as well as between Δdi-mono4S and Δdi-mono6S was somewhat affected. Baseline separation between Δdi-nonS_{CS} and Δdi-nonS_{HA} was obtained at both of these pHs, but they eluted close to each other at pH 3.50. To ensure complete separation with higher injection volumes, a pH of 3.0 seemed preferable also for analysis of the nonsulphated Δ-disaccharides. Repeated injections gave retention times with a standard deviation smaller than 1%.

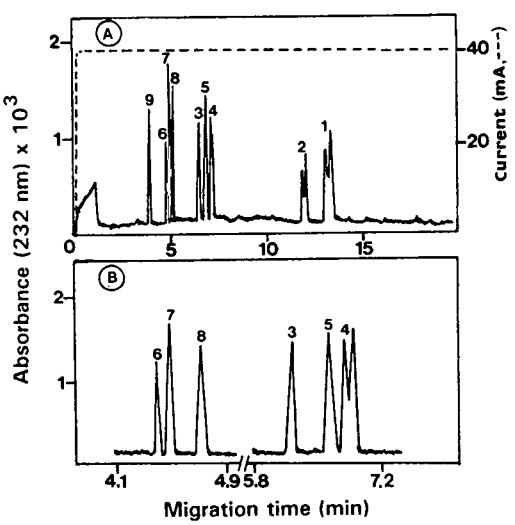

Fig. 3. (A) Typical electrophoregrams obtained at pH 3.00, showing the analysis of nine Δ-disaccharide components (1 to 9). (B) Expanded parts of the same electrophoregram showing the complete separation of individual Δ-disaccharides.

The sensitivity and linearity of the method were tested with the use of standard mixtures at various concentrations. The peak heights and the peak areas obtained were found to be linearly related to the injected amount of each Δ-disaccharide up to the 10 μg/l tested, i.e., through the entire interval tested (Fig. 4). The precision of the method was determined by six repeated determinations of all Δ-disaccharides. When 5 pmol of each disaccharide was measured, the relative standard deviations for the various sulphated disaccharides ranged from 2.6% to 3.2% of the registered value. The baseline noise was as small as 10^{-5} AU. The detection limit of these Δ-disaccharides (molar absorptivity 5500 $M cm^{-1}$), expressed as twice the baseline noise, would then correspond to 22 ng/l (32 pmol/l) for Δdi-triS, 38 ng/l (65 pmol/l) for Δdi-diS, 50 ng/l (100 pmol/l) for Δdi-monoS and 98 ng/l (250 pmol/l) for Δdi-nonS. To obtain an accurate determination of the Δ-disaccharide composition in one injection within a 95% confidence interval, as little as 15–150 fg of the GAG is required with the present injection interval of 10 s. The loading of the injector unit with 5 μl of a sample solution and the triplicate analysis using each 60 nl injection volume would then give a similar

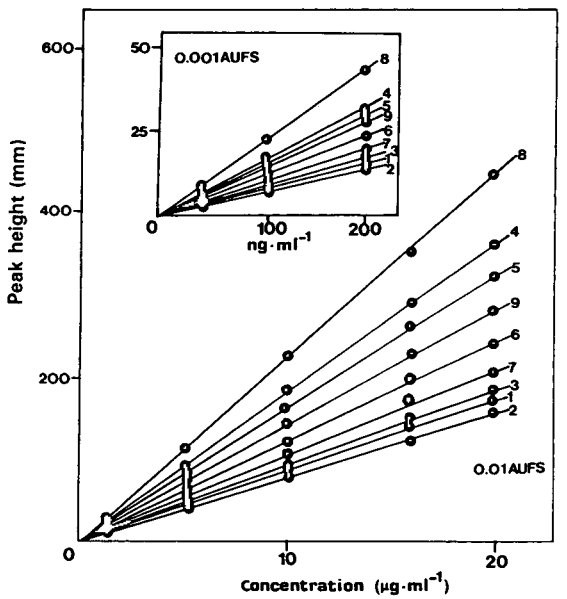

Fig. 4. Calibration curves for the analysis of disaccharides 1 to 9 showing detector response, expressed as peak heights as a function of the concentration of Δ-disaccharides in μg/l. Insert figure shows the calibration curves obtained up to 200 ng/l. Injections of 10 s time interval were performed (injection volume 60 nl). The detector responses ($AU \cdot 10^{-3}$) corresponds to the following equations for the respective disaccharides: 1, $y = 10.9x + 0.1$; 2, $y = 10.3x - 0.1$; 3, $y = 11.7x + 0.4$; 4, $y = 24.3x \pm 0$, 5, $y = 22.0x - 0.2$; 6, $y = 16.1x - 0.1$, 7, $y = 13.7x + 0.2$; 8, $y = 29.7x \pm 0$; 9, $y = 18.9x - 0.2$.

95% accuracy when the sample to be analysed contains approximately 60–200 ng/l of the various Δ-disaccharides. Detection of Δ-disaccharides in fmol levels has also been reported with HPLC by Toyoda et al. [41] and with HPCE by Honda et al. [42], however, these levels of sensitivity were obtained following precolumn derivatization with UV-absorbing substances.

3.2. Applications to the analysis of GAGs and PGs

The analysis of pure HA resulted in one split peak only, corresponding to the anomeric forms of the Δdi-OS_{HA}. Digests of GAGs from different sources, followed by HPCE analysis, showed the presence of various amounts of non-, mono- and oversulphated disaccharides (Table 1). These results were in close agreement with the previously reported composition of these tissues [19, 30–31]. The commonest location of the sulphate was C-4 and C-6 of the galactosamine. Native sulphation in C-2 of the uronic acid was detected in both mono- and disulphated Δ-disaccharides. However, the monosulphated type, Δdi-mono2S, was found only as a small fraction in CS from shark fin cartilage (Fig. 5). The trisulphated Δ-disaccharide and three types of mono- and disulphated Δ-disaccharides were completely separated with the HPCE method

Table 1
Composition of GalAGs from various sources, determined by HPCE[a]

	CSA	CSC	CSB	CSE
Δdi-$nonS_{CS}$	8.9 (9.0)[b]	1.1 (1.3)	2.2 (2.0)	2.1 (2.1)
Δdi-mono4S	64.3 (63.8)	12.5 (12.1)	72.5 (71.3)	19.4 (20.1)
Δdi-mono6S	18.9 (18.4)	64.0 (63.1)	1.2 (1.0)	9.1 (8.2)
Δdi-(2,6)diS	4.5 (5.0)	12.1 (13.4)	4.2 (3.5)	ND[c]
Δdi-(2,4)diS	ND	2.1 (1.8)	24.5 (24.1)	ND
Δdi-(4,6)diS	ND	ND	ND	69.2 (69.7)
Δdi-(2,4,6)triS	ND	ND	ND	ND

[a] Results are the average of three experiments and are expressed as per cent of the total disaccharides recovered by HPCE after digestion with both chondroitinases ABC and AC. Variations in the amounts of disaccharides measured were less than 5% in all cases.
[b] Values in parentheses were obtained from Ref. 19.
[c] Not detected.

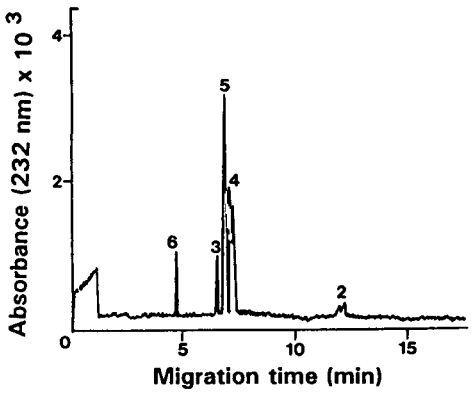

Fig. 5. HPCE analysis of CS isolated from shark fin cartilage after digestion with chondroitinase ABC.

described, even with the larger injection volumes used for analysing samples in the pg range. The identity of the migration times of these di- and trisulphated disaccharides was estimated by chromatography of standard Δ-disaccharide preparations and by observing their chromatographic behaviour after further enzymic treatment. Therefore, digestion of Δdi-di(2,4)S and Δdi-di(2,6)S with chondro-4- and 6-sulphatase, respectively, followed by HPLC analysis of the digests for monosulphated Δ-disaccharides, showed that they both migrated to the position of Δdi-mono2S. The presence of Δdi-di(4,6)S was also confirmed by the detection of Δdi-nonS_{CS} as the only Δ-disaccharide obtained after digestion with both chondro-4- and 6-sulphatases.

As shown in Table 2, the sulphation patterns obtained for the tissue extracted PGs were in close agreement with those obtained with purified GAGs. This indicates that the proposed HPCE method can also be easily and accurately used for the sulphation analysis of PG molecules present in tissue extracts. On the other hand, analysis of GAGs secreted by the two human malignant mesothelioma cell lines showed that this method is also applicable to biological preparations containing minute amounts of GAGs (approximately 1 ng of each of HA and GalAGs per 10^3 mesothelioma cells and less than 20 pg per the same number of benign mesothelial cells) which otherwise can be detected only by radiochemical techniques [43,44]. The sulphation pattern of these GAGs can also be established with the present technique. When the total amount of GalAGs is to be determined, the digest is preferably completed chondro-4- and -6-sulphatases, to collect and concentrate most of the disaccharides in the nonsulphated peak.

3.3. Determination of GlcA or IdoA clusters in DS

Clustered disaccharide structures in DS, i.e., sequences with a single type of uronic acid only, either GlcA or IdoA, can be studied by separate digestions with chondroitinase AC and B, comparing the obtained values with those obtained after digestion with chondroitinase ABC. A high rate of recovery can help in recognising such

Table 2
HPCE analysis of GalACs in human malignant mesothelioma and in tissue extracted PGs

	Δdi-nonS_{HA}	Δdi-nonS_{CS}	Δdi-mono4S	Δdi-mono6S	Δdi-diS	Δdi-triS
Fibroblast GalAGs[a]	684	425				
Epithelial GalAGs[a]	8187	5460				
Squid skin PG extract[b]	ND	3567	1200	276	1087	257
Chondroitin[b]	ND	310	ND	ND	ND	ND
CSI + CSII[b]	ND	145	198	82	25	ND
Oversulphated CS[b]	ND	152	912	202	894	185

[a] Expressed as pg per 10^3 cells and day in culture. These separations were performed only after sulphatase digestion.
[b] Expressed as ng present in mg tissue dry weight.

GlcA or IdoA clusters, whereas low a recovery indicates that the DS is rich in alternating GlcA- and IdoA-containing disaccharides (cf., Fig. 6A, B and C). The oligosaccharides resulting from such a partial digestion of chondroitinase B contain a terminal Δ-uronic acid derived from IdoA, although the remaining uronic acids in these fragments are GlcA. Corresponding fragments obtained with chondroitinase AC have a GlcA-derived Δ-uronic residue, the remaining ones are IdoA. Three such extra peaks were obtained when the DS was digested with chondroitinase B (Fig. 6C), indicating that most of the GlcA-containing disaccharides are scattered or occur in short sequences. This is also in agreement with our previous results [45], showing that the longer UV-absorbing sequences of this digest consists of one Δ-tetrasaccharide, one Δ-hexasaccharide and one Δ-decasaccharide fragment, the latter containing the linkage region. The exact identity of these oligosaccharide peaks, however, remains to be determined. The present HPCE method, in combination with the various chondroitinases, thus facilitates an understanding of the DS disaccharide sequences. Such an analytical use of chondroitinases AC and B, however, necessitates a careful interpretation of the data obtained. The exact nature of the oligosaccharide fragments remains to be elucidated.

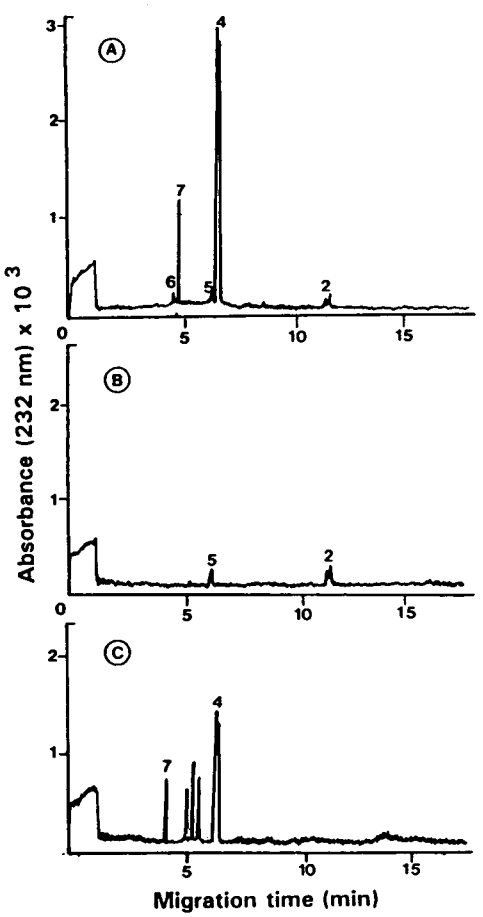

Fig. 6. (A, B and C) Analyses of CSB from porcine skin digested with chondroitinases ABC, AC and B, respectively.

Analysis of various DS digests showed the absence of IdoA-derived Δdi-mono6S, but this was found noted mainly with GlcA, indicating a non-random sulphation during synthesis. The disulphated disaccharides, Δdi-di(2,4)S, Δdi-di(2,6)S and Δdi-di(4,6)S, were obtained from GlcA- and IdoA-containing disaccharides (Table 3). These results indicated that all six disulphated disaccharides tested (GlcA- or IdoA-containing di(2,6)S, di(2,4)S and di(4,6)S can be determined in the same HPCE run.

In conclusion, the presently used HPCE method allows the separation of all the different types of Δ-disaccharides known to be present in chondroitinase-susceptible vertebrate GAGs. The

Table 3
Composition of disulphated disaccharides of various GalAGs, determined by HPCE[a]

	Disulphated Δ-disaccharides		
	(2,6)S	(2,4)S	(4,6)S
CSA	55.7[b]	ND	ND
CSC	57.4[b]	6.0[b]	ND
CS shark fin cartilage	100.0[b]	ND	ND
CSB porcine skin	6.0[c]	93.8[c]	ND
CS squid cartilage	ND	ND	100.0[b]
CS squid skin	ND	ND	10.0[b]

[a] The results are expressed as per cent of the total disulphated Δ-disaccharides recovered by HPLC after digestions with chondroitinase AC and B.
[b] Derived from GlcA-containing disaccharides.
[c] Derived from IdoA-containing disaccharides.

analysis can be performed on the attomole level. In combination with the separate use of chondroitinase AC and B, this analysis can also provide information about the types of uronic acid present.

Acknowledgements

We wish to thank Mr. Hans Kronborg, PhD, of the Beckman Instrument Co., for helping us to begin this study. This work was supported by grants from the Swedish Medical Council (Project 8274), the Swedish Cancer Fund (Project 2485) and by funds from the Karolinska Institute.

References

[1] L. Kjellén and U. Lindahl, *Ann. Rev. Biochem.*, 60 (1991) 443–475.
[2] H.J. Mankin, *Fed. Proc.*, 32 (1973) 1478–1480.
[3] B. Caterson, F. Mahmodian, J.M. Sorrell, T.E. Hardingham, M.T. Bayliss, S.L. Carney, A. Ratcliffe and H. Muir, *J. Cell Sci.*, 97 (1990) 411–417.
[4] T. Yamagata, H. Saito, O. Habuchi and S. Suzuki, *J. Biol. Chem.*, 243 (1968) 1523–1535.
[5] S. Saito, T. Yamagata and S. Suzuki, *J. Biol. Chem.*, 243 (1968) 1536–1542.
[6] S. Suzuki, *Methods Enzymol.*, 28 (1972) 911–917.
[7] A. Linker and P. Hovingh, *J. Biol. Chem.*, 240 (1965) 3724–3728.
[8] P. Hovingh and A. Linker, *Carbohydr. Res.*, 37 (1974) 181–192.
[9] J.A. Cifonely and J. King, *Carbohydr. Res.*, 21 (1972) 173–186.
[10] A. Hjerpe, C.A. Antonopoulos and B. Engfeldt, *J. Chromatogr.*, 171 (1979) 339–334.
[11] S.R. Delaney, M. Leger and H.E. Conrad, *Anal. Biochem.*, 106 (1980) 253–261.
[12] G.J.-L. Lee and H. Tieckelmann, *J. Chromatogr.*, 195 (1980) 402–406.
[13] P.J. Knudsen, P.B. Eriksen, M. Fenger and K. Florentz, *J. Chromatogr.*, 187 (1980) 373–379.
[14] G.J.-L. Lee, D.-W. Liu, J.W. Pav and H. Tieckelmann, *J. Chromatogr.*, 222 (1981) 65–73.
[15] A. Hjerpe, C.A. Antonopoulos, B. Engfeldt and M. Nurminen, *J. Chromatogr.*, 242 (1982) 193–195.
[16] A. Hjerpe, C.A. Antonopoulos and B. Engfeldt, *J. Chromatogr.*, 242 (1982) 365–368.
[17] M.E. Zebrower, F.T. Kieras and W.T. Brown, *Anal. Biochem.*, 157 (1986) 93–97.
[18] K. Murata and Y. Yokoyama, *J. Chromatogr.*, 415 (1987) 231–240.
[19] N.K. Karamanos, A. Syrokou, P. Vanky, M. Nurminen and A. Hjerpe, *Anal. Biochem.*, 221 (1994) 188–189.
[20] K. Schwarz, B. Breuer and H. Kresse, *J. Biol. Chem.*, 265 (1990) 22023–22028.
[21] M. Zebrower, F.J. Kieras and J. Heaney-Kieras, *Glycobiology*, 1 (1991) 271–276.
[22] A. Al-Hakim and R.J. Linhardt, *Anal. Biochem.*, 195 (1991) 68–73.
[23] S.L. Carney and D.L. Osborne, *Anal. Biochem.*, 195 (1991) 132–140.
[24] S.A. Ampofo, H.M. Wang and R.J. Linhardt, *Anal. Biochem.*, 199 (1991) 249–255.
[25] M.V. Novotny and J. Dudor, *Electrophoresis*, 14 (1993) 373–389.
[26] A. Pervin, A. Al-Hakim and R.J. Linhardt, *Anal. Biochem.*, 220 (1994) 182–188.
[27] Y.M. Michelacci and C.P. Dietrich, *Biochem. J.* 151 (1975) 121–129.
[28] A. Hjerpe, B. Engfeldt, T. Tsegenidis, C.A. Antonopoulos, D.H. Vynios and C.P. Tsiganos, *Biochim. Biophys. Acta*, 757 (1983) 85–91.
[29] D.H. Vynios and C.P. Tsiganos, *Biochim. Biophys. Acta*, 1033 (1990) 139–147.
[30] N.K. Karamanos, T. Tsegenidis and C.A. Antonopoulos, *Comp. Biochem. Physiol.* 85B (1986) 865–868.
[31] N.K. Karamanos, A.J. Aletras, C.A. Antonopoulos, A. Hjerpe and C.P. Tsiganos, *Eur. J. Biochem.*, 192 (1990) 33–38.
[32] N.K. Karamanos, A.J. Aletras, T. Tsegenidis, C.P. Tsiganos and C.A. Antonopoulos, *Eur. J. Biochem.*, 204 (1992) 553–560.
[33] N.K. Karamanos, *Biochem. Cell Biol.*, 70 (1992) 629–635.
[34] T. Bitter and H. Muir, *Anal. Biochem.*, 4 (1962) 330–334.
[35] N.K. Karamanos, A. Hjerpe, T. Tsegenidis, B. Engfeldt and C.A. Antonopoulos, *Anal. Biochem.*, 172 (1988) 410–419.
[36] A. Hjerpe, *Clin. Chem.*, 32 (1986) 952–956.
[37] M. Nurminen, A. Dejmek, G. Mårtensson, A. Thylén and A. Hjerpe, *Clin. Chem.*, 40 (1994) 777–780.
[38] J.E. Scott, in D. Glick (Editor), *Methods of Biochemical Analysis*, Vol. 8, Interscience, New York, 1960, pp. 145–197.
[39] C.A. Antonopoulos, E. Borelius, B. Hamnstrom and J.E. Scott, *Biochim. Biophys. Acta*, 54 (1961) 213–226.
[40] J. Klominek, K.H. Robert, A. Hjerpe, B. Wikström and G. Gahrton, *Cancer Res.* 49 (1989) 6118–6122.
[41] H. Toyoda, K. Motoki, M. Tanikawa, K. Shinomiya, H. Akiyama and T. Imanari, *J. Chromatogr.*, 565 (1991) 141–148.
[42] S. Honda, T., Ueno and K. Kakehi, *J. Chromatogr.*, 608 (1992) 289–295.

[43] V.C. Hascall, A. Calabro, R.J. Midura and M. Yanagisha, in W.J. Lennarz and G.W. Hart (Editors), *Guide to Techniques in Glycobiology* (*Methods in Enzymology*, Vol. 230), Academic Press, New York, 1994, pp. 390–417.

[44] G. Tzanakakis, N.K. Karamanos, J. Klominek and A. Hjerpe, A. *Biochem. Cell Biol.*, (1995) in press.

[45] N.K. Karamanos, P. Vanky, A. Syrokou and A. Hjerpe, *Anal. Biochem.*, (1995) in press.

ELSEVIER

Journal of Chromatography A, 696 (1995) 307–319

JOURNAL OF CHROMATOGRAPHY A

Effect of high concentrations of salts in samples on capillary electrophoresis of anions

Liguo Song[a,*], Qingyu Ou[a], Weile Yu[a], Guifang Xu[b]

[a]*Lanzhou Institute of Chemical Physics, Chinese Academy of Sciences, Lanzhou 730000, China*

[b]*Tuha Research Institute of Petroleum Exploration and Development, Shanshan 838201, China*

First received 5 July 1994; revised manuscript received 13 December 1994; accepted 22 December 1994

Abstract

The capillary electrophoretic separation of anions using direct UV detection was studied. The separation conditions, such as carrier electrolyte, pH and concentration of electroosmotic modifier, were optimized. The carrier electrolyte co-ion affected the peak shape because electromigration dispersion was non-negligible. An unsuitable anion form of the electroosmotic flow modifier would cause negative peaks on the separation baselines when the samples contain high concentrations of salts, and the separation could be adversely affected. In this work, sodium chloride with 2.0 m*M* tetradecyltrimetylammonium bromide was used as the carrier electrolyte solution, and a good separation was achieved. Taking sodium chloride to represent salts in samples, the experimental results showed that the peak height and width of a detected anion were affected by the ratio of sodium chloride concentration between the carrier electrolyte solution and sample, and correspondingly the detection limit and separation efficiency of the anion were also affected. The principle of electrostacking was used to explain this phenomenon theoretically. The reproducibility of migration time, peak height and peak area under different conditions was also examined.

1. Introduction

Capillary ion electrophoresis (CIE) [1–4] is a recently introduced capillary electrophoretic technique optimized for the rapid determination of low-molecular-mass inorganic and organic ions. In the capillary electrophoretic separation of anions, an electroosmotic modifier is added to the carrier electrolyte solution to create a layer of positive charges at the capillary inner wall and reverse or slow the electroosmotic flow [1–4]. Without the electroosmotic modifier, anions move rapidly in the opposite direction to the electroosmotic flow, which results in a very long migration time and renders the method less attractive.

Because most anions lack a chromophore, universal indirect UV detection is widely used in CIE [3–7]. In comparison with indirect UV detection, there have been only a few reports [8–10] of the use of direct UV detection. However, direct UV detection is more selective and sensitive. In the determination of a specific trace-level anion in a sample containing high concentrations of other anions, it is preferable to use direct UV detection provided that the trace-level

* Corresponding author. Present address: Department of Chemistry, Wuhan University, Wuhan 430072, China.

0021-9673/95/$09.50
SSDI 0021-9673(94)01291-1

anion shows UV absorption whereas the high-concentration anions do not.

CIE has been used in various application fields and is now recognized as a less matrix-dependent method than ion chromatography (IC). When IC is used to determine anions in samples with high concentrations of salts, there is a risk of sample overloading and consideration must be given to the total ion-exchange capacity of the column. Although CIE has not been used to determine anions in samples with high concentrations of salts, Jones and Jandik [9] successfully determined anions with disparate concentrations, such as anion impurities in 99.9% pure solid terephthalic acid. When we tried to determine anions in subterranean water, samples with high concentrations of salts were encountered (there are high concentrations of chloride, sulfate, carbonate salts, etc., in subterranean water, in which the concentration of chloride is generally the highest and can reach as high as grams per litre levels; the cation with the highest concentration is generally sodium) and the potential of CIE in the determination of anions in such samples was therefore investigated.

The objective of this study was to develop a CIE method for the determination of trace-level UV-absorbing anions in subterranean water. For this purpose, the capillary electrophoretic separation of anions using direct UV detection was studied. The separation conditions, such as carrier electrolyte, pH and concentration of electroosmotic modifier, were optimized. The effect of high concentrations of salts in samples on the separation was especially studied both experimentally and theoretically.

2. Experimental

2.1. Apparatus

The CE system used was a Quanta 4000 (Waters Chromatography Division of Millipore, Milford, MA, USA) with a negative power supply. Direct UV detection was accomplished with a zinc lamp and a 214-nm optical filter. Data acquisition was carried out with a Waters Millennium 2010 chromatography manager with a bus satellite interface and LAC/E modules connecting the data station with the CE system. Data collection was initiated by a signal cable connection between the Quanta 4000 and the bus satellite interface.

2.2. Carrier electrolyte solutions

Four carrier electrolytes, sodium sulfate, sodium acid phosphate, piperazine sulfate and sodium chloride, were used to give carrier electrolyte solutions in which tetradecyltrimetylammonium bromide (TTAB) purchased from Waters was used as electroosmotic modifier according to the literature [11] and added at a suitable concentration.

2.3. Standard solutions

Analytical-reagent grade sodium or potassium salts were purchased in China and used to prepare 1000 ppm stock standard anion solutions containing a single anion. The mixed anion solutions consisted of ten anions, fluoride, chloride, bromide, iodide, nitrite, nitrate, sulfate, phosphate, carbonate and thiocyanate, of which only five, bromide, iodide, nitrite, nitrate and thiocyanate, show UV absorbance at 214 nm. Five mixed anion solutions containing 1, 4, 10, 20 and 40 ppm of each anion were prepared to evaluate calibration graphs. Another five mixed anion solutions containing 10 ppm of each of the above-mentioned ten anions with an additional 20 ppm of thiocyanate, 10 ppm of nitrate, 10 ppm of nitrite, 20 ppm of bromide or 20 ppm of iodide separately were prepared for the purpose of peak identification in electrophorograms. Mixed anion solutions were prepared not only with deionized water, but also with 12.5, 50 or 100 m*M* sodium chloride solutions. Polyethylene containers were utilized for the mixed anion solutions.

2.4. Electrophoresis

A Waters Accu-Sep polyimide-coated fused-silica capillary was used throughout. The capil-

lary dimensions were 75 μm I.D., 60 cm total length and 52 cm from the point of injection to the detector cell. The capillary was flushed with 1 *M* potassium hydroxide solution for 1 h and then equilibrated with carrier electrolyte solution before use. All injections were performed in the hydrostatic mode at a height of 10 cm for 30 s. The applied voltage for each run was 10 kV. A 2-min capillary purge with carrier electrolyte solution by a vacuum applied to the receiving electrolyte vial was performed prior to each injection.

3. Results and discussion

3.1. Optimization of capillary electrophoretic separation of anions using direct UV detection

Three carrier electrolytes, sodium sulfate, sodium acid phosphate and piperazine sulfate, were chosen to examine the effect of carrier electrolyte on the capillary electrophoretic separation of anions. The three carrier electrolytes contained two anions, sulfate and phosphate, and two cations, sodium and piperazine, in which phosphate and piperazine could be protonated and had buffering ability. We believed that both the anion and cation of a carrier electrolyte have an effect on the separation. Carrier electrolyte solutions were prepared from 10 m*M* of sodium sulfate, phosphoric acid or piperazine with 0.5 m*M* TTAB separately, and the pH of the carrier electrolyte solutions was adjusted to 9.3 with sodium hydroxide or sulfuric acid by using a pH meter. Capillary electrophoretic separation of anions using direct UV detection was achieved as shown in Fig. 1.

It was clear that when sodium sulfate was used, peak 2 was separated from peak 3 (Fig. 1A); when sodium acid phosphate was used, peak 2 overlapped partly with peak 3 (Fig. 1B); when piperazine sulfate was used, peak 2 nearly overlapped with peak 3 (Fig. 1C). Apart from this, peak 1 was also affected. When sodium acid phosphate and piperazine sulfate was used, a negative peak occurred prior to peak 1 and rendered the calibration graph for peak 1 of

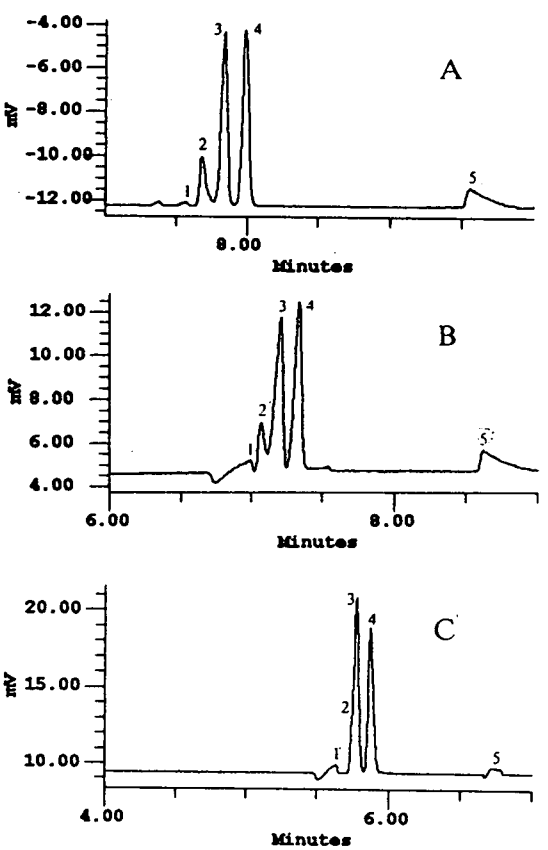

Fig. 1. Capillary electrophoretic separation of anions using direct UV detection. Carrier electrolyte: (A) 10 m*M* sodium sulfate; (B) 10 m*M* sodium acid phosphate; (C) 10 m*M* piperazine sulfate. Current: (A) 15 μA; (B) 16 μA; (C) 6.5 μA. Peaks; 1 = bromide; 2 = iodide; 3 = nitrite; 4 = nitrate; 5 = thiocyanate. The concentration of each anion in the sample was 10 ppm.

peak height or area versus concentration non-linear.

Another effect of the carrier electrolyte on separation was to change the peak shape. Fig. 2 is an enlarged view of peaks 3 and 4 of Fig. 1. With sodium sulfate, relatively symmetrical peaks 3 and 4 (Fig. 2A) were observed; with sodium acid phosphate, fronting of peaks 3 and 4 (Fig. 2B) was seen; with piperazine sulfate, slight tailing of peaks 3 and 4 (Fig. 2C) occurred. This phenomenon has been reported previously in CIE when using indirect detection, and was caused by electromigration dispersion [12–14].

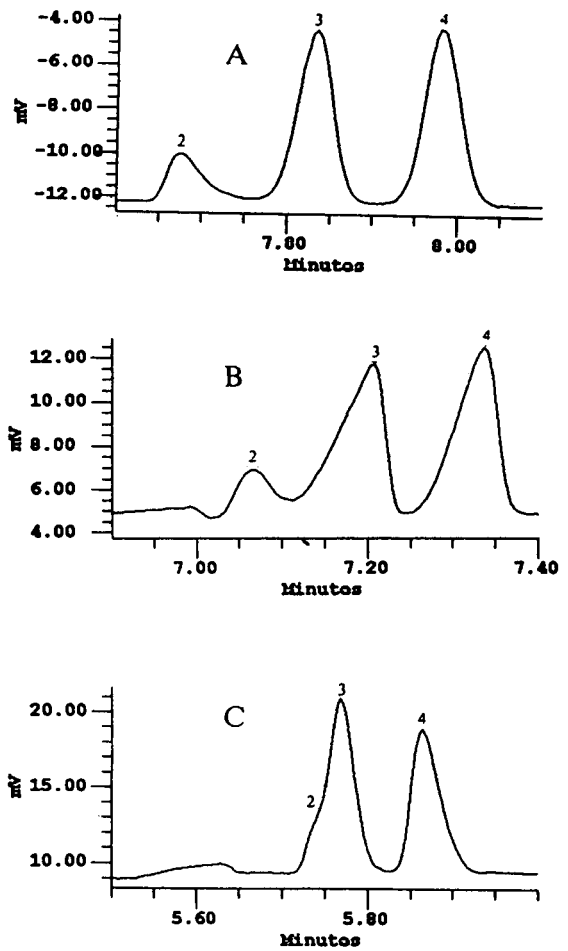

Fig. 2. Enlarged view of nitrite and nitrate peaks in Fig. 1. Peak identification as in Fig. 1.

As indicated in the literature [12–14], electromigration dispersion occurs during the migration of sample ions that possess effective mobilities different to that of the background electrolyte co-ion; the higher the concentration of the sample component is in its zone, the more pronounced the electromigration dispersion will be. Generally, electromigration dispersion is considered to be negligible when the concentration of the carrier electrolyte co-ion is two orders of magnitude higher than that of the sample ions.

In capillary electrophoresis of biological macromolecules, generally no tailing or fronting peaks occur because the concentration of the carrier electrolyte co-ion can be easily adjusted to be two orders of magnitude higher than that of the biological macromolecules. In capillary electrophoresis of anions using indirect UV detection, generally tailing and fronting peaks occur because the carrier electrolyte co-ion used will generate a UV absorption background and its concentration cannot be too high [14]. Under the experimental conditions of Fig. 2, the concentration of carrier electrolyte was 10 m*M* and that of the sample anions was 10 ppm. After the units of concentration had been converted to be the same, the ratio between the concentration of carrier electrolyte and that of the sample anions (nitrite and nitrate) was 46 (molecular mass of nitrite) and 64 (molecular mass of nitrate). Sodium sulfate is a strong electrolyte, so the concentration of the co-ion (sulfate) of the carrier electrolyte sodium sulfate at pH 9.3 was equal to the concentration of sodium sulfate, 10 m*M*. Phosphoric acid undergoes a three-step ionization with $pK_{a1} = 2.12$, $pK_{a2} = 7.20$ and $pK_{a3} = 12.36$, hence the concentration of the co-ion (phosphate) of the carrier electrolyte sodium acid phosphate at pH 9.3 was obviously lower than the original concentration of phosphoric acid, i.e., 10 m*M*. Piperazine is a base that undergoes a two-step ionization with $pK_{a1} = 9.66$ and $pK_{a2} = 5.20$, hence the concentration of the co-ion (sulfate) of the carrier electrolyte piperazine sulfate at pH 9.3 was approximately half of the original concentration of piperazine, i.e., 5 m*M*. Therefore, the concentration of the carrier electrolyte co-ion in Fig. 2A–C did not reach two orders of magnitude higher than that of the sample ions (nitrite and nitrate). Hence electromigration dispersion was non-negligible. The main reason for this can be mainly attributed to the low molecular masses of nitrite and nitrate, whereas biological macromolecules have very high molecular masses and the situation will be the opposite. Of course, in order to suppress electromigration dispersion, the concentration of the carrier electrolyte co-ion could be raised, but the anion concentration in the sample may be even higher, so it was concluded that electromigration dispersion was inevitable in capillary

electrophoresis of anions using direct UV detection.

According to the literature [15], the equivalent conductances of sulfate, phosphate, nitrite and nitrate are 80.0, 33.0, 71.8 and 71.4, respectively. As the equivalent conductances relate directly to the mobilities of ions, the following discussion using mobilities of anions was based on the equivalent conductances of the anions listed above. In Fig. 2B, the sample anions (nitrite and nitrate) were more mobile than the carrier electrolyte co-ion (phosphate), so that fronting peaks occurred. In Fig. 2C, nitrite and nitrate was less mobile than the carrier electrolyte co-ion (sulfate), so that tailing peaks were observed. However, in Fig. 2A, although the carrier electrolyte co-ion was the same as in Fig. 2C, the peaks of nitrite and nitrate did not show obvious tailing. This is because the carrier electrolyte co-ion (sulfate) had a mobility close to those of nitrite and nitrate, and the concentration of sulfate in Fig. 2A, which was nearly double that in Fig. 2C, approached two orders magnitude greater than the concentrations of nitrite and nitrate. Hence the conclusion is that the selection of a co-ion with a mobility close to those of anions in the sample is necessary in CIE not only when using indirect UV detection but also when using direct UV detection. Because iodide and thiocyanate are known hydrophobic anions that could interact with TTAB, they were not used to examine the effect of the carrier electrolyte on the peak shape.

The relationship between the response and the concentration of anions was also affected by the carrier electrolyte. Taking nitrate as an example, when sodium sulfate was used the relationship between peak height or area and concentration was linear from 1 to 40 ppm (least-squares fitting); when sodium acid phosphate was used, the relationship was linear only within the range 1–20 ppm; when piperazine sulfate was used, the relationship between peak height and concentration was linear only from 1 to 20 ppm and that between peak area and concentration from 1 to 40 ppm. The decreased linear range was caused by peak broadening and decreased separation efficiency.

The experimental results showed that as a carrier electrolyte sodium sulfate gave the best separation, but it is not a pH buffer salt. Sodium acid phosphate is a pH buffer salt, but we predicted that it would cause more fronting peaks at pH lower than 9.3. Piperazine sulfate is a pH buffer salt, and it could give relatively good separations; so piperazine sulfate seemed to be the best choice as the carrier electrolyte.

Carrier electrolyte solutions of 10 m*M* sodium sulfate with 0.5 m*M* TTAB at pH 5.8, 7.0, 9.3, 10.2 and 11.2 were used to examine the effect of pH on separation. The results showed that pH had only a slight effect on the resolution of iodide and nitrite.

Carrier electrolyte solutions of 10 m*M* piperazine sulfate with 1.0, 2.0, 2.6 and 3.0 m*M* TTAB were selected to examine the effect of the electroosmotic modifier concentration on separation. The relationship between the migration time of each anion and the concentration of TTAB is shown in Fig. 3. When the concentration of TTAB was 2.6 and 3.0 m*M*, the migration time of thiocyanate was too long, and was not measured and shown in Fig. 3; the

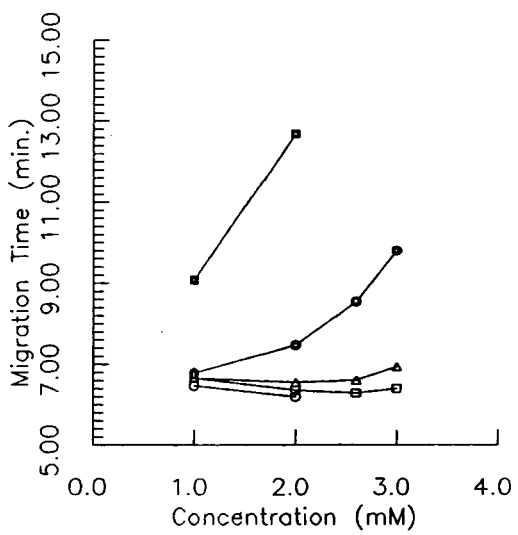

Fig. 3. Effect of concentration of TTAB on separation. ○ = Bromide; ● = iodide; □ = nitrite; △ = nitrate; ■ = thiocyanate. The concentration of each anion in the sample was 20 ppm.

bromide peak was covered by a negative peak prior to bromide, as shown in Fig. 1C, so its migration time also was not measured and shown in Fig. 3. It was observed that an increased concentration of TTAB caused longer migration times of iodide and thiocyanate and a higher resolution of nitrite and nitrate. A possible explanation of this effect involved ion pairing between nitrate and TTAB and hydrophobic interactions between hydrophobic anions (iodide and thiocyanate) and TTAB [16].

3.2. *Effect of high concentrations of salts in samples on separation*

It was shown above that the capillary electrophoretic separation of anions can be achieved by using sodium sulfate, sodium acid phosphate or piperazine sulfate as the carrier electrolyte. In each instance, TTAB was added to the carrier electrolyte solution as an electroosmotic flow modifier to reverse the electroosmotic flow. When these carrier electrolyte solutions were applied to separate anions in samples with high concentrations of salts, however, the separation became significantly poorer. In order to find the reason for this, sodium chloride was chosen to represent the salts in samples and the effect of high concentrations of sodium chloride in samples on the separation baseline was examined.

Four blank samples containing 0, 12.5, 50 and 100 m*M* sodium chloride and no analyte anions were injected and the separation baselines were monitored as illustrated in Fig. 4A and B when the sodium chloride concentration in sample was 12.5 m*M*. When sodium sulfate or piperazine sulfate carrier electrolyte solutions were used, an extremely broad negative peak followed by a very broad positive peak appeared on each baseline. Although the negative peak shown in Fig. 4A and B had different migration times, it appeared just before the bromide peak in the separation of anions and hence would seriously affect the separation. The peak width of the negative peak increased rapidly with increasing concentration of sodium chloride in the sample. Even when there was no sodium chloride in the sample there was still a small negative peak followed by a small positive peak on separation baseline when piperazine sulfate was used as the carrier electrolyte solution, but they were not present when sodium sulfate was used as the carrier electrolyte solution. This can also be seen in Fig. 1C and A. When sodium chloride was used instead of sodium sulfate and piperazine sulfate as the carrier electrolyte, similar baselines were monitored again and are shown in Fig. 4C. It was observed that only a very sharp negative peak remained (the broad peak was generated by water). The width of the sharp negative peak increased linearly with increasing concentration of sodium chloride in the sample, but the separation of anions could still be accomplished. As the carrier electrolyte co-ion, chloride has an electrophoretic mobility close to that of sulfate [15] and would not cause too much tailing or fronting of peaks, hence piperazine chloride was the best choice as the carrier electrolyte for the separation of anions in samples with high concentrations of salts. Considering that subterranean water is generally neutral, and sodium chloride as carrier electrolyte would give a wider linearity range than piperazine chloride, we chose sodium chloride as the carrier electrolyte in this experiment.

The negative peaks on the baselines in Fig. 4 could originate from the use of TTAB as an electroosmotic modifier. Bromide in TTAB made the carrier electrolyte solutions generate UV absorption at 214 nm, and the presence of chloride in samples displaced bromide and caused a decrease in absorbance as observed in Fig. 4. However, the reason for the much wider negative peaks in Fig. 4A and B than in Fig. 4C seemed to be more complicated, and may originate from electromigration dispersion caused by the different electrophoretic mobilities between chloride and the carrier electrolyte co-ion (sulfate). It is believed that when the electroosmotic flow modifier is converted into a transparent anion form, such as chloride, the negative peak will disappear.

By using sodium chloride with TTAB as a carrier electrolyte solution, the capillary electrophoretic separation of anions was achieved as demonstrated in Fig. 5. In order to increase the

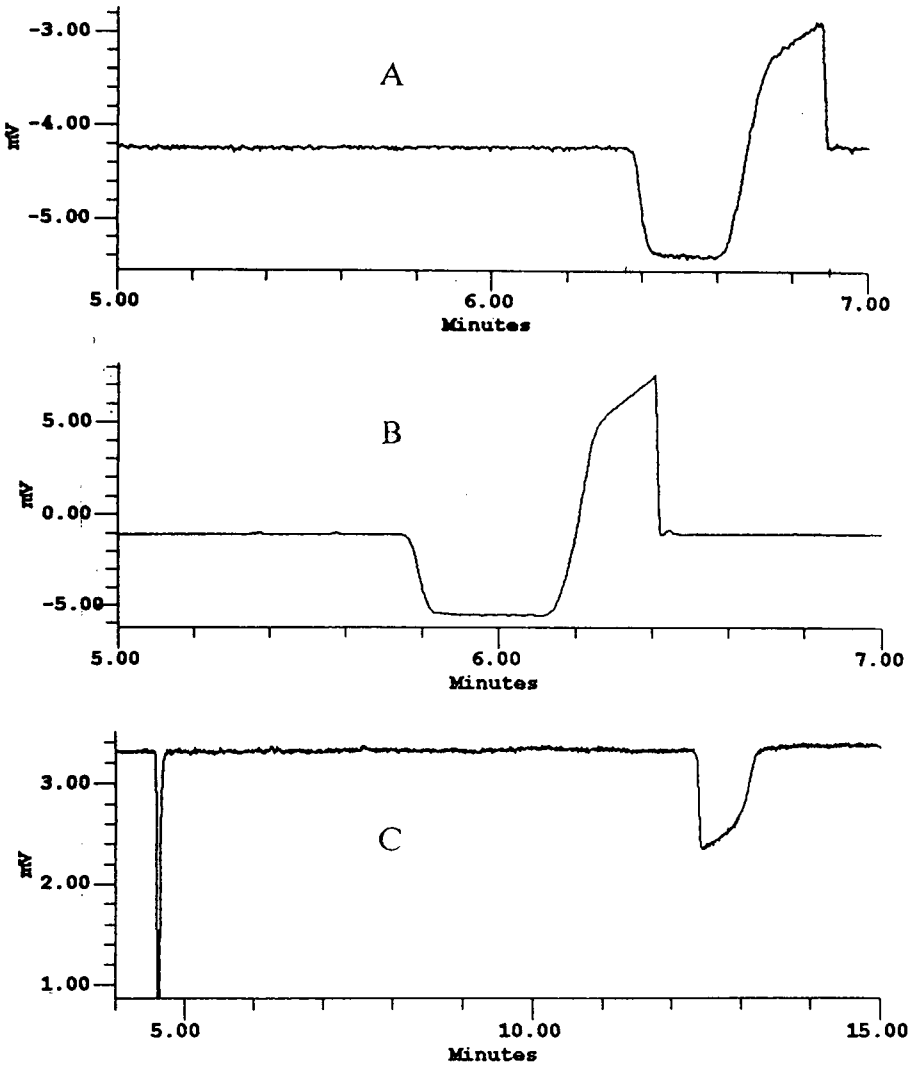

Fig. 4. Effect of 12.5 m*M* sodium chloride in the sample on the separation baseline. Carrier electrolyte solution: (A) 10 m*M* sodium sulfate with 0.5 m*M* TTAB; (B) 10 m*M* piperazine sulfate with 0.5 m*M* TTAB; (C) 25 m*M* sodium chloride with 2.0 m*M* TTAB.

resolution, 2.0 m*M* in addition to 0.5 m*M* TTAB was used. Five peaks belonging to bromide, iodide, nitrite, nitrate and thiocyanate were observed in the electropherograms when there was no sodium chloride in the sample (Fig. 5A–C). However, when there was high concentration of sodium chloride in the sample, the bromide peak disappeared owing to the negative peak caused by sodium chloride in the sample (Fig. 5D–F). It was clear that a successful separation depended on the ratio of sodium chloride concentration between the carrier electrolyte solution and the sample. When the concentration of sodium chloride in the carrier electrolyte solution was 25 m*M*, a successful separation of anions with 12.5 m*M* sodium chloride in the sample was achieved, except for bromide, but an unsuccessful separation of anions was obtained

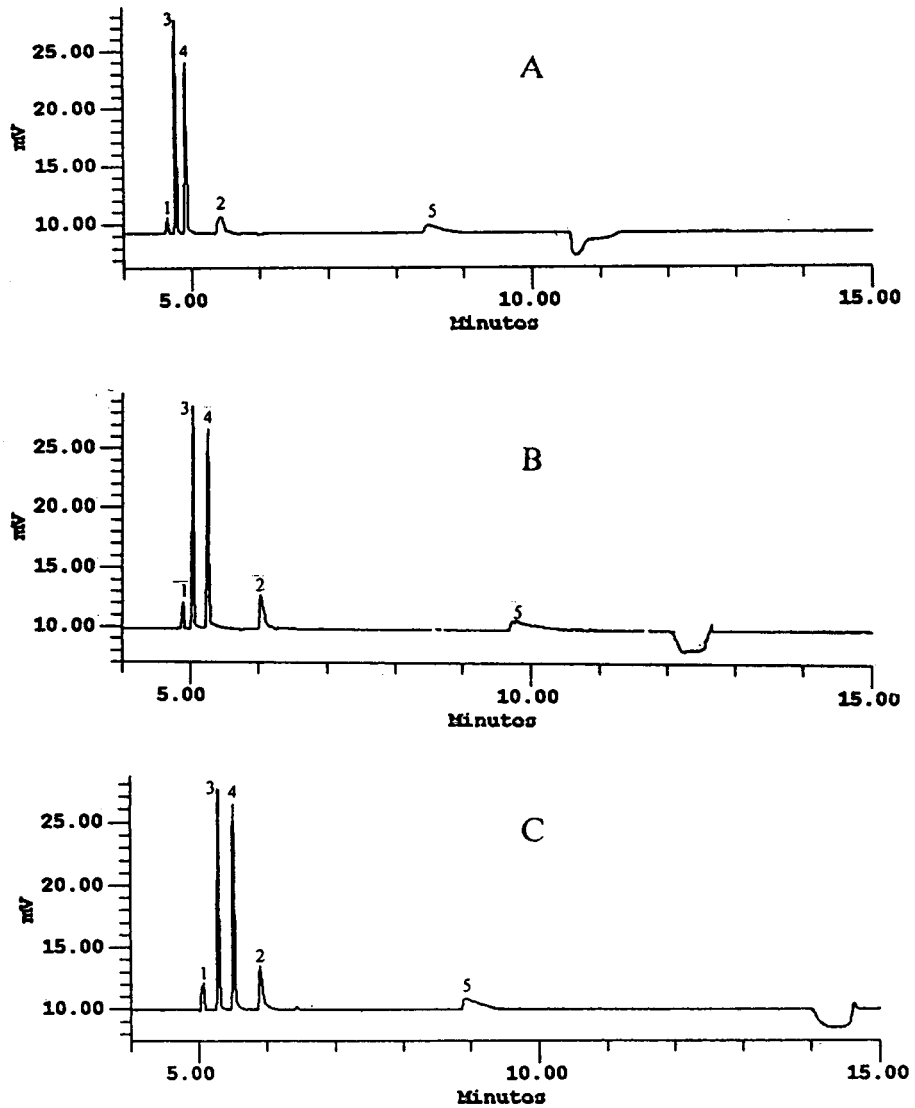

Fig. 5.

with 100 m*M* sodium chloride in the sample. This was because the peak height and width of anions depended on the ratio of sodium chloride concentration between the carrier electrolyte solution and the sample. Although the sodium chloride concentration in the sample was very high, its concentration in the carrier electrolyte solution was limited by Joule heating, so capillary electrophoresis of anions in samples with sodium chloride concentrations higher than 100 m*M* still remained a problem. It should be noted that high concentrations of sodium chloride in samples did not cause serious Joule heating problems in electrophoresis, which was concluded to be due to the slight current change cause by the high-concentration sodium chloride in the sample.

The detection limit was defined as the detectable concentration of an anion when the anion give a peak twice as high as the noise (N). For a

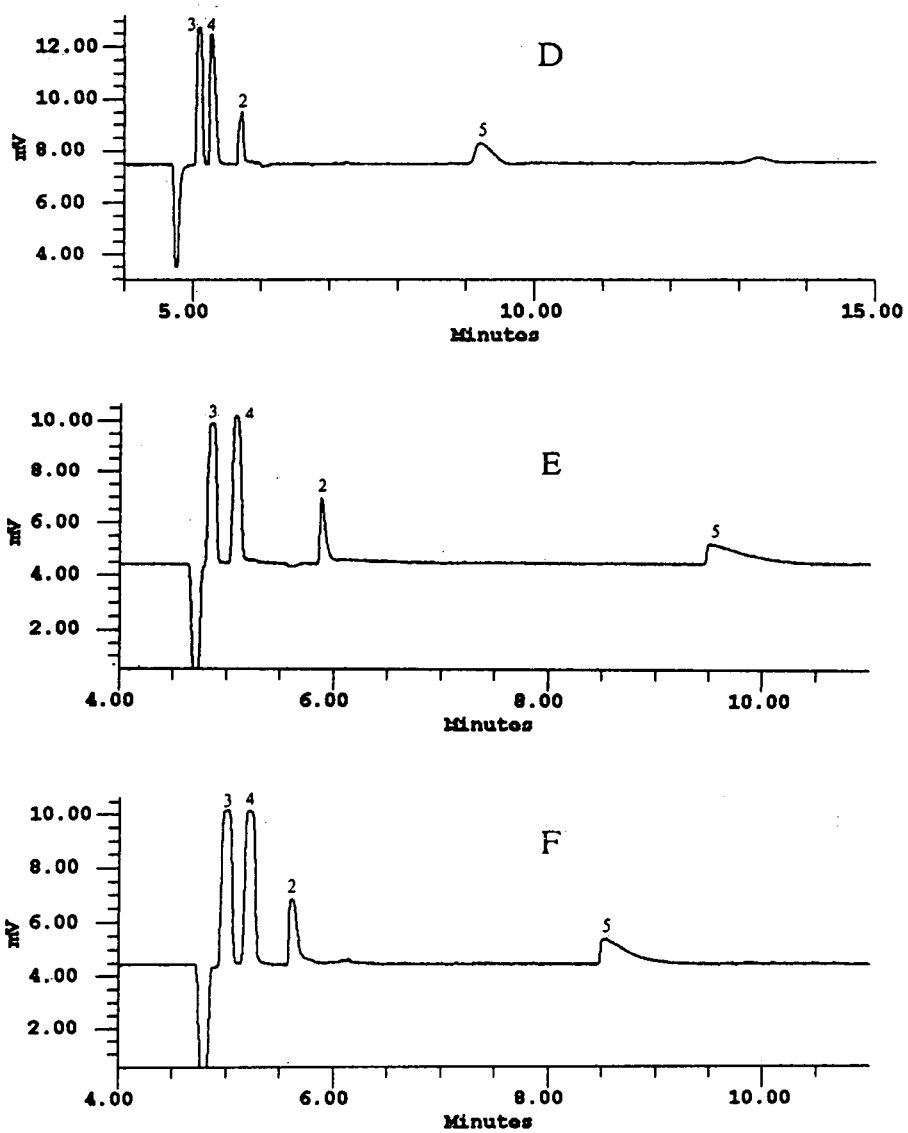

Fig. 5. Capillary electrophoretic separation of anions by using sodium chloride with 2.0 m*M* TTAB as carrier electrolyte solution. Ratio of sodium chloride concentration (m*M*) between the carrier electrolyte solution and sample: (A) 25:0; (B) 50:0; (C) 100:0; (D) 25:12.5; (E) 50:50; (F) 100:100. Peaks: 1 = bromide; 2 = iodide; 3 = nitrite; 4 = nitrate; 5 = thiocyanate. The concentration of each anion in the sample was 10 ppm.

defined change of anion concentration, its corresponding change in peak height was calculated from the slope (*SL*) of the calibration graph for the anion between peak height and anion concentration from 1 to 40 ppm. The detection limit of each anion was calculated as $2N/SL$ ($N = 55$ μV) and results are given in Table 1 under different conditions. It was observed that when there was no sodium chloride in the sample, the detection limit had an obvious tendency to decrease slightly when the concentration of sodium chloride in the carrier electrolyte solution from 25 to 100 m*M* (there was one exception). However, when the concentration of sodium

Table 1
Detection limit of each anion under different conditions

Concentration of NaCl in carrier electrolyte solution (m*M*)	Concentration of NaCl in sample (m*M*)	Detection limit (ppb)				
		Bromide	Nitrite	Nitrate	Iodide	Thiocyanate
25	0	1724	130	148	1742	3644
50	0	1048	120	130	728	–[a]
100	0	1036	120	138	648	2982
25	12.5	–[b]	418	420	–[c]	–[c]
50	50	–[b]	420	390	–[c]	–[c]
100	100	–[b]	380	378	–[c]	–[c]

[a] Not measured.
[b] Not separated.
[c] Peaks showed strong tailing and the calibration graph between peak height and anion concentration was not linear.

chloride in carrier electrolyte solution was constant at 25, 50 or 100 m*M*, the detection limit increased with increasing concentration of sodium chloride in the sample.

The separation efficiency was described by the number of theoretical plates, n, which is calculated from $n = 5.54(RT/WI)^2$, where RT is the migration time and WI is the peak width at half-height. Theoretical plate numbers of bromide, nitrite and nitrate under different conditions were calculated and are given in Table 2. Theoretical plate numbers for iodide and thiocyanate are not given because their peaks showed strong tailing. Each value of theoretical plate number in Table 2 is the average of five values obtained with five mixed anion solutions (1, 4, 10, 20 and 40 ppm) used to evaluate the calibration graphs, except the values with a superscript b, which are averages of five values obtained with five mixed anion solutions prepared for the purpose of peak identification in the electrophorograms as described under Experimental. It was observed from Table 2 that when the concentration of sodium chloride in the carrier electrolyte solution remained constant, an increased concentration of sodium chloride in sample resulted in a decreased theoretical plate number. When the concentration of sodium chloride in the sample remained at 12.5 m*M*, an increased concentration of sodium chloride in carrier electrolyte solution caused an increased theoretical plate number. However, when there

Table 2
Effect of concentration of sodium chloride in carrier electrolyte solution and sample on separation efficiency

Concentration of NaCl in buffer (m*M*)	Concentration of NaCl in sample (m*M*)	Theoretical plate number $\times 10^4$		
		Bromide	Nitrite	Nitrate
25	0	22.27	20.60	15.50
	12.5	–[a]	1.99	2.05
50	0	24.34	18.20	13.85
	12.5	–[a]	5.78[b]	6.10[b]
	50	–[a]	2.14	2.34
100	0	17.61	17.79	16.56
	12.5	–[a]	13.60[b]	11.24[b]
	100	–[a]	1.64	1.70

[a] Peak not separated.
[b] See text.

was no sodium chloride in the sample, an increased concentration of sodium chloride in the carrier electrolyte solution sometimes caused a decreased theoretical plate number, which may be attributed to increased Joule heating.

The reason why different concentrations of salts in the samples caused different detection limits and separation efficiencies of an anion can be explained by the principle of electrostacking [17] as follows. Electrostacking occurs when the injected sample has a lower ionic strength than the carrier electrolyte solution. In this experiment, the sample and the carrier electrolyte solution contained the same salt (sodium chloride), so the length of the sample zone after electrostacking can be calculated by [17]

$$l_{ib} = l_{is} C_s / C_b \quad (1)$$

where C_b and C_s are the concentration of sodium chloride in the carrier electrolyte solution (background) and sample, respectively, and l_{ib} and l_{is} are the zone length of the sample ion in the carrier electrolyte solution and sample, respectively. Eq. 1 shows that the zone length of a sample ion in the carrier electrolyte solution is inversely proportional to the ratio of the sodium chloride concentrations in the carrier electrolyte solution and sample, and the peak width is also inversely proportional to this ratio whereas the peak height is proportional to this ratio. According to the definitions of separation efficiency and detection limit used above, different peak widths and peak heights resulted in different separation efficiencies and different detection limits, respectively. It had been considered theoretically that when l_{is} was small enough that the variance of a sample zone was controlled only by molecular diffusion, as described by Jorgenson and Lukacs [18], then the separated peak would have the same height and width regardless of the value of C_b/C_s and electrostacking. However, the experimental results showed that this is difficult and the injection plug length made a contribution to the variance of a sample zone. In this experiment, l_{is} was constant and calculated to be 3.3 mm, but l_{ib} decreased with decreasing C_s/C_b. As shown in Table 2, when C_s/C_b decreased from 100:100 through 12.5:100 to 0:100 and l_{ib} decreased from 3.3 through 0.41 to 0 mm (0 mm is a theoretical value; in practice l_{ib} would be affected by other factors and be greater than 0 mm), the separation efficiency increased from 16 400 through 136 000 to 177 900. That meant that even when the injection plug length was very small (theoretically 0 mm), it still contributed to the variance of a sample zone.

When determinating anions in subterranean water, it is reasonable to choose 100 m*M* sodium chloride as the carrier electrolyte because it gave the lowest detection limit and could match samples with higher concentrations of sodium chloride. As different concentrations of sodium chloride in subterranean water could cause different peak heights with a constant concentration of an anion, the simplest approach to achieve accurate quantification was to use the standard addition technique. In this technique, a constant volume of a sample was added to a set of standard anion solutions separately and then diluted to the same volume for the purpose of quantification, so the ionic strengths of these solutions were the same and controlled by the sample. Therefore, although electrostacking has been proposed to be used as an on-column preconcentration technique [10,17,19–23], it caused quantification difficulties when a sample contained high concentrations of salts.

3.3. Reproducibility of migration time, peak height and peak area

The 10 ppm mixed anion standard solution was separated by using 10 m*M* sodium sulfate with 0.5 m*M* TTAB as the carrier electrolyte solution. The reproducibilities of migration time, peak height and peak area after five successive injections are given in Table 3.

With different concentrations of sodium chloride in the carrier electrolyte solution and sample, the reproducibilities of the migration times were calculated using five mixed anion solutions as used to evaluate the calibration graphs as described under Experimental and are given in Table 4. When an R.S.D. value in Table 4 is not marked with a superscript, it was calculated from

Table 3
Reproducibility of migration time, peak height and peak area after five successive injections

Anion	R.S.D. (%)		
	Migration time	Peak height	Peak area
Bromide	1.49	2.02	11.02
Nitrite	1.51	0.82	2.15
Nitrate	1.49	0.72	1.98
Iodide	1.52	2.40	6.49
Thiocyanate	1.78	2.16	8.03

five migration times, when it has a superscript c, it was calculated from four migration times, and when it has a superscript d, it was calculated from three migration times. Because of detection limit limitations, iodide and thiocyanate were not detected at low concentrations. It was observed from Tables 3 and 4 that the reproducibility of the migration times of all peaks was not very good. When the migration times of anions were close to each other, it was difficult to identify a peak only from the migration time when a real sample was separated. Therefore, peak identification was supplemented by analysing five anion mixture solutions containing 10 ppm of each anion with additional individual anions as described under Experimental.

When the concentration of sodium chloride in sample was 12.5 m*M*, the reproducibilities of peak height and peak area at different concentrations of sodium chloride in the carrier electrolyte solution were calculated from five values obtained with five mixed anion solutions used for the identification of each peak in electrophorograms under the same conditions, and are given in Table 5. The RSDs in Table 5 are

Table 4
Reproducibility of migration time with different concentrations of sodium chloride in the carrier electrolyte solution and sample

Concentration of NaCl in carrier electrolyte solution (m*M*)	Concentration of NaCl in sample (m*M*)	R.S.D. (%)				
		Bromide	Nitrite	Nitrate	Iodide	Thiocyanate
25	0	2.81	2.73	3.14	2.40[c]	2.15[c]
50	0	1.36	1.40	1.57	1.85[c]	–[a]
100	0	1.82	2.07	1.97	2.45[c]	3.16[c]
25	12.5	–[b]	1.65	2.93	1.50[d]	2.36[c]
50	50	–[b]	0.22	0.05	0.63[d]	1.81[c]
100	100	–[b]	0.51	0.79	0.19[d]	0.98[c]

[a] Not measured.
[b] Peak not separated.
[c] See text.
[d] See text.

Table 5
Reproducibility of peak height and peak area with a concentration of sodium chloride in the sample of 12.5 m*M*

Basis	Concentration of NaCl in carrier electrolyte solution (m*M*)	R.S.D. (%)			
		Nitrite	Nitrate	Iodide	Thiocyanate
Peak height	25	8.60	8.26	14.51	15.41
	50	6.71	6.04	9.89	17.13
	100	3.40	5.88	14.07	18.95
Peak area	25	5.68	3.50	15.03	23.93
	50	3.91	3.00	8.10	7.85
	100	5.94	5.93	6.27	9.39

not very good; the R.S.D.s for iodide and thiocyanate are higher than those for nitrite and nitrate, which is attributed to peak tailing.

Comparing Table 3 with Tables 4 and 5, it was found that the reproducibility of migration times in Table 3 was better than that in Table 4 in most instances, and the reproducibility of peak height and peak area in Table 3 was better than that in Table 5. It should be noted that more factors affect the reproducibility in Tables 4 and 5 than in Table 3, but the reproducibility in Tables 4 and 5 approached more closely the situation of quantification.

From the R.S.D.s of migration time, peak height and peak area shown in Tables 3–5, it is seen that the separation conditions studied in this work were not satisfactory for the determination of anions in subterranean water. An improved separation for the determination of anions in subterranean water has now been accomplished, and will be published in the near future.

4. Conclusions

The selection of a carrier electrolyte co-ion with an electrophoretic mobility close to those of anions in the sample is necessary in CIE, not only when using indirect UV detection but also when using direct UV detection.

An unsuitable anion form of the electroosmotic modifier would cause negative peaks on the separation baselines when samples contain high concentrations of salts, and the separation could be adversely affected.

Although electrostacking has been proposed as an on-column preconcentration technique in the CIE determination of anions, it caused quantification difficulties when the sample contained high concentrations of salts. An increased concentration ratio of sodium chloride between the sample and carrier electrolyte solution resulted in lower and wider peaks of detected anions, and correspondingly higher detection limits and a lower separation efficiency for the anion.

From the R.S.D.s of migration time, peak height and peak area shown in Tables 3–5, it is concluded that the separation conditions studied in this work were not satisfactory for the determination of anions in subterranean water.

Acknowledgement

This work was financially supported by Chinese Academy of Sciences.

References

[1] W.R. Jones and P. Jandik, *Am. Lab.*, 22 (1990) 51.
[2] W.R. Jones, P. Jandik and R. Pfeifer, *Am. Lab.*, 23 (1991) 40.
[3] P. Jandik, W.R. Jones, A. Weston and P.R. Brown, *LC · GC*, 9 (1991) 634.
[4] P. Jandik and W.R. Jones, *J. Chromatogr.*, 546 (1991) 431.
[5] J. Romano, P. Jandik, W.R. Jones and P.E. Jackson, *J. Chromatogr.*, 546 (1991) 411.
[6] W.R. Jones, *J. Chromatogr.*, 640 (1993) 387.
[7] M.P. Harrold, M.J. Wojtusik, J. Riviello and P. Henson, *J. Chromatogr.*, 640 (1993) 463.
[8] W. Buchberger and P.R. Haddad, *J. Chromatogr.*, 608 (1992) 59.
[9] W.R. Jones and P. Jandik, *J. Chromatogr.*, 608 (1992) 385.
[10] P.E. Jackson and P.R. Haddad, *J. Chromatogr.*, 640 (1993) 481.
[11] W.R. Jones, P. Jandik and M. Merion, *US Pat.*, 5 104 506 (1992).
[12] F.E.P. Mikkers, F.M. Evearerts and Th.P.E.M. Verheggen, *J. Chromatogr.*, 169 (1979) 1.
[13] F.E.P. Mikkers, F.M. Everaerts and Th.P.E.M. Verheggen, *J. Chromatogr.*, 169 (1979) 11.
[14] F. Foret, S. Fanali and L. Ossicini, *J. Chromatogr.*, 470 (1989) 299.
[15] B.F. Kenney, *J. Chromatogr.*, 546 (1991) 423.
[16] W.R. Jones and P. Jandik, *J. Chromatogr.*, 546 (1991) 445.
[17] D.S. Burgi and R.L. Chien, *Anal. Chem.*, 63 (1991) 2042.
[18] J.W. Jorgenson and K.D. Lukacs, *Anal. Chem.*, 53 (1981) 1298.
[19] D.S. Burgi and R.L. Chien, *J. Microcol. Sep.*, 3 (1991) 199.
[20] D.S. Burgi and R.L. Chien, *Anal. Biochem.*, 202 (1992) 306.
[21] A. Vinther, H. Soeberg, L. Nielsen, J. Petersen and K. Biedermann, *Anal. Chem.*, 64 (1992) 187.
[22] R.L. Chien and D.S. Burgi, *Anal. Chem.*, 64 (1992) 1046.
[23] D.S. Burgi, *Anal. Chem.*, 65 (1993) 3726.

ELSEVIER

Journal of Chromatography A, 696 (1995) 321–332

JOURNAL OF CHROMATOGRAPHY A

Application of capillary zone electrophoresis with an isotachophoretic initial state to determine anionic impurities on as-polished silicon wafer surfaces

J. Boden[a], K. Bächmann[a,*], L. Kotz[b], L. Fabry[b], S. Pahlke[b]

[a]*Fachbereich Chemie der Technischen Hochschule Darmstadt, D-64289 Darmstadt, Germany*

[b]*Wacker-Chemitronic GmbH, D-84489 Burghausen, Germany*

First received 17 August 1994; revised manuscript received 1 December 1994; accepted 14 December 1994

Abstract

Mobile inorganic anions such as chloride, sulfate and nitrate were determined up to an analyte-to-matrix-ratio (ATMR) of $1:10^4$ using capillary zone electrophoresis. On adjusting the mobility and the concentration of the co-ion of the electrolyte to an isotachophoretic initial state, the detection limit of the analytes was improved by a factor of 2 by increasing the plate numbers through the isotachophoretic state. The ATMR could be increased to $1:6 \cdot 10^4$. These optimized conditions were applied to the determination of anionogenic impurities on experimental silicon wafer surfaces ($d = 150$ mm) after dissolution of the native oxide of silicon in isothermally distilled hydrofluoric acid vapour down to the range of 10^9 anions/cm^2. The mobile organic anion oxalate was identified on silicon wafer surfaces for the first time.

1. Introduction

Metal impurities have a detrimental impact both on the fabrication yield and on the reliability of integrated circuit devices [1]. After decades of scientific investigations, device makers have gained a detailed knowledge of metallic contamination and have developed adequate analytical tools [2,3] and preventive techniques against yield losses due to metallic contamination. However, less is known about the effects of anions [4–6], owing to the lack of sufficient trace analytical methods. Recently, the advancement of capillary zone electrophoresis (CZE) has facilitated its applications to anion trace determinations in the semiconductor industry [7,8].

The determination of small anions in the presence of a matrix ion is a demanding task, because peak broadening of the analyte peaks takes place and preconcentration by electrokinetic injection or sample stacking is not applicable. A possibility for preconcentrating analyte ions in the presence of an inorganic matrix ion is to use a combination of isotachophoresis (ITP) and CZE using a coupling of two capillaries [9–14] or employing ITP and CZE on-line in the same capillary [13–17].

Theoretically, by adjusting the electrolyte composition and the sample amount to realize ITP conditions at the beginning of the CZE run,

* Corresponding author.

0021-9673/95/$09.50
SSDI 0021-9673(94)01227-X

a stacking process of the analytes occurs [18] and the matrix issue can be resolved. Thus, the matrix anion must act as either the leading or the terminating species of the CZE separation. At the end of ITP, the analytes with mobilities between those of the matrix ion and the electrolyte co-ion will have been preconcentrated by the ITP. If the analyte mobilities do not lie within that limited range, peak broadening must be expected. Reaching a uniform field strength along the capillary by electromigrative dispersion of the matrix ion, ITP is not longer sustainable. Comparing this method with the conventional ITP technique, we can emphasize a remarkable feature: the leading or terminating electrolyte arises from the matrix ion of the sample and that zone must be formed by a moving boundary mechanism first.

In this paper, we report on applications of CZE to the determination of traces of anions on as-polished silicon wafer surfaces. The method is a combination of microdissolution enrichment, based on the reaction of hydrofluoric acid vapour with the native oxide of silicon [19–21], and CZE with an ITP initial state.

2. Experimental

2.1. CZE system

We used a laboratory-made CZE system. The separations were carried out with conventional untreated fused-silica capillaries (50 and 75 μm I.D.) from CS-Chromatographie Service (Langerwehe, Germany). The capillary was suited with direct insertion for a type ABI 785A programmable absorbance detector (Applied Biosystems, Weiterstadt, Germany) of variable wavelength capability. The outlets were placed in two vials each containing 10 ml of electrolyte. The high voltage from a 30 kV power supply (F.u.G. Electronic, Rosenheim, Germany) was applied with Pt–Ir electrodes dipping into the electrolyte. The positive electrode was placed in the outlet vessel. Data were processed by an A/D board from ERC (Alteglofsheim, Germany) using APEX chromatography software (Autochrom, Milford, MA, USA). The absorbance units of the detector were transformed by the A/D board into μV, hence the output of the data was in the voltage mode.

2.2. Chemicals

All solutions, electrolytes and standards were prepared with ultra-pure water from a Milli-Q system (Millipore, Eschborn, Germany). For microdissolution, hydrofluoric acid (50%, S-ULSI Puranal) from Riedel-de Häen (Seelze, Germany) was applied. All other reagents were of analytical-reagent grade from Merck (Darmstadt, Germany).

Tetradecyltrimethylammonium hydroxide (TTAOH) was prepared from tetradecyltrimethylammonium bromide (TTAB), as described previously [22], using IRA-904 Amberlite anion-exchange resin (Serva, Heidelberg, Germany).

2.3. Sample preparation

All samples were prepared under clean-bench conditions (Class 1 by Federal Standard 209 C, VDI-2083) in poly(vinylidene fluoride) (PVDF) chambers. The dissolution enrichment technique applied has been described [19–21]. The hydrophobic HF-etched surface of as-polished and cleaned wafers (d = 150 mm) was scanned with a droplet of ultra-pure water (100 μl) to collect the dissolved contaminants. The water droplet was transferred with an Eppendorf (Hamburg, Germany) pipette into a freshly cleaned 250-μl Eppendorf vial. Recovery rates were investigated for bromide and sulfate after preparation runs.

3. Results and discussion

3.1. CZE determination of small inorganic anions in hydrofluoric acid matrix

In order to achieve a symmetrical peak shape in CZE with indirect UV detection, an electrolyte with a high molar absorptivity should be

Table 1
Mobilities of some analyte ions and electrolyte co-ions [24]

Parameter	Electrolyte					
	Chromate		Molybdate		Phthalate	Salicylate
$\mu[(cm^2/V \cdot s) \cdot 10^{-4}]$	8.1		7.4		5.5	3.7
	Analyte					
	Bromide	Chloride	Sulfate	Nitrate	Chlorate	Fluoride
$\mu_{lit}[(cm^2/V \cdot s) \cdot 10^{-4}]$	8.1	7.9	8.3	7.4	6.7	5.7
μ_{eff}[a] $[(cm^2/V \cdot s) \cdot 10^{-4}]$	8.0	7.7	7.6	7.4	6.5	5.3

[a] The effective mobilities μ_{eff} were calculated from an electropherogram without a matrix ion, using molybdate as co-ion (for conditions, see Fig. 1).

applied and the mobility of its co-ion must closely match the mobilities of the analyte ions [23]. For analytes such as chloride, sulfate and nitrate, molybdate was found to have an appropriate mobility (Table 1, Fig. 1). Because of the low wavelength of the absorbance maximum of molybdate (211 nm), nitrate was detected directly owing to its higher absorbance at this wavelength. For all other ions the indirect detection mode obtained.

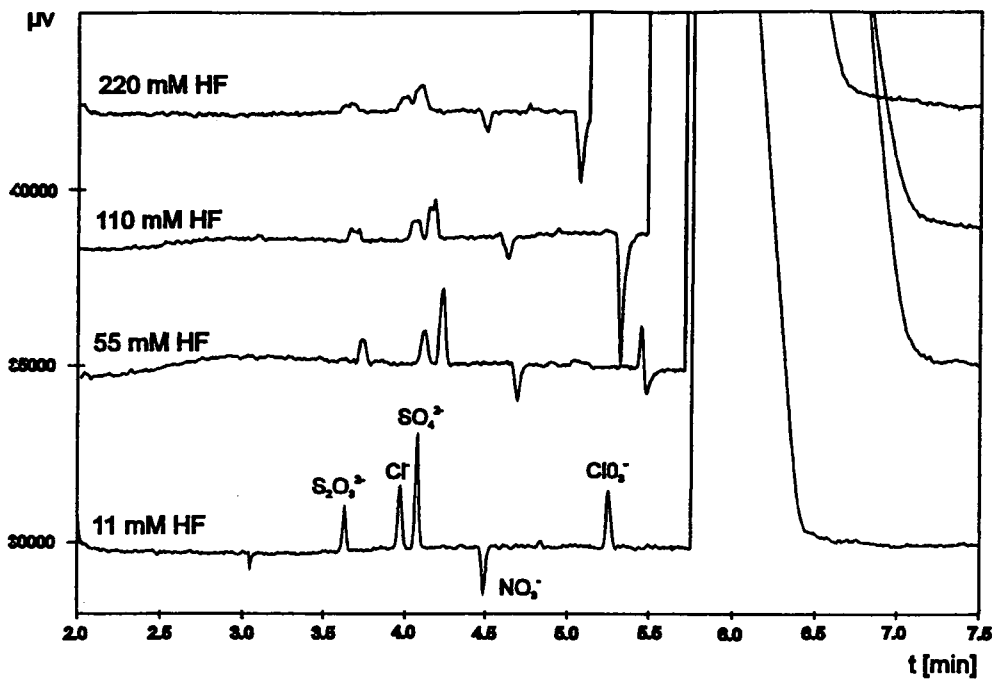

Fig. 1. Influence of HF on the peak heights using molybdate as electrolyte. Electrolyte, 5 mM sodium molybdate (pH 6.7); analytes, each 20 μM; capillary, fused silica, 60 cm to the detector, 76 cm total length, 75 μm I.D.; detection, for nitrate direct UV, for all other anions indirect UV at 211 nm; injection, hydrostatic (10 cm, 30 s); EOF, in opposite direction to the anions, $v_{EOF} = 2.7$ cm/min.

The effect of the hydrofluoric acid matrix can be characterized by the peak heights because characterization by plate number or peak area is valid only for Gaussian peaks. Obviously, the peak heights of chloride and sulfate decreased with increasing hydrofluoric acid concentration. Under the described CZE conditions, the analytes of interest can be determined up to an analyte-to-matrix ratio (ATMR) of $1:10^4$.

We investigated the effects of both the capillary I.D. and the electrolyte concentration in order to optimize the CZE conditions. Initially, we compared the separation with a capillary of 75 μm I.D. with that of a capillary of 50 μm I.D. (Fig. 2). As expected, the smaller cross-section of the latter capillary facilitated a better resolution. This is due, on the one hand, to the fact that the resolution is improved with decreasing $(dE)^2$, where d is the diameter and E the field strength, by reduced thermal zone deformation [25]. On the other hand, it is due to the decrease in sample volume (hydrostatic injection, 10 cm, 30 s) because the smaller sample volume prevented overloading of the capillary. A further analysis with a longer injection time in order to achieve a comparable injected amount using the 50 μm I.D. capillary led to the same result (not shown). Therefore, the limitation of the thermal diffusion is the main reason for the better resolution. The electroosmotic flow (EOF) is similar in both capillaries, which leads to comparable migration of the analytes in both capillaries. However, the selected I.D. must be a subtle compromise between electrophoretic resolution and detectability.

Increasing the electrolyte concentration provides additional chemical system capacity. Fig. 3 shows the influence of the electrolyte concentration on the peak heights using a 50 μm I.D. capillary. As expected, additional electrolyte

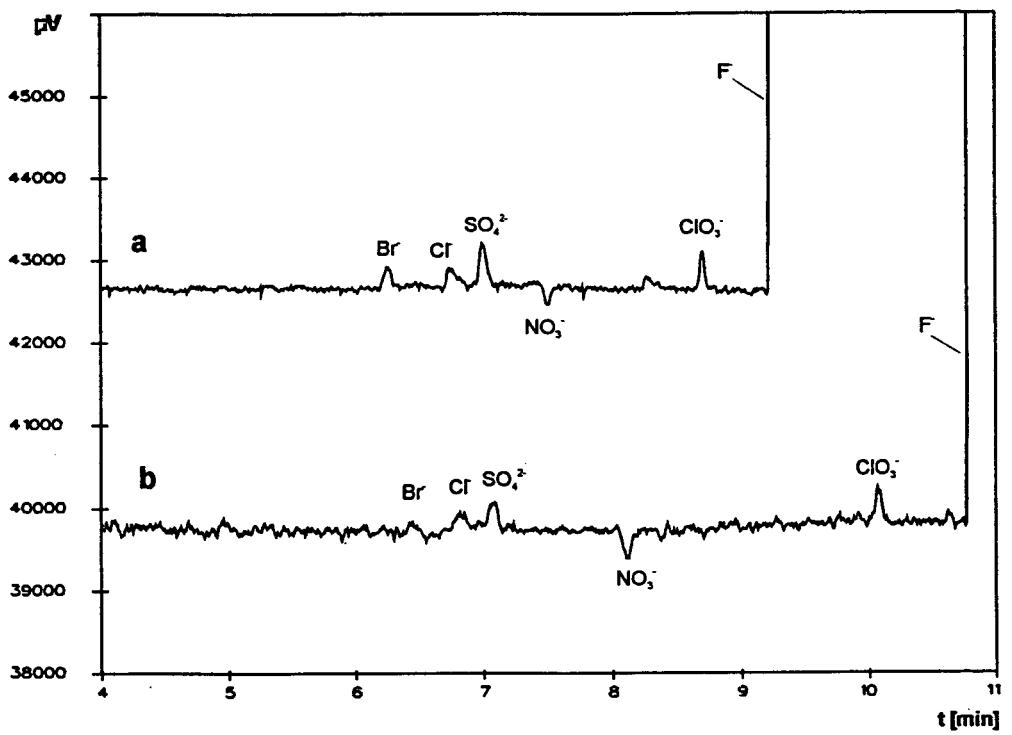

Fig. 2. Influence of the capillary I.D. (a) 50 μm I.D.; (b) 75 μm I.D. Electrolyte, 5 mM sodium molybdate; analytes, each 25 μM, HF 420 mM; capillary, fused silica, 70 cm to the detector, 86 cm total length; detection and injection, as in Fig. 1; EOF, in opposite direction to the anions, (a) $v_{EOF} = 4.5$ cm/min, (b) $v_{EOF} = 5.3$ cm/min.

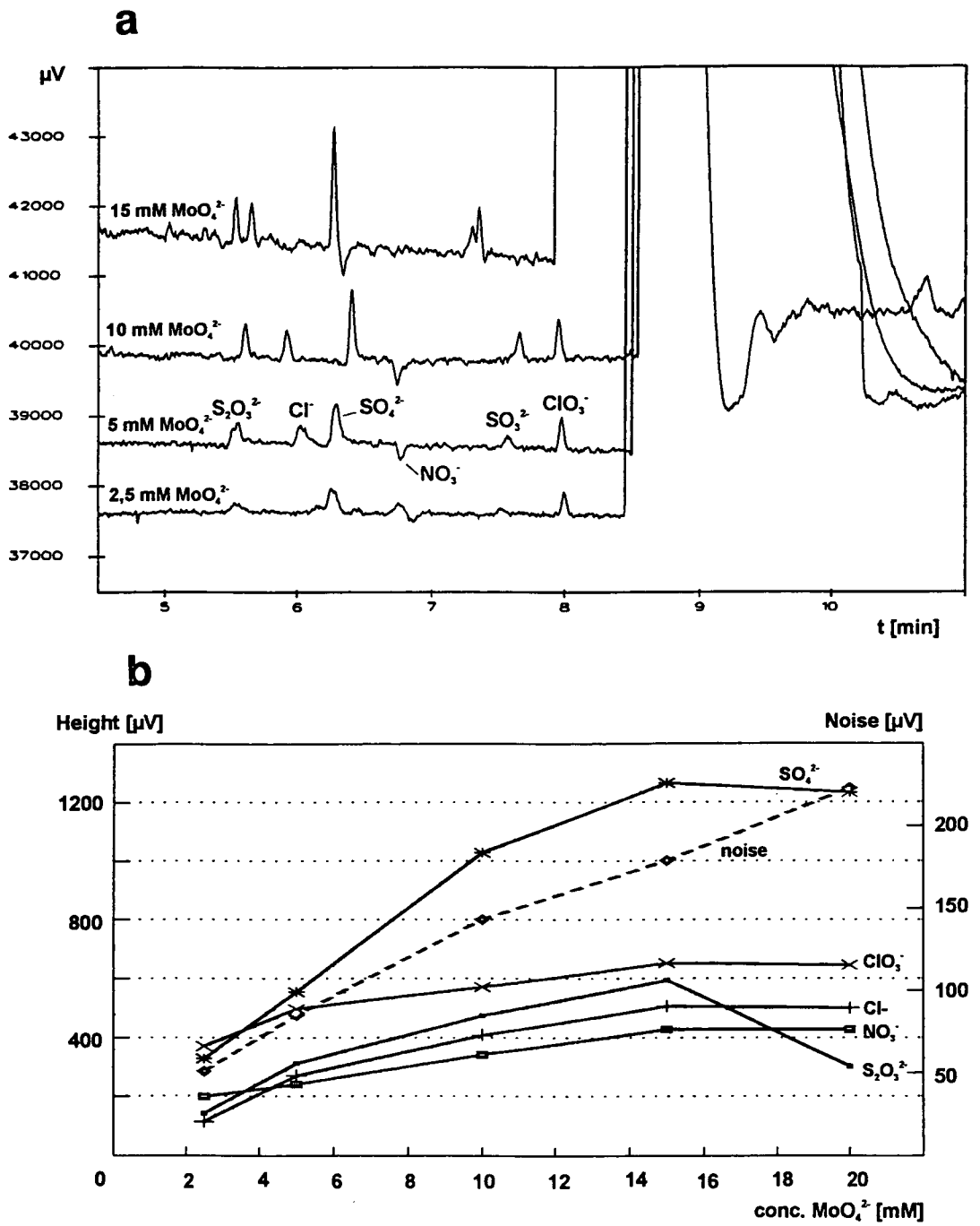

Fig. 3. Influence of the electrolyte concentration on the peak heights and on the baseline noise. (a) Electropherograms; (b) peak height and baseline noise vs. molybdate concentration. Electrolyte, different concentrations of sodium molybdate; analytes, each 25 μM, HF 420 mM; capillary, as in Fig. 2a; detection and injection, as in Fig. 1; EOF, in opposite direction to the anions, for all electrolyte concentrations nearly constant, $v_{EOF} = 3.4$ cm/min.

enlarged the peaks and increased the plate numbers. Using 10 m*M* molybdate electrolyte, the ATMR was calculated to be $1:4 \cdot 10^4$. Simultaneously, the increased baseline noise as a result of the increasing baseline signal (Fig. 3b) limited the linear response range of indirect detection. We found the optimum molybdate concentration to be within the range 8–12 m*M*. Theoretically, for direct UV detection the electrolyte concentration can be higher and is limited only by the current increase and the Joule heating.

Additionally, it can be recognized that the thiosulfate, sulfate and sulfite analyte ions migrate more slowly than the other ions when the molybdate concentration is raised. The reason is a shift in the solvation equilibrium [26,27] in the presence of an increasing counter ion (Na) concentration.

In Figs. 1–3 it was shown that by the optimization of the normal CZE run (concentration, capillary), the maximum ATMR can be increased by a factor of 4. These figures demonstrated both the capacity and the limits of CZE in the presence of a matrix ion. For many applications, an ATMR of $1:4 \cdot 10^4$ for fluoride is sufficient, but for further improvement a different approach is necessary, e.g., by using a combination of ITP and CZE.

3.2. *Determination of small inorganic anions with an ITP initial state*

During the initial stages of the separation, analyte ions can be preconcentrated in the ITP state, provided that the mobilities of the analyte ions lie between the mobilities of the electrolyte co-ion and the matrix ion. In our case, the electrolyte co-ion must have a higher mobility than the slowly migrating fluoride matrix ion and than the analyte ions to be suitable as the leading ion. On corresponding mobility data terms, chromate [28] was chosen as a leading ion (Table 1).

Because of the high pH of aqueous potassium chromate solution (7.9), the EOF is high in the direction opposite to that of the migration of the anions, thereby extending the analysis time unnecessarily. Therefore, the EOF modifier TTAOH was added to the solution to reverse the EOF. TTAOH was chosen because the common modifier TTAB produces a system peak at the migration time of bromide [22].

In contrast to the findings with molybdate as electrolyte, the peak heights of chloride, sulfate and nitrate analytes increased with increasing fluoride concentration when the chromate electrolyte was applied (Fig. 4). Having a mobility similar to that of chromate, bromide was not preconcentrated by ITP and, therefore, the peak height of bromide decreased.

From the results in Fig. 4, we estimated an improved ATMR of $1:4 \cdot 10^4$ for nitrate and of $1:6 \cdot 10^4$ for chloride and sulfate. The limit of detection (defined as twice the noise in concentration units) was found to be 3 μM for sulfate and 5 μM for chloride and nitrate (2σ) under initial ITP conditions.

Further improvement of the ATMR was limited by the worsening resolution of the analyte ions due to the increased fluoride concentration. An explanation for this effect is the prolongation of the electrodispersive depletion of the matrix ion with increased concentration of the matrix. Therefore, chromate ions need a longer time to migrate forwards through the matrix and the analyte zones, thereby starting the CZE mode. With on-line ITP–CZE coupling this leads to an increased influence of the ITP state and hence to a poorer resolution in the electropherogram. Furthermore, the analyte ions are covered one by one by the broadening of the fluoride peak. This effect can be reduced by the use of a longer capillary, but then a compromise between separation and analysis time must be found.

Under the optimized conditions, we determined the blank value of hydrofluoric acid, and so a chloride signal was detected. To determine the expected chloride contamination, the standard additions method was applied using the conditions given in Fig. 4. The regression coefficient of the calibration line of the peak area of chloride was calculated to be $r = 0.998$. Thus, we found 15 μM of chloride in 560 m*M* of hydrofluoric acid, i.e., 0.6 m*M* in the hydrofluoric acid (40%).

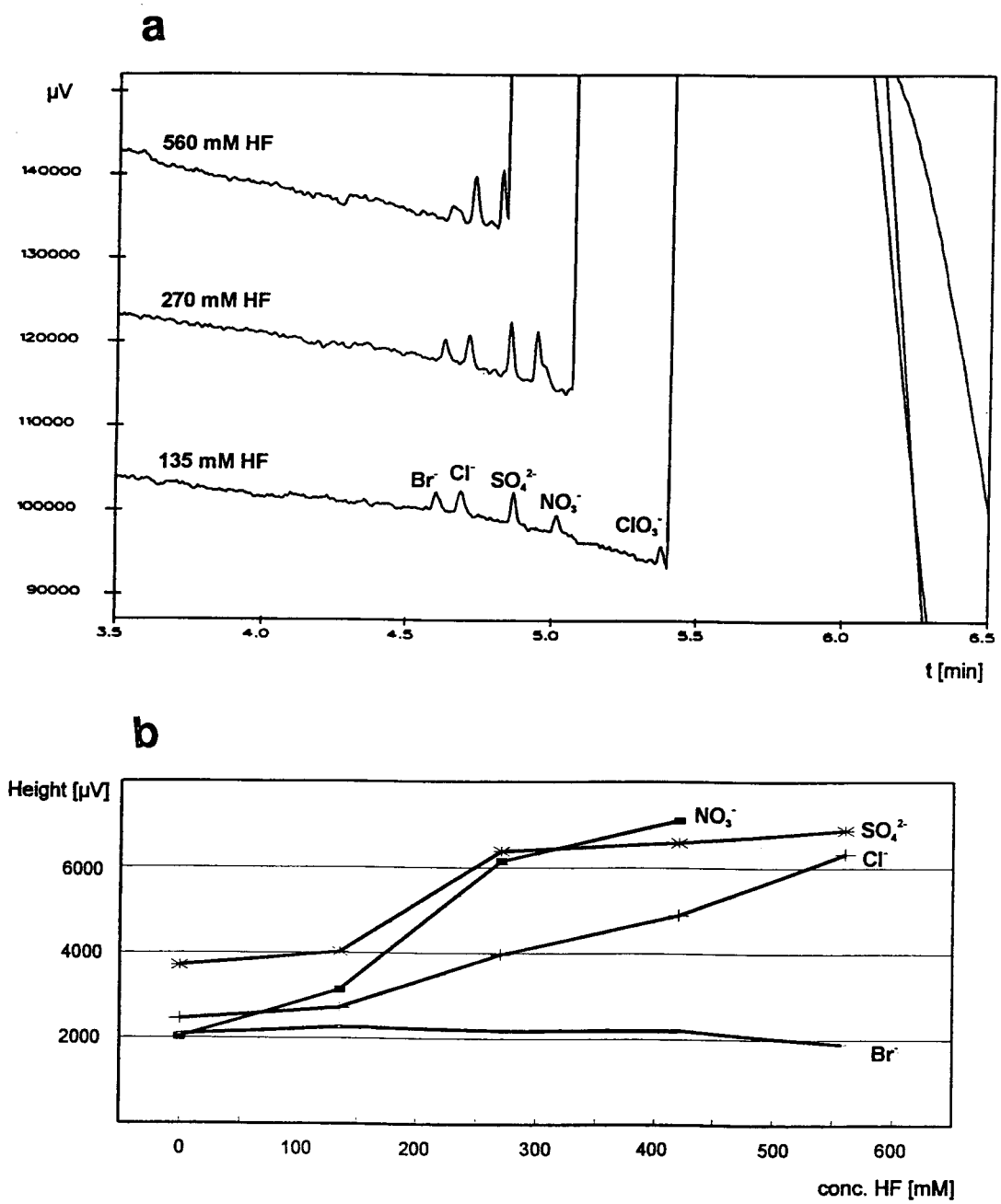

Fig. 4. Influence of HF on the peak heights using chromate as electrolyte. (a) Electropherograms; (b) peak height vs. concentration of HF. Electrolyte, 7.5 m*M* potassium chromate–0.2 m*M* TTAOH (pH 8.5); analytes, each 25 μM; capillary, 70 cm to the detector, 86 cm total length, 50 μm I.D.; detection, indirect UV at 254 nm; injection, hydrostatic (10 cm, 30 s); EOF, in the same direction as the anions, $v_{EOF} = 1.1$ cm/min.

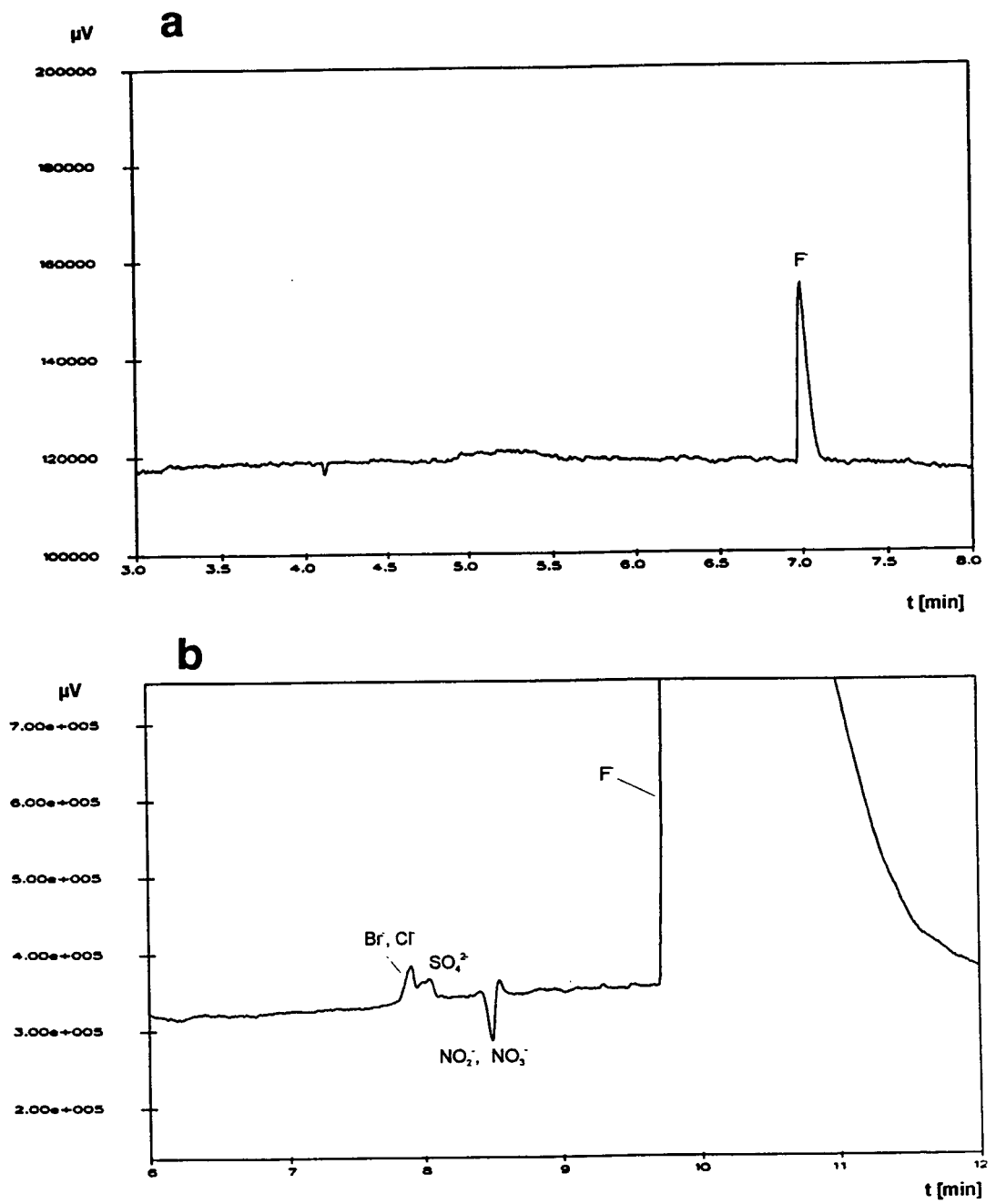

Fig. 5. Determination of anionic impurities on a silicon wafer (a) Hydrostatic injection (conditions as in Fig. 1); sample, 100-μl water droplet from repeated scanning of the wafer surface. (b) Sample stacking using molybdate electrolyte. Electrolyte, 7 mM sodium molybdate (pH 6.7); sample, as in (a); Injection (to prevent contamination of the sample droplet, the capillary was dipped into deionized water before it was transferred into the sample vial), hydrodynamic up to the detector (2.6 μl); all other conditions as in Fig. 1. (c) Sample stacking using chromate electrolyte. Electrolyte, 6 mM potassium chromate – 0.07 mM TTAOH (pH 8.1); capillary, as in Fig. 1; detection, as in Fig. 4; sample, as in (a); injection, as in (b); EOF, in opposite direction to the anions, $v_{EOF} = 2.1$ cm/min.

3.3. Analysis of low anionic contamination on as-polished silicon wafers

Only fluoride was detected under the hydrostatic CZE conditions (Fig. 5a) with a water droplet sample obtained by the applied microdissolution technique [19–21]. In order to decrease the detection limit, the sample had to be enriched by electrokinetic injection or by sample stacking [29]. We preferred sample stacking because analyte discrimination does not take place and peak correction is not necessary. The sample stacking was performed by filling the capillary with the sample up to the detector, resulting in a sample volume of 2.6 μl. After applying a high voltage, the analyte ions migrate rapidly towards the boundary between the sample and electrolyte. Simultaneously, the reverse-directed EOF removes the stacked cations and the water plug from the capillary. When the water plug leaves the capillary, a uniform field strength is reached and the CZE separation begins by itself. The sample stacking results are shown in Fig. 5b. Applying molybdate electrolyte it was possible to detect the presence of chloride, sulfate and nitrate ions. As can be seen, fluoride is enriched by sample stacking and acts as a matrix ion. However, owing to the described matrix effects, the detected species could not be quantified using the molybdate electrolyte.

To improve the separation, we adjusted the conditions of initial ITP also for sample stacking. Using chromate electrolyte with small amounts of the organic modifier TTAOH, the EOF was not reversed but slowed (Fig. 5c). Under these optimized conditions, bromide, chloride, sulfate, nitrite, oxalate and nitrate were detected. The peak identification was carried out using the standard additions method. Oxalate was identified on wafer surfaces for the first time. The reason for this contamination must be investigated.

For quantification of the analytes, the influence of the matrix ion on the peak shape, resulting in systematic errors for peak integration, must be accounted for. Therefore, the stock standard solutions for calibration (four solutions in the range 0.05–5 μM for the analytes) were applied in fluoride matrices similar to

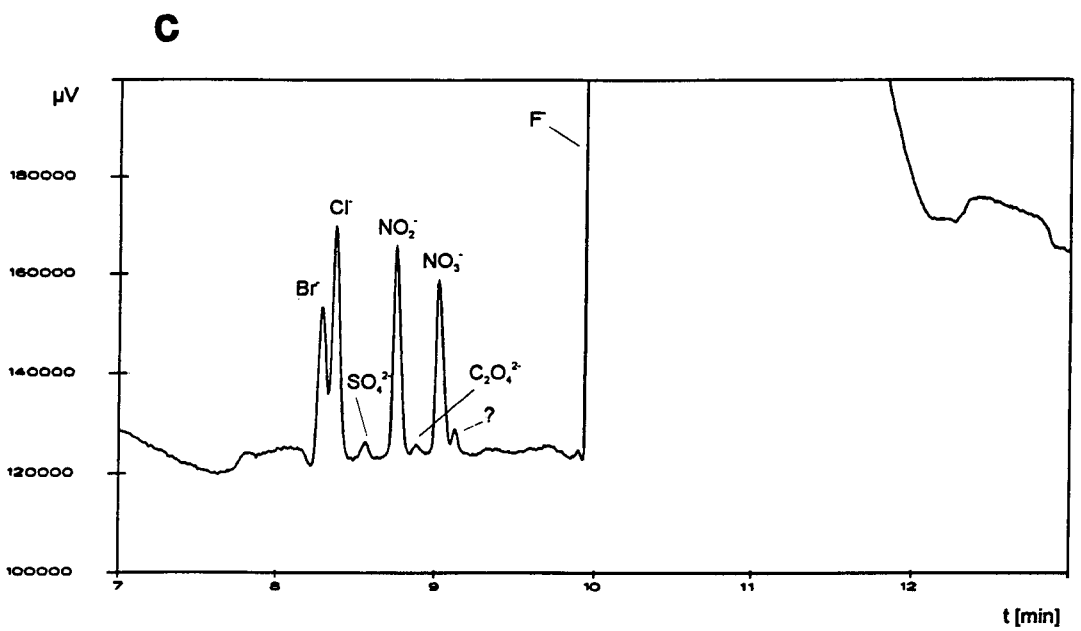

Fig. 5. (contd).

Table 2
Surface concentrations and absolute values of anionic contamination on as-polished silicon wafers after different experimental cleaning analysed with sample stacking

Sample	*Parameter*	*Anion*[a]						
		Bromide[b] ($r = 0.985$)	Chloride[b] ($r = 0.995$)	Sulfate ($r = 0.989$)	Nitrite ($r = 0.982$)	Oxalate[c] ($r = 0.983$)	Nitrate ($r = 0.989$)	Chlorate ($r = 0.993$)
Ultra-pure water blank	Concentration (μmol/l)	<0.05	0.3	0.05	0.05	<0.05	0.1	<0.05
Preclean[d] sample 1	Concentration (μmol/l)	4.4	1.6	0.35	0.6	<0.01	1.5	0.9
	Absolute value (10^{10} anions/cm^2)	151	55	12	21	<0.34	51	31
Repeated scanning	Concentration (μmol/l)	151.3	2.7	0.07	2.7	0.07	1.9	<0.02
	Absolute value (10^{10} anions/cm^2)	45	92	2.4	92	2.4	65	<0.69
Preclean[d] sample 2	Concentration (μmol/l)	3.4	0.7	0.3	0.5	<0.01	0.8	1.0
	Absolute value (10^{10} anions/cm^2)	116	24	10	17	<0.34	27	34
Repeated scanning	Concentration (μmol/l)	2.4	1.2	0.02	0.7	0.14	14	0.2
	Absolute value (10^{10} anions/cm^2)	82	41	0.68	24	4.8	48	<0.69
Clean A[d]	Concentration (μmol/l)	3.8	2.6	0.15	3.5	0.10	2.3	<0.2
	Absolute value (10^{10} anions/cm^2)	130	89	5.1	120	3.4	79	<0.69
Clean B[d]	Concentration (μmol/l)	1.5	1.5	0.04	1.15	0.09	2.1	<0.2
	Absolute value (10^{10} anions/cm^2)	51	51	17	39	3.1	72	<0.69

[a] r = Regression coefficient.
[b] Bromine and chlorine form surface species with pure silicon which are apt to hydrolyse.
[c] In the given analytical environment, low-molecular-mass acids such as oxalic acid can also be formed on the pure silicon wafer.
[d] Cleaning technology based on RCA cleaning that involves wet alkaline and acid oxidation to silicon [30].

the solved samples. The calculated regression coefficient are given in Table 2. It can be seen that the quality of the calibration lines was only moderate. The reason for this could be variations of the injection volume and of the EOF. The data show impurity concentrations in the range of $3 \cdot 10^{10}$ oxalate anions/cm^2 to $1.3 \cdot 10^{12}$ bromide ion/cm^2 (Table 2).

For recovery studies, bromide and sulfate were selected. Bromine (and more vigorously chlorine) can react with silicon and forms compounds that are unstable in hydrolysis with aqueous hydrofluoric acid solution. Sulfate does not react with silicon and therefore can be used as a standard ion for clean room conditions, since its concentration cannot be changed by chemical reaction. We obtained lower recoveries for bromide (70–30%) than for sulfate (80–93%).

4. Conclusions

We determined the optimized conditions of CZE to determine anionic analytes in samples preconcentrated on as-polished silicon wafer surfaces with an excess of fluoride solution. The combination of an electrophoretic separation with the initial ITP state was a very effective approach in improving the power of detection in the presence of matrix ions without modifying the basic CZE system. Our results suggest that an appropriate selection of the electrolyte co-ion diminishes the limitations due to the matrix ion, and that a detection power of $1:6 \cdot 10^4$ ATMR can be achieved. This ATMR value represents a six-fold increase over the results obtained in the normal CZE mode. Hence, the presence of matrix ions with a mobility very different from the mobilities of the analytes can be of advantage. In this work, the increase in plate numbers resulted in an additional improvement in the detection limits by a factor of two.

The optimization of the CZE conditions is more complicated when the mobility of the matrix ion is similar to the mobilities of the analytes. On the one hand, the analyte peaks can co-migrate with the matrix peak even at low matrix ion concentrations. On the other hand, taking the simultaneous impact of the co-ion on the ITP conditions into account, the selected co-ion must be a subtle compromise between measurement of analytes with higher or with lower mobilities than the matrix ion.

Even during calibration by sample stacking, initial ITP conditions must prevail. The quantification was carried out using calibration standard solutions with fluoride concentrations similar to those in the sample. In this way, we achieved a power of detection sufficient for surface analyses down to $5 \cdot 10^9$ ions cm^{-2}.

The mobile organic anion oxalate was identified on as-polished, experimental silicon wafer surfaces for the first time. In the same manner, electronic-grade hydrofluoric acid can be analysed for traces of anionic contaminants.

References

[1] L. Fabry, L. Köster, S. Pahlke, L. Kotz and J. Hage, *Proc. Electrochem. Soc.*, 15 (1993) 193, *and references cited therein.*
[2] L. Fabry, S. Pahlke, L. Kotz and G. Tölg, *Fresenius' J. Anal. Chem.*, 349 (1994) 260.
[3] L. Fabry, S. Pahlke, L. Kotz, E. Schemmel and W. Berneike, *Proc. Electrochem. Soc.*, 15 (1993) 232.
[4] M. Platt and J. Leo, *J. Chromatogr.*, 546 (1991) 347.
[5] D. Rathmann, *Proc. Electrochem. Soc.*, 12 (1992) 816.
[6] D. Rathmann and L. Fabry, *Proc. Electrochem. Soc.*, 12 (1992) 344.
[7] T. Talasek, B. Lucero and L. Vanatta, *Microcontamination*, 27, No. 9 (1994) 56.
[8] P. Kim Gupta, S.H. Tan, Z. Pourmotamed, F. Cristobal, N. Oshiro and B. McDonald, in *Proceedings of Electrochemical Society Spring Meeting, May 1994, San Francisco*, in press.
[9] D.S. Stegehuis, H. Irth, U.R. Tjaden and J. van der Greef, *J. Chromatogr.*, 538 (1991) 393.
[10] D.S. Stegehuis, U.R. Tjaden and J. van der Greef, *J. Chromatogr.*, 591 (1992) 341.
[11] F. Foret, V. Sustacek and P. Boček, *J. Microcol. Sep.*, 2 (1990) 229.
[12] N.J. Reinhoud, U.R. Tjaden and J. van der Greef, *J. Chromatogr. A*, 653 (1993) 303.
[13] D. Kaniansky and J. Marak, *J. Chromatogr.*, 498 (1990) 191.
[14] F. Foret, E. Szoko and B.L. Karger, *J. Chromatogr.*, 608 (1992) 3.

approach will be studied, the following aspects merit some attention.

(1) By carrying out trace enrichment and separation on one (short) column instead of using a precolumn plus a (long) analytical column, band broadening will be significantly reduced. This is especially true because the conventional SAMOS approach for practical reasons uses a copolymer sorbent in the precolumn which displays much higher retention towards most analytes of interest than does the C_{18}-bonded silica packing of the analytical column. On the other hand, breakthrough volumes will be considerably smaller in the simplified system.

(2) With the single short-column approach, the total time of analysis can be rather short. However, since the high-pressure packed short column (as yet) is not really inexpensive, repeated re-use is a necessity. Sample loading should therefore preferably be carried out at moderate flow-rates or, in other words, sample size should be limited.

It will be rather obvious that the above considerations indicate a preference for a very short rather than a moderate-size column (20 mm versus 60 mm in the present study), and that duration of run, limits of detection versus sample size, and column re-use are the main aspects of interest.

3.1. Duration of gradient run

In order to find out to which extent the time of run can be reduced without compromising the separation power of the system too much, a series of injections was performed of a standard mixture of 16 organophosphorus pesticides (OPPs) on the 20 mm column. Norberg et al. [9] —in their study on the optimisation of the 55-min linear gradient of the usual SAMOS approach— recommended a linear gradient from 5 to 95% acetonitrile (in 30 min) for the class-selective separation of a mixture of 20 OPPs on a 250 mm × 4.6 mm I.D. column. Using a 30-min gradient in our system, i.e. with the 20 mm column, baseline separation was observed for all but two of the test compounds; some peak overlap was found for fenchlorphos and bromophos-methyl only (Fig. 2). The last eluting OPP, bromophos-ethyl, had a retention time of 18.7 min as against 32.5 min on the 250 mm column.

In view of the rather unexpectedly good re-

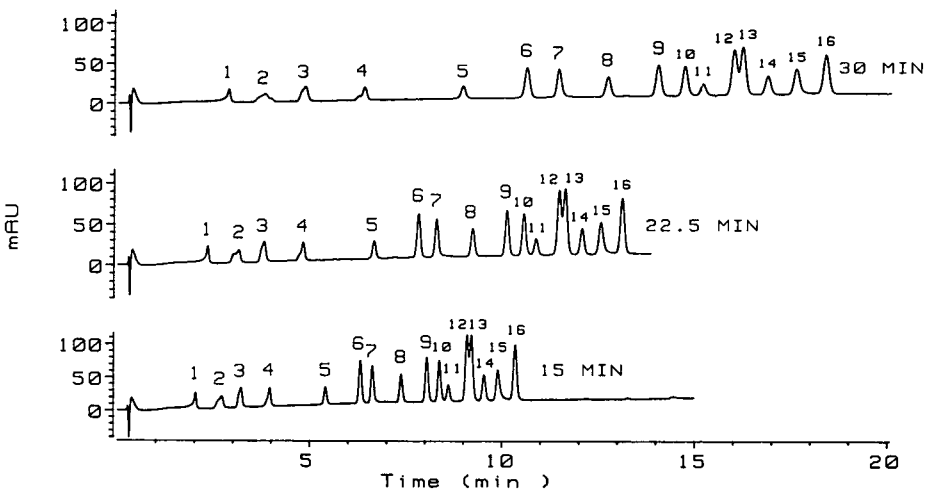

Fig. 2. Influence of gradient run time on resolution for a mixture of 16 OPPs. Column: 20 mm × 4 mm I.D. Hypersil ODS; linear gradient: 10 m*M* phosphate buffer (pH 3) to acetonitrile in 15, 22.5 and 30 min. Injection volume, 25 μl containing 5 μg/ml of each OPP. Peaks: 1 = monocrotophos; 2 = dimethoate; 3 = mevinphos; 4 = phosphamidon; 5 = paraoxon; 6 = azinphos-methyl; 7 = fenamiphos; 8 = fenitrothion; 9 = fenthion; 10 = coumaphos; 11 = phoxim; 12 = fenchlorphos; 13 = bromophos-methyl; 14 = chlorpyryphos; 15 = carbophenothion; 16 = bromophos-ethyl. UV detection at 210 nm.

sults, it was decided to omit —at least for the time being— studies dealing with the 60 mm long column, especially because preliminary results showed that this alternative primarily increased back-pressure and loading time, while the additional resolution which was obtained had no real priority anymore. Instead, restricting the study to the 20 mm long column, in a next step gradient run times of 22.5 and 15 min were used. As is evident from the pertinent chromatographic traces included in Fig. 2, even with the 15-min run (with bromophos-ethyl being eluted after less than 11 min), there still is baseline resolution for essentially all peaks. Since the main goal of our study is to achieve adequate resolution only in an early-warning situation, whilst having low limits of detection and a high sample throughput, the 15-min gradient run obviously is the best choice.

3.2. Trace enrichment

In a next series of experiments, trace enrichment was included in the operation. To this end, surface water from the river Meuse was spiked with the mixture of sixteen OPPs, and analysed on the 20 mm column according to the procedure of Table 1. In order to keep the time of analysis rather short, the sample size was only 15 ml. Subsequent analysis of five samples spiked at the 4 μg/l level, on the same column, gave relative standard deviations (peak areas) of less than 10% for all but two OPPs (dimethoate and paraoxon, 20–25%). Satisfactory recoveries of 75–95% were observed for all analytes eluting between 5 and 9 min. As was to be expected, much lower recoveries of typically 45–50% were found both for the early eluting peaks (due to early breakthrough) and the late eluting OPPs (adsorption to inner walls of the tubing, etc. because of high hydrophobicity). Whereas the former problem can only be solved —for the same sorbent material— by using lower sample volumes or a longer column, thereby decreasing the overall analyte detectability or sample throughput, the latter problem can in principle be solved by adding a few per cent of modifier (e.g. methanol or acetonitrile) to the sample solution [4,9]. A typical chromatogram of a river Meuse water sample, without and with the OPP spike (recorded after the column had been used for several such samples), is shown in Fig. 3.

The limits of detection of the OPPs typically

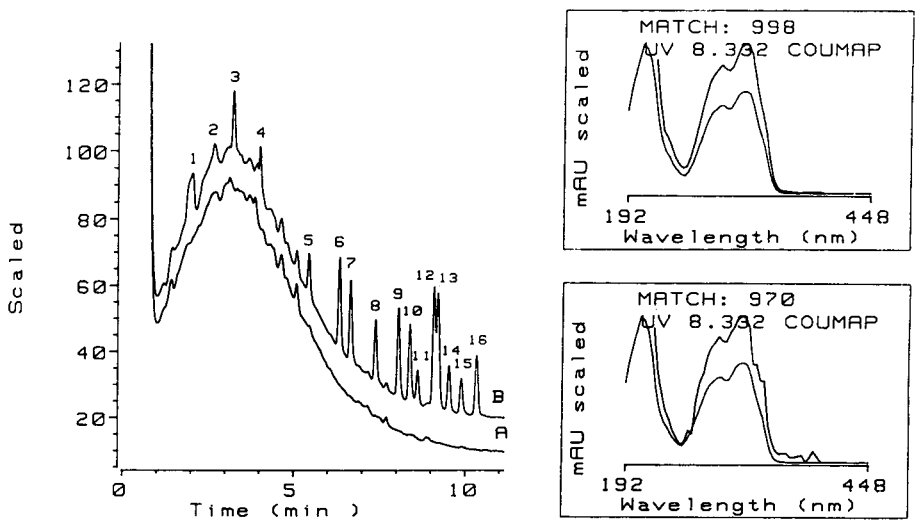

Fig. 3. Short-column LC–DAD of 15-ml samples from the river Meuse (A) without, and (B) with a 4 μg/l spike of sixteen OPPs. Insets on the right-hand side: UV spectra of coumaphos (peak 10) at 4 μg/l (top) and 1 μg/l (bottom) compared with library spectra. System characterization: 20 mm column; 15-min gradient; UV detection at 210 nm. Peak Nos. as in Fig. 2. For all other details, see text.

were about 1 μg/l in surface as well as in tap water. Actually, at the said concentration level most analytes gave good UV spectra with library matches of at least 905 for all but the first three eluting compounds. A relevant example is included in Fig. 3. Linearity was tested over the short, but relevant, concentration range of 1–8 μg/l. The results were satisfactory, with R^2 values of at least 0.992 for all but two compounds (dimethoate and paraoxon).

Column performance was remarkably good. Retention times were constant within 0.02 min, and peak widths typically were 0.1 min. Column lifetime has not been studied extensively, but on at least one 20 mm column, some 40 real samples (30 surface water and 10 tap water samples) were analysed without any noticeable column deterioration showing up. For the rest, on the basis of our (admittedly limited) experience it seems safe to state that a 20 mm column can be used for at least some 20–30 15-ml sample runs.

Other analytes

Preliminary runs were carried out with pesticides other than OPPs. Good results, i.e. detection and/or identification at the 0.5–1 μg/l level, were obtained for atrazine and for a series of phenylureas which included metoxuron, monuron, chlortoluron, diuron, chlorbromuron and neburon. Fig. 4 shows chromatograms obtained for a surface water sample spiked at the 1 μg/l level, and for a 12-μl syringe injection of a 2.5 mg/l standard solution. Recoveries were 80–100% for all but the early eluting desmethyl-metoxuron, which was not detected at this concentration as a result of early breakthrough and poor peak shape.

It is interesting to add that atrazine and diuron were identified in several of the samples tested, viz. at concentration levels of 0.2–0.5 μg/l.

3.3. Short-column LC–MS

In order to extend the scope of the present study, we briefly examined the direct on-line combination of short-column (20 mm) LC and MS. A PB interface was used, because this would enable the recording of electron impact mass spectra. The analytical conditions were as described in the Experimental section, with the exception that the aqueous part of the LC eluent now contained 0.1 *M* ammonium acetate buf-

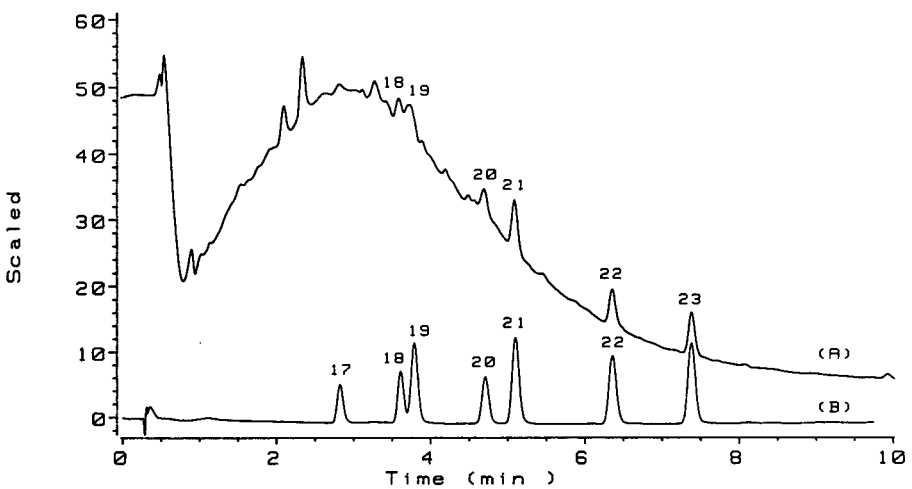

Fig. 4. Short-column LC–DAD of (A) 15-ml Meuse sample spiked with seven phenylurea herbicides at 1 μg/l and (B) a 12-μl syringe injection of a 2.5 mg/l mixture of the phenylureas. Peaks: 17 = desmethyl-metoxuron; 18 = metoxuron; 19 = monuron; 20 = chlortoluron; 21 = diuron; 22 = chlorbromuron; 23 = neburon. System characterization: 20 mm column; 15-min gradient; UV detection at 254 nm. For other details see text.

fered to pH 4 and that the flow-rate was reduced to 0.4 ml/min, which is the highest flow the PB interface can handle. Since the gradient time was kept at 15 min, the gradient itself became steeper; as a consequence peak widths were larger in time units, but smaller in units of volume.

With a series of six phenylureas (cf. [1]) as test compounds, short-column LC–PB-MS was performed with Meuse water spiked at the 0.1–10 μg/l level. Four of the test compounds could be detected over the whole concentration range in the selected ion mode (SIM), and at the 1 μg/l level with full-scan acquisition. Chlorbromuron (m/z 207) could only be detected at the 10 μg/l level (full-scan acquisition). Desmethyl-metoxuron appeared as a small broad peak in the early part of the chromatogram (cf. above), but could be detected (m/z 142) at 1 μg/l using ion extraction. Fig. 5 shows an extracted ion chromatogram of river Meuse water spiked with the six phenylureas at the 1 μg/l level. In the non-spiked sample, a peak (m/z 72) was observed with the same retention time as diuron. SIM and extracted-ion chromatograms (see Fig. 5) obtained after standard addition indicated a diuron concentration of 0.1 μg/l. Over 20 real-life samples were analysed by means of automated short-column LC–PB-MS without any deterioration of the system performance.

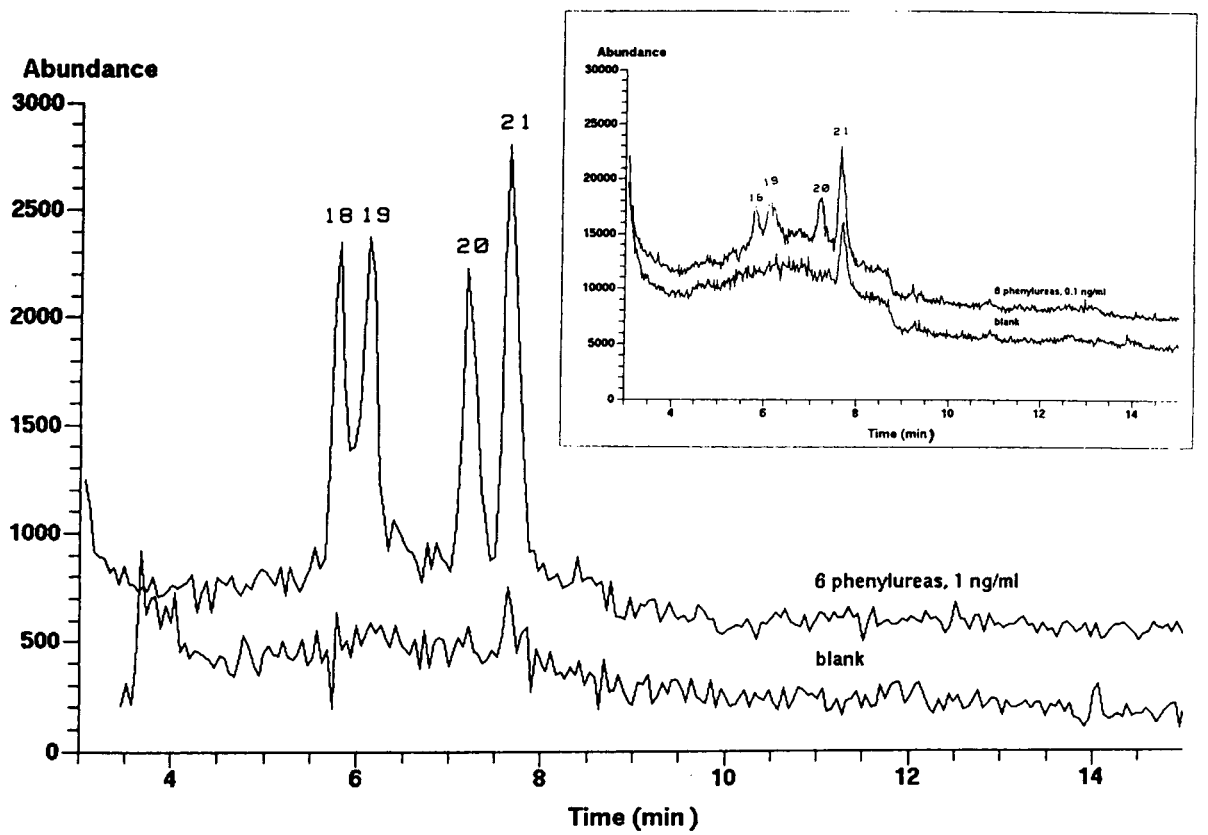

Fig. 5. Extracted ion (m/z 72) chromatograms of 15 ml of river Meuse water without (blank) and after spiking with six phenylureas at the 1 μg/l level. Inset: SIM chromatogram (m/z 72) of 15 ml of the same sample and after spiking with the six phenylureas at the 0.1 μg/l level. For analytical conditions, see text. Peaks: 18 = metoxuron; 19 = monuron; 20 = chlortoluron; 21 = diuron.

4. Conclusions

The practicality of single short-column LC for the trace enrichment and separation of polar pesticides in aqueous samples has been demonstrated. For many surface-water monitoring studies in which the number of microcontaminants actually showing up in each sample is very low, analyte detectability is much more important than high resolution. With the short-column LC–DAD system, the majority of the test analytes could be detected and identified down to concentrations of typically, 0.5–1 μg/l (8–15 ng injected). The total analysis time was 25 min, and a single 20 mm × 4 mm I.D. short LC column could be re-used some twenty times.

The results of this preliminary study and those reported in Ref. [8], and especially those on the use of MS detection instead of DAD are encouraging, and indicate that further optimisation may well lead to the development of a straightforward and relatively inexpensive procedure for the analysis of a large number of water samples in, especially, early-warning situations. Here, one should point out the distinct parallels existing between the present work and earlier studies on coupled-column LC in which two high-pressure packed short columns were used in series for the trace-level determination (large-volume injection, clean-up and separation) of highly polar analytes [10,11].

Acknowledgement

The present project was carried out within the framework of the EU Environment project EV5V-CT92-0105.

References

[1] H. Bagheri, J. Slobodník, R.M. Marcé Recasens, R.T. Ghijsen and U.A.Th. Brinkman, *Chromatographia*, 37 (1993) 159.
[2] J. Slobodník, M.G.M. Groenewegen, E.R. Brouwer, H. Lingeman and U.A.Th. Brinkman, *J. Chromatogr.*, 642 (1993) 359.
[3] R. Reupert, I. Zube and E. Plöger, *LC·GC Int.*, 5 (1992) 43.
[4] E.R. Brouwer, A.N.J. Hermans, H. Lingeman and U.A.Th. Brinkman, *J. Chromatogr. A*, 669 (1993) 45.
[5] I. Liska, E.R. Brouwer, H. Lingeman and U.A.Th. Brinkman, *Chromatographia*, 37 (1993) 13.
[6] J.M. Huen, R. Gillard, A.G. Mayer, B. Baltensperger and H. Kern, *Fresenius' J. Anal. Chem.*, 348 (1994) 606.
[7] H. Bagheri, E.R. Brouwer, R.T. Ghijsen and U.A.Th. Brinkman, *J. Chromatogr.*, 647 (1993) 121.
[8] K.-P. Hupe, M. Riedmann and G. Rozing, *Chromatographia*, submitted for publication.
[9] J. Norberg, J.J. Vreuls and U.A.Th. Brinkman, in preparation.
[10] E.A. Hogendoorn, R. Hoogerbrugge, P. van Zoonen, C.E. Goewie and P.J. Schoenmakers, *J. Chromatogr.*, 552 (1991) 113.
[11] E.A. Hogendoorn, U.A.Th. Brinkman and P. van Zoonen, *J. Chromatogr.*, 644 (1993) 307.

ELSEVIER

Journal of Chromatography A, 696 (1995) 341–348

JOURNAL OF CHROMATOGRAPHY A

Short communication

Quantitative determination of organic solvents by capillary electrophoresis using indirect UV detection

K.D. Altria*, J.S. Howells

Analytical Evaluation Group, Glaxo Research and Development Ltd., Park Road, Ware, Hertfordshire SG12 0DP, UK

First received 2 November 1994; revised manuscript received 9 January 1995; accepted 9 January 1995

Abstract

A sodium dodecyl sulphate (SDS)-based micellar electrokinetic capillary chromatography method is reported for the quantitative determination of a range of simple organic solvents employing indirect UV absorbance detection. Veronal buffer is used to provide both pH buffering and the background UV signal for indirect detection. The concentrations of both SDS and veronal buffer were optimized using an experimental design approach.

The method was shown to give acceptable performance in terms of various performance parameters including selectivity, linearity, precision and detection limits. The method was succesfully applied to the determination of the ethanol content in pharmaceutical formulations and alcoholic beverages. Good correlation was obtained between the CE results and the label claims. The method has several features including simplicity, short analysis time and robustness.

1. Introduction

The levels of organic solvents in various samples may be quantified by a variety of analytical techniques [1]. The most widely used of these techniques is GC which is very sensitive and allows detection of trace levels. However, problems of capillary fouling and blockages can occur when samples are presented which have complicated matrices. Therefore, extensive sample pretreatment may be required prior to GC analysis.

The capillary electrophoresis technique of micellar electrokinetic capillary chromatography (MECC) has been shown to resolve mixtures of aliphatic alcohols using indirect UV detection [2] or indirect fluorescence detection [3]. These reports highlighted the potential application of CE to this area. However, the separations could not be routinely applied to quantitative solvent determinations as there was insufficient resolution of the solvents from each other and from the peak due to water.

In the method reported here solvents are detected by virtue of indirect UV absorbance. This is a commonly employed detection scheme in CE as analytes with little or no chromophore are often analysed. For instance, alkylsulphate surfactants have been determined by CE employing veronal (barbitone) buffer to maintain an appropriate high pH and to provide sufficient background UV absorbance to allow indirect detection [4].

The objectives of this work were to extend previous methodology to achieve increased resolution of the organic solvents and to assess the

* Corresponding author.

0021-9673/95/$09.50
SSDI 0021-9673(95)00036-4

analytical performance of the method for quantitative analyses.

2. Experimental

A Beckman P/ACE 5000 (Fullerton, CA, USA) was employed for CE analyses, connected to a Hewlett-Packard HP1000 data handling system (Bracknell, UK). Capillaries were purchased from Composite Metal Services (Harlow, UK). All results were calculated using integrated peak areas. The polarity of the detector output was reversed to give apparently positive peaks making automated integration easier.

Both experimental designs were generated, and statistical analysis of the data was performed, using Design Ease (version 2.07) and Design Expert (version 3.05) software (Stat-Ease, Minneapolis, MN, USA).

2.1. Chemicals

Organic solvents were purchased from Rathburn (Walkerburn, UK) and BDH (Poole, UK). Barbitone buffer (5,5-diethylbarbituric acid) and sodium dodecyl sulphate (SDS) were obtained from Sigma (Poole, UK).

The separation conditions are as follows. Rinse 1: 0.5 min with 0.1 *M* NaOH; rinse 2: 0.5 min with electrolyte; set temperature: 30°C; detection: indirect UV at 230 nm; injection: 2 s pressure; separation: +5 kV; capillary: 27 cm × 50 μm.

The capillary was rinsed for 20 min with 0.1 *M* NaOH to rehydrate the surface prior to the first injection. The capillary was maintained only for use with this application.

3. Results and discussion

3.1. Method development and optimisation

The earlier reports of the separation of organic solvents by MECC [2,3] employed relatively high SDS concentrations in the range 100–150 m*M* and conventional length capillaries. Use of higher SDS concentrations would be impractical under these conditions due to excessive heating which would be generated within the capillary. In this study higher SDS concentrations, up to 300 m*M*, were employed as a combination of both a lower voltage (5 kV) and a shorter capillary (27 cm) were employed to minimise heating without unduly extending analysis time.

Barbitone (or veronal) buffer was employed to provide both pH buffering and high UV background. This buffer gives a high and reproducible electroendosmotic flow. The natural pH of this buffer is pH 9.5, no pH adjustment of any electrolyte solutions was performed. Therefore the effect of pH was not investigated in this study.

The initial stage of the method development was to optimise both the SDS and barbitone concentrations and the operating temperature. Given the number of combinations of buffer and SDS concentrations and temperature, it was decided to employ an experimental design procedure to reduce the number of experiments. A number of reports [5–10] have shown use of experimental designs on the optimisation of CE methods. The designs reported to-date include Plackett–Burman [5,6] and overlapping resolution mapping [7–10]. Another suitable design is a central composite [11] which allows evaluation of a method over a range to produce appropriate response surfaces. Central composite designs are particularly useful in the robustness of methods to small deliberate changes in method parameters. These designs are widely used in evaluation of HPLC methods [12] and have been used in an evaluation of the robustness of a CE method [11]. A central composite design was used to evaluate the effect of temperature and both electrolyte and SDS concentration during the optimisation of the separation.

The method conditions were explored in the ranges of 25–35°C for temperature, 12–28 m*M* barbitone and 150–250 m*M* SDS. The central composite design required 20 experiments, conducted in duplicate, covering a range of [SDS], [barbitone] and temperature combinations. The flexibility of controlling the entire CE instrument using a personal computer allowed this to be

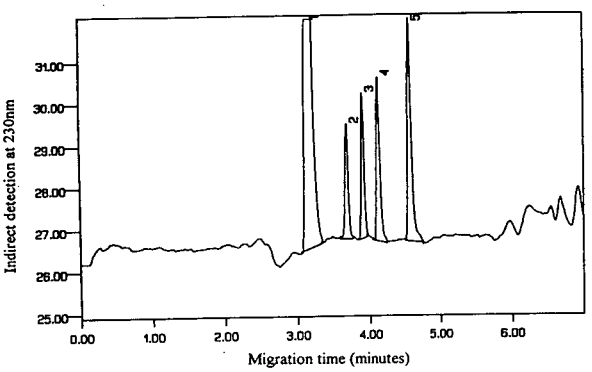

Fig. 1. Separation of 1% (v/v) test mixture of methanol, ethanol, acetone and 2-propanol. Separation conditions: as in the Experimental section using 200 m*M* SDS with 20 m*M* barbitone, 30°C. Peaks: 1 = water; 2 = methanol; 3 = ethanol; 4 = acetone; 5 = 2-propanol.

conducted in an overnight sequence. The test sample employed was a 1% (v/v) aqueous solution of methanol, ethanol, 2-propanol and acetone. Fig. 1 shows the separation achieved at the mid-point value of the ranges explored i.e. 30°C, 20 m*M* barbitone and 200 m*M* SDS. Peak 1 is due to water and is also obtained from analysis of a blank solution. A minimum resolution criteria of 2.0 was applied to ensure baseline resolution of all components. Statistical analysis showed that temperature had no significant effect on resolution in the range evaluated. Fig. 2 shows a response surface for the resolution between methanol and ethanol to be most critical to [SDS] requiring SDS concentration of greater than 180 m*M* to achieve the resolution requirement of 2.0.

The following limits were applied to the method: SDS concentration 200 m*M* ± 10; barbitone buffer concentration 20 m*M* ± 2; temperature 30°C ± 5. Higher SDS concentrations resulted in improved resolutions but with longer analysis times. Variation in buffer temperature, or SDS concentrations, had no significant effect on either peak height or areas.

3.2. Detector wavelength

The detection wavelength was varied and assessed at 200, 214, 230, 254 and 280 nm (being

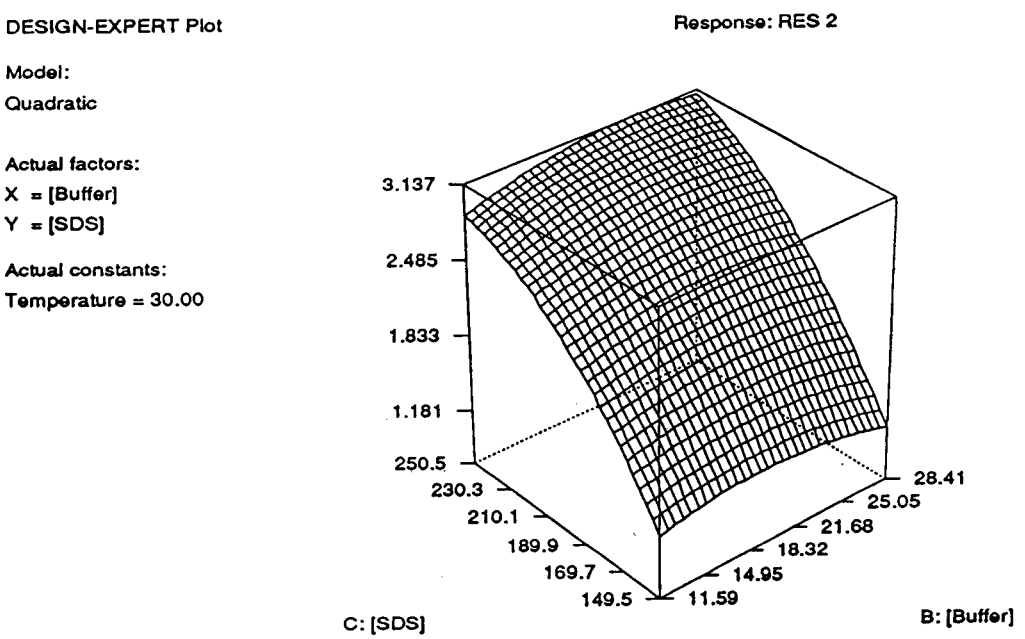

Fig. 2. Response surface plot for the resolution of methanol and ethanol with changes in [SDS] and [buffer].

the wavelength filters available on the particular CE instrument employed). No peaks were observed at 280 nm, whilst smaller peaks were seen at 200, 214 and 254 nm. Therefore 230 nm was selected as the wavelength for indirect detection in the final method.

3.3. Operating voltage

Voltage was assessed between +3 to +7 kV. Operation at +7 kV produced a considerably faster analysis (peak 5, 3.3 min) at the expense of reduced resolution and increased baseline noise. Operation at +3 kV produced increased resolution with longer analysis times (peak 5, 7.8 min). Therefore, the earlier value of +5 kV was employed in all further studies.

3.4. Peak identification

The range of solvents of interest was extended to methanol, ethanol, 2-propanol, 1-propanol and acetone. It is also necessary to confirm the migration position of butan-1-ol which is a likely interferent. A test mixture containing 1% (v/v) of each of the solvents in water was prepared and analysed (Fig. 3). Aliquots of this test mixture were spiked with 1% (v/v) of each individual solvent to confirm identity. The migration order was confirmed as water > methanol > ethanol > acetone > 2-propanol > 1-propanol > butan-1-ol (last).

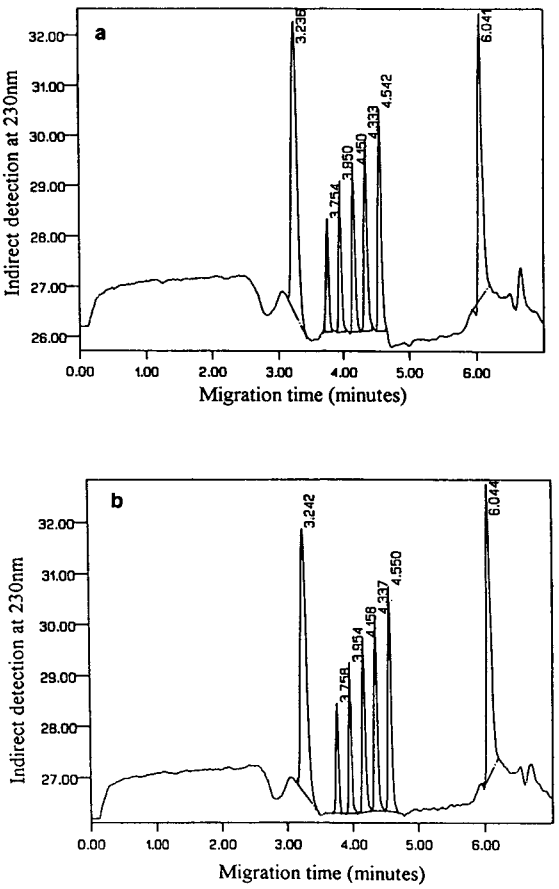

Fig. 3. Injection repeatability. (a) First injection; (b) tenth injection. Separation conditions as in Fig. 1. Migration order: water, methanol, ethanol, acetone, 2-propanol, 1-propanol, butan-1-ol.

3.5. Assessment of analytical performance

The validation criteria commonly employed in the evaluation of a CE method are similar to those tested for in HPLC [13]. Preliminary evaluation of this method included assessments of linearity, precision and detection limits.

Precision

A 1% (v/v) mixture of the six solvents in water was injected using the method settings given in the experimental section. Fig. 3 shows the first (Fig. 3a) and the tenth (Fig. 3b) injection. Table 1 shows that the migration time precision was excellent, R.S.D. values of <0.1% being obtained for all solvents, indicating good performance of the method for qualitative analysis. Peak area precision for the solvents was in the region of 2–3%. However, when using peak area ratios, precision was improved to 0.7–2.8% which supports the use of an internal standard [14]. Precision was worse for methanol as it had the smallest peak area and precision in CE is highly dependent on concentration and peak area [15,16]. This performance suggests, however, that the method is entirely suitable for quantitative determination of solvents.

Table 1
Precision of injection

	Area (R.S.D., %)	PAR (R.S.D., %)	Height (R.S.D., %)	Relative height (R.S.D., %)
Methanol	4.8	2.8	2.3	0.9
Ethanol	3.0	2.9	2.1	1.4
Acetone	2.9	1.8	2.0	1.0
2-Propanol	2.8	0.7	2.1	0.8
1-Propanol	2.4	0.7	1.6	0.8

Relative height and peak-area ratio (PAR) with respect to butan-1-ol; $n = 10$.

Linearity

Detector response was measured over the range 0.05–5% (v/v) spiking of the various solvents. Seven solutions were prepared within this range which were analysed in duplicate. Peak area linearity correlation coefficients over this range were typically 0.996. The correlation coefficients of peak height over the range 0.05–2.5% (v/v) spiking were typically 0.997. Higher spiking levels did not lead to linear increases in peak height due to peak broadening, as has been established previously [17].

Detection limits

Peaks at three times the signal-to-noise were obtained for 0.05% (v/v) standards which represents an approximate limit of detection. A 0.1% (v/v) standard was injected ten times (Fig. 4) giving average peak area ratios in the region of 5–10% R.S.D. This level represents a limit of quantitation for the solvents. It is noted that these figures are not as sensitive as GC and other techniques [1].

3.6. Applications

Many liquid pharmaceutical formulations contain levels of ethanol as a preservative. These formulations also contain a range of other excipients such as sugars and colouring agents as well as the active ingredients. These components can foul GC columns and may require sample pre-treatment. A syrup sample containing drug (at 10 mg/ml) and ethanol at 6.0% (v/v) was tested. An internal standard (2-propanol) was employed at 1% (v/v) for increased precision and to compensate for any viscosity differences between sample and standard solutions (as the injection volume in CE is related to solution viscosity). The syrup was appropriately diluted with internal standard solution and then injected directly (Fig. 5a) onto the capillary. Other peaks observed for the injection of the syrup samples are attributed to excipients in the syrup formulation. The peak due to drug migrated considerably later than the peaks of interest and did not interfere. The rinse steps between injections

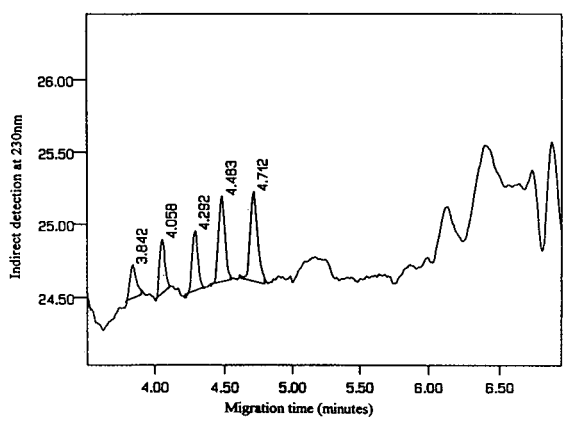

Fig. 4. Limit of quantitation (0.1%, v/v, for each solvent). Separation conditions as in Fig. 1. Migration order: methanol, ethanol, acetone, 2-propanol, 1-propanol.

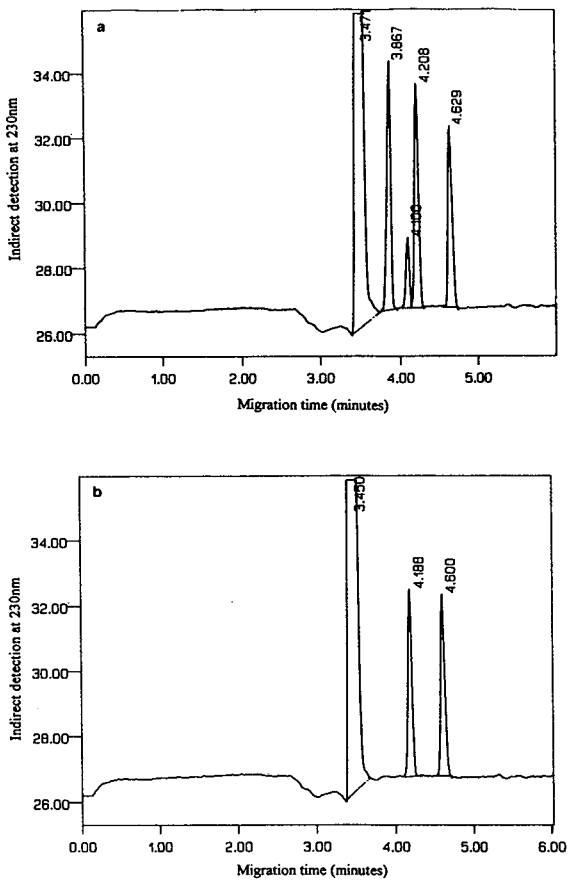

Fig. 5. Quantitation of ethanol content in syrup sample. (a) Injection of diluted syrup sample; (b) injection of a calibration solution containing 1% (v/v) of both 2-propanol and ethanol.

removed the drug and other unquantified material from within the capillary. The ethanol content was directly quantified by employing standards (Fig. 5b) containing both ethanol and 2-propanol at 1% (v/v). Results were calculated employing peak area ratios. Table 2 shows that the method gave results in line with the 6.0% ethanol label claim with good precision for migration times, relative migration times and response factors.

A further quantitative application of alcohol determination is shown in Fig. 6 which shows the analysis of alcoholic beverages. A sample of whisky (label claim of 40%, v/v, ethanol) was diluted with internal standard solution and directly injected (Fig. 6a), and no interfering peaks were observed. The results obtained (Table 2) were in good agreement with the label claim. An alcohol-free beer (<0.05% ethanol) was directly injected and confirmed as containing <0.05% alcohol (Fig. 6b), the origin of the early migrating peak(s) being unknown. This direct injection illustrates the robustness of the CE method to sample composition.

Qualitative identity confirmation is often required for input solvents in a manufacturing environment. For this testing, simple quantitative confirmation of the identity of solvent is required, and may be conventionally performed by IR and/or GC. This CE method is extremely suitable for such purposes given the good migration time and peak area precisions.

Table 2
Quantitative analysis results

	Result
Response factor ($n = 8$)	0.47% R.S.D.
MT of water ($n = 20$) (min)	3.48 (0.9% R.S.D.)
MT of 2-propanol ($n = 18$) (min)	4.65 (1.0% R.S.D.)
RMT of 2-propanol ($n = 18$)	0.35% R.S.D.
Syrup (6.0% nominal ethanol content)	(6.0, 6.1) (6.1, 6.1) average = 6.1
Whisky (40% nominal ethanol content)	(40.8, 4.12) average = 41.0%
Alcohol-free beer (<0.05% ethanol)	ND (less than 0.05%)

MT = Migration time; RMT = relative migration time; ND = not detected.

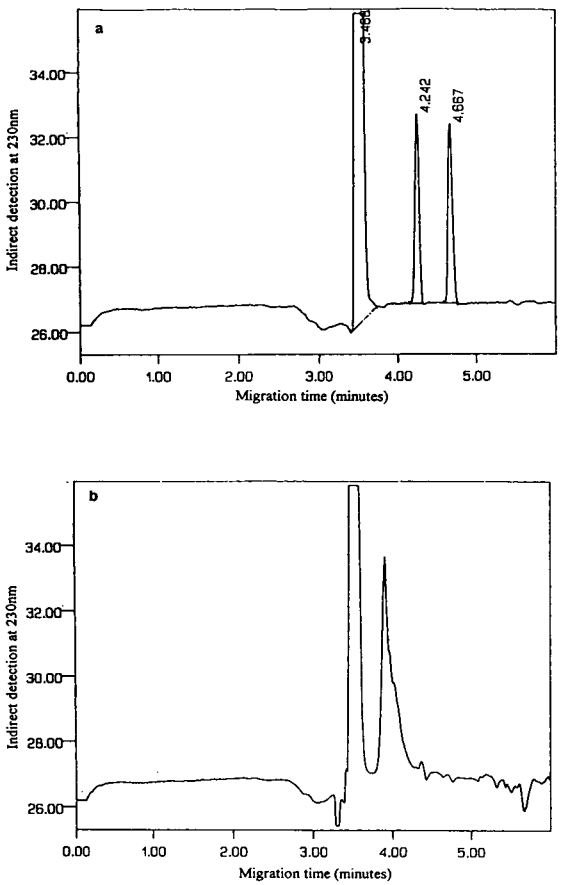

Fig. 6. Quantitation of ethanol content in alcoholic beverages. (a) Injection of diluted whisky sample; (b) direct injection of an alcohol-free beer.

3.7. Features of the method

The method is simple and robust, and the buffer can be prepared and stored for several weeks. The set-up time for the method is a matter of a few minutes resulting in quicker overall analysis times. Expenses are minimal compared to many alternatives as the reagents and consumables are very inexpensive. A particular feature is that samples of considerable complexity may be analysed with no fouling of the capillary, whereas extensive sample pretreatment may be required for other separative techniques. In addition, the testing is performed on conventional CE instrumentation using standard, inexpensive capillaries.

4. Conclusions

A MECC method has been developed and optimised for the quantitative determination of a range of organic solvents. A central composite experimental design and appropriate statistical analysis were employed in the optimisation of electrolyte composition and temperature. Acceptable performance of the method has been demonstrated in terms of precision, linearity and limits of detection. Features of the method compared to other analytical test procedures include robustness, simplicity and reductions in both overall analysis time and expense. The major disadvantage is reduced sensitivity which limits the scope of current applications.

Possible applications of the method include semi-quantitative identity confirmation of input solvents and determination of alcohol content in both liquid pharmaceutical formulations and alcoholic beverages. Undoubtedly further improvements in detector sensitivity and methodology will considerably improve the applicability and sensitivity of the method.

Acknowledgement

Thanks are extended to Sharon Filbey of Glaxo for her assistance with the experimentally designed optimisation work.

References

[1] F. Tagliaro, G. Lubli, S. Ghielmi, D. Franchi and M. Marigo, *J. Chromatogr.*, 580 (1992) 161.
[2] R.K. Szucs, J. Vindevogel and P. Sandra, *J. High Resolut. Chromatogr.*, 14 (1991) 692.
[3] L.N. Amankwa and W.G. Kuhr, *Anal. Chem.*, 63 (1991) 1733.
[4] M.W.F. Nielen, *J. Chromatogr.*, 588 (1991) 321.

[5] J. Vindevogel and P. Sandra, *Anal. Chem.*, 63 (1991) 1530.
[6] M.M. Rogan, K.D. Altria and D.M. Goodall, *Chromatographia*, 38 (1994) 723.
[7] C.L. Ng, H.K. Lee and S.F.Y. Li, *J. Chromatogr.*, 598 (1993) 133.
[8] C.L. Ng, C.P. Ong, H.K. Lee and S.F.Y. Li, *Chromatographia*, 34 (1992) 166.
[9] C.L. Ng, Y.L. Toh, S.F.Y. Li and H.K. Lee, *J. Liq. Chromatogr.*, 16 (1993) 3653.
[10] S.K. Yeo, C.P. Ong and S.F.Y. Li, *Anal. Chem.*, 63 (1991) 2222.
[11] K.D. Altria and S.D. Filbey, *Chromatographia*, 39 (1994) 306.
[12] M. Mullholland and J. Waterhouse, *Chromatographia*, 25 (1988) 769.
[13] G.S. Clarke, *J. Pharm. Biomed. Anal.*, 12 (1994) 643.
[14] E.V. Dose and G. Guiochon, *Anal. Chem.*, 63 (1991) 1154.
[15] S. Ryder, *J. Chromatogr.*, 605 (1992) 143.
[16] H. Watzig and C. Dette, *J. Chromatogr.*, 636 (1993) 3.
[17] D.M. Goodall, S.J. Williams and D.K. Lloyd, *Trends Anal. Chem.*, 10 (1991) 272.

ELSEVIER

Journal of Chromatography A, 696 (1995) 349–352

JOURNAL OF CHROMATOGRAPHY A

Short communication

Separation of fast anions by capillary electrophoresis without flow reversal

G.W. Tindall*, R.L. Perry

Research Laboratories, Eastman Chemical Company, Kingsport, TN 37662, USA

First received 22 July 1994; revised manuscript received 16 November 1994; accepted 14 December 1994

Abstract

Anions with high electrophoretic mobilities (fast anions) cannot easily be separated on bare silica columns by capillary electrophoresis unless the electroosmotic flow is reversed. The materials used to reverse flow limit the selection of indirect chromophores as well as complicate the direct detection of ions that do not need indirect detection. The availability of columns permanently coated to reduce electroosmotic flow could provide the means to separate fast anions without the need for a flow reversal agent. Useful separations of fast anions were achieved on commercially available silane-coated columns. These columns were particularly useful for the analysis of anions that could be detected by direct detection.

1. Introduction

Numerous applications of capillary electrophoresis have been reported for the determination of anions [1–9]. Bare silica capillaries are normally used and their surface is negatively charged at the pH typically used for separation. A corresponding positive charge in the capillary electrolyte results in bulk flow (electroosmotic flow) when voltage is applied. The net velocity of an anion is the vector sum of its electrophoretic velocity and its electroosmotic flow velocity. In anion analysis, an electroosmotic flow modifier may be added to reverse the direction of this flow. If the detector end of the capillary is positive, the electrophoretic and electroosmotic velocities are toward the detector. This configuration provides rapid separation of a wide variety of ions.

Quaternary salts, for example myristyltrimethylammonium bromide, can be used to reverse flow. The use of a quaternary salt, in combination with chromate as an indirect chromophore, has been described by Jones et al. [10] for anion analysis. A disadvantage of this approach, other than limitations imposed by the patent, is compatibility of the indirect chromophore with the quaternary salt. Vanadate, for example, forms a precipitate with some quaternary salts used for flow reversal [9].

Flow reversal is unnecessary for the separation of many anions, for example aliphatic and aromatic acids [8]. By using small-diameter columns and high pH, electroosmotic flow velocity is faster than the electrophoretic mobility of many anions and they will reach the detector in reasonable times even though their electrophoretic

* Corresponding author.

0021-9673/95/$09.50
SSDI 0021-9673(94)01229-6

migration is away from the detector. However, without flow reversal some very fast anions cannot be practically analyzed because the vector sum of their electrophoretic velocity and flow velocity is small [6]. For example, if the detector is negative, they migrate away from the detector nearly as fast or faster than flow toward the detector. In these cases the analysis time is unacceptably long or impossible because the analyte never reaches the detector. Reducing electroosmotic flow would result in practical separation times for these anions.

Additives such as water-soluble polymers have been reported to slow electroosmotic flow, but we were unable to significantly slow flow at neutral or basic pH. However, there are now a variety of coated columns available. High coverage of the silica surface should result in much reduced flow. The objective of this investigation was to evaluate coated (low flow) columns for fast anion analysis.

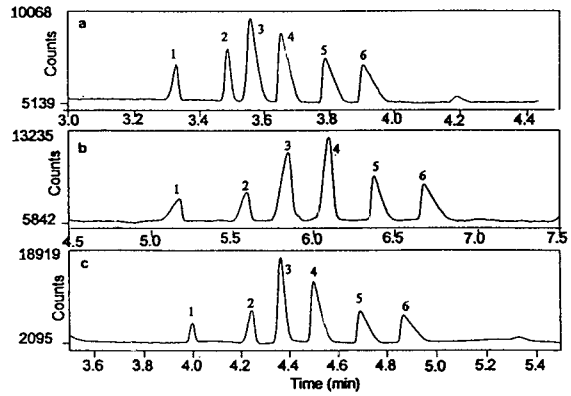

Fig. 1. Separation of fast anions with various indirect chromophore-electrolytes. Capillary: 72 cm (50 cm to detector) × 50 μm I.D. DB-1. Voltage: +25 kV at detector end. Column temperature: 30°C. Sample injection: 5 s by vacuum at 5 in.Hg (1 in.Hg = 3386.38 Pa). (a) 4 m*M* Sodium chromate, 270 nm; (b) 7.5 m*M* sodium vanadate, 254 nm; (c) 7.5 m*M* sodium iodide, 226 nm. Peaks: 1 = thiosulfate; 2 = bromide; 3 = chloride; 4 = sulfate; 5 = nitrite; 6 = nitrate. Concentration: 10 mg/l.

2. Experimental

The 270A-HT electrophoresis instrument was manufactured by PE-ABI (Foster City, CA, USA). A 0.05-μm film thickness DB-1 (C_1 phase), 72 cm × 50 μm I.D. column made by J & W Scientific (Folsom, CA, USA) and CElect-H50 (C_1 phase), H150 (C_8 phase) and H250 (C_{18} phase) 72 cm × 50 μm columns made by Supelco (Bellefonte, PA, USA) were used for anion separations. Separations were made with the detector end of the column at +25 kV and a column temperature of 30°C.

3. Results and discussion

Fig. 1 shows the separation of six fast ions on the DB-1 column. The ions all separate in a relatively short time and can be detected with a variety of indirect chromophore-electrolytes. One advantage of not using a quaternary salt electroosmotic flow modifier is the freedom to use any indirect chromophore that is compatible with the column and analytes. Factors to consider when choosing the indirect chromophore have been discussed [11]. The best dynamic range for separation will be achieved when the mobilities of the analyte and electrolyte match. The molar absorptivity and mobility of the indirect chromophore will affect sensitivity. The electrolyte should not react with any of the analytes of interest. Therefore, we do not recommend iodide for the determination of thiosulfate because it may contain iodine as an impurity or as a result of electrolysis.

Fig. 2 shows the separation of the six fast anions on the Supelco columns with chromate as the electrolyte. These columns differ in column coating which affects their charge and electroosmotic flow. Increased flow results in improved resolution, but at the expense of longer analysis time. This effect can be seen by comparing the separation of bromide and iodide on the DB-1 column and the H50 column (Fig. 3). This H50 column has slightly higher flow resulting in slightly longer migration times and higher resolution for iodide and bromide. The length of a column can be adjusted to optimize analysis time and resolution.

We found column life was typically limited by

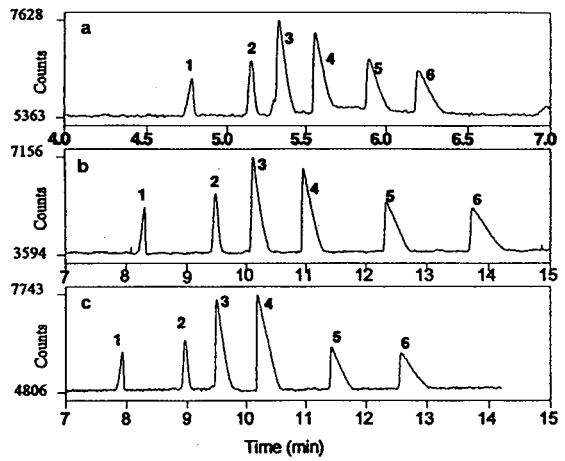

Fig. 2. Separation of fast anions on various Supelco capillaries. Capillary: 72 cm (50 cm to detector) × 50 μm I.D. Voltage: + 25 kV at detector end. Electrolyte: 4 m*M* sodium chromate. Detector: 270 nm. Column temperature: 30°C. Sample injection: 5 s by vacuum at 5 in.Hg. (a) CElect-H50, (b) CElect-H150, (c) CElect-H250. Peaks: 1 = thiosulfate; 2 = bromide; 3 = chloride; 4 = sulfate; 5 = nitrite; 6 = nitrate. Concentration: 10 mg/l.

stability of the coating. The columns investigated show some initial instability that results in slightly increasing migration times, but the times stabilize after a few runs. The lowest flow columns evaluated in this investigation have remained stable for weeks of use at neutral or slightly basic pH. However, the coatings are not stable at very high or low pH. When the coating starts to hydrolyze, as evidenced by increasing migration times, flow can increase in a matter of hours to a point where separation time is too long to be practical.

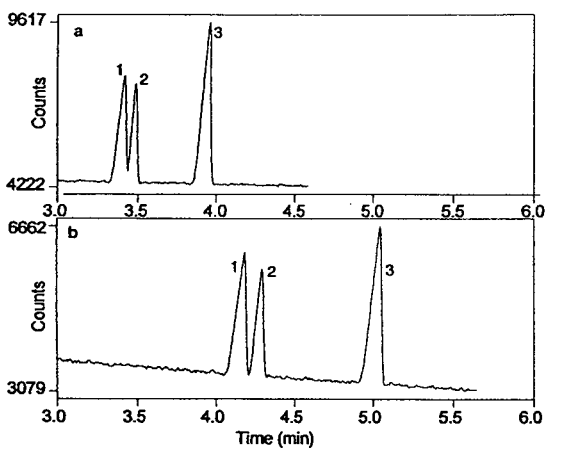

Fig. 3. Comparison of the separation of bromide and iodide on the DB-1 (a) and CElect-H50 (b) columns. Capillary: 72 cm (50 cm to detector) × 50 μm I.D. Electrolyte: 10 m*M* sodium phosphate (pH 7). Detector: 200 nm. Voltage: + 30 kV at detector end. Column temperature: 30°C. Sample injection: 5 s by vacuum at 5 in.Hg. Peaks: 1 = bromide; 2 = iodide; 3 = nitrate. Concentration: 10 mg/l.

Electrolyte concentration affected the separation in several ways. A higher electrolyte concentration produced better peak shapes at high analyte concentrations, but reduced sensitivity. The wavelength must be chosen to optimize absorbance once peak shape and sensitivity are optimized [11]. All the columns had some amount of electroosmotic flow that was slowed by increased electrolyte concentration. Migration times of anions decreased with increasing concentration of electrolyte, as a result of decreased flow, which under the conditions used is away from the detector. Electrolyte concentration also affected mobility (see Ref. [12], p. 407). When the ionic strength of the electrolyte is increased, divalent ions are slowed more than monovalent ions. As a result, electrolyte concentration affects selectivity in cases where anions of different charge are present in the sample. An example of this effect is illustrated in Fig. 4. At low electrolyte concentration sulfate migrates to the detector faster than chloride. As the electrolyte concentration is increased, sulfate mobility is reduced more than chloride and their positions in the electropherogram reverse. Because the electroosmotic flow decreases, both ions reach the detector quicker.

The use of the coated columns is particularly advantageous for the determination of anions that do not require an indirect chromophore. Tetraalkylammonium salts are typically available as the bromide salt. The bromide must be exchanged for a UV-transparent ion for direct determination of anions with flow reversal. This inconvenience is avoided by using coated columns. With direct detection, the baseline typically has less noise, consistent with the observation of Wang and Hartwick [13] that fluctuation in chromophore-electrolyte concentration is the

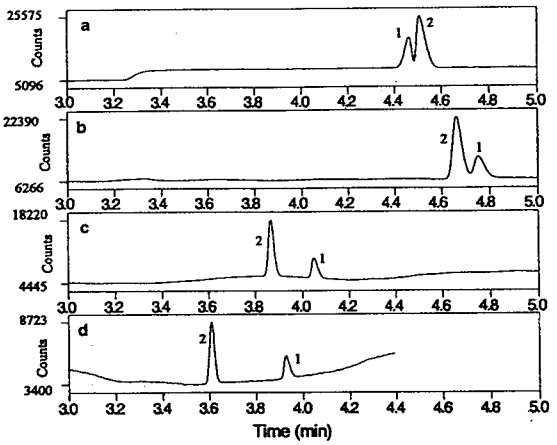

Fig. 4. Comparison of the effects of electrolyte concentration on selectivity. Capillary: 72 cm (50 cm to detector) × 50 μm I.D. DB-1. Detector: 226 nm. Voltage: + 25 kV at detector end. Column temperature: 30°C. Sample injection: 5 s by vacuum at 5 in.Hg. Sodium iodide concentration: (a) 2 m*M*, (b) 5 m*M*, (c) 10 m*M*, (d) 20 m*M*. Peaks: 1 = sulfate; 2 = chloride. Concentration: 10 mg/l.

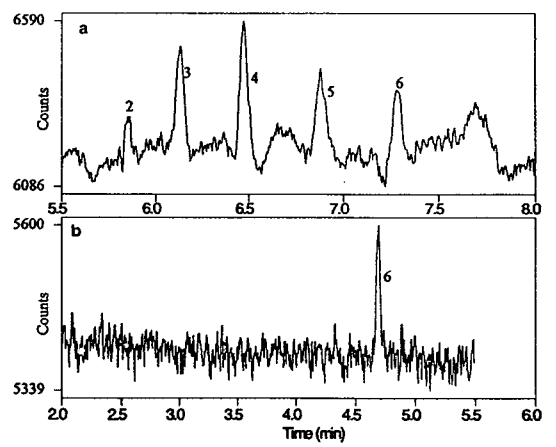

Fig. 5. Comparison of baseline noise with indirect and direct detection. Capillary: 72 cm (50 cm to detector) × 50 μm I.D. CElect-H50. Column temperature: 30°C. Sample injection: 5 s by vacuum at 5 in.Hg. Peaks: 2 = bromide; 3 = chloride; 4 = sulfate; 5 = nitrite; 6 = nitrate. (a) Indirect, conditions: 7.5 m*M* sodium iodate, detector at 226 nm, all components at 0.3 mg/l; (b) direct, conditions: 10 m*M* phosphate, pH 7, detector at 210 nm, nitrate concentration 0.15 mg/l.

noise limiting factor with indirect detection. An example of the improved baseline with direct detection is shown in Fig. 5. While the high-frequency noise attributed to the detector is similar for direct and indirect detection, the baseline with indirect detection has low-frequency fluctuations that makes accurate integration of low-concentration peaks difficult.

Acknowledgements

The authors thank both J & W Scientific and Supelco for providing the columns used in this investigation.

References

[1] K.D. Altria and C.F. Simpson, *Chromatographia*, 24 (1987) 527.
[2] S. Hjertén, K. Elenbring, F. Kilar, J. Liao, A.J.C. Chen, C.J. Siebert and M. Zhu, *J. Chromatogr.*, 403 (1987) 47.
[3] X. Huang, J.A. Luckey, M.J. Gordon and R.N. Zare, *Anal. Chem.*, 61 (1989) 766.
[4] B.F. Kenny, *J. Chromatogr.*, 546 (1991) 423.
[5] T. Wang and R.A. Hartwick, *J. Chromatogr.*, 589 (1992) 307.
[6] P. Jandik, W.R. Jones, A. Weston and P.R. Brown, *LC·GC*, 9 (1991) 3.
[7] M.W.F. Nielen, *J. Chromatogr.*, 588 (1991) 321.
[8] G.W. Tindall and R.L. Perry, *J. Chromatogr.*, 633 (1993) 227.
[9] P. Jandik and W.R. Jones, *J. Chromatogr.*, 546 (1991) 431.
[10] W.R. Jones, P. Jandik and M. Merion, *US Pat.*, 5 104 506 (1992).
[11] G.W. Tindall, D.R. Wilder and R.L. Perry, *J. Chromatogr.*, 641 (1993) 163.
[12] J.C. Reijenga and E. Kenndler, *J. Chromatogr. A*, 659 (1994) 403.
[13] T. Wang and R.A. Hartwick, *J. Chromatogr.*, 607 (1992) 119.

ELSEVIER

Journal of Chromatography A, 696 (1995) 353–354

JOURNAL OF CHROMATOGRAPHY A

Book Review

Fractionation by Packed-Column SFE and SFC, Principles and Applications, edited by M. Saito, Y. Yamauchi and T. Okuyama, VCH Weinheim, New York, Basel, Cambridge, Tokyo, 1994; XVI + 276 pages, 131 figures, 33 tables; DM 198.-, £80.-; ISBN 1-56081-591-4.

The book is split in two main parts: (I) Principles and techniques, (II) Applications.

Part I (133 pp.) is an introduction to the principles and instrumentation for performing SFC.

The first chapter gathers the "history" of SFC and SFE. It is well organized and references despite the fact that it mixes the technical aspects and the aim of these techniques. Chapter two describes the main properties of fluids and mixtures of fluids relevant to chromatography and extraction. Using references and data presented here, readers can obtain critical parameters of mixtures. This will also be useful for experienced chromatographers using exotic mixtures. Chapter 3 is entitled "Fundamentals of packed-column supercritical fluid chromatography and extraction". This title is very surprising because the SFE fundamentals do not appear at all in this chapter! Basic chromatographic parameters such as capacity factor, efficiency, resolution and so on are detailed. In my opinion, even SFC beginners, coming from the field of GC or HPLC, are familiar with all these data which thus could have been simplified. Part I ends with a chapter on instrumentation where all parts of apparatus are well described and illustrated.

Part II begins with "Recent advances in applications of SFE and SFC to industry". Here, despite the title, SFE is the purpose of the chapter. Unfortunately, recent here means 1990. No research papers published in the period from 1991 until now are referenced. The authors used the results of a survey published in 1991. It would have been desirable to include SFC and more recent results (several special issues of chromatographic journals were devoted to SFE and SFC during this period). The next 8 chapters are devoted to various applications. Chapters 6 and 7 are devoted to lemon oil extraction and fractionation and could have been organized in only one chapter (chapter 6 is devoted to data published in 1985 and 1988). Chapter 11, devoted to chiral separation, is simple but gives a clear approach of the advantages of SFC in this topic. Other chapters are interesting examples of the advantages of SFE extracts over extracts obtained by other methods for further application. Unfortunately, no real optimization of SFE or SFC conditions is described. For example, in chapter 3, related to SFE/SFC of carbon clusters, it is said that efficiency could be improved by changing extraction conditions such as pressure, volume ratio of CO_2/toluene and temperature, but no real description is given! Generally, conditions are given without explanation. It

0021-9673/94/$07.00
SSDI 0021-9673(95)00188-3

would have been very desirable, particularly for beginners in the field, to select and describe examples for which optimisation was given.

To conclude, this contribution to the understanding of SFC/SFE is a little disappointing because it lacks essential data on the optimization of SFE conditions and recent references, despite the fact that some examples are interesting and that the first part is well organized.

Paris, France M. Caude

Author Index

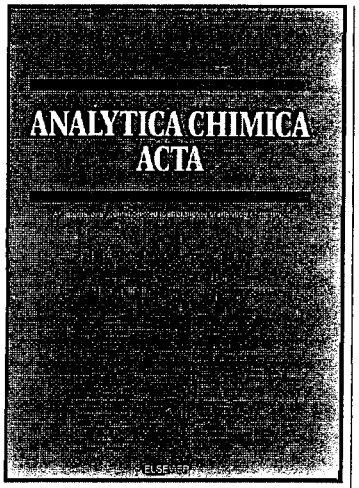

ANALYTICA CHIMICA ACTA

An International Journal Devoted to All Branches of Analytical Chemistry

Editors

Aims and Scope

Analytica Chimica Acta publishes the highest quality refereed research papers, reviews and preliminary communications covering all aspects of analytical science, and particularly those areas at the forefront of analytical development. **Full Author, Subject and Technique Indexes** are provided every 10 and 50 volumes.

Abstracted/Indexed in

Aluminum Abstracts, Analytical Abstracts, BIOSIS, Biological Abstracts, Chemical Abstracts, Current Contents: Physical, Chemical & Earth Sciences, EMBASE, Engineered Materials Abstracts, Index Medicus, Mass Spectrometry Bulletin, Material Business Alert, Metals Abstracts, Science Citation Index.

Audience

Chemists (all disciplines) in academic institutions, industry, independent laboratories and consulting firms.

1995 Subscription Data

Volumes 297-314 (in 54 issues)
Subscription price: Dfl. 6804.00 (US$ 3581.00)
ISSN 0003-2670

Elsevier Science B.V.
P.O. Box 211
1000 AE Amsterdam
The Netherlands
Fax: +31 (20) 485 3598

In the USA and Canada:
P.O. Box 945
New York
NY 10159-0945, USA
Fax: +1 (212) 633 3680

I would like ☐ a free sample copy of **Analytica Chimica Acta.**
☐ Instructions to Authors.
☐ to enter a subscription for 1995.
Please send me a Proforma Invoice.

Name .....
Address .....
.....
.....

The Dutch Guilder price (Dfl.) applies worldwide except in the Americas (North, Central and South America). US$ price quoted applies in the Americas only. Customers in the European Community should add the appropriate VAT rate applicable in their country to the price(s).

CALL FOR PAPERS

Fourth International Symposium on

HYPHENATED TECHNIQUES IN CHROMATOGRAPHY
HYPHENATED CHROMATOGRAPHIC ANALYZERS
(HTC 4)

The Saint John's Conference Center, Bruges (Belgium), February 6 - 9, 1996

The purpose of this fourth symposium will again be to highlight and treat in-depth recent developments and progress in the field of chromatographic hyphenations. It will cover all fundamental aspects, instrumental developments and applications of the various hyphenated chromatographic techniques e.g. coupling of LC to LC,GC and SFC ; MS, FTIR, AED and other techniques coupled with GC, (HP)LC, SFC and CZE; on-line air traps GC; purge-and-trap-GC, etc. Emphasis will also be placed on the design of hyphenated, on-line and at-line chromatographic analyzers.

The **scientific programme** will include oral presentations in plenary and parallel sessions, poster presentations and discussion sessions with prominent scientists. A **technical exhibition** will give an overview of instruments, books and accessories. The latest developments in instrumentation will be presented during workshop type **seminars**. Finally, a social and an accompanying persons programme including optional tours in Bruges and Northern Belgium will be offered.

The symposium will be preceeded by **workshops** on February 5 and 6, 1996.

A special volume of the *Journal of Chromatography* will be dedicated to the accepted and reviewed papers, which will be channelled through the usual refereeing system.

Participants who wish to present a paper are hereby invited to submit an abstract. Deadline for abstracts : **June 30, 1995** and for last minute posters : **December 15,1995.**

Submission forms for papers, enquiries about the technical exhibition and all other information may be obtained from the HTC 4-Congress Secretariate, Lucas Henninckstraat 18, B-2610 Wilrijk (Belgium), tel.: + 32 (3) 561.28.31, fax : + 32 (3) 828.89.61

PUBLICATION SCHEDULE FOR THE 1995 SUBSCRIPTION

Journal of Chromatography A and *Journal of Chromatography B: Biomedical Applications*

MONTH	1994	J	F	M	A	M	
Journal of Chromatography A	Vols. 683–688	689/1 689/2 690/1 690/2	691/1 + 2 692/1 + 2 693/1 693/2	694/1 694/2 695/1 695/2	696/1 696/2 697/1 + 2 698/1 + 2	699/1 699/2 700/1 + 2 702/1 + 2	The publication schedule for further issues will be published later.
Bibliography Section				713/1			
Journal of Chromatography B: Biomedical Applications		663/1 663/2	664/1 664/2	665/1 665/2	666/1 666/2	667/1 667/2	

INFORMATION FOR AUTHORS

(Detailed *Instructions to Authors* were published in *J. Chromatogr. A*, Vol. 657, pp. 463–469. A free reprint can be obtained by application to the publisher, Elsevier Science B.V., P.O. Box 330, 1000 AH Amsterdam, Netherlands.)

Types of Contributions. The following types of papers are published: Regular research papers (full-length papers), Review articles, Short Communications and Discussions. Short Communications are usually descriptions of short investigations, or they can report minor technical improvements of previously published procedures; they reflect the same quality of research as full-length papers, but should preferably not exceed five printed pages. Discussions (one or two pages) should explain, amplify, correct or otherwise comment substantively upon an article recently published in the journal. For Review articles, see inside front cover under Submission of Papers.

Submission. Every paper must be accompanied by a letter from the senior author, stating that he/she is submitting the paper for publication in the *Journal of Chromatography A* or *B*.

Manuscripts. Manuscripts should be typed in **double spacing** on consecutively numbered pages of uniform size. The manuscript should be preceded by a sheet of manuscript paper carrying the title of the paper and the name and full postal address of the person to whom the proofs are to be sent. As a rule, papers should be divided into sections, headed by a caption (*e.g.*, Abstract, Introduction, Experimental, Results, Discussion, etc.). All illustrations, photographs, tables, etc., should be on separate sheets.

Abstract. All articles should have an abstract of 50–100 words which clearly and briefly indicates what is new, different and significant. No references should be given.

Introduction. Every paper must have a concise introduction mentioning what has been done before on the topic described, and stating clearly what is new in the paper now submitted.

Experimental conditions should preferably be given on a *separate* sheet, headed "Conditions". These conditions will, if appropriate, be printed in a block, directly following the heading "Experimental".

Illustrations. The figures should be submitted in a form suitable for reproduction, drawn in Indian ink on drawing or tracing paper. Each illustration should have a caption, all the *captions* being typed (with double spacing) together on a *separate sheet*. If structures are given in the text, the original drawings should be provided. Coloured illustrations are reproduced at the author's expense, the cost being determined by the number of pages and by the number of colours needed. The written permission of the author and publisher must be obtained for the use of any figure already published. Its source must be indicated in the legend.

References. References should be numbered in the order in which they are cited in the text, and listed in numerical sequence on a separate sheet at the end of the article. Please check a recent issue for the layout of the reference list. Abbreviations for the titles of journals should follow the system used by *Chemical Abstracts*. Articles not yet published should be given as "in press" (journal should be specified), "submitted for publication" (journal should be specified), "in preparation" or "personal communication".

Vols. 1–651 of the *Journal of Chromatography*; *Journal of Chromatography, Biomedical Applications* and *Journal of Chromatography, Symposium Volumes* should be cited as *J. Chromatogr.* From Vol. 652 on, *Journal of Chromatography A* (incl. Symposium Volumes) should be cited as *J. Chromatogr. A* and *Journal of Chromatography B: Biomedical Applications* as *J. Chromatogr. B*.

Dispatch. Before sending the manuscript to the Editor please check that the envelope contains four copies of the paper complete with references, captions and figures. One of the sets of figures must be the originals suitable for direct reproduction. Please also ensure that permission to publish has been obtained from your institute.

Proofs. One set of proofs will be sent to the author to be carefully checked for printer's errors. Corrections must be restricted to instances in which the proof is at variance with the manuscript.

Reprints. Fifty reprints will be supplied free of charge. Additional reprints can be ordered by the authors. An order form containing price quotations will be sent to the authors together with the proofs of their article.

Advertisements. The Editors of the journal accept no responsibility for the contents of the advertisements. Advertisement rates are available on request. Advertising orders and enquiries can be sent to the Advertising Manager, Elsevier Science B.V., Advertising Department, P.O. Box 211, 1000 AE Amsterdam, Netherlands; Tel: 31 (20) 485 3796; Fax: 31 (20) 485 3810. Courier shipments to street address: Molenwerf 1, 1014 AG Amsterdam, Netherlands. *UK*: T.G. Scott & Son Ltd., Tim Blake, Portland House, 21 Narborough Road, Cosby, Leics. LE9 5TA, UK; Tel: (0116) 2750 521/2753 333; Fax: (0116) 2750 522. *USA and Canada*: Weston Media Associates, Daniel S. Lipner, P.O. Box 1110, Greens Farms, CT 06436-1110, USA; Tel: (203) 261 2500; Fax: (203) 261 0101.